THE UNIVERSITY
of EDINBURGH

Dynamic signal processing by the glucose sensing network of *Saccharomyces cerevisiae*

Luis Fernando Montano-Gutierrez

Thesis submitted in fulfilment of the requirements for the degree of Doctor of Philosophy
University of Edinburgh
September 2017

To Mom, Dad and Brother, who are always on my mind.

Declaration

I declare that this thesis was composed by myself and that the work contained herein is my own. Contributions of other authors have been explicitly stated in the text. This work has not been submitted for any other degree or professional qualification except as specified.

(*Luis Fernando Montano-Gutierrez*)

Acknowledgements

I would like to thank the support provided by the Mexican National Comission of Science and Technology (CONACYT), and grant number 099819 awarded to me by the Wellcome Trust. This work would not have been possible without the contribution, help and support of the following people. Infinite gratitude:

- To my supervisor Peter Swain, for 4 years of advice and patience while dealing with an anxious biologist.
- To Iseabail Farquhar, for the construction of many of the yEGFP tagged strains and deletions that were crucial for completion of this work.
- To Emily Johnston, for the construction of most of the MoClo strains used in section 3.7, and her passionate dedication to our ongoing collaboration.
- To Jill Zhang, for her excellent data on long–term incubation of yeast, which I reanalysed in Appendix section A.4.
- To Jamie Auxillios, for her valuable contribution to the library of HXT promoters.
- To Melissa Bothe, for her insightful exploration of networks, included in section 5.4), and figure 5.3, which was taken from her thesis.
- To Gasper Tkaĉik, for his valuable advice on the linear decoding based on environmental history in chapter 5.
- To Christos Josephides, Elco Bakker, and Julian Pietsch for going out of their way to discuss my results and for their constant eagerness to help.
- To Ivan Clark for all his patience in teaching me the ways of yeast at the beginning of my PhD.
- To Uriel Urquiza, my lifelong friend and colleague, who has been always there to support and coach me in the toughest times inside and outside academia.
- To Silvia Visentin, for her kindness and never ending support during the writing of this thesis.
- To my dear friends Emiliano Alvarez, Guillermo Ortiz, Lorenzo Conti, Francesc Levrero, Ruth Shah, Alice Mari, Adrian Mallory, Siraj Sabihuddin, who have kept my spirit up.
- To Samuel Casasola, Efrain Zarazua, Gonzalo Mendoza, Louise Hansen, Tim Najuch, Utibe Utmoh, Becky Tillotson, Jean Paul Morrisey and Shane Burns, who have made this an unforgettable PhD experience, and without whom these years would have been very dull.
- To my family, for their everlasting love and understanding, and for believing in me.

Abstract

Organisms must constantly face and adapt to environmental change. Although unpredictable events may inevitably impose threats, temporally correlated
changes may also provide opportunities from which an organism can profit. An evolutionarily successful microbe must collect enough information to distinguish threats from opportunities. Indeed, for nutrient transport, it is not clear how organisms distinguish one from the other. Fluctuations in nutrient levels can quickly render any transporter's capabilities obsolete. Identifying the environment's dynamic identity is therefore a highly valuable asset for a cell to elicit an accurate physiological response.

Recent evidence suggests that the baker's yeast Saccharomyces cerevisiae can exert anticipatory responses to environmental shifts. Nevertheless, the mechanisms by which cells are able to incorporate information from the environment's dynamic features is not understood. A potential source of complex information processing is a highly intricate biochemical network that controls glucose transport. The understanding of this network, however, has revolved around its ability to adjust expression of 17 hexose transporter genes (HXT) to glucose levels. In this thesis, I postulate that instead the glucose sensing network is dynamically controlling the 7 major hexose transporters. By studying transporter dynamics in several scenarios, I provide substantial evidence for this hypothesis.

I find that hexose transporters with similar reported affinities (Hxt2 and Hxt4) are robustly allocated to separate stages of growth for multiple initial glucose concentrations. Using single-cell studies, I show that Hxt4 expresses exclusively during glucose downshifts, in contrast with Hxt2. From multiple approaches, I demonstrate that Mig1 is mostly responsible for reporting on the time derivative of glucose, and harnessing it to differentially regulate both transporters. I also provide evidence for the roles of Rgt2 and Std1 in modulating long-term glucose repression of Hxt4.

This work extends our ideas on the functionality of transport and gene regulation beyond the established steady-state models. The ability to decode
environmental dynamics is likely to be present in other signaling systems and may impact a cell's decision to use fermentation - a decision which is of fundamental interest both for cancer research and for biotechnology.

Resumen en español

Todo organismo debe enfrentar y adaptarse a los cambios en su entorno. Aunque los cambios impredecibles son una amenaza inminente, ciertos cambios temporalmente correlacionados podrían ofrecer oportunidades provechosas para un organismo. Cualquier sistema que permita distinguir dichas oportunidades entre las amenazas brindará ventajas evolutivas. Específicamente, en el contexto del transporte de nutrientes, no está claro cómo los organismos hacen esta distinción, pues las fluctuaciones en las concentraciones de un nutriente podrían atrofiar repentinamente el funcionamiento de cualquier transportador. Por esta razón, detectar la 'identidad dinámica' de un ambiente sería de utilidad para preparar una respuesta fisiológica a tiempo cuando un nutriente está por agotarse. Bastante evidencia sugiere que la levadura de cerveza *Saccharomyces cerevisiae* puede anticipar transiciones ambientales. Sin embargo, no se conocen los mecanismos mediante los cuales las células leen y almacenan la información dinámica del ambiente. Una potencial fuente de procesamiento de información es una compleja red bioquímica que regula el transporte de glucosa en este organismo. Sin embargo, dicha red se ha entendido principalmente como ajustadora de la expresión de 17 transportadores de hexosas (HXT) de acuerdo con niveles externos de azúcar. En esta tesis, postulo la alternativa que la red controla temporalmente los principales transportadores HXT1-7, y ofrezco evidencia diversa en apoyo de esta hipotesis.

En el texto, muestro que dos transportadores con afinidades similares, Hxt2 y Hxt4, se alocan robustamente a estadíos distintos de crecimiento microbiano. Mediante estudios de celulas individuales, demuestro que el gen HXT4 se expresa exclusivamente durante una caída de glucosa ambiental, en contraste con HXT2. Desde ángulos diversos demuestro que el represor Mig1 es mayormente responsable de reportar al sistema sobre la tasa de cambio de la glucosa para regular diferencialmente ambos transportadores. También presento evidencia sobre el papel de Rgt2 y Std1 en la represión de HXT4 a largo plazo.

Este trabajo extiende nuestras ideas sobre la funcionalidad del transporte celular y regulación génica más allá de los modelos de estado estacionario. Posiblemente, la capacidad de decodificar la dinámica ambiental se encuentre en otros sistemas y podría impactar la capacidad de una célula para fermentar. Dicha capacidad es de interés fundamental en el estudio del cáncer y la biotecnología.

Lay Summary

Every living organism must adapt to change to survive. Environmental fluctuations can be unexpected or predictable, like a sudden loss of nutrients or the change of day to night. Even though stress and hardship may be inevitable, organisms that are able to anticipate events may have an evolutionary advantage. For example, we know that plants prepare for photosynthesis before the sun rises. Recent evidence shows that microbes, such as the bakers yeast, can similarly anticipate environmental shifts. We know that microbes must use the regulatory circuits encoded by their genes to perform these calculations. For example, a single yeast cell must store and compare information from different points in time. Yet exactly how the cells do this is not well understood. In this thesis I study the biochemistry that yeast evolved to sense glucose and to regulate hexose transporter proteins (HXT) that import glucose. We understand this network of proteins as being responsive to glucose levels. Nevertheless, for a single yeast cell, a particular amount of glucose could be ambiguous, perhaps signalling thriving conditions or the need to prepare for depletion of the sugar. Confusing those cues could be fatal. Here, I show that this complex network can integrate information about temporal sequences of glucose. In particular, I show that a protein in the network, Mig1, is able to monitor when sugar is either rising or falling. Mig1 then uses that information to specifically stop synthesis of Hxt4 when glucose rises and allow synthesis when glucose falls. Consequently, Hxt4 appears exclusively in preparation for glucose depletion. This finding is striking because currently no model explains why a transporter should be expressed exclusively in transient conditions. The results are an initial exploration of how the dynamics of a signal (its history and temporal trend) affects how single–celled organisms enter fermentation, which is a key metabolic process for industrial biotechnology and is present in diseases such as cancer.

Contents

List of Figures

List of Tables

0.1 List of Relevant Abbreviations

Gene notation (X symbolises any letter)

:

- XXXX- Usually a functional gene
- Xxxx- A protein
- xxxxΔ- deletion of the XXXX gene, or a non functional gene.
- pXXXX- indicates a promoter in text. In tables it may be a plasmid.

Commonly mentioned gene names (usually with a number)

- HXK- Hexokinase.
- HXT- Hexose Transporter.
- MIG- Multicopy Inhibitor of GAL1.
- MTH- MSN Three Homolog.
- RGT- Regulator of glucose transport.
- SNF- Sucrose Non Fermenting.
- STD- Suppresor of TBP Deletion.
- YCK- Yeast Casein Kinase.

Other abbreviations

- ADH- a class of promoter/terminator system for induction in yeast
- ALCATRAS- a microfluidic system created by the Swain Lab
- ABC-SMC- Approximate Bayesian Computation-Sequential Monte-Carlo. An algorithm
- A_{xxx}- Absorbance at xxx nanometers
- ACCESSPR- software for plate reader data processing
- ATP- Adenosine Triphosphate.
- AutoFL- Autofluorescence.
- BY4741- a strain
- cy5- a far–red fluorophore
- DNA- Deoxyribonucleic acid.
- GFP- Yeast Green Fluorescent Protein
- GR- Growth Rate
- IQR- Inter Quartile Range
- K_d- dissociation constant
- K_{cat}- catalytic constant
- SC- Synthetic Complete
- LFSC- Low Fluorescence SC
- LB- Luria Broth
- MoClo- Modular Cloning
- MOI- Moment Of Inertia. A metric defined in the study based on a physical property.
- NAD(H)- Nicotin Adenine Dinucleotide.
- OD- Optical Density.
- ODE- Ordinary differential equation
- PCR- polymerase chain reaction
- PEG- Polyethylene glycol
- RNA- Rybonucleic Acid.
- ROC- Receiver Operating Characteristic
- SCM- Synthetic Complete for Microfluidics

- SGA - Synthetic Genetic Array
- SEM - Standard Error of the Mean
- SEP- Super Ecliptic Phluorein
- STRE- Stress Response Element
- TEF- a class of promoter/terminator system for induction in yeast.
- UTR- Untranslated Region.
- URA- marker for selection in media without uracil
- yEGFP- Yeast optimised Green Fluorescent Protein

Chapter 1

Introduction

1.1 On the general mechanisms for biological decision making in the face of environmental uncertainty

1.1.1 Environmental change is a ubiquitous condition for all lifeforms.

The only constant element for all life forms is change, especially in a planet that renovates itself in scales of hours, months, decades and millions of years. Take, for example, the microorganisms undergoing nutrient starvation on the surface of a grape, patiently waiting for the sudden rupture of the fruit. Despite the highly nutritious content of this new environment, an individual cell must first make sure not to undergo an osmotic shock caused by the high density of sugar in the grape's flesh. At the same time being too cautious may result in being pushed out by members or another species–or even its own. Consider now a motionless cactus in a desert: its survival depends on withstanding the long hours of excruciating heat, while at the same time resisting, in the same day, the freezing temperatures at which water crystals could shatter its tissues. Finally, consider the Great Oxygen Catastrophe around 2.3 billion years ago, caused by the appearance of efficient photosynthetic organisms (Kopp et al. (2005)). The massive increase of

free oxygen levels in the atmosphere forced the decimation of life that depended on anaerobic (oxygen-free) and reducing (hydrogen and methane-based) atmospheric conditions. We, the inhabitants of Earth, are the descendants of the beings able to adapt to (or even benefit from) such gradual, yet schismatic changes in the chemistry of our surroundings. Adaptability to change is therefore not only an optional attribute for organisms; it is a fundamental requirement for all living beings.

1.1.2 Homeostasis, a default device against unpredictable fluctuation

Let us decompose the spectrum of environmental change along 2 axes (Figure 1.1) Change can be gradual or sudden; at the same time, it can be frequent or infrequent. This spectrum of change will bring enormous challenges to an organism. How then must an organism cope with all these numerous, unpredictable situations? As the exact number of threats is realistically uncountable, There has been a strong selective pressure for rather general mechanisms to counter the biological effects of environmental uncertainty. In an attempt to illustrate this, for a moment consider an airplane. Somehow, a massive piece of flying metal must maintain stability regardless of turbulence, snow, thunderstorms and many other harsh weather conditions. Airplane engineers have therefore designed systems that enable planes to cope with unpredictable changes in the plane's behaviour such that any imperfections in the plane's state can be measured and compensated (King (1998)). In biology, an organism's ability to maintain a constant internal state in the face of unexpected conditions has been termed homeostasis. Homeostasis has become a cornerstone paradigm in the modern biological sciences (Cooper (2008)), and how organisms achieve homeostasis upon environmental stress has been a fundamental question since the foundation of modern biology (Bernard (1885)). The notion is powerful because, regardless of the physical implementation, for homeostasis it is relevant to compensate any effects on the physiology, whereas the precise nature and source of the stress becomes of less importance. Homeostasis still dominates our understanding of how organ-

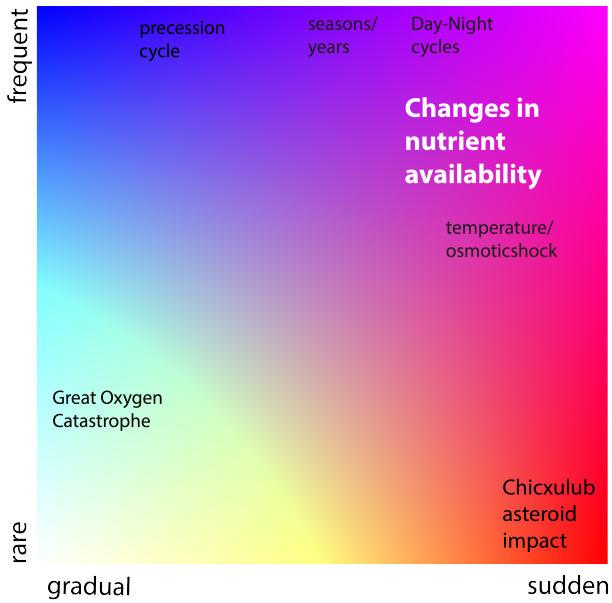

Figure 1.1: A spectrum of environmental change according to how gradual or sudden, and how frequent a phenomenon is. A few examples of changes across the spectrum are given. The present thesis focuses on environmental nutrient changes (white). These changes are frequent enough to impose a threat to any organism's survival, but are predictable enough that a link between external cues and biological responses can arise through evolution. Biology offers plenty examples of such tuning for most phenomena in the upper right side of this spectrum, some of which are briefly discussed in this chapter.

isms respond to environmental threats, and thus guides our biological questioning to this day (Levy et al. (2011), Mony et al. (2016)). It is deeply rooted in the biochemistry of every living cell (Engelhart et al. (2016)), however simple, and thus believed to be essential for life since the earliest of times.

1.1.3 Pressure for accurate decisions

Despite the fact that species can rely on homeostasis for survival, just coping with the environment is not enough for high fitness. Environmental uncertainty not only includes changes in time and space; it places organisms in fierce competition against each other for the same resources, even whilst belonging to the same species. Thus, a strong competitive advantage would come from more precision, nuance and context in physiological decisions, and from choosing the most adequate strategy among multiple possibilities. The discovery of system-level mechanisms that enable precise environmental decoding is driving a paradigm

shift from a homeostasis-centric biology, where advantageous decision-making are equally as important as merely surviving stress. One may immediately attribute optimal sensing and decision making to animals (Gabbiani et al. (2002)), many of which have complex neural networks and specialized organs for sensory perception; However, in recent years, there has been an explosive number of discoveries which have unveiled complex spatio-temporal decoding of information in plants (Scialdone et al. (2013)) and even single celled organisms (Yi et al. (2000), Tagkopoulos et al. (2008), Mitchell et al. (2009), Escalante-Chong et al. (2015), Muzzey et al. (2009), Venturelli et al. (2015), Balázsi et al. (2011)). A fascinating example is the detailed molecular mechanism by which the bacterium Escherichia coli swims towards increasingly higher concentrations of relevant molecules (i.e. chemotaxis) (Alon et al. (1999), Hansen et al. (2008)).

1.1.4 Predictable environmental variation: a platform for the evolution of temporal information processing

When it comes to performing the most optimal decision in a changing environment, a large asset for an organism is the information about the frequency and predictability of an environmental stimulus. For a moment, let us go back to the problem of the desert cactus (section 1.1), which faces particularly steep changes of scalding and freezing temperatures within hours of each other. These temporally correlated shifts in light and temperature not only present threats but also opportunities (Millar (2016)) for plants and other organisms to profit from. Intense research has revealed innate mechanisms to sense such spatio-temporal correlations, such as day-light photoperiods, in plants and animals. To cope with day-night cycles, organisms have developed autonomous physiological oscillations generally called the 'circadian rhythm', whose molecular basis has been deeply studied. Capturing such environmental variation enables plants to initiate particular physiological programs in anticipation of dawn (Dodd et al. (2005)). Similarly, neural circuits in mice are known to produce consecutive spikes in response to navigation (Chadwick et al. (2015)) or looming objects, which are then converted into neuromotor responses (Gabbiani et al. (2002)). Internal represen-

tations of the environmental sequences, which I will momentarily call correlative processing, have been also described in single-celled organisms (Tagkopoulos et al. (2008), Mitchell et al. (2009)). This adds to the notion that complex signal processing is widespread in evolution.

1.1.5 Environmental correlations can be genetically encoded

So where can the 'ability to remember' be found? In several studies, correlative information processing has been affected by genetic perturbations that ultimately alter the molecular and cellular mechanisms guiding these responses (Naylor et al. (2000), Mitchell et al. (2009), Wulff et al. (2009)). Genetic encoding of mechanisms that enable decoding environmental correlations is thus a valuable resource for living organisms, and it follows that genetic variation leads evolution to perfect the capture and exploitation of environmental patterns. Genetics thus provides a path to understanding the mechanisms behind the encoding of environmental patterns.

1.1.6 Clock-work genetic programmes are hampered by stochasticity

Despite the fact that mutations can enable very precise and tailored responses over evolutionary time, over-adapted strategies may become unreliable with a slight change in circumstances and thus, genetics is not a panacea for adaptability. For instance, an individual flowering plant must integrate subtle, long-term cues in light and temperature to decide on the right moment to flower. The difficulty of this task increases with the imminent variability of weather conditions. Hence, plants from the same species can show significant differences in flowering time from year to year and from one plant to another. Phenotypic variability is particularly predominant at the level of single cells: the same gene can achieve vastly divergent levels of expression amongst individuals of a genetically identical population of cells, at a given time (Elowitz et al. (2002), Swain et al. (2002)).

For these cells, the stochastic effects of molecular behaviour - generally called molecular noise - are exacerbated, even causing two identical copies of a gene within the same cell to follow distinct expression patterns (Elowitz et al. (2002)). Additionally to environmental changes, Noise during the events of gene expression is called intrinsic noise, which can cause differences between genes sharing the same cell environment. In contrast, noise coming from fluctuations in other cellular components, which affects two identical gene copies in the same way, is deemed extrinsic noise (Elowitz et al. (2002)). Therefore, any molecular sensing system must either be robust to noisy, confounding molecular variability, or harness the properties of external variation as another measure of environmental information (Bowsher et al. (2013)). Some molecular systems may have evolved to perform bet-hedging where the probabilities of eliciting a response may relate to the probabilities of environmental events (Perkins & Swain (2009)). The mechanisms through which cells thus integrate environmental fluctuations and remain robust to intrinsic and extrinsic noise remain largely elusive.

1.1.7 Despite simpler alternatives, robust and complex molecular information processing is commonplace

There is an appealing simplicity to generating a diverse population where some individuals will survive by chance (Balaban (2004), Yaakov et al. (2017)). However, the ability of many cellular systems to elicit responses of nearly deterministic precision to environmental cues despite molecular noisiness remains astounding. For instance, the nuclei in early stage drosophila embryos, initially placed into an equally spaced grid, are able to decode their spatial location with unprecedented, quantifiable precision (Dubuis et al. (2013)) . Furthermore, such positioning is strikingly resilient to genetic perturbations in molecular cues. How genetic systems like this are established to achieve precise environmental decoding and robustness to noise is subject of intense study for the field of systems biology. In that context, in the following section, the molecular machinery that enables such sensing is summarised.

1.1.8 The molecular machinery behind cellular signal processing

A single cell may sense and respond to environmental stimuli by assembling several layers of complexity into an integrated biochemical circuitry (Broach (2012)). The most basic of these layers is composed of physical changes (e.g. light, temperature, ions) or single molecules (ligands) usually bound by specific moieties in macromolecules, such as RNA or proteins. It is often the case that the binding of a ligand, or stimulation by physical phenomena, triggers a conformational change in the receptor. This change can be followed by chain reactions whose downstream targets are other effector molecules and genes. Among those actuators are kinases and phosphatases, which respectively phosphorylate and dephosphorylate substrates with speed and specificity. Transcription factors are often found among downstream effectors. Their role is generally to bind upstream sequences in genes (i.e. promoters) and thus induce or repress their expression. Systems that transfer information from the exterior are typically referred to as 'signal transduction pathways'. Examples across different life domains encompass the two-component signaling systems in bacteria, mitogen-activated protein kinase (MAPK) pathways and G-protein coupled receptors (GPCR).

1.1.9 Interconnections increase the topological complexity in pathways

Molecular response pathways, however, are seldom a linear arrangement. Effectors often activate or inhibit other pathway intermediates or themselves, and event sequences may eventually branch into sometimes contradictory outputs; downstream genes may themselves be transcription factors that affect genes within the same pathway, albeit at a slower timescale than enzymatic reactions. Moreover, biochemical networks often present circular action loops, where an output feeds back into the input (i.e. feedback loops) or feed forward loops (Alon (2007), Goentoro et al. (2009)) and often present cross-talk among pathways. In some cases, as we will see for some organisms, the redundancy and connectivity of

biochemical pathways can be overwhelming. A central problem is why evolution has opted for such degree of complexity in biochemical networks. One potential explanation is that the complexity of these networks reflects the complexity of the environment organisms evolved in.

1.2 Brief historical account on the studies of molecular decision making

1.2.1 First efforts describing biochemical network function

For the more than half a century, important efforts have been made towards abstracting and understanding the design principles of complex regulatory networks, and in elucidating their functional potential in the presence of environmental change. In the first half of the 20th century, in a time when the physical anatomy of a gene was yet to be identified, Conrad H. Waddington proposed that a dense network of gene functionality could create an 'epigenetic landscape' (WADDINGTON (1957)) that constrained the physiology of an organism towards particular states. In the 1960's, Francois Jacob and Jacques Monod integrated concepts of enzyme kinetics with cybernetics (according to Gayon (2015)) to pioneer the regulatory logic of known biological components. One outcome of their work was the concept of the lac operon: a self-contained gene-regulatory unit in Escherichia coli in charge of de–repressing lactose import in response to lactose availability– and hence the concept of repressor Jacob & Monod (1961). From this followed the description of positive gene activation, and a regulatory circuit controlling whether the bacteriophage lambda infecting Escherichia coli would enter lysis or lysogeny (Young (1992)). Standing on the shoulders of these cornerstone studies was the finding that certain molecules formed a spatial gradient during the development of organisms, which correlated with the rise of specific cell lineages. The concept sparked the interest of theoretical biologists, which have been developing models to explain how levels across molecular gradient could determine

phenotypic states. An example of such models is the french flag model (Wolpert (1969)). In sum, the quest for abstracting the regulatory basis of decision making has been as old as molecular genetics.

1.2.2 From genes to network motifs to system level information processing

Many keystone interdisciplinary advances have demonstrated that certain systems enable organisms to achieve adaptation and exert tailored responses to stimuli. The study of chemotaxis eventually proposed how a particular molecular system was able to detect fold-changes in concentration of a ligand (Alon et al. (1999)) and connect such detection to the torque of a molecular motor and achieve perfect adaptation (Yi et al. (2000)). In recent years, particularly with the advent of genomics and transcriptomics, large-scale screenings of transcription factor binding sites allowed major characterisation of gene regulatory networks, but also revealed how the frequencies of certain network substructures were statistically more represented than what was expected by chance. These substructures came to be called network motifs (Milo (2002), Alon (2007)). For around fifteen years, the information processing potential of these small motifs has been heavily investigated. These network configurations are known to account for a large plethora of behaviours upon specific types of stimuli.

1.3 General aim of this work

Despite the increasing understanding of the capabilities of small network motifs, to this day it remains difficult to understand the evolutionary, environmental forces that cause large, complex network configurations to become fixed in a population. In an attempt to tackle this problem, this work seeks to address whether the complexity of biological networks reflects the complexity of the environments organisms have evolved in. A complex network may be an organism's arsenal of strategies to identify and cope with more diverse classes of environmental kinetics, both the simple and the complex ones.

I hypothesise that the functional potential of a pathway may become more evident as the dynamic complexity of the environment increases, and the subtleties in the network connections start to impact a cell's decision-making. In the next section, I will elaborate on why *Saccharomyces cerevisiae* is an ideal organism to address this hypothesis for many reasons.

1.4 The yeast *Saccharomyces cerevisiae*, an intriguing decision maker

Saccharomyces cerevisiae, (a.k.a. budding yeast, baker's yeast) is a unicellular fungus with an asymmetric cell division, in which new cells grow from the mothers as small buds (hence its common name). It is a ubiquitous and vastly successful organism whose influence in human history is hard to compete with. It is found in most human-inhabited corners of the Earth, and is robust to a wide range of environmental conditions and changes (Chambers & Pretorius (2010)). For humans, it has been a fruitful collaborator, even in cultural terms. At the center of that success and influence is the yeast's ability to grow in environments rich in diverse sugars, but perhaps its most relevant asset is to produce ethanol as a byproduct of consuming sugar a process normally referred to as fermentation. Ethanol, besides being the obvious appeal for human use, also kills many competing, potentially pathogenic microbes. But despite the ecological advantage of ethanol production, fast depletion of carbon sources from the medium and away from competitors (Josephides & Swain (2017) might make yeast such a highly successful invader of new ecological niches. Hence, the earliest human civilisations adopted the organism as a valuable guarantee for safely drinkable beverages and, along with other fermentative organisms, for enhancing the nutritional value of foodstuffs such as leavened bread. The utilization of yeasts to enhance our food was a biotechnological breakthrough on its own, and as part of the larger agricultural revolution. The drive to understand, exploit and improve yeast's metabolism has naturally been of strong biotechnological interest ever since Louis Pasteur indicated that yeast was responsible for fermentation

(Pasteur (1876))

As implied before, The budding yeast is not the only organism capable of fermentation. In fact, most organisms capable of aerobic growth can ferment under specific circumstances, particularly when environmental oxygen is scarce. The choice to move away from fermentation is often attributed to its inefficiency. In yeast, glycolysis occurs via the Emden-Meyerhoff-Parnas (EMP) pathway and has a net yield of 2 molecules of ATP for every molecule of glucose (De Kok et al. (2012)) whereas respiration yields at least 10 times that amount(Fraenkel et al. (2011), Kregiel (2012), Nilsson & Nielsen (2016)). Third, in a highly oxidative atmosphere, oxygen is an extremely destabilizing compound. Besides, inefficient fermentation often releases toxic byproducts such as lactic acid or ethanol (Lehninger et al. (2008)). This is the case even for yeast; even though some industrial strains might resist high concentrations of ethanol, higher doses ultimately inhibit all microbial growth. However, in low sugar or non–fermentable carbon sources such as glycerol or ethanol, yeast opt for the far more efficient respiratory metabolism (Broach (2012)). As yeast actively choose to ferment despite being in a respiration friendly, aerobic environment, the question of why yeast then favour fermentation as a first metabolic choice has remained highly contended. The exact reasons and mechanisms that control this metabolic switch are not fully understood and thus are subject of intense investigation.

1.4.1 The rise of *S. cerevisiae* as a model organism for cellular decision making

In addition to *cerevisiae*'s biotechnological resourcefulness, a combination of other factors led to the rise of yeast as a prime model organism for molecular and cellular biology. First, it was ubiquitous and easy to grow. Second, it belonged to the domain Eukarya, which placed its cells closer to animal cells than bacteria in the evolutionary tree. Third, in 1956 Otto Heinrich Warburg (a Nobel laureate-to-be at that time) published the observation that several tumours developed on high rates of glycolysis followed by lactic acid fermentation even if oxygen is abundant. This came to be known as the Warburg hypothesis (Warburg (1956)), and its

uncanny resemblance to *cerevisiae*'s aerobic fermentation (Barford & Hall (1979)) suddenly placed the single-celled organism in the spotlight of cancer research - a gatekeeper of the secrets of cancer metabolism. Since then, yeast studies have come to be the foundation of many scientific breakthroughs in genetics, cellular and molecular biology, and a proxy for understanding our own biology.

1.4.2 Yeast batch culture growth as a dynamic environment

A normal yeast cell can face a vast range of environmental nutrient conditions during its lifespan: from prolonged starvation periods to ephemeral moments of nutrient abundance. One example is the standard batch fermentative growth. A starved yeast cell, placed in rich medium, will adjust its machinery and metabolism for growth in the new medium without dividing (the 'lag' phase) (Yates & Smotzer (2007)). Once the cells have adjusted, they begin producing biomass and new generations of dividing cells; such growth is of exponential nature (logarithmic growth). As soon as the cell population starts doubling, the concentration of the carbon source starts dropping. At a certain point during growth, cells transition from a glycolytic to a respiratory metabolism and start consuming ethanol, partly due to its abundance and the scarcity of glucose (a period called diauxic shift or lag). Respiratory growth during the diauxic shift can last several days and be of different intensities, depending on the strain , the abundance of respiratory carbon sources and oxygen availability. When no further carbon source is present in the environment, or when other nutrients become limiting, cells enter the 'stationary phase', where the cell population is no longer growing. Finally, after a prolonged period without growth, the cell population enters a death phase, where an OD drop may be seen. Transition through these phases can be quantified by the optical density (OD) of a culture the amount of light that passes through the culture is inversely proportional to the amount of cells in it. It will be learned in later sections that, particularly during glucose fermentation, a phenomenon called catabolite repression orchestrates the transition through these stages.

1.5 Glucose repression is a strong driver of decisions in yeast

Glucose, the most abundant monosacharide on Earth (Sabina & Brown (2009)), is a highly valuable carbon source. Most known organisms are both to catabolise it as an energy source (glycolysis), and to synthesise it from other energy sources (gluconeogenesis). It is thus a modular component of other disacharides (such as maltose and lactose) and other reserve polysacharides. Among these are starch, which is most common in plant tissues, and glycogen, which is used as energy reserve in fungal and animal cells. The exact reason why glucose is so ubiquitous is not known; however, it a resource that organisms are prepared to exploit, and hence for which they fiercely compete (Sabina & Brown (2009)). *Saccharomyces cerevisiae* is a heavy contender in this competition; it strongly prioritises glucose over essentially every other carbon source. The way this priority is established is generally known as catabolic repression, and more specifically glucose repression. This means that the presence of glucose not only activates the molecular machinery needed to import and metabolise glucose, but shuts down the pathways to use other carbon sources as a commitment to glucose consumption. Catabolite repression is central to the appearance of diauxic growth in microbial cultures. In yeast, concentrations of 18 mM have been found to cause repression of genes of alternative sugar metabolism Meijer et al. (1998). Moreover, as shown by monod curves, the maximal growth rate in glucose is achieved with similarly low concentrations of the sugar (Meijer et al. (1998)).

Glucose repression has been well described at the molecular level. The main executor of glucose repression is the transcription factor Mig1, a shorthand for 'Multi-copy inhibitor of GAL1' [1]. Shortly after glucose is detected, cytoplasmic Mig1 shuttles into the nucleus Bendrioua et al. (2014), causing immediate repression of alternative carbon source genes. Similar to Mig1 are paralogous genes Mig2 and Mig3, which have a common evolutionary origin and have overlapping functions. Mig1 is known to come into action at low glucose concentrations,

[1] GAL1 is one of the main genes required for galactose metabolism

whereas Mig2 repression becomes relevant at higher glucose levels. However, Mig1 function seems to be the dominant effector of glucose repression. Some regulatory specificity has been suggested to arise from combinatorial regulation of the three repressors (Westholm et al. (2008)).

1.5.1 Factors affecting Mig1 function

Mig1 function is largely regulated by the Snf1 Kinase complex, comprised of the main protein subunits Snf1, Snf4 and accessory proteins Sip1, Snf4, Gal83, that bring the complex to different locations (Vincent et al. (2001)). Low glucose concentrations generally correlate with an active form of Snf1, which causes phosphorylation of Mig1, forcing the repressor to leave the nucleus (Treitel et al. (1998), Kayikci & Nielsen (2015)). At higher glucose levels, the Reg1/Glc7 phosphatase complex dephosphorylates both Snf1 (Rubenstein et al. (2008), Ludin et al. (1998)) and Mig1 (Shashkova et al. (2017)), forcing the former to leave the nucleus and Mig1 to repress its targets. Nucleo-cytoplasmic shuttling of Mig1 is coupled to parallel translocation of Hexokinase 2, which binds to nuclear Mig1 and forms a repressor complex. Recent studies suggest that whether Mig1 binds a promoter together with Hxk2 influences its final effect on regulation, however the effects of such coupling remain to be determined (Ahuatzi et al. (2007), Fernańdez-García et al. (2012)). Hxk2 changes from a close to an open configuration in high glucose. For this reason, and its intersection with Mig1 and Snf1, Hxk2 is regarded as an internal glucose sensor. Therefore it is said that glucose metabolism triggers repression by Mig1 (Vega et al. (2016)) (Figure 1.4, green triangle). The specific way in which the metabolic signaling reaches Hxk2 or Snf1 is still to be understood.

Upon entry to the cells Snf1 itself is also a target of multiple regulation layers, for example the Protein kinase A (PKA) complex and the Target of Rapamycin complex (TORc), whose actions couple overall growth signals to glucose levels (Broach (2012)); however, the detail of such regulation is beyond the scope of this work.

1.5.2 Glucose repression in the face of environmental uncertainty and change

Vast research has placed Mig1 as a switch mediating transcriptional repression, induced to enter the nucleus within two minutes of exposure to glucose levels as low as 0.01% (Bendrioua et al. (2014)). However, this understanding does not solve an obvious ambiguity for the cell: a low glucose concentration might imply a poor, but reliable source of glucose or the presence of a high glucose source nearby. Alternatively, low glucose concentration could signal that nutrient starvation is imminent and looming, and hence that production of reserve molecules (such as glycogen or trehalose) must be prioritised. Cells must be able to distinguish between all these scenarios in order to maximise fitness, as each of them require specific time, resources and machinery to cope with. Several clues indicate that yeast are able to distinguish amongst these scenarios, for which yeast have evolved a complex, specialised machinery.

1.5.3 Mig1/2/3 as central players in metabolic reprogramming of yeast

Yeast batch growth has been deeply studied in the post-genomic era. In fact, the first transcriptomics study of all time addressed the reprogramming of yeast transcriptome across all batch growth phases (DeRisi (1997)). A more recent study provided extensive detail about the sequence of molecular events leading the to shift from glycolytic to gluconeogenic metabolism (Zampar et al. (2013)). While the moment of glucose exhaustion indicated the starting point of ethanol consumption, the study found a large number of events that happen prior to glucose depletion. The first of these is a change in glycolytic flux, which leads to upregulation of certain transcription factors and an increment of reserve molecules glycogen and trehalose. Production of the latter two molecules is essential for survival during starvation, is known to occur near halfway through glucose consumption (Lillie & Pringle (1980)) Kutty, and is genetically controlled by transcription factors Mig1/2 (de Virgilio (2012)).

1.5.4 Nuance and context in Mig1/2 mediated glucose repression

Among the genes canonically repressed by Mig1 are those required for galactose metabolism (the GAL network). A number recent studies have challenged the widely studied diauxic model for mixtures of galactose and glucose. One of them (Venturelli et al. (2015)) showed that a subpopulation of cells was able to activate expression of GAL genes prior to glucose depletion. Another study (Escalante-Chong et al. (2015)) has shown that a ratio of glucose to galactose, rather than a specific concentration, determines the activation of GAL genes. Deletion of both MIG1, and GAL80 was sufficient to obliterate this phenotype. In sum, these observations suggest that mig1/2-controlled glucose repression can be deactivated while glucose is still present, in a context-dependent, at times anticipatory fashion.

1.5.5 Is the glucose sensing network dynamically controlling glucose repression?

Through the information presented above, I intend to emphasize that even though Mig1 enters the nucleus immediately after glucose addition, repression cannot depend solely on glucose levels. A particular set of studies has explored how yeast that are starved and subsequently exposed to 0.5% glucose enter periodic cycling between fermentative and respiratory metabolism; this state has been coined 'the yeast metabolic cycle' (Tu (2005)). This cycling could be a direct consequence of the inability of the glucose level alone to determine a metabolic fate. Thus, the exact environmental cues that enable catabolic derepression, and the reading of those cues by the cellular machinery, remain to be elucidated. Glucose transport, in charge of the supply of glucose, is likely to be important for the respiration/fermentation decision when its flux is limiting relative to the downstream (demand) steps of glycolysis (van Heerden et al. (2015)). In support of this, the metabolic switching of yeast has shown to be manipulated into respiration by redesigning a glucose transporter (Otterstedt et al. (2004)). Furthermore, deletion

of the external glucose sensing promotes derepression of respiration (Youk & van Oudenaarden (2009)). The results of Zampar et al. (2013) and Escalante-Chong et al. (2015), Otterstedt et al. (2004) and Youk & van Oudenaarden (2009) thus withhold valuable clues central to this problem: They hint that glucose flux, influenced (somehow) by the glucose sensing and transport machinery, is in the spotlight of complex information processing and decision making. Therefore, the dynamic signal processing capabilities of the glucose sensing and transport network of *Saccharomyces cerevisiae* are the central focus of this work.

1.6 The yeast glucose sensing and transport network as a model for cellular decision making

1.6.1 Nutrient transport as the first front of cellular decisions

The nutrient transport machinery of every cell is at the forefront of interaction with the outside world, and is the gateway to a cell's survival. Control of transport allows a cell to connect specific cellular demands with the environmental circumstances. A mismatch between demands and circumstances could be lethal for a cell (van Heerden et al. (2014)). Thus, nutrient transporters are controlled by often immense layers of regulation (Broach (2012), Horák (2013)). The presence of a transporter on the surface of the cell can hence be considered an output of cellular decision making. Passive transport (which does not require energy) can be divided into channels/permeases, which allow the pass of a certain molecule by a preformed aqueous permeation, and facilitated diffusion, which generally involves two events: a) recognition, which is a ligand-induced conformational change in the transporter/carrier, and b) the subsequent release of the ligand into the cell (Figure 1.2). Thus, a perfect transporter would be able to efficiently bind the ligand and readily release it (Hernndez & Lisboa (2004)). In reality,

real transporters are far from this perfection. The binding and unbinding of a ligand to a transporter is captured by the rate constants K_f and K_r, whereas the rate at which bound ligand is effectively released into the cell is captured by the K_{cat} (Figure 1.2). the affinity, or the concentration at which half the transport rate is achieved, can be derived by integrating these parameters into by the Michaelis–Menten constant K_M (Fersht (1999)):

$$K_M = \frac{K_r + K_{cat}}{K_f} \tag{1.1}$$

Generally low affinity transporters are presumed optimal for higher ligand concentrations (due to a high K_M), where as high affinity transporters can achieve transport at lower ligand concentrations (due to a lower high K_M) and achieve saturating uptake rates at higher concentrations, for which a lower affinity may be bettersuited.

1.6.2 The decision landscape of nutrient transport

The physical chemistry of transport imposes imposes strict rules and trade-offs which constrain the cell's decision landscape. If a transporter is required to import high amounts of a ligand, then its affinity for such molecule must be relatively low. This means that at lower concentrations of the ligand, dissociating molecules will be at least as frequent as associating molecules Levy et al. (2011), thus neutralising total transport. Additionally, a low affinity transporter may be less specific and could also let in other molecules (Diallinas (2014)). At lower ligand concentrations, a high affinity transporter will be able to bind the ligand effectively; yet such strong attachment (low K_M) will lower the K_{cat}, which affects the rate at which sugar enters the cell. This constrains the rate at which the molecule can be metabolised. Additionally, the relative values between the K_{cat} and Km are further constrained as they cannot violate the equilibrium between substrate (external glucose) and internal glucose (product), as established by the Haldane relationship:

$$\frac{(K_{cat}/K_M)_S}{(K_{cat}/K_M)_P} = K_{eq} \tag{1.2}$$

Where K_{eq} is the equilibrium constant between substrate and product.

Another transport option, active transport, can be both fast and specific, but involves energy expenditure. Finally, not having transporters would mean depending on the diffusion of a molecule, which would not be optimal for highly competitive, membrane-impermeable or slowly diffusing molecules. In order to maximise fitness, a cell must strike a balance among all of these caveats. Such decision is not particularly simplified by the fact that external nutrient concentrations may be changing fast.

1.6.3 A 'dual transporter' motif is common in microbial transport systems

One common transport strategy used by organisms is a dual transporter motif, where cells use both a high-affinity transporter and a low-affinity transporter for the same molecule (Levy et al. (2011)). Why would a cell need more than one permease when a high affinity transporter could satisfy nutrient import at any concentration? (Levy et al. (2011)) propose how the dual transporter system could be used to trigger a 'mock' starvation response when nutrients drop below a certain concentration. The drop below the K_d of the low affinity transporter would trigger a starvation response, while the high-affinity transporter would still be present to import the nutrient. Thus, dual transport could imply a simple way for cells to cope with a changing sugar environment. However, this model contains several assumptions and caveats. First, the model assumes that both transporters must be active at the same time, which is not necessarily true. Transporters outside their conditions are often found in the vacuole or lysosomes, either stored or being targeted for degradation (Krampe et al. (1998)). This suggests that coexistent transport modes may be unfavourable to a cell. Secondly, a 'starvation response' in the presence of nutrients is a somewhat paradoxical concept and, without actual starvation, an additional system must account for detection of nutrient decrease. This possibility is offered by nutrient transport systems which have have additionally evolved transport-independent (external) nutrient sensing. External sensing is not explained either- the model accounts

for systems with exclusively internal sensing. In short, the simple, elegant logic of the dual transporter system as posited by Levy et al. (2011) is not sufficient to explain the elaborate regulation that many nutrient transporters receive in biological contexts. A particularly rich example of this is the glucose sensing-transport network in yeast. In this network, a large number of sensors, kinases and transcription factors regulate the expression of an arsenal of transporters.

1.6.4 20 transporters for the transport of hexoses in yeast

Nearly 20 years ago, it was found that knockout of 20 *Saccharomyces cerevisiae* genes encoding hexose transporters was required to compromise viable growth on all hexoses such as glucose and galactose (Wieczorke et al. (1999)). These genes were Hexose transporters 1-17 (Hxt1-17), galactose transporter GAL2, AGT1, YDL247w and YJR160c). Viability in glucose was eliminated by knocking out hexose transporters 1 to 7, which happened to be the most highly expressed ones. It is generally understood that Hxt1 and 3 encode low-affinity transporters ($K_m \approx 50 - 100mM$); Hxt2, Hxt4 are of intermediate affinity ($K_m \approx 10mM$), whereas Hxt6 and 7 are of high affinity ($K_m = 1.5mM$) (Reifenberger et al. (1997)). Hxt2 was also shown to have a low affinity component ($K_m \approx 60mM$) (Reifenberger et al. (1997)). Hxt5 has also been described as of moderate affinity ($K_m \approx 10mM$) (Diderich et al. (2001)), however it has been found to be controlled by growth rates (Verwaal et al. (2002)), and to be important for growth reinitiation after starvtion (Diderich et al. (2001)). The transporters have been described to be expressed in concentrations overall inversely proportional to their affinity: Low affinity transporters show high expression levels at high glucose concentrations ($> 1\%$); intermediate affinity transporters show expression at low to intermediate glucose levels (0.1%-0.5%) and high affinity transporters are expressed at low glucose levels ($< 0.1\%$). Together with the knowledge about glucose repression, there appears to be a general correlation between glucose levels, transport modes, and the decision between fermentative (high glucose) or respiratory (low glucose) metabolism. Given that one glucose transporter is the minimal requirement for viability in glucose and 2 for efficient uptake in high and low environments, the

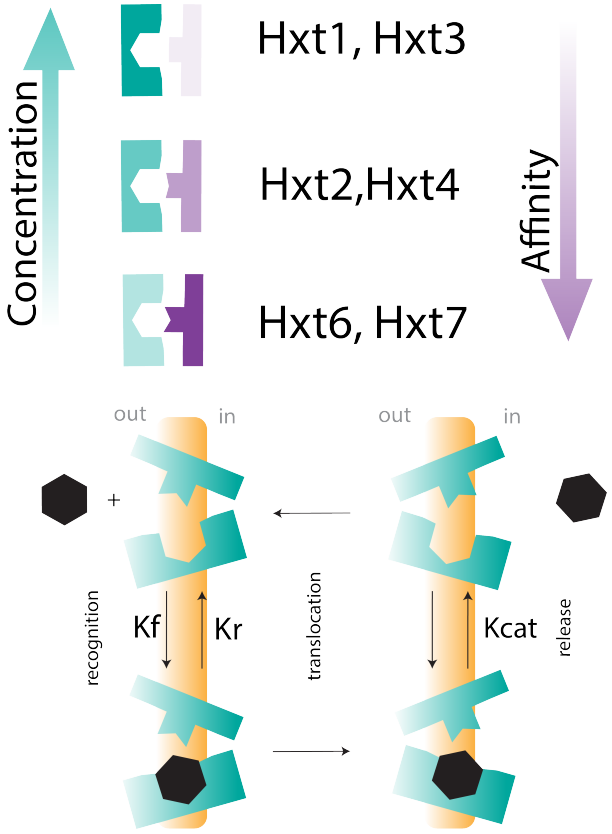

Figure 1.2: The major hexose transporters of *Saccharomyces cerevisiae* and their properties. Top panel: Hxt1-4 and hxt6-7 coloured by the concentration range at which they are expressed (bottom to top) Ozcan & Johnston (1995) and their increasing affinities, top to bottom (Reifenberger et al. (1997)). Bottom panel: Of the many kinetic steps to membrane transport, the model shown is widely used to understand facilitated diffusion. Kinetic constants collapse these phenomena into recognition and release. The dissociation constant $K_d = \frac{K_r}{K_f}$ is a concentration at which half of the glucose molecules that bind a transporter will dissociate from it. The catalytic constant K_{cat}, on the other hand, determines how effectively the transporter+glucose complex will release the glucose into the cell, reflected in the number of glucose molecules internalised per unit of time. Internal glucose may also bind a transporter from the cytoplasm, implying more reversibility than other enzymatic processes.

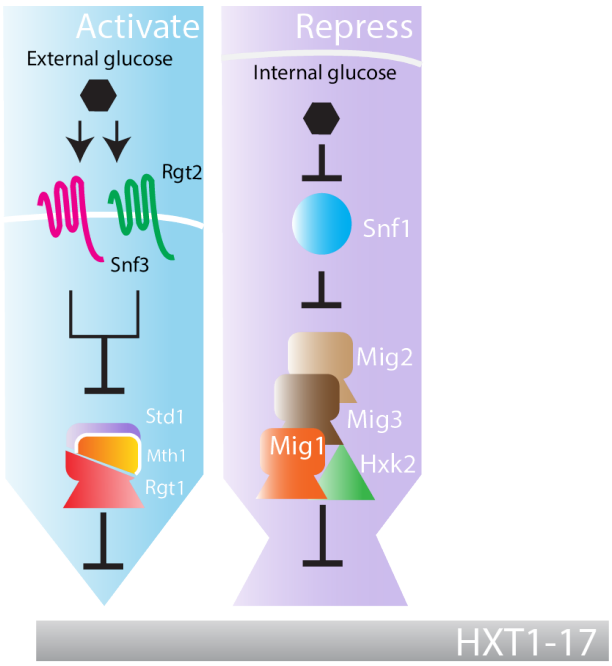

Figure 1.3: Overview of the yeast glucose sensing network.
An activator branch senses external glucose through sensors Snf3 and Rgt2 to release repression by the Rgt1/Mth1/Std1 complex. Internal glucose is sensed by enzyme/transcription factor Hexokinase 2, causing repression of HXT genes through Mig1/Hxk2, Mig2 and Mig3

contributions to fitness of the set of 7 transporters combined, and justifications for their extensive regulation remain elusive.

1.6.5 Overview of the yeast glucose sensing network

Hexose transporters are, in general, controlled by an activator branch, in which external glucose stimulates glucose sensors Snf3 and Rgt2, which derepresses transcription of the HXT genes. A repressive branch, orchestrated by the metabolism of internal glucose, then represses a select set of HXT genes by the action of internal glucose sensor hexokinase 2 (Hxk2), inhibition of the Snf1 kinase complex, and nuclear shuttling of repressors Mig1/2/3. both branches enable adjustment of transport to specific set points (Figure 1.3).

1.6.6 Regulatory logic of the components in yeast glucose sensing

Figure 1.4 describes with larger detail the regulatory interactions in the yeast glucose sensing network. Transporter expression is repressed by a complex composed of transcription factor Rgt1 and paralogs Mth1 and Std1. In the absence of glucose, the repressor complex remains bound to HXT promoters, thereby inhibiting their expression. At the cell membrane, such repression is controlled by signals from membrane-bound, paralogous glucose sensors Snf3 and Rgt2. Snf3 and Rgt2 sense low and high glucose respectively (Ozcan et al. (1996), Özcan et al. (1998). Their similarity to transporters indicates that they were initially transporters that lost the ability to import sugar. The binding of glucose to Snf3 and Rgt2 induces a conformational change that stimulates the contact between the cytosol-oriented C-terminal tail of the sensors with membrane-bound yeast casein kinases 1 and 2 (Yck1/2) (Babu et al. (2004)). The interaction of sensors with the kinases triggers a 'glucose signal' that stimulates degradation of Mth1 and Std1, which in turn disrupts the Rgt1 repressor complex and thus induces HXT expression. Once glucose enters the cell, Hexokinase 2 acts as an internal glucose sensor which, together with Mig1, forms a repressor complex (Vega et al. (2016)) that enters the nucleus and represses the HXT genes (See next section). Mig1, Mig2 and Mig3 have also been found to bind the HXT promoters to different extents. Titration of the influence of these two branches should allow for expression of HXTs at different glucose levels. Yet another pathway transmits general glucose signals to proliferation and growth via the G protein-coupled receptor Gpr1, but in general no strong evidence has linked this pathway to HXT expression. Glucose-induced degradation of high affinity transporters Hxt6 and 7 has additionally been described (Krampe et al. (1998)), controlled by E3 Ubiquitin ligase Rsp5 and adaptor Arrestin 6 (Art6) (Sen et al. (2016)).

1.6.7 Metabolic feedback and role of internal glucose during repression

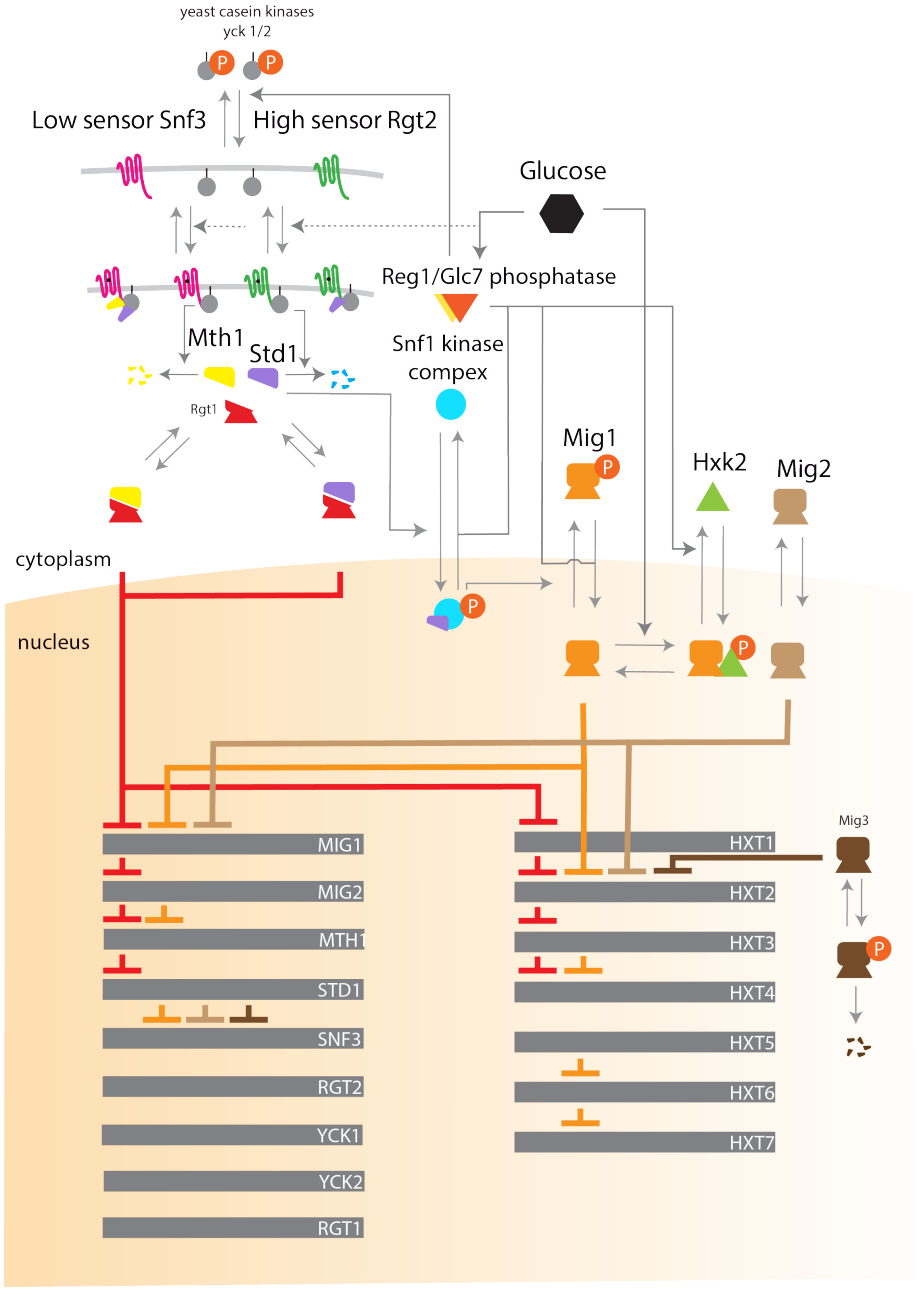

Figure 1.4: The regulatory logic of the yeast glucose sensing/import network. **Glucose activation**: Glucose binds sensors Snf3 and Rgt2 (magenta and green line) which then bind kinases Yck1/2 (gray circles) at the membrane. The sensors interact with corepressors Mth1 (yellow) and Std1 (violet) which are targeted for degradation. Mth1 has not been found to bind Rgt2. Mth1 and Std1 form a repressor complex with Rgt1, which disassembles in glucose. **Glucose repression**: The Snf1 kinase complex (cyan circle) and Mig1 (orange anvil) are dephosphorylated by the Reg1/Glc7 phosphatase (yellow/orange triangles), forcing Mig1 into the nucleus, where it binds hexokinase 2 (Hxk2), an internal glucose sensor. Mig2/3 (brown anvils) are two other specialised glucose repressors. Lines indicate the targets of combinatorial repression of Rgt1 and Mig1/2/3.

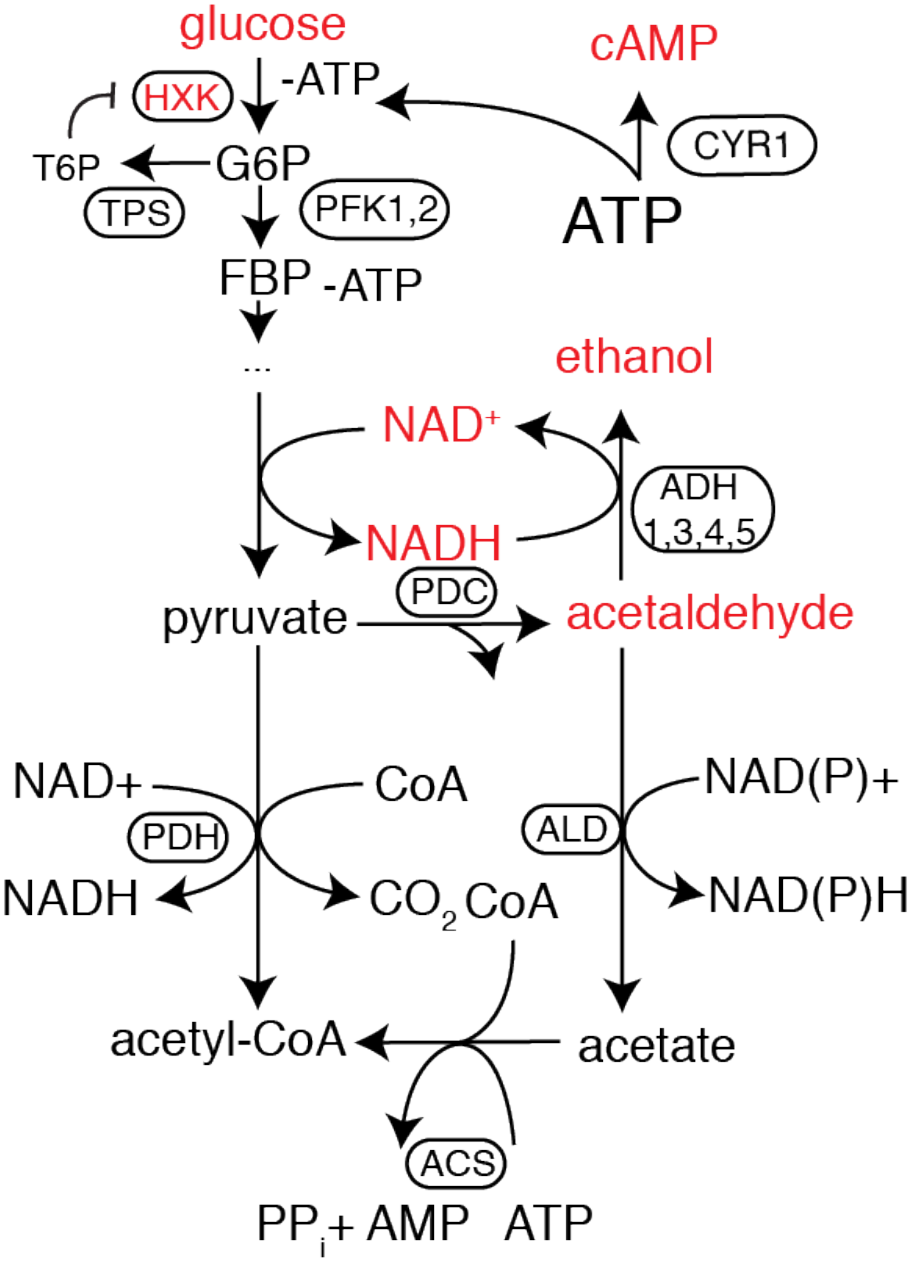

Figure 1.5: Feedback inputs from metabolism on transporter activity and glucose flux. The diagram shows sections of glycolisis whose products influence the metabolic and transport modes in yeast. Red indicates studied influence. Enclosed names are genes of yeast enzymes involved in catalysis of the reaction nearby. Internal glucose can lower the rate of high affinity transport into the cell. Hexokinase receives internal glucose metabolism signals to repress HXT genes, and is in turn inhibited by trehalose 6 phosphate. Acetaldehyde synchronises metabolic oscillations in a cell population. the NADH to NAD ratio has shown influence over respiratory metabolism.

Internal glucose levels within seconds of glucose addition have been quantified to be about 1.5 mM in cells exhibiting high affinity transport(Teusink, Walsh, Van Dam & Westerhoff (1998)). In a model where a transporter is inhibited by its product, the glucose consumption rate could be reduced by up to 50% by this level of intracellular glucose (Teusink, Walsh, Van Dam & Westerhoff (1998)).

Intracellular glucose was found to be almost negligible in cells undergoing low affinity transport (Teusink, Walsh, Van Dam & Westerhoff (1998)).This could potentially imply that low affinity transport takes longer to cause an accumulation of glucose, or that conversion of such glucose into other metabolites could be immediate (Teusink, Walsh, Van Dam & Westerhoff (1998)). Such is the role of Hexokinases HXK1, HXK2 and GLK1 which mark the starting point of glucose metabolism. Hexokinases are in charge of phosphorylation of glucose into Glucose 6-phosphate (G6P). Out of the three kinases, Hxk2 seems to be the only one able to direct glucose repression (Peláez et al. (2010)). Hxk2 has two domains which independently confer its catalytic or transcriptional regulator activities respectively (Peláez et al. (2010)). High glucose changes Hxk2 to an open configuration capable of exerting repression through Mig1. Hexokinase activity, particularly that of Hxk2, seems to be inhibited by trehalose–6–phosphate (T6P) (Blázquez et al. (1993)). In tpsΔ mutants, unable to synthesise T6P, glucose upshifts cause an enlarged accumulation of metabolic intermediates such as Fructose–1,6– bisphosphate (FBP), causing a depletion of inorganic phosphate (P_i) and causing subpopulations of non–growing cells (Teusink, Diderich, Westerhoff, Van Dam & Walsh (1998), van Heerden et al. (2014))Having T6P inhibit Hxk2, together with futile cycling of T6P through the trehalose pathway (van Heerden et al. (2014)) would potentially mitigate such metabolic overload. Glycolytic flux (Figure 1.5) meets an important crossroads at the pyruvate branchpoint, where Pyruvate decarboxylase (PDC) and Pyruvate dehydrogenase (PDH) decide on the metabolic fate of the precursor. Glucose overflow is understood to stir the cell towards the faster PDC branch, which yields acetaldehyde and subsequently ethanol, with low yields of ATP (Otterstedt et al. (2004)). Such low yield of ATP, together with its consumption, feedback to produce an even larger glycolytic flux to sat-

isfy the demands of the cell (Vemuri et al. (2007)). This phenomenon is dubbed the Crabtree effect, and the source of this feedback is probably a combination of the lower capacity of respiratory metabolism, glucose metabolism or the cell's NADH to NAD ratio (Vemuri et al. (2007)). Ethanol and acetaldehyde permeate through cell membranes, and thus act as cis or trans feedback inputs into metabolism. Acetaldehyde, for example, induces synchronisation of NADH oscillations across cells Richard et al. (1996); Finally, addition of glucose to yeast causes a fast, near 5-fold increase in the intracellular cyclic AMP (cAMP) levels (ERASO et al. (1987)). cAMP stimulates growth and proliferation through the PKA pathway, which promotes Rgt1 phosphorylation and enhance hexose transporter activity. In sum, metabolism promotes plentiful inputs that tune hexose transporter function.

1.6.8 Ever-growing interaction landscape in glucose sensing

Even though the activation and repression branches of glucose sensing have been generally described in an independent manner, increasing evidence is suggesting several interconnections between the two pathways, further increasing the network's complexity. For instance, the SNF3 gene seems to be actively repressed by Mig1,Mig2 and Mig3 (Kaniak et al. (2004)). The Reg1/Glc7 phosphatase complex is known to dephosphorylate Snf1 (Rubenstein et al. (2008)),Hxk2 (Fernańdez-García et al. (2012)), Mig1 (Shashkova et al. (2017)) and kinases Yck1/2 (Gadura et al. (2006)). Reg1/Glc7, together with sensor Rgt2 and Yck1/2, has shown a role in maltose permease degradation (Gadura et al. (2006)). Rgt1 itself, besides acting as a repressor, has been reported to act as an activator upon phosphorylation by Protein Kinase A (PKA) (Kim & Johnston (2006)), which is also in charge of Snf1 activation. Additionally, interaction between Std1 and Snf1 has been found to enhance Snf1 activity. As more contradictory and redundant interactions in the pathway are described, the general understanding of the pathway's function in terms of glucose levels becomes less evident, and the evolutionary motivation to maintain all these redundancies and interactions becomes more

enigmatic.

1.7 Why the glucose sensing network may perform dynamic signal integration

Despite all the unanswered questions about the glucose sensing network's complexity and the elusive relationship between glucose and growth, the paradigm for understanding the function of the glucose sensing/import network has remained rather unchanged: Glucose levels activate both expression and repression of several transporters, and therefore transporter function is constrained to specific concentration regimes.

I hypothesise that the hexose transporters of Saccharomyces cerevisiae are subject to high dynamic control. That is, expression of the transporters is not only a function of concentration, but of time–evolving conditions. Considering the information presented in the previous sections, there are several arguments for this reasoning. First, the regulatory actions in the network span several timescales, from instantaneous enzymatic reaction to gradual accumulation and inhibition. Different kinds of environmental transitions might call for exploiting all these timescales. Second, HXT genes are under direct control of Mig1, whose localisation dynamics is intricate, nuanced, conditional and elusive (Section 1.5). Third, the fact that transporters have been characterised during mid-log phase, balanced growth and chemostats does not mean that transporter functionality is limited to such conditions. Uptake rate studies have been done from a balanced growth standpoint, often based on mid-log sampling (Ozcan & Johnston (1995), Reifenberger et al. (1997)) or chemostat (Teusink, Diderich, Westerhoff, Van Dam & Walsh (1998), Daran-Lapujade et al. (2004), Verduyn et al. (1992)), and have revealed the influence of glucose levels on transporter expression. These experiments have justifiably been designed trying to remove the environment and growth history from the study of transporter expression. Even though such data is of high value, dismissing such context could obscure hidden dynamic functionality of transporters when transitioning into and out of balanced growth. Furthermore,

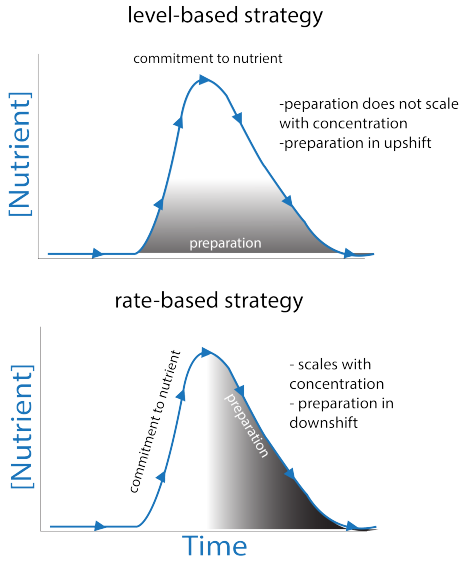

Figure 1.6: Two potential strategies for yeast to decide when to prepare for nutrient shifts or depletion. Top panel: triggering preparation by reaching a glucose level and would not take advantage of larger nutrient amounts. Preparation time could be affected by faster depletion, and would misclassify low but steady nutrient inputs as a preparation signal. Bottom panel: a strategy in which the rate of change is harnessed for preparation is scalable with nutrient amounts and can prepare faster if the depletion rate increases.

even during balanced growth, the impression that hexose transporter expression is controlled by glucose levels may be a direct consequence of transporter expression kinetics as different dynamic mechanisms could yield the same response curve while observed at a single timepoint or steady state, (Figure 1.7, top panel) and sampling at different timepoints may yield discrepancies in the interpretation (Figure 1.7, bottom panel). These assumptions about transporter function may become increasingly difficult to hold, especially after recent theoretical predictions of hexose transporters pulsing (Kuttykrishnan et al. (2010)). Finally, as cells can prepare for environmental shifts (de Virgilio (2012), Venturelli et al. (2015), a mechanism that controls preparation as a function of environmental change rates would be more advantageous (Figure 1.6). In sum, a wider functional potential of hexose transporters and their control mechanisms cannot be fully appreciated under the current experimentation paradigm. In contrast, transporter dynamics can be readily studied using the currently available technology.

1.7.1 On the sensitivity to dynamic features of a signal

A system may respond not only to input levels, but also to dynamic features like its first and higher order time derivatives, the integral of the input over time, or a combination of any of these. Additionally, environmental change frequencies or categorical transitions may be tracked and stored. Finally a system's response may depend on specific nutrient history, where the trajectory of arrival to one state may vary depending on where the system is at a given time. I refer to all of these dynamic sensitivities as the processing of dynamic signals. One can test for dynamic feature processing by providing control of the input signals in time and testing how dependent the response is to input trajectories. In the glucose sensing network, the presence of paralogs with asymmetric properties and feed forward loops hint at the network's ability to perform integration of information from sequences of events.

1.7.2 Asymmetric paralogs as a design principle in glucose sensing

As described above (Section 1.6.6), several of the regulators in the glucose sensing network are partially redundant paralogs. However, key to understanding their function are the differences between them. For example, paralog Mth1's glucose-induced degradation is immediately responsive to addition of glucose, whereas the levels of Std1 do not seem majorly altered in the same timescale (Sabina & Johnston (2009). This asymmetry was revealed to be due to negative self-regulation of Std1 (Kim et al. (2006)), encoded at the pSTD1 promoter. Upon exchange of the promoter for a constitutive one, Std1 levels dropped as fast as those of Mth1 in the presence of glucose (Kim et al. (2006), Sabina & Johnston (2009)). Additionally, a Yeast 2 hybrid assay revealed a stronger Rgt2-Std1 interaction than a Rgt2-Mth1 interaction (Schmidt et al. (1999)). Glucose sensors have been assumed to be redundant in their sensing function and hence the network has been modeled assuming a single sensor system (Kuttykrishnan et al. (2010)). However, their differential affinities for glucose or Yck1/2, or their expression

over time might have large effects on their function. Finally, Mig1/2/3 combinatorially regulate different HXT and network promoters (Westholm et al. (2008)). If several components in the system are sensitive to different glucose or internal variable concentrations, a specific transition from one concentration to another may allow different sequences of events to be internalised in the cell's molecular states. As different sequences of events may call for specific transport demands, channeling those molecular states to hexose transporter regulation may allow for tailored, even preemptive adjustment of glucose transport towards specific physiological requirements. Connections in the network that favor internalisation of event sequences would thus provide a strong selective advantage.

1.8 Chapter description

Chapter 2 introduces all the materials, analysis methods and protocols used in different sections of this study.

In Chapter 3 I describe the behaviour of the 7 major hexose transporters in batch cultures. I focus on the gene transporter Hxt4, whose intricate dynamics makes it an ideal model to study the principles behind hexose transporter timing. I show that the dynamics of Hxt4 is set by a growth staging mechanism, which is able to allocate Hxts to different growth phases robustly at multiple glucose concentrations. Such mechanism is able to distinguish between rising and falling growth rates, an intrinsically dynamic property. In the chapter, I also show how some deletions (RGT2 and STD1) drastically affect the gene's expression dynamics with respect to growth even though growth itself and total expression levels remain comparable. I also show that the promoter, which is sufficient to reproduce the gene's activation kinetics, can be engineered to modulate or bypass such dynamic signals from the network (particularly those from Mig1/2/3) and activate strongly and constitutively in glucose. Together, the results provide a novel framework to understand the network's contributions to scaling and delay of the decisions that take place during glucose-based growth, and how this timing can be readjusted and tuned for each gene by a few changes in a promoter.

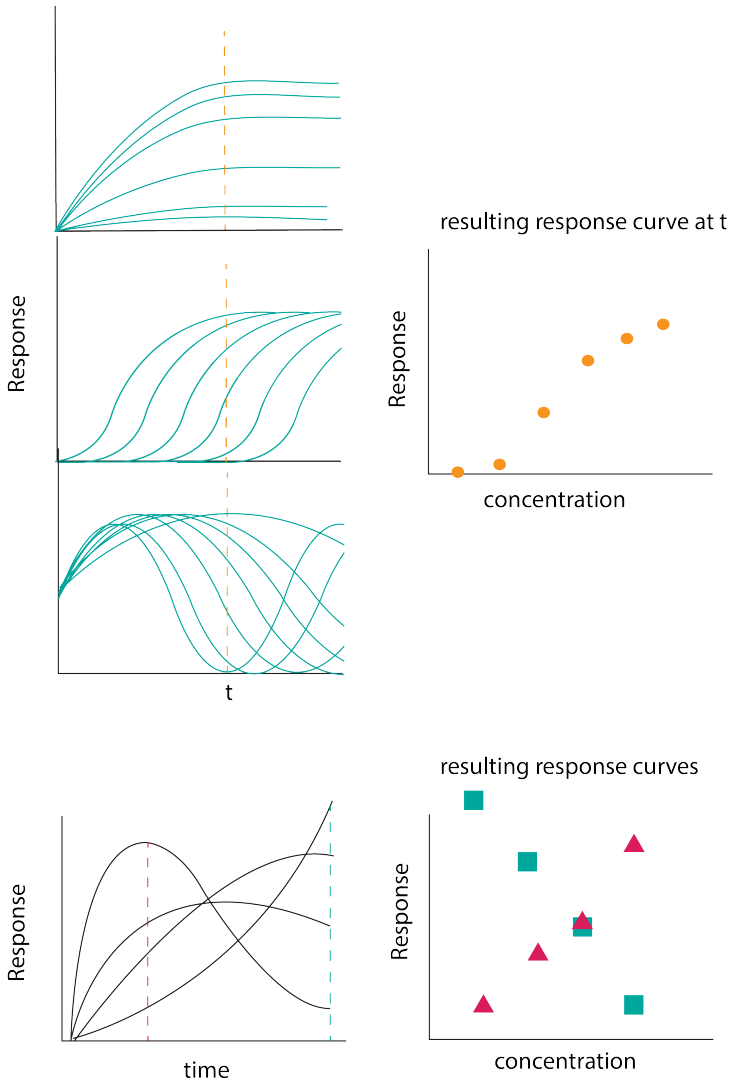

Figure 1.7: A dynamic system may cause ambiguity in dose response curves. Top panel: three different dynamic mechanisms sampled at the same time can yield the same dose response curve. Bottom panel: sampling a dynamically evolving system at different times may yield different, even contradictory interpretations.

In chapter 4, I examine more closely the activation dynamics of HXT genes at a single cell to elucidate the environmental cues and mechanisms that lead to each transporter's expression. By controlling the input trajectory of glucose as well as the level, I find that the transient glucose regimes reveal little temporal overlap across transporter groups, with each transporter performing different processing of the glucose signal. Even Hxt2 and Hxt4, transporters of similar reported affinities, show distinct activation to similar environmental transitions. In particular, transporter Hxt2 is the only one found expressed in regime of low but rising glucose, and Hxt4 is uniquely triggered by a falling glucose signal and accumulates exclusively prior to glucose depletion. Later in the chapter, I closely examine the dynamic asymmetry that causes the 'falling glucose' activation of Hxt4. I provide evidence that MIG1 and RGT2 account as dynamically distinct sources of Hxt4 repression, and that Mig1 localisation dynamics reports on the derivative of the glucose signal. Such derivative is the source of dynamic asymmetry that keeps Hxt4 repressed in glucose upshifts. The data suggest a role for STD1 in countering these repressive effects as deleting it exacerbated repression. These results expand the functional potential for hexose transporters, and reveal the key dynamic regimes at which the lack of key transporters may cause a disadvantage to the cell.

Chapter 5 describes initial efforts in mathematical modelling to elucidate the mechanisms in control of HXT activity. Using data driven modelling, I show that the upcoming localisation of Mig1 can be predicted from past glucose history. I find the approximate calculation that Mig1 performs on the glucose signal to report its derivative. Together with collaborators, we find a couple of 3 component networks that nearly recover the glucose downshift response of Hxt4. Finally, I show a preliminary dynamic model of Hxt4 function that includes the derivative reporting of Mig1, and shows qualitative agreement with the dynamics of Hxt4 in mutant strains.

Chapter 2

Materials and Methods

2.1 Media used in this study

Table 2.1: Microbial growth media used.

Abbreviation	Composition	Use
SC	0.2% Yeast Nitrogen Base (YNB) , 0.5% ammonium sulfate	Pre-cultures
LFSC	YNB w/o riboflavin, folic acid 0.5% ammonium salts	Plate reader
XY Glucose	YEP + 0.1% adenine + 0.2% tryptophan +2% glucose	Yeast transformation
LB	Lysogeny broth	E. coli transformation
SCM	SC + 0.002% BSA + 2 mg/l cy5	microfluidics

2.2 Plasmids used in this study

Table 2.2: Plasmids used in this study.

Plasmid name	rep. origins,markers (ec) [y]	purpose
PKT127	ColE1 (AMP)[KAN]	super ecliptic phluorin
PKT128	ColE1 (AMP)[HIS]	yeast-optimised EGFP
pFA6a-KAN	ColE1 (AMP)[KAN]	knock out [KAN]
pFA6a-Hph	ColE1 (AMP)[Hph]	knock out [Hph]
PYTK001	ColE1 (CamR)	MoClo entry vector
pYTK096	ColE1 (KanR)	URA3 Integration
pE087	(ColE1 AMP) [2micron URA3]	CRISPR-Cas9 cutter, @URA3 integration
pTwist32 Chlor	ColE1 (CamR)	Twist entry vector

2.3 Yeast strains

All strains made for this work derive from BY4741, referred to as the wild type or WT strain in the text. Table 2.3 describes the genotype of each strain.

2.4 Microbial culture

2.4.1 Plate growth

Wild type BY4741 cells were kept in XY or SC media plates containing 2% glucose. Depending on their respective marker, modified strains were grown in plates with added antibiotic G418 (Geneticin) or Hph hygromycin, or synthetic dropout media lacking the nutrient of interest for strains with auxotrophic markers.

2.4.2 Incubation

Pre-cultures for most experiments (unless otherwise specified) were prepared by inoculating single yeast colonies in SC media complemented with 2% of the respective carbon source for 24 hours. Incubation medium was always SC complete to minimise auxotrophy-dependent effects (Alam et al. (2016)) In general, 5 ml overnight cultures were subjected to strong agitation in test tubes 260 rpm at a 45-60 degree angle. After 24 hours, this yielded an OD_{595} greater than 1 for both 2% glucose and 2% galactose.

2.4.3 Pyruvate pre-culture incubation

A special case had to be made for pyruvate incubation as cells divided significantly slower than in glucose or galactose. Pyruvate cultures were pelleted and replenished with fresh medium at 24 hours and 45 hours of incubation, and then used for experimentation at 48 hours.

Table 2.3: Strains used in this study.

Strain ID	in–text description	Genotype/background
PS077/PS229	BY4741 (WT)	MATa, his3Δ1, leu2Δ0, ura3Δ0, met15Δ0, ura3Δ0
PS567	SGA query strain Y6547	Matα can1Δ::pMFA1-LEU2 lyp1Δ ura3Δ0 leu2Δ0 his3Δ1 met15Δ0
PS621	rgt2Δ	PS567 rgt2::Hph
PS612	std1Δ	PS567 std1::Hph
PS618	mth1Δ	PS567 mth1::Hph
PS668	mig1Δ	PS567 mig1::Hph
PS620	mig2Δ	PS567 mig2::Hph
PS614	snf3Δ	PS567 snf3::Hph
PS669	yck1Δ	PS567 yck1::Hph
PS615	yck2Δ	PS567 yck2::Hph
PS498	Hxt1-yEGFP	PS229 HXT1-yEGFP::HIS
PS480	Hxt2-yEGFP	PS229 HXT2-yEGFP::HIS
PS485	Hxt3-yEGFP	PS229 HXT3-yEGFP::HIS
PS409	Hxt4-yEGFP	PS229 HXT4-yEGFP::HIS
PS487	Hxt5-yEGFP	PS229 HXT5-yEGFP::HIS
PS488	Hxt6-yEGFP	PS229 HXT6-yEGFP::HIS
PS566	Hxt7-yEGFP	PS229 HXT7-yEGFP::HIS
PS747	Hxt4-yEGFP mig1Δ	PS409 x
PS748	Hxt4-yEGFP rgt2Δ	PS409 x PS621
PS749	Hxt4-yEGFP std1Δ	PS409 x PS612
PS750	Hxt4-yEGFP yck1Δ	PS409 x
PS751	Hxt4-yEGFP yck2Δ	PS409 x PS615
PS796	Hxt4-yEGFP mth1Δ	PS409 x PS618
PS798	Hxt4-yEGFP snf3Δ	PS409 x PS614
PS732	pHXT1-yEGFP	PS229 pHXT1e1-yEGFP@ura3
PS719	pHXT4-yEGFP	PS229 pHXT4-yEGFP@ura3
PS720	pHXT5-yEGFP	PS229 pHXT5-yEGFP@ura3
PS721	pHXT6-yEGFP	PS229 pHXT6-yEGFP@ura3
PS722	pHXT4R001-yEGFP	PS229 pHXT4R001-yEGFP@ura3
PS723	pHXT4R004-yEGFP	PS229 pHXT4R004-yEGFP@ura3
PS724	pHXT4R005-yEGFP	PS229 pHXT4R005-yEGFP@ura3
PS725	pHXT4R007-yEGFP	PS229 pHXT4R007-yEGFP@ura3
PS726	pHXT4R008-yEGFP	PS229 pHXT4R008-yEGFP@ura3
PS730	pHXT4D001-yEGFP	PS229 pHXT4D001-yEGFP@ura3
PS727	pHXT4D004-yEGFP	PS229 pHXT4D004-yEGFP@ura3
PS728	pHXT4M001-yEGFP	PS229 pHXT4M001-yEGFP@ura3
PS731	pHXT4noSTRE-yEGFP	PS229 pHXT4noSTRE-yEGFP@ura3

2.4.4 Culture preparation for microfluidics

For most microfluidics experiments unless otherwise specified, a standard 2% galactose preculture was diluted 1/100 in fresh 2% galactose medium and incubated for 7-9 hours to reach an OD between 0.15 and 0.2. The culture was then directly used for the experiment. Galactose was used as a good compromise between fast growth and a non-inducing condition for most of the genes studied.

2.4.5 Microfluidic pumping media

For microfluidics experiments, 40 ml of one of the two media was complemented with 160 ul of .0025 mg/ml cy5 and the other with 160 μl ddH20. Both media were additionally complemented with 80 ul of 2.5% BSA. BSA was added to saturate reactive groups and helped reduce undesired cell clogging.

2.5 Molecular biology and strain engineering

2.5.1 Yeast transformation

Following a standard protocol (Burke et al. (2000)), a 50 ml yeast cell culture was grown in XY 2% glucose for 3 hours and washed with 25 ml water, and resuspended in 1 ml water. A mixture was prepared which contained 240 ul PEG 4000, 5 ul of YeastMaker carrier DNA (Clontech), 32 ul 3M Lithium Acetate, 50 ul of purified insert DNA, and a 100 ul of the dense cell suspension. The mixture was shaken and incubated for 40 minutes in a 42C waterbath. Cells were either resuspended in PBS and pelleted directly onto auxotrophic plates, or resuspended in rich medium, incubated for 2 hours and plated into antibiotic plates in the case of a resistance marker.

2.5.2 Gene deletion and C-terminal protein tagging

Gene deletion and tagging were performed by PCR-based integration and replacement of constructs (Baudin et al. (1993), Longtine et al. (1998)).

C-Terminal Translational fusion (Tagging)

For C-terminal tagging, plasmids pKT128 and pKT127 (Sheff & Thorn (2004)) were obtained from a commercial repository (AddGene). Sequencing revealed pKT127 to contain super-ecliptic phluorin::KAN: (Miesenböck et al. (1998)) rather than the reported yEGFP::KAN::. The FP-Marker tagging cassettes were PCR amplified using primers F5 and R3 (Sheff & Thorn (2004)) with 50 nucleotide overhangs corresponding to the pre and post 'stop codon' sequence respectively. The PCR product was directly transformed and positive colonies were tested by PCR and sequencing. yEGFP was chosen as the main fluorophore of this study because a) previous Hxt work successfully incorporated this tag (Youk & van Oudenaarden (2009)), b) It yielded brighter signals and was less stable than the more traditionally used GFP(S65T).

Deletion

For gene deletion an analogous procedure was used, but using a forward primer and overhang spanning the whole coding region of the gene of interest. The deletants from the deletion collection were thus generated using pFA6a::KANMXn plasmids (Shoemaker et al. (1996), Longtine et al. (1998)), whereas Hph strains were created by PCR-based amplification of the HpH cassette from pYM40 (Janke et al. (2004)). Colonies resistant to the respective antibiotic were then confirmed by 2 PCRs spanning each edge of the deletion site and sequencing.

2.5.3 SGA double tags and tagged deletions

Double marker strains were designed to maximise compatibility between HIS markers with a TEF promoter/terminator (coming from plasmid pKT128) and a Hph marker driven by a ADH promoter/terminator (obtained from plasmid pYM40). All tagged strains can be found in table (2.3)

2.5.4 Genomic sequences

Promoter and primer sequences were obtained from the Saccharomyces reference genome version R64-2-1 for strain S288C through the Saccharomyces Genome Database (Engel et al. (2014)).

2.5.5 MoClo assembly

The MoClo (MOdular CLOning) system (Lee et al. (2015)) was developed with the aim of enabling fast, combinatorial assembly and prototyping of synthetic DNA constructs in budding yeast. In MoClo assembly, modular 'parts' (i.e. promoters, coding sequences, terminators, linkers among others) are created, each with specific sequential barcode overhangs. Each of these barcodes can only anneal with an overhang from another specific part. For example, promoters (part 2) can only anneal with coding sequences (part 3), which in turn only anneal with terminators, etcetera. As a result, when mixing multiple parts of each kind together, a wide number of part combinations can arise but only in coherent sequences.

Preparation of sequences for MoClo assembly

Promoters pHXT2/3 were obtained by genomic amplification from BY4741 (Jamie Auxillios). Promoters pHXT1/4/5/6 were obtained by DNA synthesis. pHXT7 was not possible to obtain by any of the methods tried.

MoClo compatible synthetic versions of the HXT promoters were designed in the following way. Genomic promoter sequences for HXT1-7 were obtained by extracting the 1000 bp upstream of the first codon of the ORF. Some of the sequences were then adapted and modified for DNA synthesis and MoClo assembly. This adaptation involved three steps: 1) removing BsmB1, Bsa1, Not1 sites, 2) shortening the length of single nucleotide repeats as required by the standards of Gen9 (now Ginkgo Bioworks), 3) addition of MoClo assembly overhangs. The overhangs consist of an outer BsmBI and an inner BsaI site, followed by part-specific 4 letter overhangs. Such overhangs were added to amplified promoters

through PCR amplification. A MoClo compatible version of yEGFP (part 3) was also synthesised. All parts were then placed into the pYTK001 MoClo entry vector following using BsmBI assembly as instructed (Lee et al. (2015)). These modifications did not differ significantly from the native promoter as shown by the correlation between the dynamics of the synthetic promoter and the protein-yEGFP dynamics (Figure 3.7)

Description of synthetic promoter modifications for MoClo

The specific nucleotides that were removed from each version of the pHXT4 promoter are found in tables 2.4 and 2.5. For the sequences with single sites removed, the sequence was named as the site removed.

Table 2.4: Rgt1 core and accessory bases in the HXT4 promoter.

site ID	strand	core site start	motif
R001	F	-758	ATAGCGGAAACA
R002	F	-679	AAACCGGAACCA
R003	F	-425	ACTTCGGATAAA
R004	F	-296	ACAACGGAGGAA
R005	R	-711	GACTCGGATATT
R006	R	-696	ATCCCGGAACCA
R007	R	-647	AAAGCGGATAAA
R008	R	-627	TGTACGGATTTT

Table 2.5: Putative Mig1-2-3/Msn2-4 core and accessory bases in the HXT4 promoter.

site ID	strand	core site start	motif
M001	F	-519	CTGACCCCTTTT
M002	F	-502	CCCACCCCCCCC
M003	F	-498	CCCCCCCCGGTT
M004	F	-476	GGGGCCCCATAT
M005	F	-467	TATTCCCCCGCC
M006	R	-480	GGGGCCCCATGG
M007	R	-446	CTTTCCCCAAGT
M008	R	-248	ACCACCCCACCT
M009	R	-184	CATTCCCCAGTG

Table 2.6 contains a description of the modifications performed to adapt the promoters for MoClo assembly. As can be observed in the results (Figure 3.7) significant effects due to these alterations are unlikely.

Table 2.6: Modifications to original HXT promoters for MoClo compatibility

Promoter	Modification	contributed by
pHXT1	BsaI(-66) removed	Emily Johnston
pHXT2	None. Amplified from BY4741	Jamie Auxillios
pHXT3	None modification. Amplified from BY4741	Jamie Auxillios
pHXT4	T(-567) changed to A to remove a BsmBI site	Luis Montano
pHXT5	T(-802) changed to A to remove a BsaI	Luis Montano
pHXT6	None	Luis Montano

MoClo assembly protocol and cutter-induced integration of pHXTn-yEGFP cassettes

The MoClo assembly was performed using the 'BsaI assembly' as described by Lee et al. (2015). Each part 2 (promoter) plasmid was then mixed in equimolar amounts (20 fmol) with the part 3 yEGFP plasmid, the part 4 tTDH1 terminator plasmid (pYTK056), and the preassembled URA3 integration vector (pYTK096). The plasmid mix was added to a Master mix containing Buffer, BsaI and T7 ligase. The mix was then put through 25 cycles of digestion and ligation (2 minutes at 42 °C, 5 minutes at 16 °C), then a final digestion (10 minutes at 60 °C), to finally inactivate the enzymes (10 minutes at 80 °C). The plasmid was linearised through a NotI-HF digestion (37 °C for 1 hour, followed by 20 min at 65 °C).

An auxiliar 'cutter' plasmid was assembled from the MoClo library, whose purpose was to optimise the efficiency of integration of the linearised insert into the ura3 locus, as recommended by Lee et al. (2015). The system takes advantage of the CRISPR-Cas9 methodology to generate a double strand break of the native URA3 locus. The break can only be repaired by the insertion of the desired cassette, thereby increasing efficiency of integration.

Cells were transformed with 500 ng of the cutter plasmid and 500 ng of the linearised insert. The cutter plasmid, under a 2 micron replication origin, contains the URA+ marker, which was used for positive selection of transformants. Afterwards, colonies whose insert was verified by sequencing were grown on 5-FOA[1] to select for colonies who lost the URA3 marker.

[1]5-Fluoroorotic Acid Monohydrate. The molecule is toxic to cells producing the enzyme orotidine-5-phosphate decarboxylase, produced by the gene URA3.

Table 2.7: MoClo part plasmids synthesised in this study

Swain Lab ID	project ID	MoClo part name (part type)	vector
103	pLM01	pHXT4R001(2)	pYTK001
104	pLM02	pHXT4R002(2)	pTwist32 Chlor
105	pLM03	pHXT4R003(2)	pTwist32 Chlor
106	pLM04	pHXT4R004(2)	pYTK001
107	pLM05	pHXT4R005(2)	pYTK001
108	pLM06	pHXT4R006(2)	pTwist32Chlor
109	pLM07	pHXT4R007(2)	pYTK001
110	pLM08	pHXT4R008(2)	pYTK001
111	pLM09	pHXT4D001(2)	pYTK001
112	pLM10	pHXT4D002(2)	pYTK001
113	pLM11	pHXT4D003(2)	pYTK001
114	pLM12	pHXT4D004(2)	pYTK001
115	pLM14	pHXT4M001(2)	pYTK001
116	pLM15	pHXT4STRE(2)	pYTK001
117	pLM13	pHXT4D005(2)	pTwist32 Chlor
118	pLM16	pHXT4SR001(2)	pTwist32 Chlor
119	pLM17	SR023(2)	pTwist32 Chlor
120	pLM18	SR045(2)	pTwist32 Chlor
121	pLM19	SR006(2)	pTwist32 Chlor
122	pLM20	SR007(2)	pTwist32 Chlor
123	pLM21	SR008(2)	pTwist32 Chlor
124	pLM22	STRER001(2)	pTwist32 Chlor
125	pLM23	pChunk(2)	pTwist32 Chlor
126	pLM24	woHalfmigC(2)	pTwist32 Chlor
127	pLM25	woHalfmigG(2)	pTwist32 Chlor
128	pLM26	quartermig repeats(2)	pTwist32 Chlor
129	pLM27	quartermig no repeats(2)	pTwist32 Chlor
130	pLM28	p02STRE(2)	pTwist32 Chlor
131	pLM29	p02SR01(2)	pTwist32 Chlor
132	pLM30	p02SR02(2)	pTwist32 Chlor
133	pLM31	p02SR03(2)	pTwist32 Chlor
134	pLM32	p02SR04(2)	pTwist32 Chlor
135	pLM33	p02SR05(2)	pTwist32 Chlor
136	pLM34	p02SR06(2)	pTwist32 Chlor
137	pLM35	p04Rgt1(2)	pTwist32 Chlor
138	pLM36	Halfmig(2)	pTwist32 Chlor
139	pLM37	p04Chunk2(2)	pTwist32 Chlor

2.6 General experimental design

2.6.1 Plate reader experiments

24 hour pre-cultures (generally in SC 2% glucose) were diluted 1/6 in ddH20, which yielded an OD_{595} of 0.3-0.35. They were pelleted and resuspended in the

Table 2.8: MoClo part plasmids synthesised in this study (continued).

Swain Lab ID	project ID	MoClo part name (part type)	vector
140	pLM38	yEGFP(3)	pYTK001
141	pLM39	pHXT4(2)	pYTK001
142	pLM40	pHXT5(2)	pYTK001
143	pLM41	pHXT6(2)	pYTK001
144	pLM42	pICL1(2)	pYTK001
145	pLM43	pHXT1e1(2)	pYTK001
146	pLM44	pADH2e2(2)	pYTK001
147	pLM45	pSUC2e1(2)	pYTK001

same volume of LFSC medium. 180 ul of cell resuspension was added to black, transparent microplate wells (THERMO) containing 20 ul 10x sugar solution and mixed gently by pipetting, then covered with a short plastic lid without circles. An untagged strain was added to all experiments in all media conditions to correct for autofluorescence. Time lapse reads were performed automatically in a Tecan M-200 plate reader incubating at 30 °C, with linear shaking at 6mm amplitude. Data was acquired as described in Table 2.6.1. For each condition, between 4-7 technical replicates in each plate and 2 biological replicates were collected. Outlier replicates that showed bumps (usually because of bubbles) were discarded from the analysis as long as several unaffected curves remained.

Table 2.9: Plate reader acquisition parameters

$Channel_{nm}$	Gain	No. Flashes
OD_{595}	N/A	25
$GFP_{485/525}$	70, 80, 100	10
$AutoFL_{485/585}$	100	10

2.6.2 Glucose consumption time course assay

After standard incubation in SC 2% glucose, wild type untagged and Hxt4-yEGFP cells were washed with water and diluted to a starting OD_{595} of 0.3 in LFSC with 0.4, 1 and 2% glucose. 2 technical replicates for each condition were included, for a total of 12 cultures. The cultures were placed to shake in parallel in 12 well trough box (INTEGRA) at 60-70 rpm on a benchtop orbital shaker at 30 °C. Every 30 minutes, 200 microliter samples of each culture were taken, for which the OD and fluorescence were measured. To remove the cells

and keep the medium for later glucose assays, the same culture was transferred to a 96 well filter plate and spun down for 1 minute at 4000 rpm on a benchtop centrifuge. The flow-through was immediately frozen.

Once all samples were collected, glucose was quantified using a commercial enzymatic glucose assay kit GAHK20 (SIGMA). The assay uses enzymes Hexokinase and glucose-6-phosphate dehydrogenase G6PDH, whose coupled reactions generate 6-Phosphogluconate + NADH in the presence of NAD and causes a change in absorbance at 340 nm. Such change is linearly correlated with glucose concentration (B.8). The assay was adapted for plate reader use in the folowing way. The original samples were diluted 1/80, and 10 μl of each sample were mixed into microplate wells containing 190 μl of the glucose assay reagent. The plate was incubated for 1 hour at 30 °C without shaking. Due to time sensitivity, several A_{340} reads were performed until the measurements reached steady state. The assay read at time point 0 was used as a standard because a water-based standard yielded a different linear relationship than a cell culture-based standard.

As the plastic lid in the microplate added extraneous noise during the measurement, all glucose assay reads were performed without a microplate lid.

2.6.3 Microscopy

All microscope experiments were performed on a Nikon Eclipse Ti inverted microscope with filter sets for GFP and cy5 imaging. In order to control the temperature, the microscope stage was contained inside an incubation chamber (Okolabs) held at a constant temperature of 30 °C. The experiments were imaged using a 60X 1.2NA water immersion objective or a 100X 1.4NA oil objective (Nikon). The Nikon Perfect Focus System (PFS) maintain accurate focus over many hours. Images were taken using an Evolve EMCCD camera (Photometrics).

In all the experiments shown unless otherwise specified, imaging was performed for all recorded positions every 5 minutes. Each imaging cycle included 3-5 DIC/Brightfield stacks, 1 GFP and 1 cy5 acquisition per position. GFP imaging was kept at low intensity (1 Volt, 30 milliseconds) to minimise phototoxicity.

Image acquisition was programatically controlled using custom-made scripts

in MATLAB (Mathworks) controlling the Open Source imaging application MicroManager.

2.6.4 Microfluidics

Device fabrication

Microfluidics devices were created through standard soft lithography procedures (Qin et al. (2010)). A rigid master mold containing device negatives was filled with a degassed mixture of Polydimethylsiloxane (PDMS) and silicone curing agent at a ratio of 10:1, then casted at 65 C for $>$ 4 hours. A positive device cast was cut out and media inlet holes were punched with a 1 mm biopsy punch. The device was then subjected to 30 seconds of plasma treatment and bonded to a clean microscope coverslip. The device was then primed by filling it with the initial microfluidics media for the experiment, typically with no sugar.

Cell loading and media pumping

A ready cell culture was transferred to a syringe and gently pumped into the device through each chamber's media outlet. Filters on top of the chamber prevented flow of cells into adjacent chambers and media inlets, thus preventing cross-contamination among chambers. After enough cells accumulated at the filter, they were pushed into the traps by media pumping.

Media was delivered using two syringe pumps (New Era Pump Systems, model NE100), located in an incubator set at 30C and set at a total flow rate of 4 $\mu l/min$ throughout the extended imaging period. Mixing from both media pumps was external, and was implemented through an external mixer (STC). A dynamic mixing programme was controlled by real-time pump adjustment, dictated by custom matlab scripts and the pump's software.

2.7 Data analysis, modeling and bioinformatics

2.7.1 Plate reader data Analysis

Plate reader data preprocessing

Plate reader results were processed with the Swain Laboratory's Platereader software (version 4.62) written in python 3.5 (Lichten et al. (2014), Swain et al. (2016)). This software was used to perform correction of fluorescence data by the spectral unmixing method (Lichten et al. (2014)). Briefly, the method uses fluorescence reads at 2 emission wavelengths (525 nm and 585 nm) to quantify what proportion of the autofluorescence spectrum bleeds through the 525 nm wavelength. This method has been considered the most appropriate method available for correction of green autofluorescence (Mihalcescu et al. (2015)).

OD measurements were processed by subtracting the media values for the entire time series. Then a correction was made to account for the non linearity in the OD measurement due to high cell density. This was done by applying the following regression:

$$OD_{corrected} = 0.1713(OD)^2 + 0.2303(OD) + 0.004 \tag{2.1}$$

where OD is the OD obtained from the measurement. Then a gaussian process fit was used to infer growth rates and estimate errors from the OD replicates (Swain et al. (2016)).

Plate reader data integration

Integration of data from biological replicates and multiple experiments was done through the ACCESSPR software (Montano-Gutierrez (2017)).

Different biological replicates could be sampled at different times, and hence may be subject to differences in lag time. Biological growth replicates from different experiments were therefore merged by setting each timepoint of the curve relative to the point of maximum growth rate. The growth curves were then sampled at the exact same time (relative to the point of maximum growth

Figure 2.1: Linear fit of GFP (525/585) from different gains between Tecan M200 plate readers 1 (SN:1006006292) and 2 (SN:1411011275). The measurements were obtained by reading a plate with serial dilutions of fluorescein in both plate readers.

rate) across all replicates. This processing eliminated artificial variance caused by lags across curves.

Plate reader experiments coming from two machines differed despite identical experimental conditions. This was because of the intrinsic measurement gain of each machine. Particularly measurements from machine PR1 were consistently lower from those of PR2. A linear transformation was applied to the GFP values from PR1 to account for this consistent difference according to the formula in the following equation:

$$PR2 = 2.26PR1 + 2.48 \tag{2.2}$$

Correction of missing values arising from overflow.

GFP measurements were generally taken at gain 70 and 80 (occasionally 100), and GFP80 was mainly used for analysis. Missing values caused from overflow in the GFP80 channel were corrected by applying a linear fit between GFP70 and GFP80, and linearly transforming the GFP70 values according to that fit. The transformed GFP70 values were essentially identical to the original GFP80 values

in most cases. In cases where the values could not be corrected in this way (such as when there was overflow in both channels), the missing values were averaged from other replicates or left blank.

2.7.2 Microfluidics data analysis

Computer vision assisted cell segmentation

Cell areas were segmented and tracked in brightfield image stacks using the Swain lab's DISCO software written in MATLAB (Bakker et al. (2017)). In it, the probability of any pixel being a cell centre was calculated using a computer vision model based on a support vector machine (SVM). The SVM was trained on image transformations of real cells. Based on the centres, the cell area was found by performing an active contour algorithm (Bakker et al. (2017)), where a deformable ellipse (specifically the lengths of 6 equidistant radii) was adjusted to fit the cell outline in a stack of brightfield images). X–Y drift was adjusted by locating the traps at one position and using cross-correlation to find the trap's displacement over time. After adjusting for XY drift, cells were then tracked over time by penalising large displacements or changes in area from one timepoint to the next. The outline was then used to extract data from the cy5 and GFP channels. Wherever a GFP Z-stack was acquired, the maximum projection of the images was used. For most fluorescence intensity data, the mean of the pixels of the cell area was used.

Processing of glucose signals from cy5 images

The glucose signal in the experiment was obtained from the time average of the cy5 signal of the image background of each cell. The average from all cell backgrounds was then normalised by subtraction of the smallest value (usually found at the beginning of the experiment) and scaled between 0 and the maximum percentage of glucose in the medium.

Processing of Glucose ramp slopes

In order to obtain the slopes of glucose ramps, sections of the timelapse between the cy5 crossing 10% and 90% of the intensity were fit by linear regression. More weight was given to the points at the centre of the slope due to non linearities at the edges. To achieve this parametrically, weights were obtained directly from a gaussian probability density function with mean 0.5 and standard deviation of 0.1.

Pre-processing of individual cell traces and expression rates

Cell traces with 5 or less missing values were used. Each cell trace was interpolated across 500 uniform intervals. Then, to remove high frequency noise, each trace was subjected to a smoothing spline, based on piece–wise polynomial fitting. The smoothing parameter used was generally 0.9.

Quantification of transient responses

The rationale of this measure was to add all increments in expression during the ramp. To this end, I reasoned that finding the sum of all positive sections in the derivative (i.e. non steady–state or transient) per unit of time could be an indicator of the instant reaction of a gene. To find these, I relied on finding the zero–crossings of the derivative, which indicated the incremental and decremental sections. Only the glucose ramp sections were used. for the calculation. Each experiment's mean was processed as done with the cell traces in the section above. With these processed means, the positive and negative zero crossings of the derivative were used to heuristically determine the incremental sections in the response, and the sum of the areas of those positive sections in the derivative was used as the transient response.

Data processing for rate chymographs of cell populations

After interpolating and smoothing the cell traces as specified in section 2.7.2, the temporal gradient of each cell trace was then obtained, yielding a $m \times n - 1$ matrix where m is the total number of cells and n is the number of time points.

An image of such matrix was plotted using a cyan-black-magenta symmetric colourmap from -15 to 15, and saturating beyond those values.

2.7.3 Subcellular localisation measures

Nuclear localisation calculations

To quantify Nuclear localisation of Mig1-yEGFP, the average of the 5 brightest pixels divided by the median of the cell's fuorescence was taken as a proxy for nuclear localisation. This measure has been proven to be accurate and used in other studies (Cai et al. (2008), Hersen et al. (2008), Granados et al. (2017)).

Bud site localisation calculation

Localisation of fluorescence to the budding site was measured with a custom metric. The positions of the 20 brightest pixels (weighted by their fluorescence) were averaged, and the city block distance from that average position to the cell centre was divided by the radius. Bud site localisation would hence be closer to 1. A threshold θ=0.9 was used to call bud site localisation. The measure's performance was tested on real images (Area under the ROC Curve > 0.91).

2.7.4 feature map generation

Feature map images were generating by a standard pipeline in the Regulatory Sequence Analysis Tools website (Medina-Rivera et al. (2015). HXT promoter sequences were inserted into the dnapattern tool to seach for CGGA and CCCC on both DNA strands. The result of dnapattern was pipelined into the feature map tool and the resulting image was stored.

Calculation of localisation to the vacuole

Localisation to the vacuole is distinguished by loose–shaped, central placement of fluorescence in the cell, which contrasts with fluorescence decrease in the surrounding areas. In order to obtain a proxy for central or membrane localisation, the moment of inertia (MOI) was calculated based on the spatial distribution of

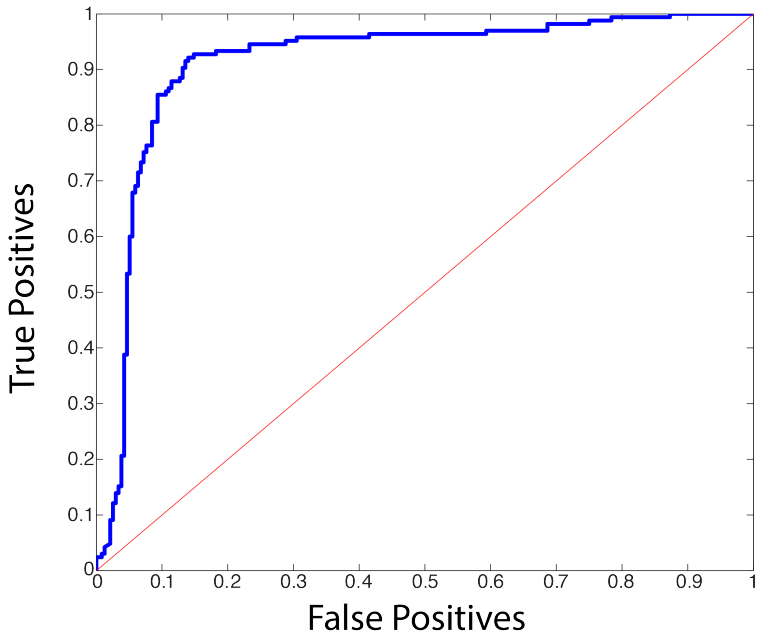

Figure 2.2: Receiver operating characteristic (ROC) curve for detection of bud site localisation. 400 cells were manually classified by hand into 8 different categories: membrane, vacuole, one focus, many foci, unidentifiable, nucleus, not a cell, budding site. Cells were then ranked from the highest to the lowest mass deviation score. The threshold is gradually lowered and the total number of true and false positives is counted. It is expected to preferentially accumulate true positives and climb to prove that the metric is accurate. Accumulation of most budding site cells at highest values causes a sharp climb on the true positive axis, whereas accumulation of other cells (false positives) causes the curve to move right until all cells have been collected. A random measure will ascend through the diagonal, as the same number of false positives and negatives is accumulated. With this information, an adequate detection threshold can be chosen.

the cell's fluorescence. The MOI is interpreted, in physical terms, as the torque needed to cause a desired angular acceleration around a rotational axis. For an image in which each pixel's brightness is weighted, clustering of the brightest pixels near the center of a cell would constitute a small moment of inertia relative to the same pixels dispersed to the edges (i.e. if fluorescence is localised to the membrane). In the latter case, a higher MOI would mean that the cell is heavier to rotate. The moment of inertia of a cell area was calculated with the formula

$$I = \sum_{p}^{P} pr^2 \tag{2.3}$$

where p is the intensity of pixel p, P is the total number of pixels, and r is the

cityblock distance between the pixel p and the centre of the fluorescence mass (c). The centre of mass is defined as the average position of all pixels weighting each pixel by its intensity. The normalised moment of inertia (I_N) as shown below:

$$I_N = \frac{I_{real}}{I_{shuffled}} \tag{2.4}$$

Where I_{real} is the moment of inertia of a real cell image, and $I_{shuffled}$ is the moment of inertia for the same cell image with permutated pixel values. This normalisation is important because the moment of inertia is sensitive to the total brightness of the cell. For both images, the centre of mass of the real cell was used for the calculation of distance r. $I_N > 1$ therefore means localisation to the cellular membrane, and $I_N < 1$ means a centralised fluorescence mass. The measure does not yield values exceptionally > 1 for membrane localisation, presumably due to low signal strength and high backgrond. In contrast vacuole localisation is distinguished as well by depletion of fluorescence from non membrane other cell regions, making $I_N << 1$.

The calculation of the moment of inertia was implemented with a custom MATLAB script. Such script called another script which calculated the center of mass (Wells (2013)).

2.7.5 Prediction of responses based on input history

Let $x(t)$ be an input signal, and $g(t)$ be a cellular response. Then let X be a design matrix made of rows of all possible input history traces of size w $x(t_{i-w})...x(t_{i-1})$. Also let $\hat{g}$ be a vector of future responses at $g(t_i)$. Based on X, a dynamic filter $\hat{k} = [K_0, K_{t-w}...K_{t-1}]$ was found by ordinary least squares to satisfy

$$X\hat{k} = \hat{g} \tag{2.5}$$

In other words, each element of the filter contains weights for each point of the glucose history trace such that the future response $g(t_i)$ can be expressed as a linear combination of the previous history states:

$$g(t_i) = K_0 + K_{(t_i-w)}x(t_i - w) + ...K_{(t_i-1)}x(t_i - 1) \tag{2.6}$$

In practice, sliding windows of input traces (glucose or OD) of size $w = 10$ (each differed by $s = 1$ timepoint) were used to populate design matrix X, with each row corresponding to an input trace. When mapping glucose history to nuclear localisation of Mig1, equation 2.6 was applied with the restriction $\forall i > w$. This was possible because of the long baseline before glucose addition. When mapping plate reader growth features to fluorescence, windows where $i < w$ were also used to exploit all the information in the time series. For the missing values of those windows, $x(-1), x(-2)....x(-w)$ were set to be $x(0)$. Having obtained the filter, the prediction was generated by constructing X for any input and multiplying $X\hat{k}$.

2.7.6 Bayesian model discrimination of the Hxt4 downshift response

The approach for model selection, which followed an ABC-SMC algorithm (see section 5.4), is detailed in Bothe (2016). The resulting model of an incoherent type 3 feed forward loop is found in equations 2.7. The input is described as I, rate constants of X on Y as k_{XY}, and Michaelis constants of X on Y as K_{XY}. The equations describe the rate of change of agents A, B and C. Background enzymes F_A and F_B were added to stabilise the dynamics of each main agent, and their concentration was fixed at 0.5. The parameter values for the equation were not included by Bothe (2016)) and thus not reported here. However, it is expected that many parameter sets achieve a similar behaviour robustly as ths network accounted for 75% of the posterior distribution.

$$\begin{aligned}
\frac{dA}{dt} &= Ik_{IA}\frac{(1-A)}{K_{IA}+(1-A)} - F_A k_{F_A A}\frac{A}{A+K_{F_A A}} \\
\frac{dB}{dt} &= Ak_{AB}\frac{(1-B)}{K_{AB}+(1-B)} - F_B k_{F_B B}\frac{B}{A+K_{F_B B}} \\
\frac{dC}{dt} &= Bk_{BC}\frac{(1-C)}{K_{BC}+(1-C)} - Ak_{AC}\frac{C}{C+K_{AC}}
\end{aligned} \tag{2.7}$$

2.8 Dynamic modeling of the Hxt4 response using ODEs

Dynamic models of Hxt4 regulation were generated using Sencillo, (which is a version of Facile (Siso-Nadal et al. (2007)) implemented in Python instead of Perl). Equation (.eqn) files with all the parameters were processed with Sencillo to generate ODE model functions in python. The ODEs were solved numerically using standard scientific python (scipy) function odeint using custom scripts.

2.8.1 processing of Glucose Input and Mig1 signal for models and ODE solver

Normalised glucose signals (see 2.7.2) and nuclear Mig1 fold change signals (see 2.7.3) were inserted into the models as interpolation functions. Such functions were provided to the solver as arguments, and could be evaluated by the ODE solver at any real value of time.

The nuclear localisation signal of Mig1 for any given glucose step was predicted directly from any glucose signal by applying the dynamic filter shown in Figure (B.12) to the glucose time series as detailed in 2.7.5.

2.8.2 Parameter fitting of the Hxt4 response

In attempts of parameter estimation, a simulation was run using initial parameter guesses, and evaluated according to the squared error between the expression mean and the simulation output. To estimate the best fits, the error was subjected to a particle swarm optimisation algorithm in which multiple particles (simulations) explore the parameter space, and the starting values of the next particle set are chosen in the direction of the best particles of the previous round. Such optimisation yielded low quality fits, so table 2.8.3 shows the best manually fit parameters found.

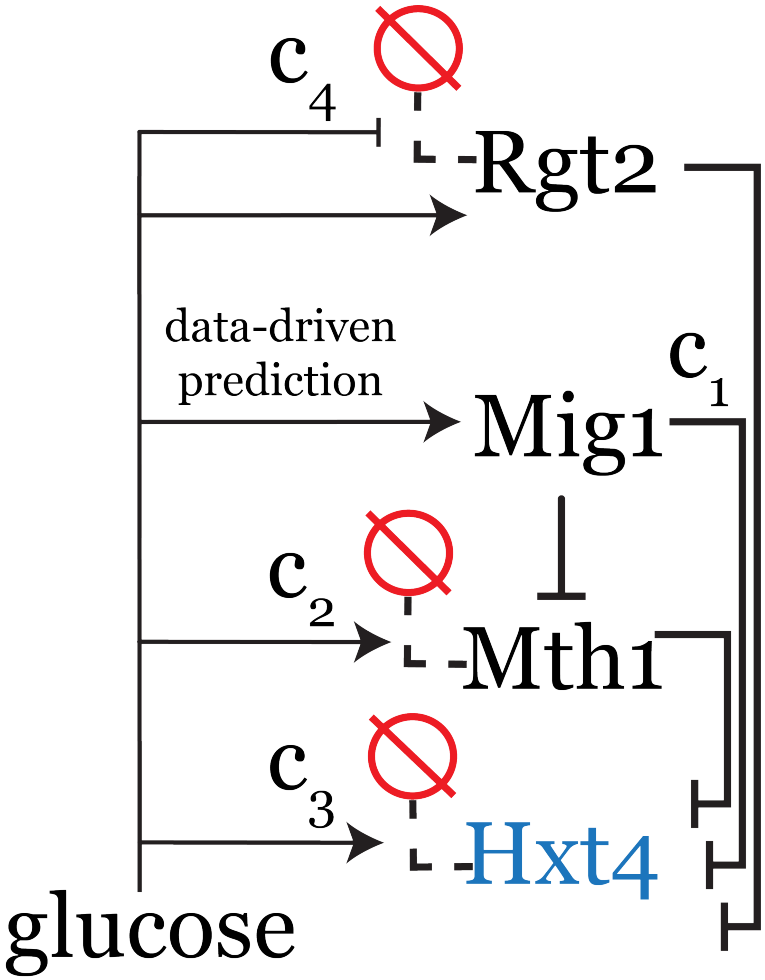

Figure 2.3: Overview of the model. Nuclear Mig1 is predicted from the glucose signal and represses Mth1. Rgt2 is activated by glucose and degraded by its absence. Mth1, Mig1 and Rgt2 represses Hxt4, and both Mth1 and Hxt4 are are degraded in glucose. The output of the system is Hxt4, with no translation explicitly modeled

2.8.3 Equations for the model

The purpose of the model was to recover the qualitative dynamics of Hxt4 in the wild type and the mutants. The rate of change of each agent with respect to time can be understood through the following equations:

$$\begin{aligned} \frac{dHxt4}{dt} &= A_{Hxt4} - B_{Hxt4} \\ \frac{dMth1}{dt} &= A_{Mth1} - B_{Mth1} \\ \frac{dRgt2}{dt} &= A_{Rgt2} - B_{Rgt2} \end{aligned} \tag{2.8}$$

In the equations 2.8, the rate of change of each agent is composed of additive terms A and subtractive terms B. In the following description, symbols for parameters are: β for maximum production rates, α for basal degradation/dilution rates, K for Michaelis constants and n for Hill coefficients. Constants $C_{1...j}$ correspond to gain factors applied to specific processes.

For simplicity, the Hxt4 product was generated as if from transcription with no explicit modeling of translation. The production rate of Hxt4, A_{Hxt4}, was controlled through additive Hill repression from Mig1, Mth1 and Rgt2. As Mig1 levels coud not be controlled, the Mig1 signal was scaled by parameter C_1 in order to alter the sensitivity of Hxt4 to the same input signal:

$$\begin{aligned} A_{Hxt4} &= \frac{\beta_{Hxt4}}{1 + M + T + R} \\ M &= (\frac{C_1 \cdot Mig1}{K_{RepMig1Hxt4}})^{nHxt4Mig1} \\ T &= (\frac{Mth1}{K_{RepMth1Hxt4}})^{nMth1Hxt4} \\ R &= (\frac{Rgt2}{K_{RepRgt2Hxt4}})^{nRgt2Hxt4} \end{aligned} \tag{2.9}$$

The production rate of Mth1 was placed under Hill repression by Mig1. As for Rgt2, it was set under Hill activation by glucose:

$$\begin{aligned} A_{Mth1} &= \frac{\beta_{Mth1}}{1 + (\frac{Mig1n}{KMth1Mig1})^{nMth1Mig1}} \\ A_{Rgt2} &= \frac{Gluc^{nRgt2}}{(K_{Rgt2})^{nRgt2} + Gluc^{nRgt2}} \end{aligned} \tag{2.10}$$

All three agents were subject to basal degradation/dilution rates. The subtractive term for Mth1, B_{Mth1}, was composed of basal degradation plus a glucose induced degradation term, whose intensity was controlled by constant C_3. Hxt4 was also subject to glucose induced degradation since it was observed in the vacuole when in high concentrations in the presence of glucose. It was controlled with the same the same Hill parameters as Mth1, but with different intensity C_2. As opposed to the above two, degradation of Rgt2 was inhibited by glucose, thereby imitating the stabilisation of the sensor at the membrane. The intensity of such stabilisation was regulated by constant C_4. To achieve greater steepness in the decay of Rgt2, basal degradation/dilution of Rgt2 was also made proportional to the concentration of Mth1. This simplification ensures that Mth1 and Rgt2 cannot coexist in an active form.

$$
\begin{aligned}
B_{Hxt4} &= \alpha_{Hxt4} \cdot Hxt4 + C_2 \cdot Hxt4 \cdot \frac{(\frac{Gluc}{K_{Mth1}})^{nMth1}}{1 + (\frac{Gluc}{K_{Mth1}})^{nMth1}} \\
B_{Mth1} &= \alpha_{Mth1} \cdot Mth1 + C_3 \cdot Mth1 \cdot \frac{(\frac{Gluc}{KMth1})^{nMth1}}{1 + (\frac{Gluc}{K_{Mth1}})^{nMth1}} \\
B_{Rgt2} &= \alpha_{Rgt2} \cdot Mth1 \cdot Rgt2 + (C_4 \cdot \frac{Rgt2}{1 + \frac{Gluc}{K_{Rgt2}}})
\end{aligned}
\tag{2.11}
$$

$$
\begin{aligned}
\frac{dHxt4}{dt} &= A_{Hxt4} - B_{Hxt4} \\
\frac{dMth1}{dt} &= A_{Mth1} - B_{Mth1} \\
\frac{dRgt2}{dt} &= A_{Rgt2} - B_{Rgt2} \\
A_{Hxt4} &= \frac{\beta_{Hxt4}}{1 + (C_1 \cdot \frac{Mig1n}{K_{RepMig1Hxt4}})^{nHxt4Mig1} + (\frac{Mth1}{K_{RepMth1Hxt4}})^{nMth1Hxt4} + (\frac{Rgt2}{K_{RepRgt2Hxt4}})^{nRgt2Hxt4}} \\
A_{Mth1} &= \frac{\beta_{Mth1}}{1 + (\frac{Mig1n}{KMth1Mig1})^{nMth1Mig1}} \\
A_{Rgt2} &= \frac{Gluc^{nRgt2}}{(K_{Rgt2})^{nRgt2} + Gluc^{nRgt2}} \\
B_{Hxt4} &= \alpha_{Hxt4} \cdot Hxt4 + C_2 \cdot Hxt4 \cdot \frac{(\frac{Gluc}{K_{Mth1}})^{nMth1}}{1 + (\frac{Gluc}{K_{Mth1}})^{nMth1}} \\
B_{Mth1} &= \alpha_{Mth1} \cdot Mth1 + C_3 \cdot Mth1 \cdot \frac{(\frac{Gluc}{KMth1})^{nMth1}}{1 + (\frac{Gluc}{K_{Mth1}})^{nMth1}} \\
B_{Rgt2} &= \alpha_{Rgt2} \cdot Mth1 \cdot Rgt2 + (C_4 \cdot \frac{Rgt2}{1 + \frac{Gluc}{K_{Rgt2}}})
\end{aligned}
\tag{2.12}
$$

Table 2.10: Parameter values for the dynamic model of Hxt4

Parameter	Value
α_{Mth1}	0.3
α_{Hxt4}	0.001
α_{Rgt2}	0.6
$\beta_M th1$	30
β_{Hxt4}	$800*1 + \frac{\frac{\beta_{Mth1}}{(\alpha_{Mth1}}}{K_{Hxt4Mth1})^n_{Hxt4Mth1}\alpha_{Hxt4}}$
β_{Rgt2}	1
K_{Mth1}	.5
$K_{Mth1Mig1}$	1
$K_{RepMig1Hxt4}$	11
$K_{Hxt4Mth1}$	14
K_{Rgt2}	0.1
$K_{Hxt4Rgt2}$	.085
n_{Mth1}	2
$n_{Mth1Mig1}$	1
n_{Rgt2}	2
$n_{Hxt4Rgt2}$	4
$n_{Hxt4Mig1}$	2
$n_{Hxt4Mth1}$	4
C_1	100
C_2	5
C_3	0.028
C_4	5

Chapter 3

Analysis of the dynamics of hexose transporters of yeast in batch cultures

3.1 Glucose level information alone is insufficient for survival in fast changing environments

In natural conditions, yeast cells reside on the surface of fruit and seeds to break open and release sugar and other nutrients. Upon such events, both the cells and the environment start to influence each other, leading to a complex, dynamic interaction. As the yeast utilise the sugar for growth, glucose levels naturally start dropping until eventually the sugar is depleted. Thus, in a growing culture there is uncertainty that a cell must cope with due to its potential implication in fitness: How much environmental sugar is there at a given time? For how long will sugar be present? When must a cell stock up on nutrients? How likely the sugar is to reappear once it has been depleted? If the environment is changing fast, is it worth adapting to the transient condition? A wide number of studies have established that hexose transporters 1-7 are expressed and functional at specific glucose levels (Ozcan & Johnston (1995), Youk & van Oudenaarden

(2009), Reifenberger et al. (1997)). From these studies it not clear how cells would reconcile activation by glucose levels with fast-changing circumstances, where a concentration change may quickly render a transporter obsolete. In sum, knowing glucose level information does not resolve relevant ambiguities about the cell's environment, and thus may not be sufficient for survival. This is particularly the case if resolving such ambiguity could enable advantageous decision making (for example, anticipatory behaviour) in competitors.

3.2 Hypothesis

One study attempted to assess the contribution of individual transporters to glucose flux and fitness (Youk & van Oudenaarden (2009)). They constitutively expressed single transporters in a strain where all other transporters were knocked out (Wieczorke et al. (1999)). Doing so revealed non-linear relationships between the glucose concentration and growth rate. Deletion of both sensors SNF3 and RGT2 entirely removed the dependency between growth and glucose in these strains, making growth rate uniform across all glucose concentrations (Youk & van Oudenaarden (2009)). Though a contribution of sensing to fitness was proven, the exact mechanisms that connect sensing to transport and growth remain unclear.

The continuum of events from one cellular and environmental state to another may contain information that a cell could harness to reduce environmental uncertainty and therefore impact fitness. I hypothesised that the glucose sensing network exerts dynamic control of each transporter in relation to environmental event sequences as opposed to the instantaneous glucose levels in the culture. In other words, that the glucose sensing network is able to process dynamic signals. Therefore, I sought to address whether the temporal dynamics of transporter expression could be explained solely by the initial glucose levels, the instant glucose levels at a given time, the kinetics of environmental glucose, or other environmental conditions.

3.3 Strategy: plate reader experiments to analyse expression dynamics

To this aim, Hexose transporters 1-7 were C-terminally tagged with the yeast-optimised Green Fluorescent Protein (hereafter referred to as yEGFP). Tagging of transporters was done in collaboration with Iseabail Farquhar. In the following section, by mentioning a transporter, like Hxt1, I refer to strain BY4741 whose native HXT open reading frame is c-terminally tagged with yEGFP and has a ::HIS:: nutritional marker. The experiments shown were all done in complete medium to avoid nutrient difference effects. We characterised the expression dynamics of each transporter in a growing culture using a plate reader.

3.4 Plate reader data processing challenges

Quantification of gene expression dynamics per cell introduces several challenges when using a plate reader in order to get a measure of fluorescence and microbial growth, judged by optical density (OD). Figure 3.1 provides an overview of the entire strategy used to quantify fluorescence and growth using a plate reader.

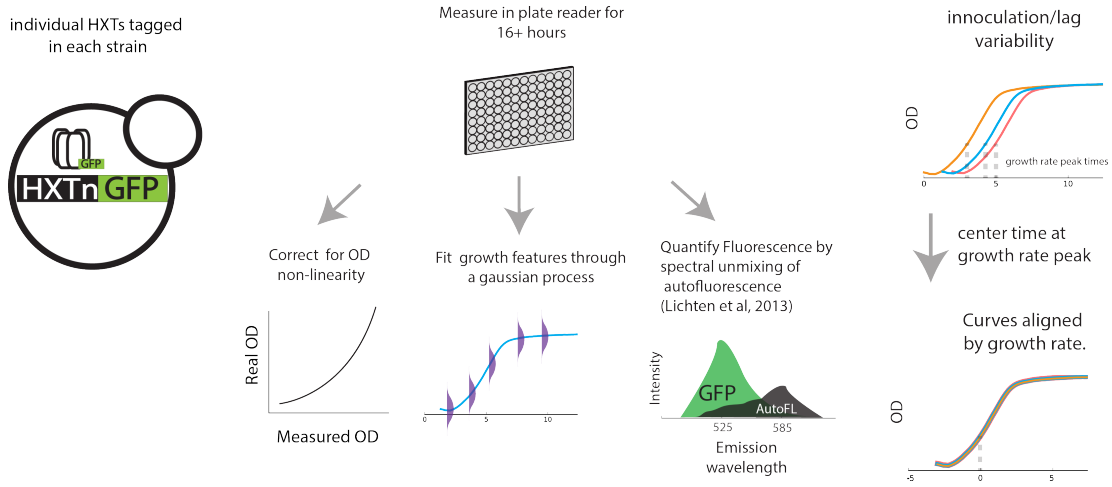

Figure 3.1: Plate reader experiment and analysis overview. Left: Each of *Saccharomyces cerevisiae* HXT proteins (n=1-7) were C-terminally tagged with yEGFP in different strains. Middle: Expression dynamics during growth is monitored using a 96 well plate reader. The data is processed to a) correct OD nonlinearity, b) find subtle changes in growth rate over time with a non-parametric, gaussian process based estimation of instantaneous growth rates and c) Removing the proportion of the fluorescence intensity that corresponds to autofluorescence. Right: heterogeneous replicates are integrated by centering time at the point of max growth rate to account for shifts in growth caused by different lags or innoculate sizes.

The first of these challenges is that the measured OD in a plate reader does not have a linear correspondence with the number of cells. To address this, the machine OD was transformed to real OD according to (Lichten et al. (2014)).

Second, as yeast cells are naturally autofluorescent, we quantified GFP fluorescence using the spectral unmixing method developed by our group (Lichten et al. (2014). See methods section 2.7.1). Third, growth-altering events, such as diauxic lags, are difficult to quantify using standard logistic growth fitting. Our group developed a method to quantify growth statistics by fitting a gaussian process to the OD data (Swain et al. (2016)), making it possible to account for precise growth features in gene expression dynamics. Adoption of this non-parametric fitting of instantaneous growth rates allows the detection of changes in growth rate over time. These features have previously remained difficult to quantify.

Finally, a small change in growth conditions (like a small difference in lag time) may propagate into the variation of expression dynamics, especially when integrating several experiments with inconsistent time sampling. Therefore, instead of combining replicates directly, we first centered the time of all replicates at the time of maximum growth rate. Having set the time of max growth rate to 0, all replicates were then sampled all replicates at equal timepoints by interpolation.(Figure 3.1, right panel, and appendix section A.4.1). An integrated software for analysing plate reader data (ACCESSPR) was developed to facilitate analysis and integration of ever-growing plate reader datasets (Montano-Gutierrez (2017)).

Each fluorescently tagged strain was incubated overnight in glucose, and placed in rich media with 7 glucose concentrations: 0.2%, 0.4%, 0.6% 0.8%, 1%, 1.5% and 2%. Figure 3.2 shows how individual transporters comprise a diverse family of complex fluorescence dynamics.

In order to see whether these dynamics matched previous knowledge of transporter expression, this data was compressed into a dose response curve (Figure 3.3) and compared to other studies (Ozcan & Johnston (1995), Youk & van Oudenaarden (2009)). Such curves have been obtained at around 4 hours of growth in glucose. In general, the curve obtained for the transporters is in agreement with

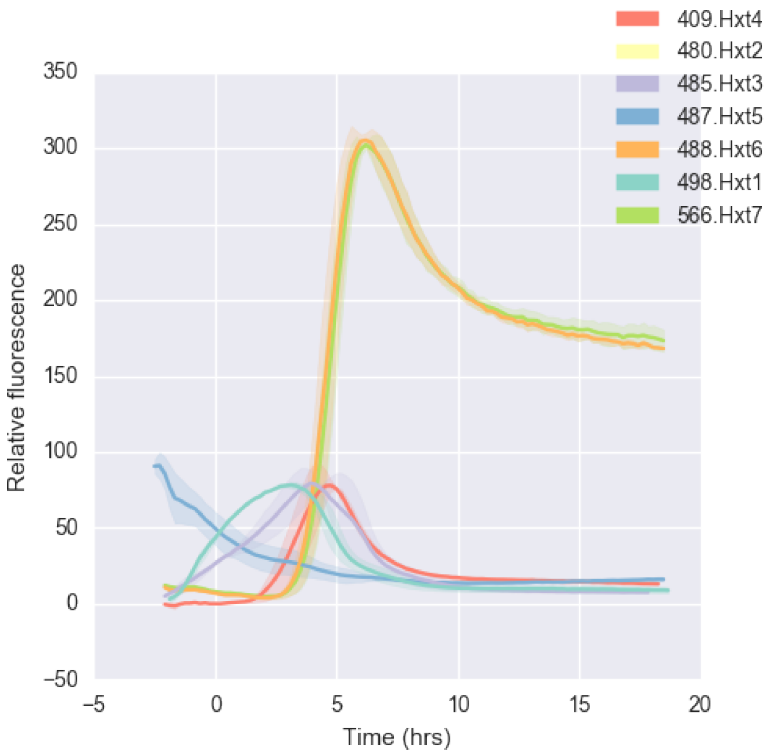

Figure 3.2: Dynamics of Hexose transporters 1-7 in 2% glucose. The curves correspond to the mean of 2 biological replicates of pre-growth in 2% pyruvate

other reports.

Dose response curves are standard in enzymatic kinetics and thus are the basis of concentration-based biochemical modelling. We therefore wondered how the observed transporter dynamics affected the dose response curve. Figure 3.3 shows the time dependence of dose response curves for several transporters. For some proteins, the overall shape of the curve remains consistent for several time points. However, for transporter Hxt4 this is not the case: sampling the curve at earlier timepoints gives results that are consistent with the literature, whereas sampling at later timepoints induces a change in the shape and thus the interpretation of the induction curve the transporter would appear to be expressed at low, intermediate, and higher glucose concentrations rather than intermediate ones. Altogether, we conclude that the glucose response of hxt4 is time dependent.

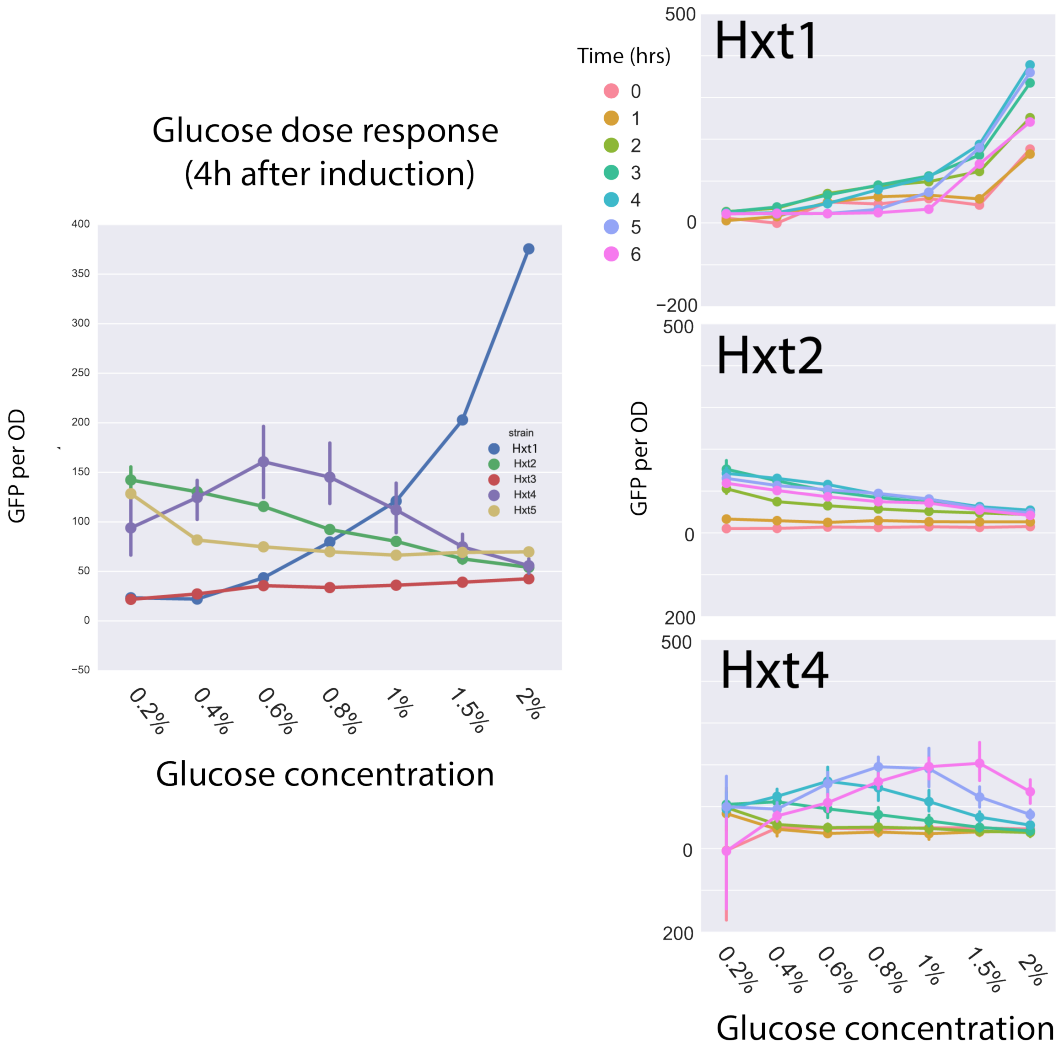

Figure 3.3: The glucose dose response of Hxt4-yEGFP is time-sensitive. Left: Dose response curves for Hxt1-5 4 hours after glucose induction (2+ biological replicates). Hxt6 is not shown due to its relatively high levels. Right: Glucose dose responses for Hxt1 (top), Hxt2 (middle) and Hxt4 (bottom) taken at different sampling times (from 0 to 6 hours, depicted by each colour). For Hxt1 and Hxt2, the same overall shape is found for all sampling times, whereas the shape changes every time point for Hxt4, suggesting that a dynamic system is controling the response. Error bars denote the standard deviation across 2 or more biological replicates, which may vary in each case.

3.5 Intermediate affinity transporters Hxt2 and Hxt4 are dynamically allocated to distinct growth stages

I sought to find factors that could explain the temporal sensitivity in the dose response curve of transporter Hxt4. I found no major impact of pre-culture conditions on the dynamics of Hxt4 (appendix A). Hxt2 and Hxt4 have been considered transporters with similar affinities expressed at low to medium concentrations of glucose, and of intermediate affinity (Ozcan & Johnston (1995), Horák (2013), Reifenberger et al. (1997)). I thus compared the dynamics of transporters Hxt2 and Hxt4 more closely (Figure 3.4).

Hxt2 appears to activate immediately after glucose addition at any concentration tested, whereas Hxt4 shows a glucose-dependent delay in its activation: higher glucose levels induce a longer delay in the Hxt4 response. Additionally, Hxt2 levels per unit of OD appear to decrease with higher initial glucose, whereas Hxt4 levels per OD show a general increase with higher initial glucose. This observation suggests that Hxt2 levels get degraded/diluted as the population grows, whereas Hxt4 gets derepressed in the growing population, and thus Hxt2 and Hxt4 are allocated to distinct growth stages. To translate this in terms of growth rate, we reasoned that growth rate itself could not explain this activation asymmetry. Rather, the activation regimes of both genes could perhaps be better explained by a rising growth rate phase ($dGR/dt > 0$) and a falling growth rate phase ($dGR/dt < 0$). The lower row insets of Figure 3.4 show the expression rate of Hxt2 and Hxt4 as explained by growth rate and the derivative of the growth rate. It can be seen how high Hxt2 expression rates become more allocated to the right quadrant as growth rate increases, whereas Hxt4 levels show a shift to the left quadrant with higher growth rates (induced by higher glucose). Altogether, we conclude that the Hxt2 and Hxt4 despite their similar reported affinities, show distinct temporal allocation upon identical glucose and growth environments. This allocation appears to be coordinated not by cell density or growth rate, but by the change in growth rate with respect to previous instants.

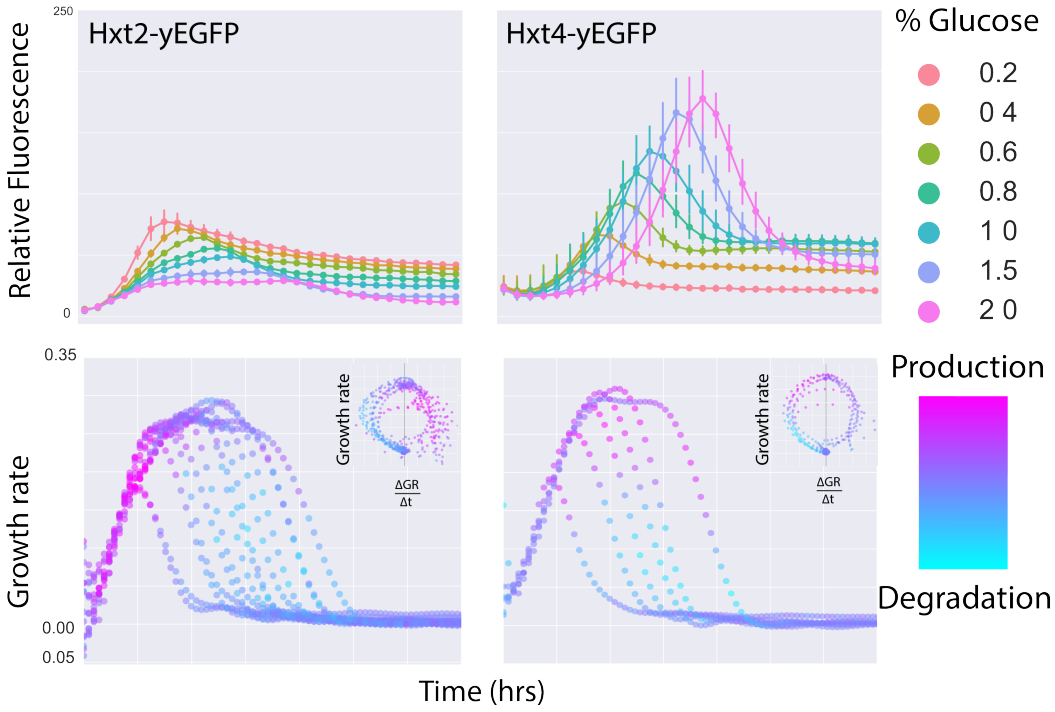

Figure 3.4: Dynamic differences between the intermediate affinity hexose transporters. Hxt2 and Hxt4 and their relationship to growth stages. Top two panels: distinct activation patterns of both transporters in response to glucose, at different glucose levels. Error bars indicate standard deviation in two biological replicates. Bottom panels: growth rate dynamics for the curves above. Larger curves correspond to higher glucose concentrations. Dot colors indicate the GFP expression rate (magenta for active GFP production, cyan for dropping GFP levels. Insets show the same data, plotted relative to the growth rate and its derivative, to emphasize how each gene majorly expresses in either 'rising' (right side) and 'falling' (left side) growth stages

This constitutes evidence for glucose level-independent information processing in the underlying network controlling these two hexose transporters.

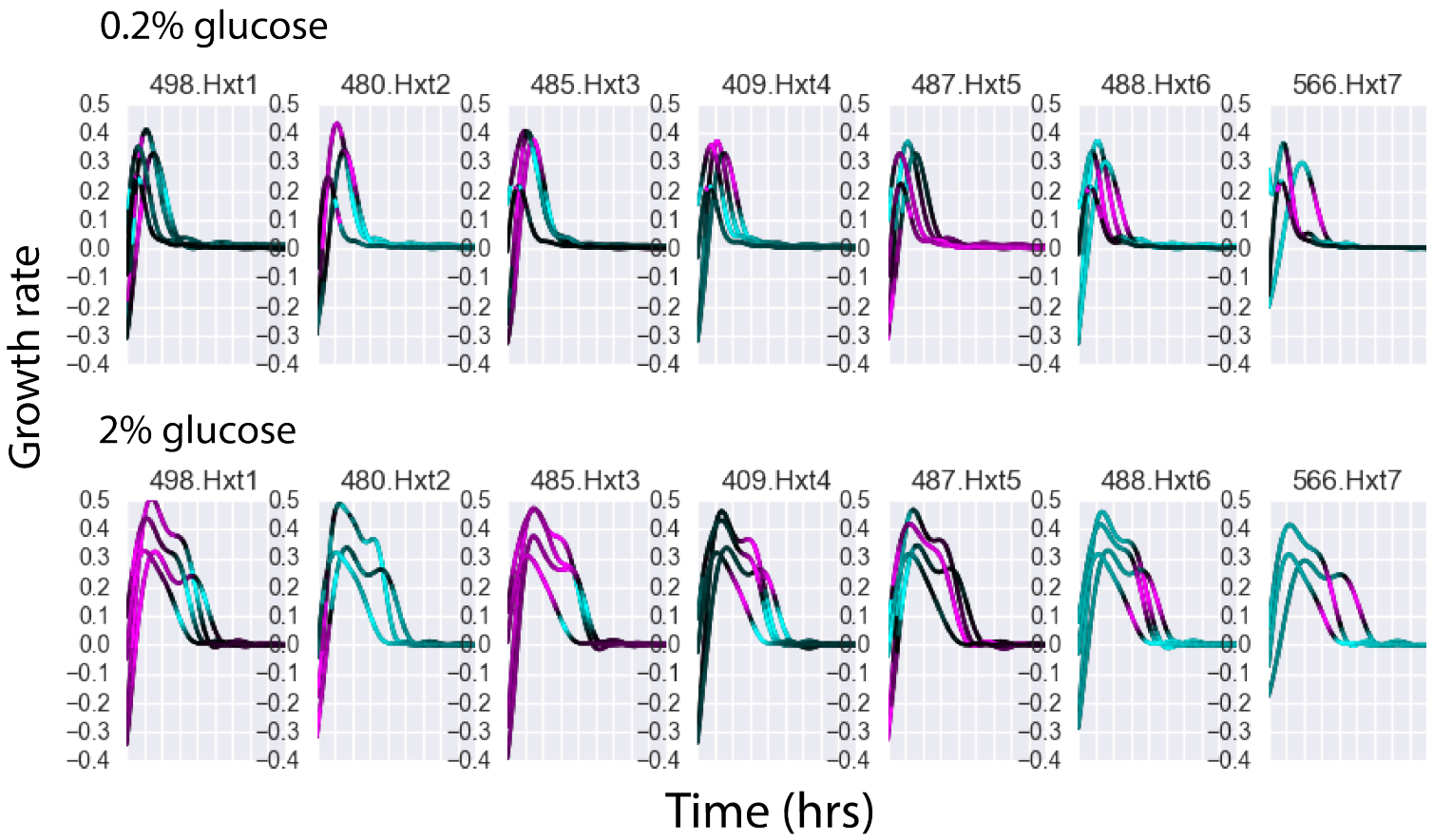

Figure 3.5: Expression of different hexose transporters is subject to a growth staging mechanism. Each plot shows growth rate over time for one strain carrying an Hxt-yEGFP construct, and all lines come from different experiments in 0.2% glucose or 2% glucose. Magenta, black and cyan line sections indicate rising, steady or falling protein levels respectively. The colour pattern is qualitatively similar across concentrations (e.g, Hxt3 and Hxt4 activate in accelerating and decelerating growth phases respectively). The patterning is preserved for curves of different duration. This suggests a general mechanism of growth staging, which robustly orchestrates activation patterns for each Hxt.

3.6 Hxt4 expression is triggered independently of glucose concentration and shows a relationship with a glucose 'drop'

The temporal allocation of Hxt4 to a falling growth rate partially explains the time varying relationship between Hxt4 expression and glucose. However, the results presented so far do not imply a causal relationship between the change of growth rate and Hxt4 expression. It could be that the drop in growth rate is caused by the fall of glucose below a particular glucose concentration, thereby supporting the model that transporters are expressed at particular glucose levels. Alternatively, the glucose sensing network may be responding to other features of the glucose signal, which may not involve glucose levels. To test this hypothesis, I designed an assay to quantify OD, GFP fluorescence and environmental glucose in a growing yeast culture starting from 3 different glucose concentrations: 0.4%, 1% and 2%. I reasoned that, if Hxt4 expression is subject to glucose levels, the expression onset should be triggered any time the glucose concentration is around a specific neighbourhood of concentrations. For example, if the optimal concentration is 0.4, then expression should be triggered around 0.4% regardless of whether initial levels were higher.

I measured glucose with an enzymatic assay which yielded a linear relationship between initial glucose concentration and OD at 340 nm (Figure B.8).

Before detailing the results of the glucose assay, I must point out an unexpected rise of the assay's value after the first timepoint, resulting in an ambiguity of the exact glucose levels throughout the experiment. For an explanation on why this is not expected to interfere with the overall conclusion of the assay, please see Appendix C.2.

Figure 3.6 and Appendices B.8, B.9 show the results of the glucose assay in cultures starting at different concentrations. In all cases, cultures showed delay in the activation of Hxt4 which was longer when the starting concentration was higher. In the three cultures, Hxt4 expression was activated at a similar rate; yet, the threshold concentration at which Hxt4 activated was different for all three

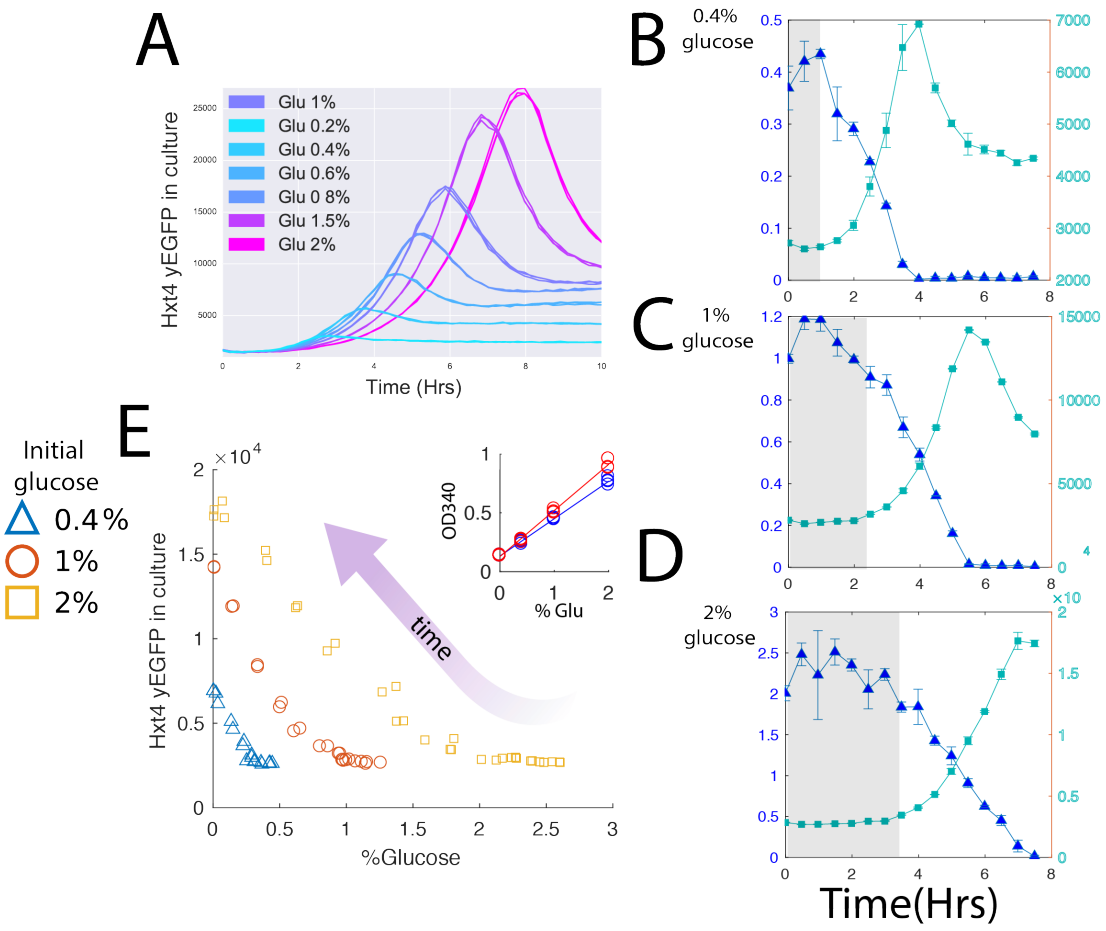

Figure 3.6: The expression onset of Hxt4 is concentration independent. A) Raw Hxt4-yEGFP response at multiple concentrations. BCD) Glucose assay where parallel cultures were simultaneously initiated at 0.4, 1, and 2% glucose. Curves indicate the glucose assay reads (blue), Hxt4 yEGFP (turquoise). Appendix Figure B.9 shows same data organised by type. Shaded areas depict the initial delay in activation of Hxt4. E) Hxt4 activation occurs at different concentrations. For 0.3% glucose, there are several values of Hxt4, as its levels had more time to accumulate in the higher concentration culture. Inset shows the glucose quantification using the first(blue) and second timepoint (red) as a reference for quantification. The blue regression is used throughout.

cultures (Fig 3.6 E). As the initial concentration is increased, the activation set point for Hxt4 becomes higher. Hence, there are multiple possible levels of Hxt4 for a given glucose level depending on the sugar's history. I therefore conclude that hxt4 expression is not controlled by extracellular glucose levels. Nevertheless, the onset of Hxt4 expression was delayed until glucose started dropping steadily, and production abruptly stopped upon glucose depletion. This suggests that a glucose 'drop' could be the trigger for Hxt4 expression prior to glucose depletion.

However, it could also be that Hxt4 or other transporter's activity causes sugar depletion in the medium. Even though this causality is not resolved in this chapter, Chapter 4 provides evidence that the falling glucose signal is sufficient to trigger Hxt4 expression.

3.7 The HXT4 promoter is sufficient to recover the induction dynamics of Hxt4

I asked what mechanisms would allow for the complex activation dynamics of HXT4. In the results so far shown, the observable is the Hxt4 protein-an output of the glucose signaling pathway. It could therefore be that regulation is being exerted at the promoter level i.e. through transcriptional activators or repressors, or perhaps post-transcriptionally through the 5' UTR (untranslated region). Alternatively, protein degradation could account for the protein dynamics observed. To resolve this, in collaboration with Emily Johnston, we used the MoClo assembly system to place yEGFP downstream of the HXT4 promoter (pHXT4). We inserted such construct into the URA3 locus of S. cerevisiae[1]. In the strain holding the construct, the native Hxt4 gene was left unaltered. I reasoned that, if regulatory control of the Hxt4 protein was exerted at the promoter level, the pHXT4-yEGFP transcriptional fusion should recover the activation dynamics of Hxt4-yEGFP. Alternatively, if regulation is exerted at the translational level, then there would be weak correlation between the expression of both constructs. To test between these alternatives, I performed a plate reader experiment in which the pHXT4-yEGFP and Hxt4-yEGFP strains were grown in parallel in 7 glucose concentrations (Fig 3.7). The results of these experiments show that the activation dynamics of both constructs is strongly correlated in time for all glucose concentrations tested up until the Hxt4 fluorescence peak (the glucose depletion point). The temporal correlation is high for all glucose concentrations despite the fact that more Hxt4-yEGFP proteins are observed over time per ev-

[1]Such locus is a common heterologous gene insertion site. The native locus has been spliced out to induce auxotrophy for uracil in strain BY4741

ery yEGFP produced directly with the promoter. Such discrepancy could be due to a difference in the 5' UTR between the sequences, chromosomal positioning, a higher translation rate for the native ORF (perhaps due to higher ribosome occupancy (Ingolia et al. (2013)) or a slower degradation rate control for the native protein) or a combination of all of these factors. One last possibility is that an extra promoter titrates out the levels of transcription factors needed to elicit a fast response. Despite this discrepancy, expression stopped at similar points for both strains, suggesting a coordination between transcriptional and post-transcriptional repression at glucose depletion.

3.8 Hxt4 expression dynamics and growth staging are independent of respiratory growth.

Previous studies have linked the sensors and kinases in the pathway to the repression of respiration (Reddi & Culotta (2013)), which could potentially feed back on Hxt4 regulation. As Hxt4 is expressed during late exponential growth, close to the respiratory regime, it remained a possibility that transition towards respiration was either correlated, causative of or influenced by Hxt4 expression. I hypothesised that Hxt4 expression could be either shut down or enhanced upon addition of the antifungal antimycin A. Antimycin A is a compound that binds and disrupts the function of cytochromes, thereby inhibiting mitochondrial respiration. Therefore, untagged and Hxt4-yEGFP cells were grown in 0.2%[2] and 2% glucose. Half of the wells were treated with antimycin, with the other half left untreated as a control.

Figure 3.8 A shows how diauxic growth is completely abolished in 0.2% glucose plus antimycin, consistent with the fact that cells enter respiratory growth during this stage. However, Hxt4 induction was nearly as high (even slightly higher) in both the untreated and treated cultures, suggesting that Hxt4 activation is not dependent of respiratory activity. In high glucose, Hxt4 was significantly

[2]0.2% glucose was chosen as it had previously shown clear post-diauxic growth, whereas higher concentrations led to a significant flattening of the OD curve in stationary phase. This flattening is generally indicative of no respiratory activity.

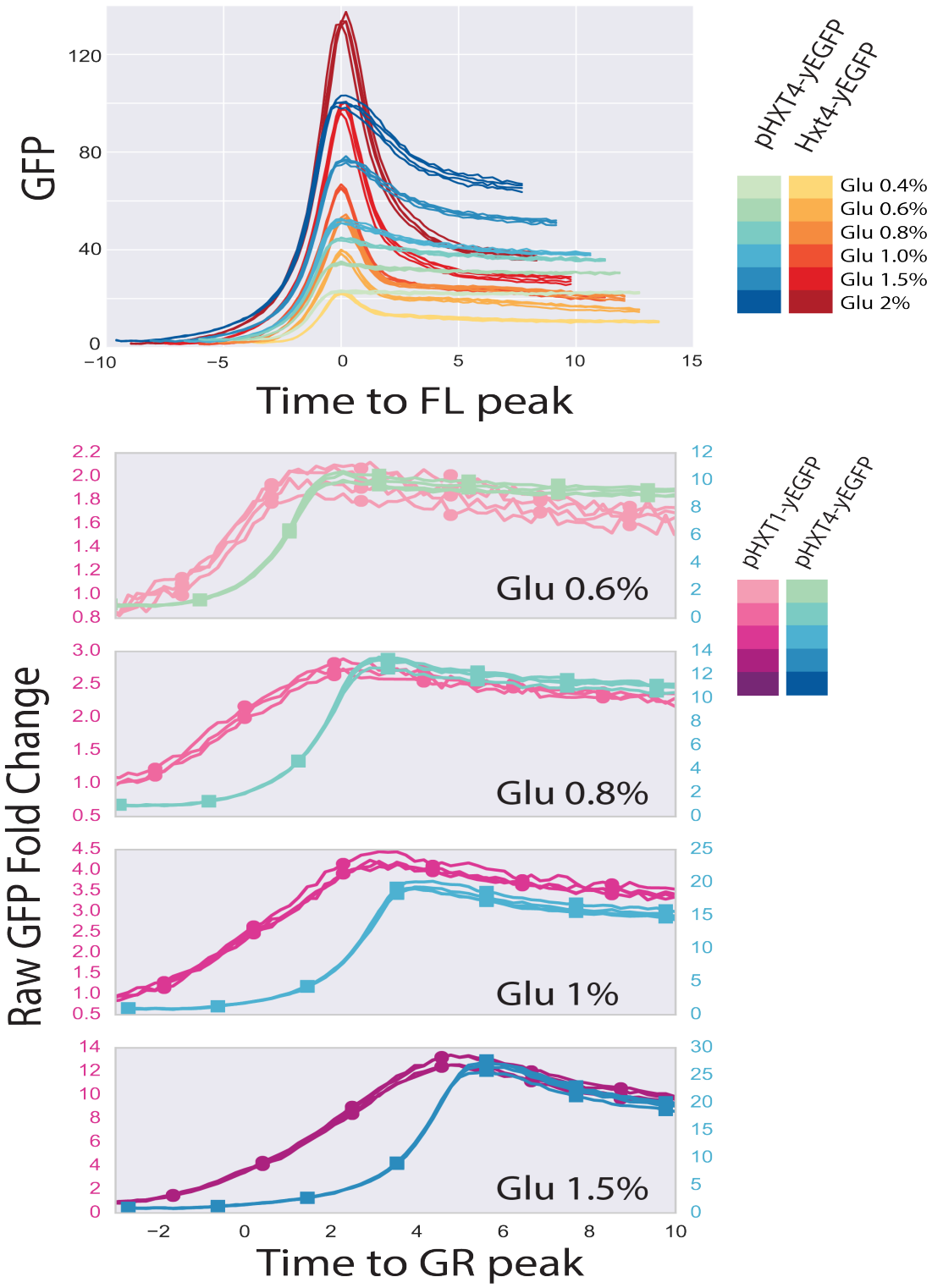

Figure 3.7: The HXT4 promoter is sufficient to recover the activation dynamics of Hxt4-yEGFP. Top: Overlay of Hxt4-yEGFP and pHXT4-yEGFP dynamics relative to the fluorescence peak of each curve, to emphasise the kinetic similarity between both strains. Bottom: pHXT4 conserves a characteristic activation dynamics, different from that of pHXT1, at multiple glucose concentrations. Magenta and blue axis and gradients correspond pHXT1 and pHXT4 respectively. The fold change is calculated relative to the start of the experiment, where values are comparable to the untagged strains.

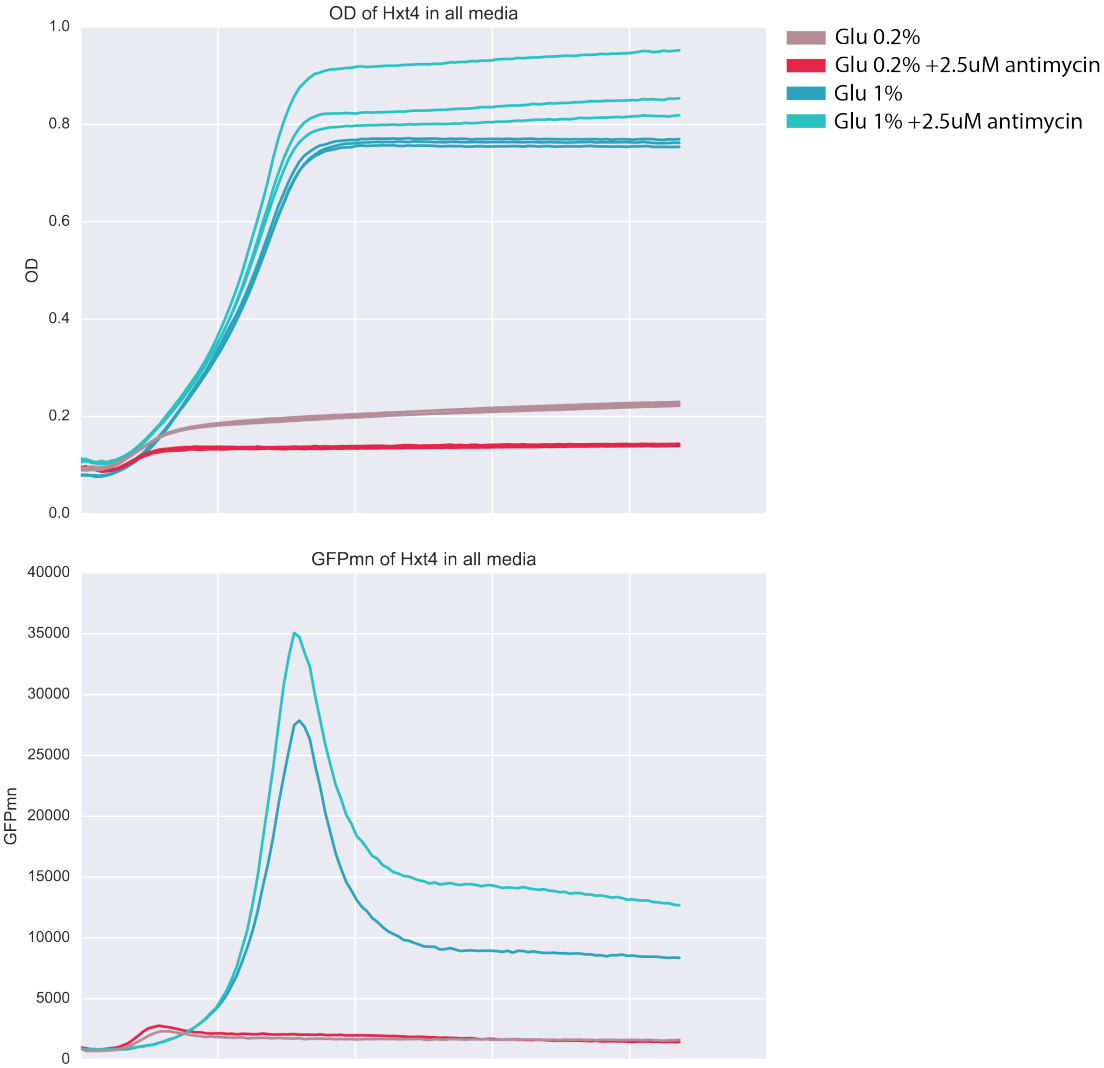

Figure 3.8: Hxt4 activation is not dependent on respiration. Results are shown for strain PS409 (Hxt4-yEGFP), both in 0.2% and 2% glucose. Red and cyan indicate treatment with antimycin, whereas blue and brown are untreated controls. Top: the low glucose, antimycin-treated curve (red) is unable to enter post-diauxic growth compared to the control (brown). Bottom: Hxt4 expression shows slighly higher levels of Hxt4 in antimycin and complete lack of diauxic growth (respiration) in low glucose. The difference is likely due to lower cell density in the red culture. The temporal trend is unaffected. As for the high glucose, higher cell density is achieved in the antimycin A culture. Wild type BY4741 has been reported to be insensitive to antimycin A in high glucose (Schmidt et al. (1999)). Higher final ODs were observed for the antimycin treated culture, and higher levels of Hxt4 were obtained for this condition as well.

expressed for both conditions, suggesting that Hxt4 expression is not inhibited when cytochromes are inhibited. However, other antimycin A insensitive pathways of respiration could be involved in the increased growth for the antimycin treated curves in high glucose (Fig 3.8, cyan curves).

Further experiments are needed to elucidate whether Hxt4 activation could be part of a sequence of events directly influencing the transition toward respiration. For example, it could be asked whether deletion of Hxt4 affects the respiratory rate in a glucose limited chemostat, similar to the experiments performed by Daran-Lapujade et al. (2004).

3.9 Genetic determinants of the Hxt4 response at the promoter level

I have shown so far that the Hxt4 response is cell density-independent, happens at multiple sugar concentrations, is concomitant with a glucose drop in batch cultures (Section 3.6), shows precise allocation to a falling growth rate (Section 3.5), and is largely independent of pre-culture conditions (Appendix section A). It have also shown that the promoter alone can reproduce the dynamic response observed (Section 3.7), which contrasts with the activation of the HXT1 promoter. This strongly suggests that this complex signal processing is genetically encoded within the promoter, rather than just a general effect from growth shared by all genes. As such it can potentially mutate, be modularly inherited and transferred to other promoters. Thus, I sought to address the genetic determinants of such dynamics.

Control of transporter expression is understood to be excerted mainly through the binding of transcription factors (TFs) to motifs in the promoters of HXT genes. The two most studied TF groups in this context are repressors Rgt1 and Mig1/2/3. A fair amount of biochemical evidence assays has been collected describing associations between Mig1/2/3 and Rgt1 at the promoter upon specific glucose stimuli (Kaniak et al. (2004), Westholm et al. (2008), Flick et al. (2003)). In general, addition of glucose releases Rgt1 from the HXT promoters and pro-

motes binding of Mig1/2/3. However, the relationship between the binding of these TFs, the binding motifs and expression output has remained elusive.

The first reason for the elusive genetics of this system is that the binding sites for both TFs are highly degenerate, with their core motifs being reduced to 4 or 5 bases: 'CGGA' in the case of Rgt1 and 'GGGG' in the case of Mig1/2/3. Not only must the Mig1 motif allocate distinct binding of Mig1,2, and 3; it also must serve to provide specificity (along with other nucleotides) from Msn2/4 binding, which is known to bind to the sequence CCCCT (commonly known the stress response element STRE) (Westholm et al. (2008), **?**). The second reason may become apparent by looking at the distribution of CGGA and CCCC at the HXT promoters (3.9). Microarray evidence shows that pHXT1 is not regulated by Mig1/2/3, even though some putative Mig1 sites are present (Westholm et al. (2008)). In contrast, pHXT6/7 are highly expressed after glucose depletion regardless of claims of Rgt1 binding (Schmidt et al. (1999)). Nevertheless, core motifs for all these transcription factors are present in all HXT promoters, with no obvious correlation in order or abundance of these sites that may directly explain Hxt behaviour.

I reasoned that the complex expression dynamics of Hxt4 could provide insight into the role of specific binding motifs on HXT regulation. Thus, starting from the WT promoter as a basis, synthetic promoters were made in which certain sites were removed. Specifically, Hxt4 has 8 potential Rgt1 core binding motifs, 4 of which are on the forward strand and 4 on the reverse strand(Figure 3.10. I designed 8 promoters with each of the Rgt1 sites removed and one where all of the Rgt1 sites were removed at once. Another synthetic promoter was cleared of all CCCC and GGGG repeats to test for Mig1-2-3 binding. Since such core motif overlaps with the the Stress Response Element (STRE), this promoter version was called noSTRE for generality. Additionally, another site (M001) was deleted of a site that exactly matched the consensus Msn2/4 binding motif CCCCT. Finally, in order to test for neighbourghood and distance effects of the regulation, the native promoter was divided in 5 fragments of equal size, and each of them was removed in an additional 5 variants. Figure 3.10 shows an overview of all the

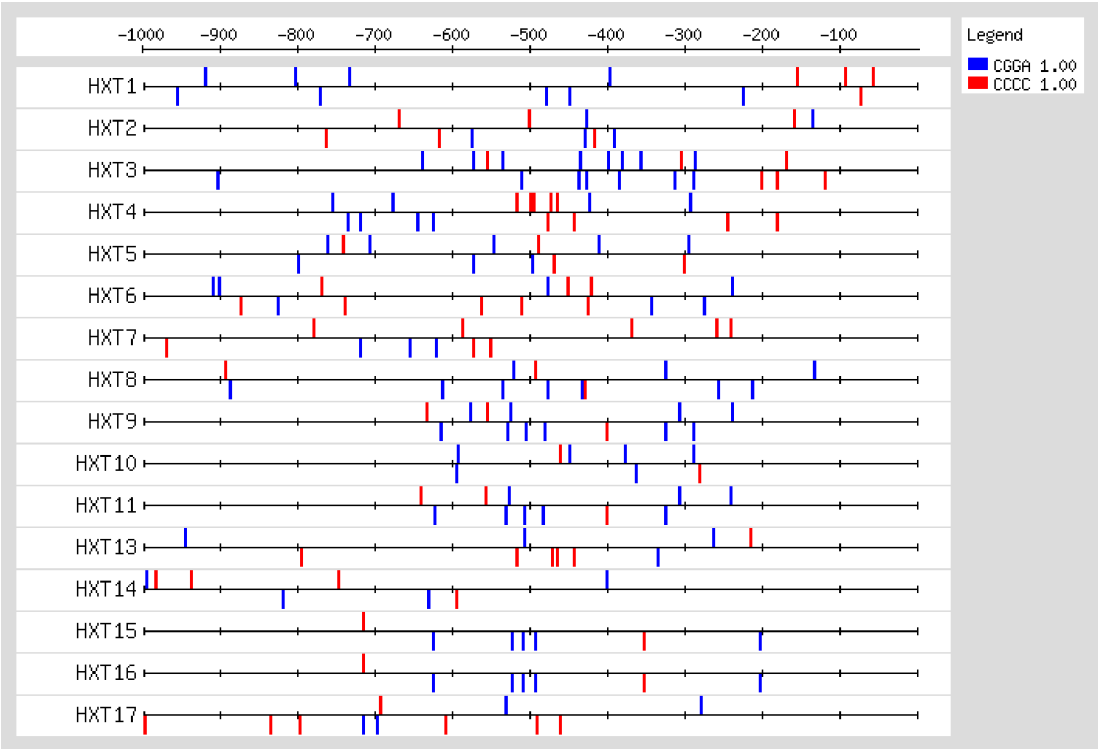

Figure 3.9: Distribution of Rgt1 and Mig1 core motifs along the promoters of HXT1-17. Image generated by using the dna-pattern and feature map tools on the Regulatory Sequence Analysis Tools (RSAT) website (Medina-Rivera et al. (2015))

designs, sites and their design logic. [3]

3.9.1 Expression dynamics of synthetic promoter variants differs from that of the native HXT4 promoter

In total, 10 synthetic promoters were obtained and screened in 0.2% and 2% glucose following the standard plate reader procedure. Figure 3.11 shows how different promoter variants diverged from the original pHXT4 response when screening their activity in 2% glucose, with several mutants specifically altering the timing of the response relative to the max growth rate. Strikingly, variant R001 had no strong alterations in timing but its expression was 10-fold higher than the native promoter. In contrast, in the pHXT4_STRE variant, the HXT4 time delay effect was completely lost. GFP levels constantly increased from the beginning of the time course, which enabled a 600 fold induction from the start of the experiment. This induction level is comparable with the widely-established GAL1 promoter, and 20 fold higher than pHXT1e1. Altogether, these 2 promoters demonstrate that the timing and expression levels of the pHXT4 can be modulated independently.

3.9.2 Response scaling of pHXT4 by the Rgt1 sites

It has been generally established that Rgt1 serves as a repressor. Removal of repressor binding sites should therefore cause higher expression levels, as is the case for pHXT4R001. However, the relationship was less trivial in other Rgt1 site deletions. Removal of other sites resulted in lower, if not minimally changed expression levels. For example, removal of site R004 caused a slight decrease in expression relative to the native promoter (Figure 3.11). In contrast, the deletion of the promoter region including this site caused a stronger expression. Strikingly, the native, R004 and D004 promoters fall into highly overlapping

[3]Due to technical problems in the synthesis process with the company Gen9, some of the variants were not possible to synthesise at the time of this writing: the LMP04_RGT1 variant, region deletion variants D002, D003, D005, and Rgt1 site deletion variants R002, R003 and R006. Nevertheless, despite the incompleteness in this set, I will show that the sequences screened provide valuable insight about Hxt4 regulation.

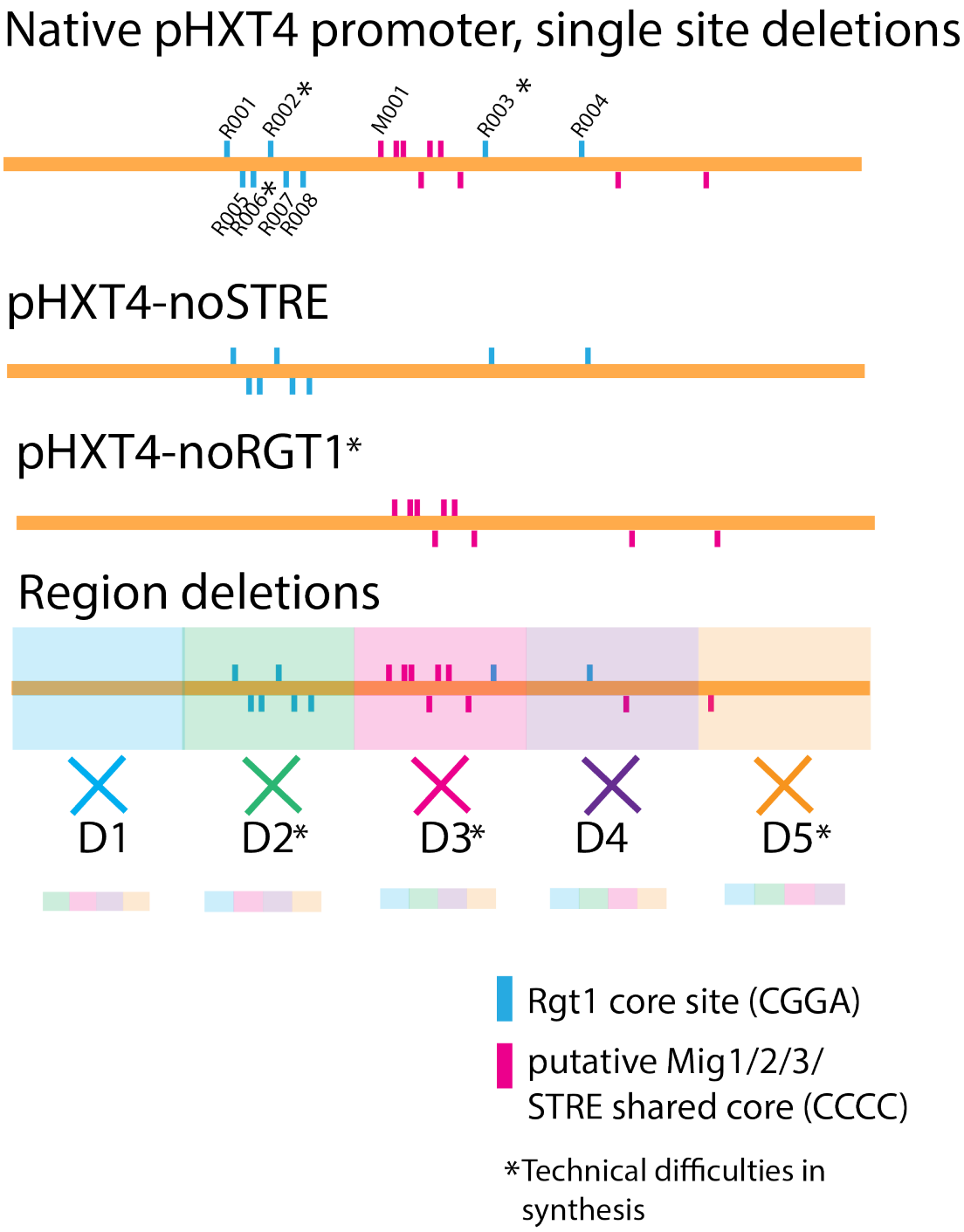

Figure 3.10: Design of synthetic promoter variants to understand pHXT4 regulation. Top: (potential Rgt1 binding sites (CGGA/TCCG, cyan) and potential Mig1/STRE sites (CCCC/GGGG), cyan. Second to top: variant where all potential Mig1 sites have been removed. Third to top: variant where all the RGT1 sites have been removed. Bottom: Schematic for region deletions: variant DX means that chunk number X of the native promoter was removed. *: the variant could not be synthesised due to technical difficulties.

induction kinetics when the curves are normalised between 0 and 1. Similarly, promoters M001 and R001 impact the response magnitude in opposite ways, yet expression timing is equally as delayed relative to the native promoter in both cases. Such changes could potentially be understood as a linear transformation (a scaling). This transformation could manifest biologically in terms of fidelity with which the promoter reads signals from the network. Too many sites could make it difficult to release repression, whereas too few of them could render the promoter insensitive to glucose signals.

In general,the variability in timing observed for the native HXT4 promoter is wider, whereas the timing of the variants was more consistent. The overlap among growth curves and consistency across replicates suggests that variability is not simply due experimental error. Minor growth deviations from wild type were observed in the synthetic genes (Figure 3.11 bottom panel, t 5), yet they had little impact on the timing of their response. Altogether, changing the configuration of sites in the variants affects the probability of activating at particular times, with some variants yielding more concise responses than the wild type. However, more replicates are needed for closer examination of timing distributions.

3.10 Potential explanations for uneven Rgt1 binding site contributions to expression

The uneven contribution of different core RGT1 sites to the pHXT4 response strength could be due to 3 potential reasons:

a) Out of the sites screened, only R001 is one of the only sites capable of binding RGT1, and many others are not functional RGT1 binding sites. This would predict R001-like sites in other HXTs to bind RGT1 as well, and thus be major regulators of HXT expression. b) Some of the RGT1 core binding sites are, in fact, binding sites for activators. This would explain why removal of some sites might decrease expression levels. c) R001 exerts strong epistasis over all other sites, perhaps due to its strength or position as first in the promoter; therefore, its presence masks the regulatory functionality of the other sites. This would imply

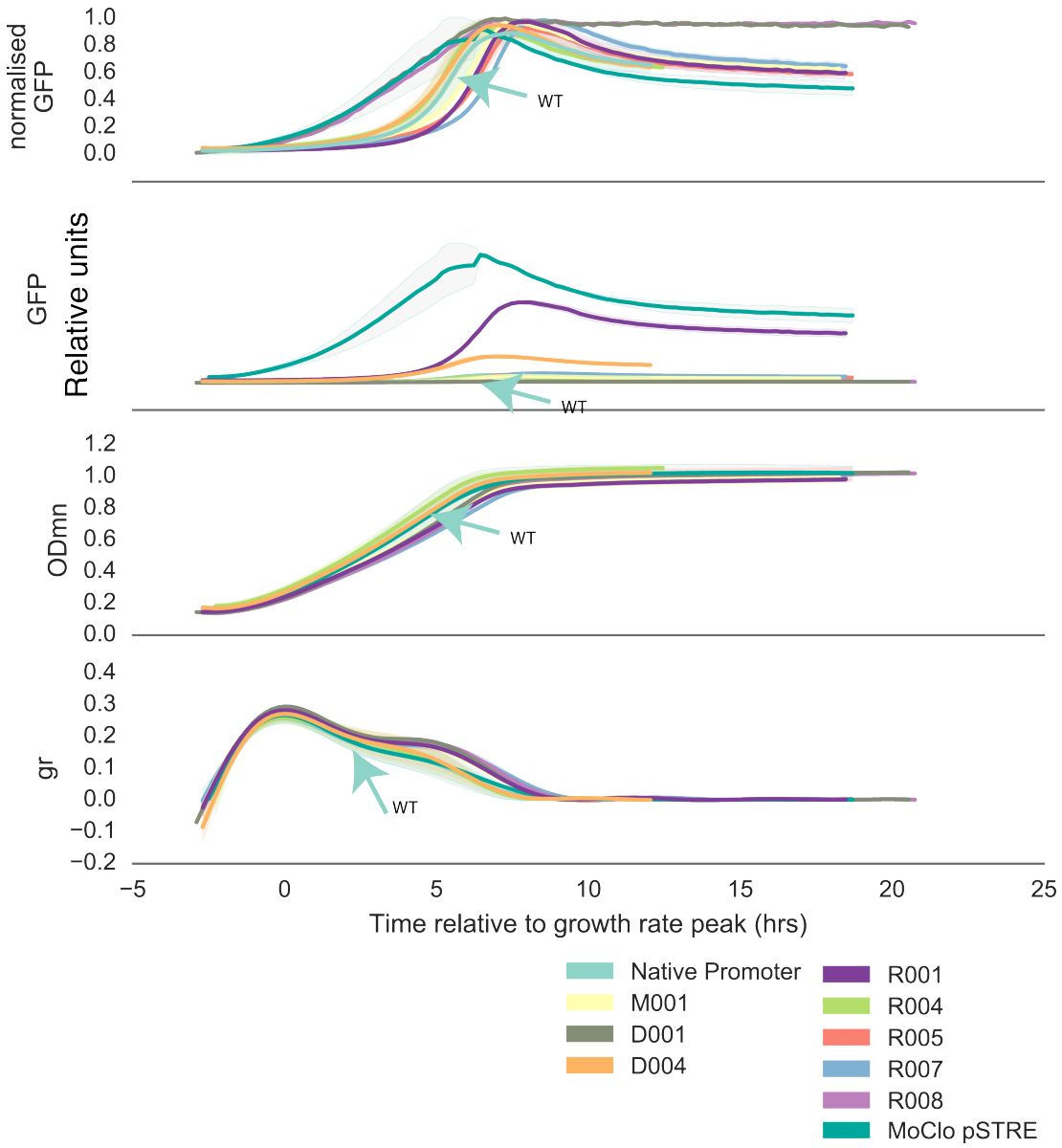

Figure 3.11: Synthetic variants of pHXT4 alter both the timing and magnitude of the response compared to the native promoter. Light blue arrows indicate the data for the strain with the native promoter. Top: Normalisation of the GFP traces between 0 and 1 to emphasise the differences in timing. Second to top: same data without normalisation. Note that R001 shows similar timing to WT but is expressed to a larger scale. pSTRE and pR008 have lost all the timing effect, but STRE reaches the highest levels of the sample. Second to bottom: OD_{595} for all the strains. Bottom: Growth rates for all the strains

that removal of R001 should allow to see a clearer effect of other sites. d) The closer an Rgt1 site is to a Mig1 site, the more likely there is epistasis between the two sites. For instance, binding of one regulator may affect the binding of the other. This could explain why removal of site R004 lowered expression and removal of chunk D4, which contained the site R004 and a Mig1 site (Figure 3.10), yielded stronger activity.

3.11 Role of the glucose sensing network in Hxt4 expression dynamics

The glucose sensing pathway controls expression of the HXT genes by mapping glucose signals to the control of transcription factors Mig1/2/3 and Rgt1. The specific nature of those glucose signals remains unknown. Moreover, the robust growth staging of Hxt4 gene expression was largely found to be independent of an initial glucose level, yet controlled at the promoter level by Rgt1 (CGGA) and potential Mig1/2/3 (CCCC/GGGG) core motifs (Section 3.9). Yet, how the network's signal processing might enable such growth staging based on the regulation of Rgt1 and Mig1 is not clear.

I therefore set to investigate how specific pathway mutations might alter the expression dynamics of Hxt4. To do this, the Hxt4 protein was tagged with yEGFP in strains carrying individual deletions for genes in the pathway. The deletant strains used were, in the case of these results, obtained from the knockout collection, and hence are in the BY4741 background. All the strains with deletions were then screened in 7 glucose concentrations in order to investigate how glucose and growth influenced Hxt4 expression in the mutants. To make sure that the phenotype was not caused by the independent Gpr1 glucose sensing pathway or the general stress response, the gpr1 Δ deletion and a msn2Δ msn4Δ deletant strain were also tested (Appendix figure B).

Appendix figures B.10 and B show how the dynamics of Hxt4 is altered at several concentrations of glucose for different mutant backgrounds. Overall, deletion of gpr1 or MSN2/4 had little or no impact in the induction dynamics of

Hxt4-yEGFP, suggesting that the Hxt4 response is mostly autonomous and does not depend on the general stress response or other pathways. In general, the expression peak time remained unaltered for most of these deletions as well. Most of these single mutants had no obvious growth phenotype, at least in the standard experimental procedure I tested. The only exceptions were a minor effect on the std1Δ strain only at higher glucose concentrations (Figure 3.13 right, bottom panel), and a lower overall growth rate limit the gpr1Δ deletion.

The rest of the pathway deletions had stronger and diverse effects on Hxt4 regulation (Figure 3.13), although with no obvious shared features across mutants. For example, the mth1Δ strain showed a timing close to wild type, albeit with significantly larger levels. The rgt2Δ and std1Δ strains showed major changes in the response timing. Before proceeding with their description, I will attempt to decompose the dynamics of the Hxt4 response into 3 different features. The first component of this response is an initial delay in expression, which happens regardless of the initial sugar concentration, and is mostly corrected when aligning curves at the growth rate peak time. In contrast, genes Hxt1 and 2 do not show such delay: their levels start to rise immediately after glucose addition. The second component to this is a glucose-dependent delay, additional to the first one; aligning the growth curves at the max growth rate does not account for this delay. The third component is the steepness of the response. Several proxies for steepness can be used, but the steepness can be defined as the slope in the dynamics between half the response and the peak.

In particular, the Hxt4-yEGFP mig1Δ strain lost the initial response lag 3.12. In the std1Δ deletion the glucose-dependent delay was exacerbated, and the response was overall steeper, whereas in the rgt2 strain such delay was lost. This observation suggests that Rgt2 and std1 act in opposite regulatory directions, potentially in the same mechanism. Figure 3.13 (top left) and Figure B.10 summarise the timing effects for all the relevant mutants.

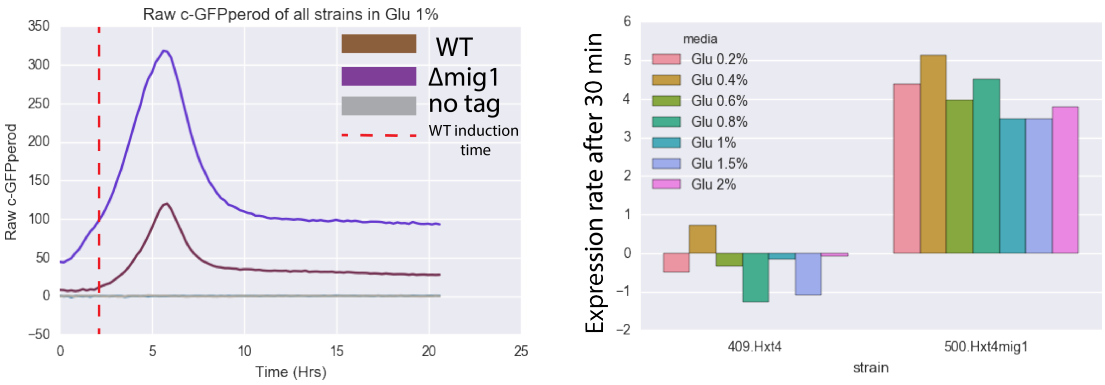

Figure 3.12: Deletion of MIG1 eliminates the initial delay in the Hxt4 response. Left: Hxt4-yEGFP per OD over time for WT and mig1Δ. The untagged version has been left to compare to the uninduced Hxt4. Dotted line indicates the moment when Hxt4 expression is triggered in the wild type strain. Right: Expression rates 30 minutes post induction at for the wild type and mig1Δ, suggesting immediate Mig1-mediated repression of Hxt4 and its subsequent release after 2-3 hours (red line)

3.12 Section summary

Altogether, these results show that the components in the glucose sensing network, rather than other general factors, are active determinants in the strength and timing of Hxt4 expression. Together with the previous section, the results suggest that both network activity and promoter decoding of this activity are required for a precise determination of Hxt4 dynamics.

3.13 Network perturbations alter the link between Hxt4 and growth.

I have previously shown that the timing of each glucose transporter's expression can be dynamically staged with respect to two features of growth rate: its amplitude and its dynamics (whether it is rising or falling), at both low and high glucose concentrations (Figure 3.4). For example, Hxt1 and 2 are allocated to a rising growth rate, whereas Hxt4, 6 and 7 are assigned to a growth deceleration phase, though the amplitude of the growth rate may be high (Figure 3.5). I asked whether these growth features themselves were causative of the allocation. In the conditions for which growth was indistinguishable among strains, the expression

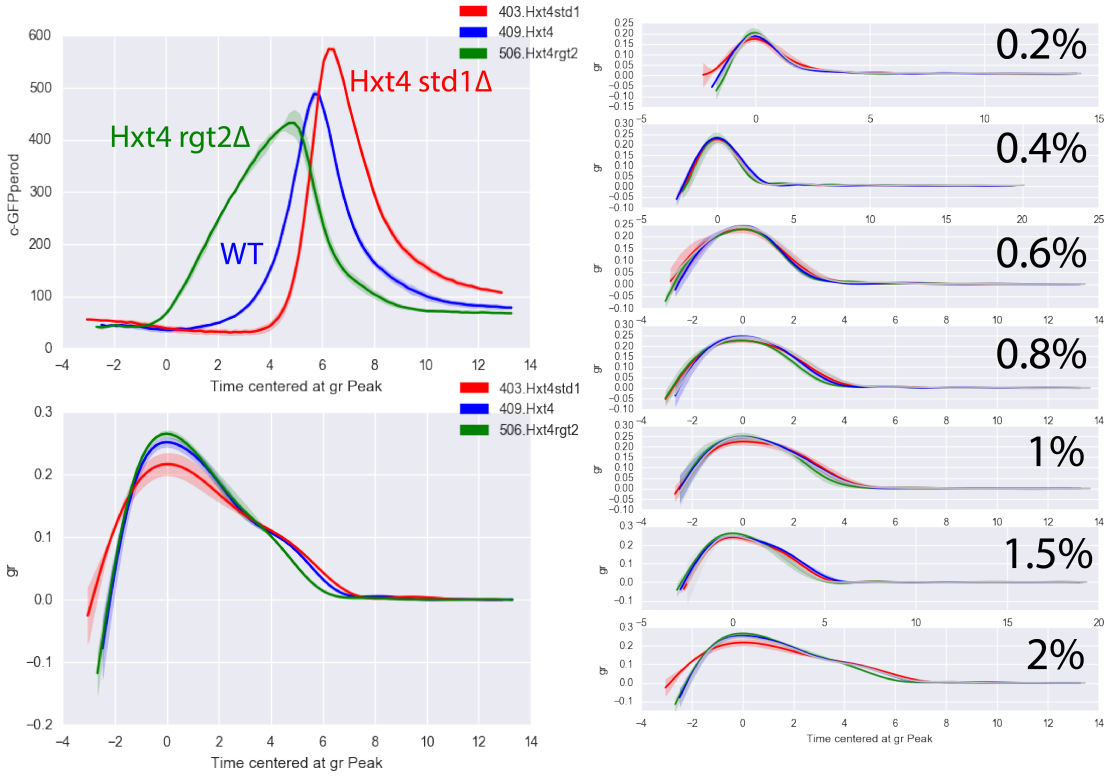

Figure 3.13: Deletion of RGT2 and STD1 have opposing effects on the dynamics of Hxt4. Neither of these two deletions removed the delay entirely. Left: dynamic alterations on the mutants for highly similar growth phenotype. Right: minor growth differences are only visible at certain concentrations of glucose.

dynamics was still drastically different among the wild type, the std1Δ and the the rgt2Δ strain, suggesting that growth differences are not causative of the diverse dynamics observed, and that Hxt4 expression is not causative of the growth defect.

In the wild type, Hxt4 production is constrained to falling growth rates below a threshold. It could be that the mutations warp the growth rate curve, thus displacing the timing of Hxt4 expression, or that the relationship of Hxt4 with growth rate was altered. Closer examination revealed that Hxt4 expression became induced in high growth rates in the rgt2Δ strain. This suggests that glucose sensing network components have an active role in establishing the relationship between growth and expression even with no detectable alterations in growth or total expression levels.

3.14 Chapter 3 discussion

In this chapter, I have intended to show that hexose transporter expression in actively growing batch cultures is not obviously dictated by initial glucose levels or instant glucose concentrations. Rather, the glucose dose response curve for some transporters is sensitive to time and history (Figure 3.3, 3.6), and each transporter's production is generally subject to specific growth staging (Section 3.5). Such staging is robustly achieved at a wide range of starting glucose concentrations. Both the magnitude and kinetics (the time derivative) of growth rate are considered for transporter expression. Using Hxt4 as a model to study this phenomenon, I have found that growth staging does not depend on pre-culture conditions, cell density (Appendix A) or respiratory metabolism. Moreover, promoter activity alone can largely recover the response magnitude and kinetics at several glucose levels, mostly through the effect of Mig1 and Rgt1 binding sites. Finally, sensor Rgt2 and co-repressor Std1 significantly warped the relationship between growth and Hxt4, without abrupt changes in either growth or total expression levels. Altogether, these observations provide evidence of dynamic signal processing by the glucose sensing network in *Saccharomyces cerevisiae*.

3.14.1 Clues about the growth-staging mechanisms of hexose transporter expression

Hxt2 and Hxt4 are differently staged in growth 3.4 despite having similar affinities for glucose. The specific signals that induce growth staging of hexose transporters have not been completely dissected. However, multiple observations hint at possible underlying events orchestrating this process.

If the Rgt1 complex and Mig1 are regulating both promoters, there is no obvious explanation why Rgt1 complex would be destabilised in one promoter and not in another. Different promoter affinities cannot explain this, unless there is a way that the Hxt4 binding isoforms of Rgt1 escape glucose destabilisation. Similarly, upon the same Mig1 dynamics, a similar (or at least not opposite) output dynamics would be expected.

Asymmetry at the level of Mig1 repression

Hxt4 expression is initially subject to a delay in activation. Such delay is gone in a mig1Δ strain, suggesting that Mig1 mediated repression is responsible for the hxt4 delay upon immediate exposure to glucose. Consistently, removal of all potential Mig1/2/3 core sites from the promoter eliminated all delays in the HXT4 promoter, and with them, the gene's growth staging. I thus conclude that Mig1 activity plays a direct role in control of the growth staging of Hxt4.

As Hxt4 is induced during the falling growth stage it follows that Mig1 loses the ability to sustain repression of its target a) while there is still glucose b) at different glucose concentrations c) at a particular point in growth. What, then, is driving Mig1 to derepress the Hxt4 promoter? I will attempt to address those mechanisms in the following chapters.

3.15 Asymmetry at the level of the sensors

The Snf3 deletion lost the ability to induce Hxt4 at initial glucose concentrations of 0.4 or below. However, Hxt4 expression dynamics (shape) was more comparable to the wild type at higher concentrations. Taken together with the fact

that the rgt2 deletion removed the glucose dependent delay but its levels were comparable (slightly lower) than wild type, the data reveal differential effects in shape and timing of the Hxt4 response. Snf3 has a larger impact on the response strength, whereas Rgt2 has a larger impact on the delay of the response.

Asymmetry at the level of Rgt1 repression

Mth1 and Std1, albeit their paralog status, have non identical effects over Hxt4. A Mth1 deletion causes a 'scale up' of the Hxt4 response below 1% glucose, and a 'scale down' at higher concentrations B. In contrast, STD1 deletion causes a delay, resulting in a sharp increase of Hxt4 levels later during growth. The Mth1 deletion suggests control in the basal transcript levels, with smaller effects in timing. But the Std1-induced delay suggests role of Std1 in de-repression of Mig1/2/3. As deletion of RGT2 causes an earlier derepression (Figure 3.13) it could mean that the relationship between Std1 and Rgt2 determines the exact moment of induction of Hxt4. Later chapters will elaborate on this issue.

3.16 Chapter conclusion

To conclude, the batch culture experiments performed in this chapter are provided as evidence that the yeast glucose sensing network is able to perform dynamic signal processing, due to its ability to perform dynamic growth staging of hexose transporters that scales with growth magnitude (section 3.5), glucose concentration and cell density (section A.4), and it differentiates between two states of the growth derivative: rising and falling growth rate. This mechanism, exerted by the network's behaviour (3.13) can differentially stage transporters of similar reported affinities (3.5). Staging is exerted by the network components (3.13), and is encoded at the HXT promoters (section 3.7), which may harness the same network's dynamic signals in different ways. The fact that this processing happens at the promoter level (Section 3.7) provides a platform for the tuning of responses to a global sequence of events, and thus can be adapted and tinkered by evolution while avoiding pleiotropic consequences.

The specific cues that trigger growth staging, and particularly the activation of Hxt4, have yet to be discovered. To this end, in the following chapter I explore the role of environmental glucose kinetics as an organising stimulus of HXT expression in single cells.

Chapter 4

Single cell studies of hexose transporter regulation

4.1 On the advantages of single cell studies for hexose transporter analysis

The batch experiments performed in the previous chapter have been valuable for two major reasons. First, they have provided insight about how specific transporters can be dynamically organised as cells face a changing, albeit predictable environmental condition. Second, they have been useful to identify key general principles which govern the regulation of hexose transporter genes by the network: Its components are able to establish a relationship between different growth stages and the HXT promoters. In the following chapters, I attempt to shed light on the underlying cues and mechanisms governing the kinetics of these genes. However, studying cell behaviour in batch cultures can bring limitations about our understanding of the system's biology for several reasons.

4.1.1 A feedback between the population and the environment blurs causality

In a batch culture it is difficult to disentangle the causality of certain phenomena as not only the cells are dividing and growing, but the environment is being

changed by the cells, potentially establishing a causation ambiguity: a change in cell behaviour may cause a change in the cell environment, and this environmental change may feedback into the observed cell behaviour. Take, for example, the strong delay in Hxt4 gene expression in the std1Δ background (Figure 3.13, left, top panel). Is this delay caused by the cell's inability to read a signal appropriately? Is it caused by the fact that glucose consumption was severely impaired? Such impairment would cause a longer time to consume the sugar, therefore delaying the transporter's activation, which would delay sugar consumption even further. Even though biomass accumulation and growth have been barely affected, it is impossible to trace down the sequence of causal events from this data. Looking at the rich batch culture data of Zampar et al. (2013), the large numbers of parallel events observed further complicate pinning down the signals that are being decoded by the cells. In fact, it is usually assumed that the many parallel events are all tightly linked, and thus cannot be readily decomposed to a single organising stimulus. [1].

4.1.2 Populations average out sources of variation

The second problem with batch cultures is that the signal obtained arises from a population average, assuming that most cells behave the same way. In fact, this is known to be false (Elowitz et al. (2002)), with only a fraction of cells behaving as the population's mean or mode. Moreover, the dynamics of sub-populations, often masked by batch growth, are fundamental to accurately determine the underlying mechanism of expression. For example, a steady-state time average may be given by a uniform population of cells at steady state, or by a population of unsynchronized, oscillating cells. Additionally, the population's time average may be widely affected by individual cell cycles, sizes, types, ageing, etcetera.

[1]The finding that the timing of Hxt4 expression was completely controlled by the promoter provided an opportunity to disentangle the effects of signaling over this promoter without altering glucose transport

4.1.3 Control of localisation can render a transporter obsolete

The third problem comes specifically when trying to connect transporter expression to fitness, as transporter expression does not necessarily match transporter activity. A transporter may be at very high levels, but be rendered inactive by being targeted to the yeast vacuole. To accurately estimate and measure the mechanistic determinants of Hxt expression and the physiological contribution of every Hxt, it is imperative to study their induction dynamics at the single cell level.

4.2 Available approaches for single cell studies

4.2.1 Microfluidics and microscopy as a state–of–the–art technology

Two main types of approaches have become widely used for studying gene expression in single cells. With the rise of fluorescent expression markers, fluorescence microscopy has become an ideal option and live cell imaging has become a method of choice for cell biology (Ettinger & Wittmann (2014)). However, the information obtained from these images remained mostly qualitative due to many challenges. Specifically, transformation of pixel intensities into absolute molecule numbers is a challenging task subject to a large number of variables. Despite these difficulties, the quality of quantitative measurements through image analysis has grown substantially in the last years (Gordon et al. (2007), Waters (2009)). To this day, despite the difficulties of absolute quantification, relative fluorescence has become of standard acceptance in quantitative cell imaging. In parallel, the development of microfluidic technologies for biology (Wheeler et al. (2003), Zare & Kim (2010)) has allowed cells to be kept under precise, constant and controlled environments where they are less subject to the intrinsic harshness of a microscope surrounding. This has led to monitoring cellular behaviour for increasingly longer periods of time. At the expense of a less 'natural' environ-

ment for the cells, the submission of cells to a microfluidic environments opens the possibility of changing the cell environment at will, and thus disentangling how cellular responses might be linked to specific external stimuli.

4.2.2 Flow cytometry allows the study of phenotypic distributions of a population of cells at a tradeoff with temporal resolution

The powerful insights and resolution that can be obtained with microfluidics and microscopy have come at a large trade off with throughput. Most of the technologies are able to screen, at most, 200 cells per condition per experiment, which can be limiting when trying to resolve the phenotypic distribution of a population. For this latter purpose, a technique called flow cytometry offers a large number[2] of cells sampled at the trade-off of resolution. In flow cytometry (Brown & Wittwer (2000)), particles are flown through a channel, one after the other. As particles pass through the flow, they are screened for different properties. Particles are typically measured for the among of light that directly bounces back to the source (Forward scatter, usually associated with particle size) and the light that is refracted in a different direction from the source (the side scatter, usually associated with sample's 'complexity'). Finally, the particle can be monitored for fluorescence by shining light of the appropriate wavelengths. A limitation of the flow cytometry approach is the need for heuristic gating of the forward and side scatter based on sample knowledge.

Flow cytometry has been previously used to study hexose transporter expression levels and activities during logarithmic growth (Youk & van Oudenaarden (2009)). This group characterised the dose response curve of the hexose transporters using flow cytometry and their results are in qualitative agreement with the plate reader dose response curve obtained in figure 3.3 (left panel), despite the difference in strain background between studies[3]. However, they reported mea-

[2]One flow cytometry read is able to measure millions of cells

[3]Youk & van Oudenaarden (2009) used CENPK-1C as background, whereas I have used BY4741.

suring this curve 4 to 6 hours after glucose addition. I attempted to reproduce the flow cytometry measurements for Hxt2 and Hxt4, and the results revealed a time dependence for the response curve with Hxt2 and Hxt4 expression being comparable only at 6 hours post induction, and an essentially unresponsive Hxt4 at 4 hours. This delay was comparable to the dynamics observed for Hxt4 (Figure 3.6 top left panel). Because of this time dependence, its redundancy with the plate reader experiments, and the absence of enough technical throughput, it was decided that timelapse fluorescence microscopy was better suited for temporal characterisation of single cell Hxt dynamics. It is important to note an unexpected discrepancy: Hxt2 effectively showed full repression at 6 hours in the plate reader, whereas its levels were larger than Hxt4 in the flow cytometer sample. The latter sample was obtained from a flask culture, and subject to higher oxygenation.

4.3 The ALCATRAS microfluidics platform for single cells of yeast

Our group has recently developed a microfluidics- timelapse microscopy platform to monitor gene expression dynamics in single yeast cells for a significantly long time (up to 60 hours) (Crane et al. (2014)). This platform includes the design of a microfluidics device (Figure 4.1) which is able to trap single yeast mother cells between two pillars of silicone polymer PDMS [4]. Cells that bud off this trapped mother cell can freely flow away, while the mother remains in the trap. The device can also be used for studying ageing under the microscope (Crane et al. (2014)), in an analogous fashion to the 'Mother machine' device developed for Escherichia coli (Wang et al. (2010)). Mother trapping enables the study of long term events on cell fitness at the tradeoff of short term monitoring of newly budded daughters. However, daughters that are still attached to the mother can be also analysed. A machine learning algorithm then detects the cells in brightfield or DIC or brightfield images in order to find cell region information

[4] full name: Polydimethylsiloxane

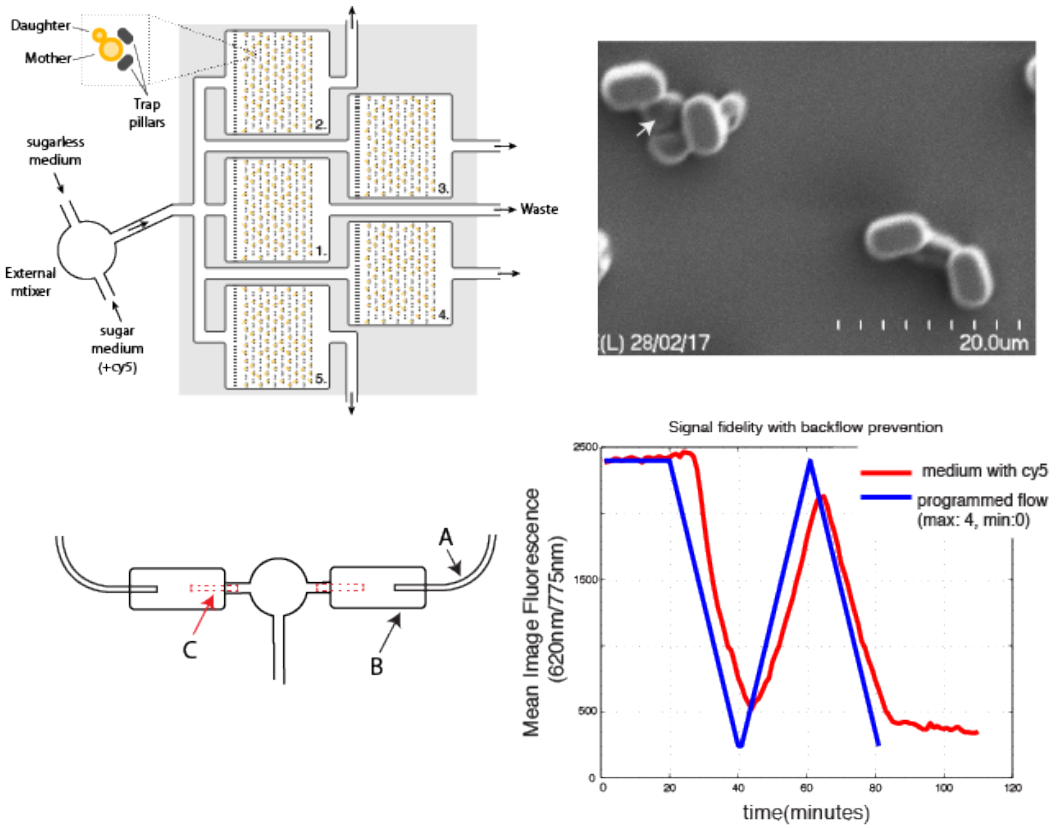

Figure 4.1: Adaptation of the ALCATRAS microfluidic system for multiplex single cell analysis in transient glucose environments. **Top left**: Schematic of the ALCATRAS device (Crane et al. (2014)), whose original design was expanded to simultaneously screen 5 independent strains. Each chamber contains arrays of trap pairs that hold mother cells (orange) in place while daughters are washed away (see inset). Gradual transitions in the extracellular medium are achieved through an external mixer which combines the flow from 2 pumps carrying sugarless medium and sugar medium. cy5 is often added to the sugar medium in order to monitor the media transition independently of the GFP channel. Schematic was created in collaboration with Julian Pietsch. **Top right**: Scanning electron microscopy image of the traps in the ALCATRAS device (courtesy of Ivan Clark). White arrow indicates a mother yeast cell in the trap. **Bottom left**: Detail of the setup for the external mixing, which I proposed. This setup largely prevents backflow, which disrupts real time control of mixing. A piece of internal thin tubing (C, red dotted lines) is placed inside the T-junction's arm. Thick tubing (B) holds the mixer, T-junction and media source tubing (A) together. A and C are the same kind of tubing. **Bottom right**: Results of the first experiment with the backflow control in the bottom left panel. Comparison of an input flow programme (blue) with the output, measured by the average intensity in the cy5 images. The plot shows a small delay, which had to be taken into account for the design of transitions.

independently of fluorescence (Bakker et al. (2017)). The original ALCATRAS microfluidics device contained only one imaging chamber for a single strain, with an array of 500 traps per chamber. In collaboration with Matthew Crane and Elco Bakker, I proposed a new design to enable up to five chambers with different strains in a single device, with a shared medium. The final design (Figure 4.1, top left) was implemented into a functional microfluidics device by Matthew Crane. This design enables the loading of the cells through the media outlet, and chamber filters block the cells from invading other chambers.

4.3.1 Implementation of gradual nutrient transitions in the ALCATRAS device

A particular advantage of microfluidics is the ability to directly apply dynamic environmental stimuli to the cells. In the ALCATRAS setup, a fast change between two different culture media can be produced with the aid of two syringe pumps. The change from one medium to another can be performed automatically, with a programme that instructs either pump to infuse at the required rate. Typically, microfluidics/time-lapse microscopy experiments rely on applying a stimulus through an immediate environmental shift (commonly conceived as a 'step' input), to which cells will respond and adapt. For this project it is of particular interest to explore how glucose kinetics might influence transporter expression. Such transitions have proven key to discrimnating biological mechanisms behind protein dynamics (Granados et al. (2017), Muzzey et al. (2009)).

To create gradual glucose transitions it is essential to enable real time mixing of the media sources. This task is challenging in microfluidic devices because they promote laminar flow, which effectively prevents turbulence (and thus mixing) of the media. To generate mixing in the device, I implemented an external mixing system based on a T junction (4.1, top left). The final, successful mixing protocol implemented 2 features: a) Tailored adapters for the T junction (Figure 4.1, Bottom left) consisting of interlocked pieces of tubing, which would prevent direct flow from one media source to the other by inhibiting backflow. b) Resetting the

pumping programme every minute. In order to monitor media changes, cy5[5] was added to one of the 2 media (the glucose one). Cy5 would avoid bleed–through with fluorescent protein and autofluorescence spectra. Figure 4.1 (bottom right) shows the differences between the programmed input and the cy5 signal received in the images. It can be seen that there is close resemblance between input and output despite a delay. With this setup it was possible to perform both an upshift and a downshift in the same experiment with high reproducibility, as well to tune the transition from one media to another in a parametric fashion. A no glucose environment was guaranteed by pumping sugarless media after the transitions (see section 4.10.5)

4.4 The activation dynamics of Hexose transporters during composite glucose shifts

With this setup, I characterised the induction dynamics of individual transporters upon an upshift and a downshift of glucose. According to the accepted model of Hxt regulation, the presence of glucose would stimulate degradation of Mth1 and Std1, which would then release Rgt1 from the Hxt promoters and stimulate expression. Shortly afterwards, glucose metabolism should cause repression of some HXT genes, thereby setting their expression level to steady state (Section 1.6.6, Ozcan & Johnston (1995), Horák (2013), Broach (2012), Kuttykrishnan et al. (2010)). We decided to grow the cells in sugarless SC, and then submit them to an upshift, and subsequently return them to the original medium, causing a downshift of glucose 8 hours afterwards. Figure 4.2 shows the diverse, yet reproducible responses of Hxt1-7 to the combined upshift and downshift step (hereafter called a 'hat') across several biological replicates.

[5]Cy5 is a fluorophore on the far red spectrum.

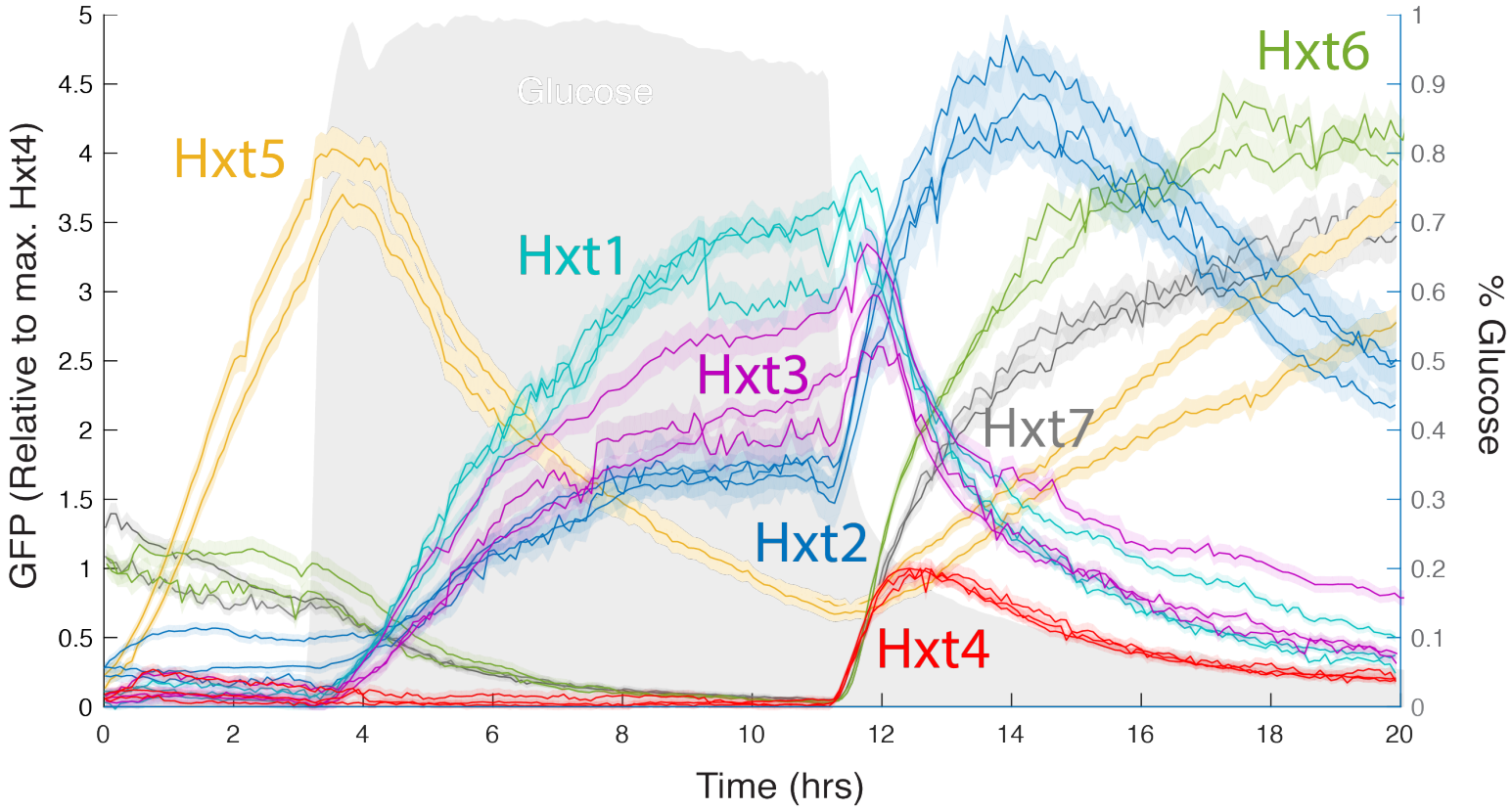

Figure 4.2: Exposure to composite glucose shifts ('hats') reveals diversity of dynamic responses of the hexose transporters. Galactose-grown cells were placed into the device in SC without sugar, then subjected to a 1% glucose upshift, and a downshift to the initial medium. The plot shows the mean fluorescence in the GFP channel over time (hours), while shaded areas indicate ± SEM. Lines of the same colour are biological replicates for the same strain. Shaded area is a reference for the glucose environment experienced (the exact time may change for a particular replicate).

As can be seen in the above figure, Hxt1 and Hxt2 and Hxt3 are induced (albeit at different levels) upon glucose exposure, whereas Hxt5 and 7, whose levels are initially high, start dropping. This is presumably due to repression plus degradation/dilution, and it is consistent with previous studies (Krampe et al. (1998), Verwaal et al. (2002)). The downshift showed an increase in the expression rate of Hxt2, 5 and 7. Levels of Hxt5 and 7 kept increasing long after glucose depletion, whereas Hxt2 levels started dropping shortly after depletion. The activity of these genes is overall consistent with the literature. I note that the responses of Hxt1, 3, and 2 show a similar induction dynamics, however they are distinguished by significant increase of Hxt2 levels during the downshift.

4.5 Hxt4 is expressed exclusively during glucose downshifts

The most unorthodox of the responses to a glucose hat was that of Hxt4 (4.2, red line). Batch culture studies had previously shown that expression of Hxt4 was concomitant with the onset of glucose depletion at several concentrations, but it was unclear from those experiments whether glucose depletion itself could be a trigger for Hxt4 activation. In accordance with this, Hxt4 remained unresponsive during glucose upshifts, but activated during the downshift of glucose, to then reach its peak in the vicinity of glucose depletion. This response was highly reproducible and observed for single cells (Appendix Figure B.1). Figure 4.3 shows a single Hxt4-yEGFP cell responding to the glucose downshift. In sum, these results suggest that a transporter can be allocated exclusively to a transient condition. Since the response happens before glucose depletion, it suggests that Hxt4 activation may be part of an anticipatory response to depletion.

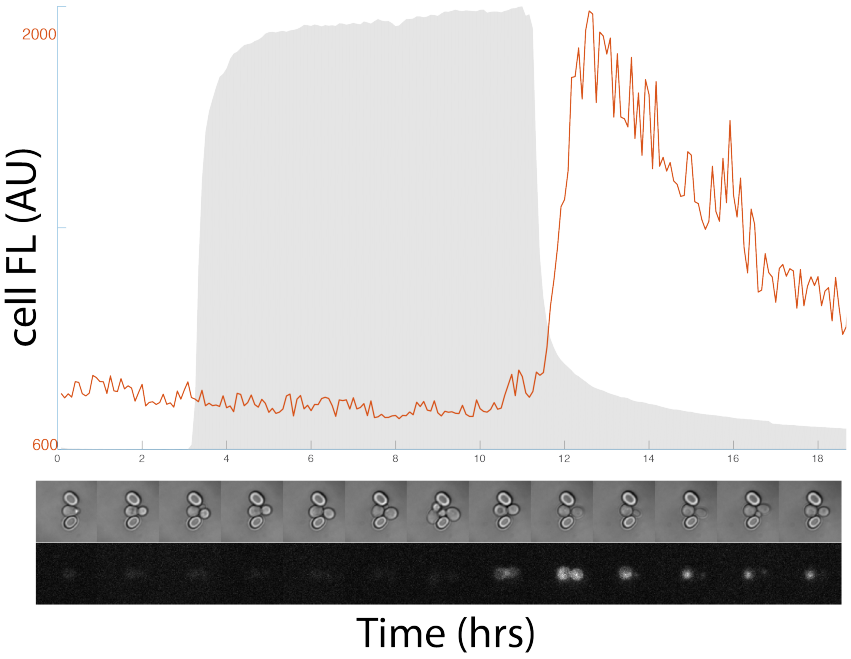

Figure 4.3: An example of an Hxt4-yEGFP cell exposed to a 1% glucose hat. Top: raw cell fluorescence (GFP channel) for the target cell (background level is around 800). First image row: Brightfield images showing the target cell trapped between ALCATRAS pillars. Bottom image row: GFP images for the same cell. Pixel intensity has been normalised across all images.

4.5.1 A glucose downshift is causative of the Hxt4 response

It could be that the observed Hxt4 response is pre–programmed, and just happened to coincide with the stimuli that we submitted the cells to, and thus the falling glucose signal is correlated but not causative. To test this, I submitted the cells to 4 hour glucose ramp, half the duration of the original one to account for length effects. Figure 4.4 shows how the response of the 4 hour ramp is just as strong as one of 8 hours. It could also be that a delay will never let the gene express in such a fast upshift. Therefore I submitted Hxt4 tagged cells to 3 glucose hats (4.11, top panel), two of which are within the reported expression regime of Hxt4 (Figure 3.3, left panel, Ozcan & Johnston (1995), Youk & van Oudenaarden (2009)). The levels of Hxt4 always spiked during a sugar downshift. Altogether, I conclude that a glucose downshift is causative of Hxt4 expression, and its strength can be modulated by glucose levels

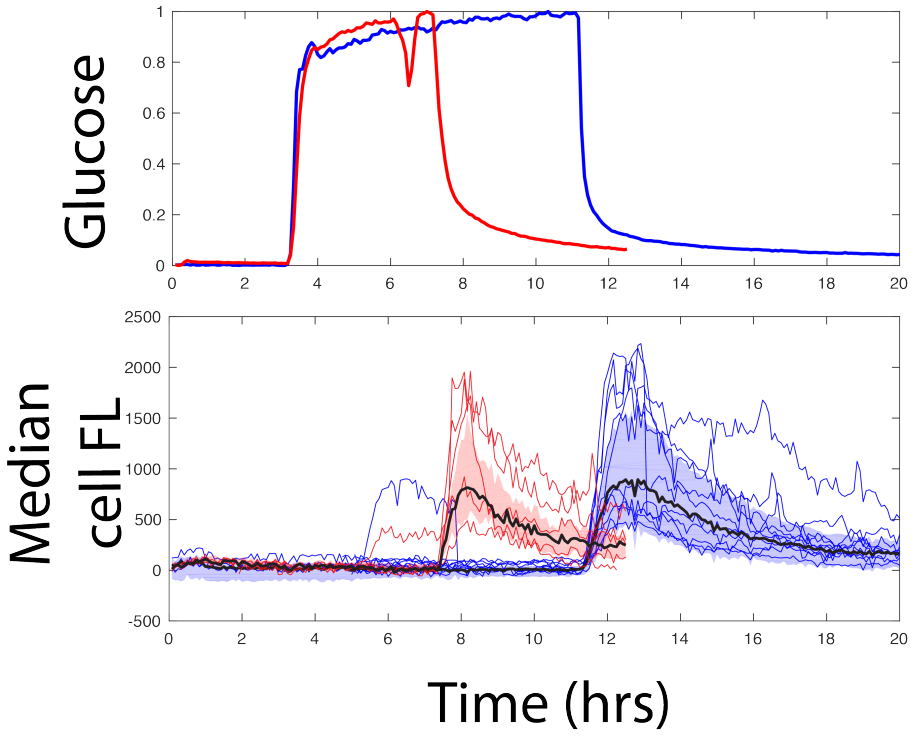

Figure 4.4: A glucose downshift exclusively causes Hxt4 expression. Plot shows median expression over time (black) for Hxt4 exposed to 1% glucose hats of 4 hours (red) or 8 hours (blue). Shaded area corresponds to the inter quartile range. Randomly sampled traces are shown for each case.

4.6 The downshift response of Hxt4 is robust to glucose concentrations and competing carbon sources

To see whether the Hxt4 downshift response was robust even in confounding environments such as a competing carbon source, the yeast cells were subjected to a hat transition from 1% galactose to 0.4% glucose. The mixing protocol transits from full galactose to 0.4% glucose, passing through every intermediate mixture, thereby creating a confounding environment where the cell experiences glucose and galactose at the same time. In this experiment (Figure 4.5), Hxt4 was exclusively sensitive to the downshift as well.

Hxt4 has previously been reported to show expression at low to medium levels of glucose (Ozcan & Johnston (1995), Youk & van Oudenaarden (2009)), and thus it could be that the sharp transition to 1% glucose does not allow the transporter

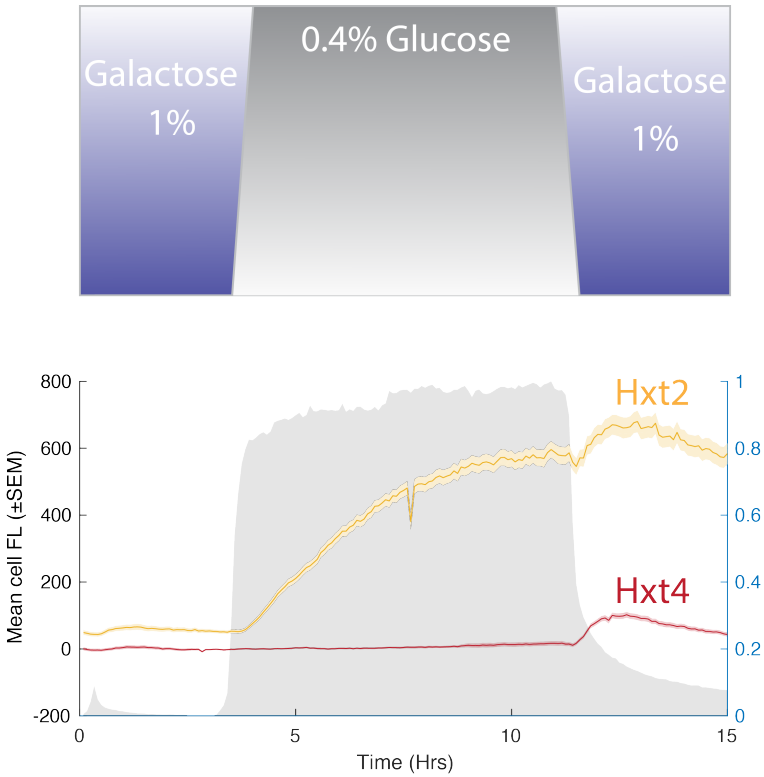

Figure 4.5: The downshift response of Hxt4 is robust to the presence of galactose. Top panel: schematic of the transition to which cells were subjected. Bottom panel: responses of Hxt2-yEGFP (yellow) and Hxt4-yEGFP (red) ± standard error of the mean. Fluorescence units differ from those of other figures.

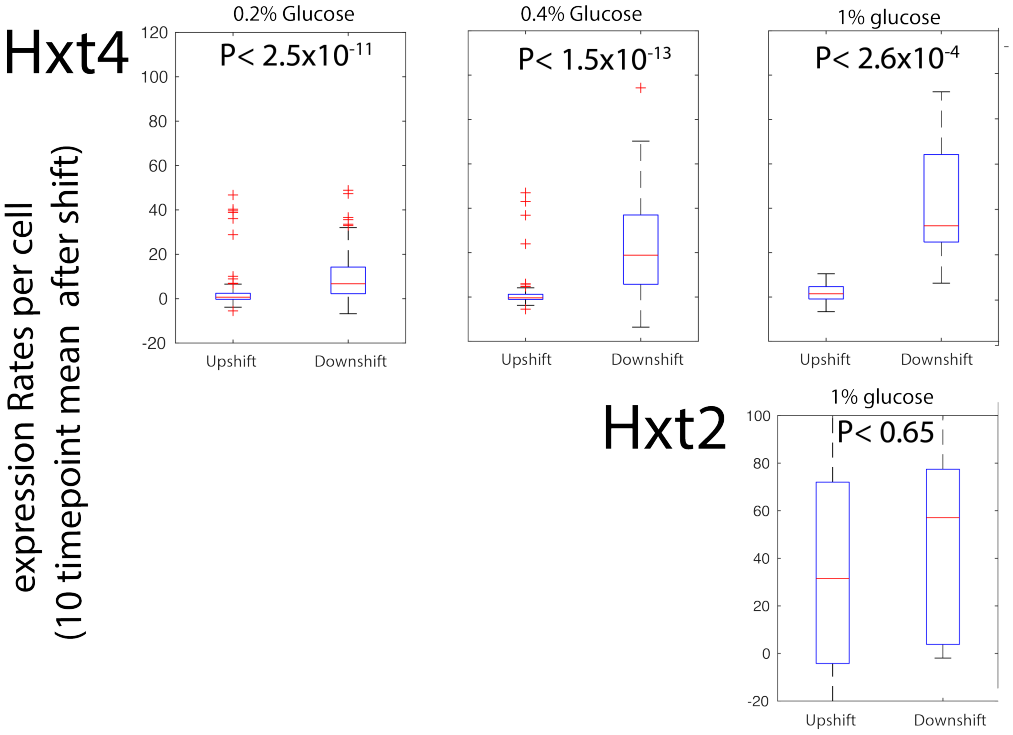

Figure 4.6: Hxt4 shows asymmetric expression rates in response to glucose upshifts and downshifts, in contrast with Hxt2. Boxplots show distributions of mean expression rates over 10 timepoints after an upshift or a downshift for individual cells after a glucose. Top row: Hxt4 in several concentrations. The time series can be observed in Figure 4.11. Bottom row: Hxt2, a transporter with similar affinity to Hxt2, at 1% glucose (data from Figure 4.2). P values were obtained for a Wilcoxon rank sum test on different medians.

to express at its activation regime, reported as similar to Hxt2-yEGFP. To test this, Hxt2 and Hxt4 cells were subjected to additional hats of 0.2% and 0.4% glucose. The response was significantly stronger in the downshift than in the upshift at all these concentrations for Hxt4-yEGFP (Figure 4.6, top row). In fact the downshift response became modestly stronger when glucose concentration was increased. In contrast, for Hxt2-yEGFP, expression was indistinguishably strong in both upshifts and downshifts (Figure 4.6, bottom row). In sum, Hxt4 expression is unequivocally responsive to a glucose downshift, whereas Hxt2 activation is more (if not completely) symmetrical.

Finally, to investigate the moment in which transporters localise to the vacuole or membrane, I designed a metric that quantified the distribution of the fluorescence mass across the cell area, yielding values < 1 for vacuole localisation

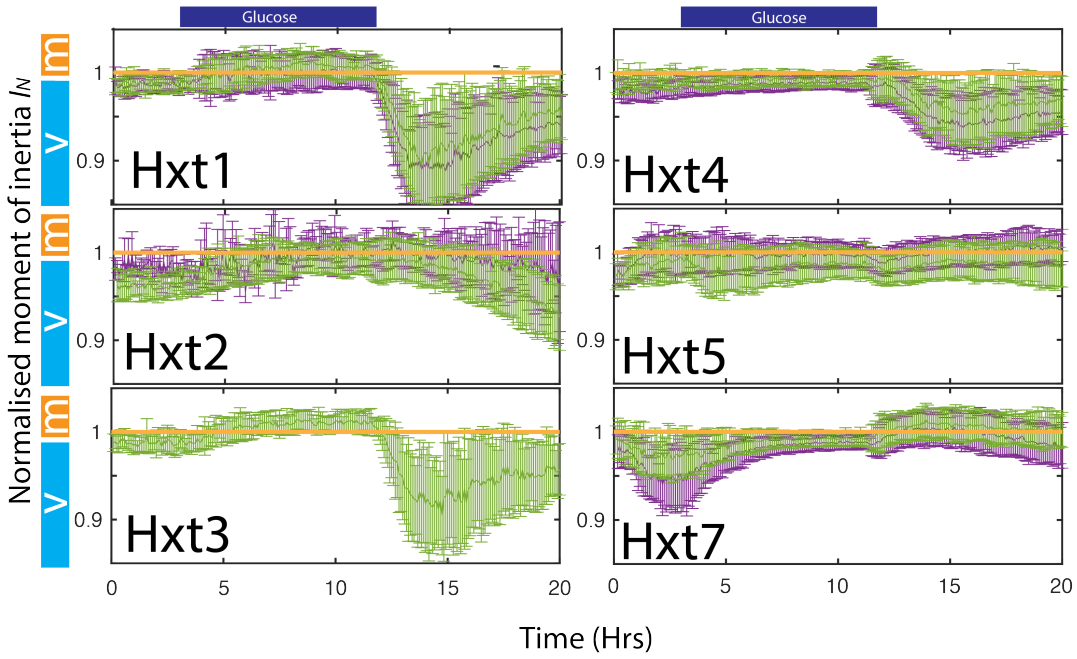

Figure 4.7: The normalised moment of inertia shows a reproducible vacuole internalisation dynamics. Each panel shows the normalised moment of inertia, which is meant to correspond to membrane ($I_N > 1$) and vacuole ($I_N < 1$) localisation respectively. Each panel shows data for a single Hxt in 2 independent experiments (no the same experiments per color). The line corresponds to the median with error bars corresponding to the interquartile range. Despite higher sensitivity to vacuole localisation than to membrane localisation, the trends are consistent. Navy blue bar above indicates the approximate glucose regime, while side bars are a reference regarding vacuole(v) or membrane (m) localisation.

and > 1 for membrane localisation, and values ≈ 0 for indistinct localisation. Figure 4.7 shows how membrane localisation is reproducible and consistent with gene activity, but not identical to it, and how Hxt4 appears at the membrane only during the downshift. Altogether, the network's ability to allocate Hxt4 to a glucose downshift, but not other transporters, supports the hypothesis that the function of hexose transporters is dynamically specified. The network can distinguish a dynamic feature of the glucose signal (its derivative) and harness those to dynamically allocate the expression of transporter Hxt4 [6]. Future work will improve on the metric's sensitivity to membrane localisation, whose sensitivity is not optimal and underestimates membrane localisation.

[6] low but rising levels of glucose ($dGlucose/dt > 0$) are processed differentially from low but falling levels of glucose ($dGlucose/dt < 0$)

4.7 Gradual glucose transitions (ramps) provide insight on the dynamic control mechanisms of hexose transporters

The above experiments have shown that the cell can control decisions regarding transport during a rather fast glucose transition. However, a gradual but consistent environmental change constitutes a different, perhaps more confounding situtation for the cells to respond to. I therefore hypothesised that slower transitions would provide insight on the dynamic asymmetry of Hxt4, and potentially reveal more subtle dynamic control of transporters. Therefore, the yEGFP-tagged strains were subjected to gradual transitions (ramps) of several duration from no sugar to 1% glucose medium and vice versa. Rather than monitoring expression levels, I quantified activation and de-activation of the genes by looking at the expression rate. For detailed explanation of why rates have been chosen used to monitor gene activity, please see the section C.3 of the appendix.

Figure 4.8 shows chymographs (image profiles of single cells) of the glucose ramps performed: a slow upshift and slow downshift. The chymographs correspond to the expression rates for each cell present in the entire experiment. In the following sections I describe in detail the responses of the Hxts, which I divide in categories.

4.7.1 Hxt1 and 3

It can be seen that Hxt1 and Hxt3, besides having qualitatively similar activation, undergo a precise rate switch already during the glucose ramp (Figure 4.8, region after black rectangles). This behaviour is not immediately obvious from the core network logic, as even small glucose amounts have been shown to cause major release of repressor Rgt1 from the promoter (Flick et al. (2003)). Immediate activation of Hxt2 and Hxt7 upon glucose exposure, and fast activation of Hxt1 upon a faster glucose upshift (Figure 4.8, top red asterisk) upon glucose exposure rules out a delay in transcription or translation as a cause for the delay

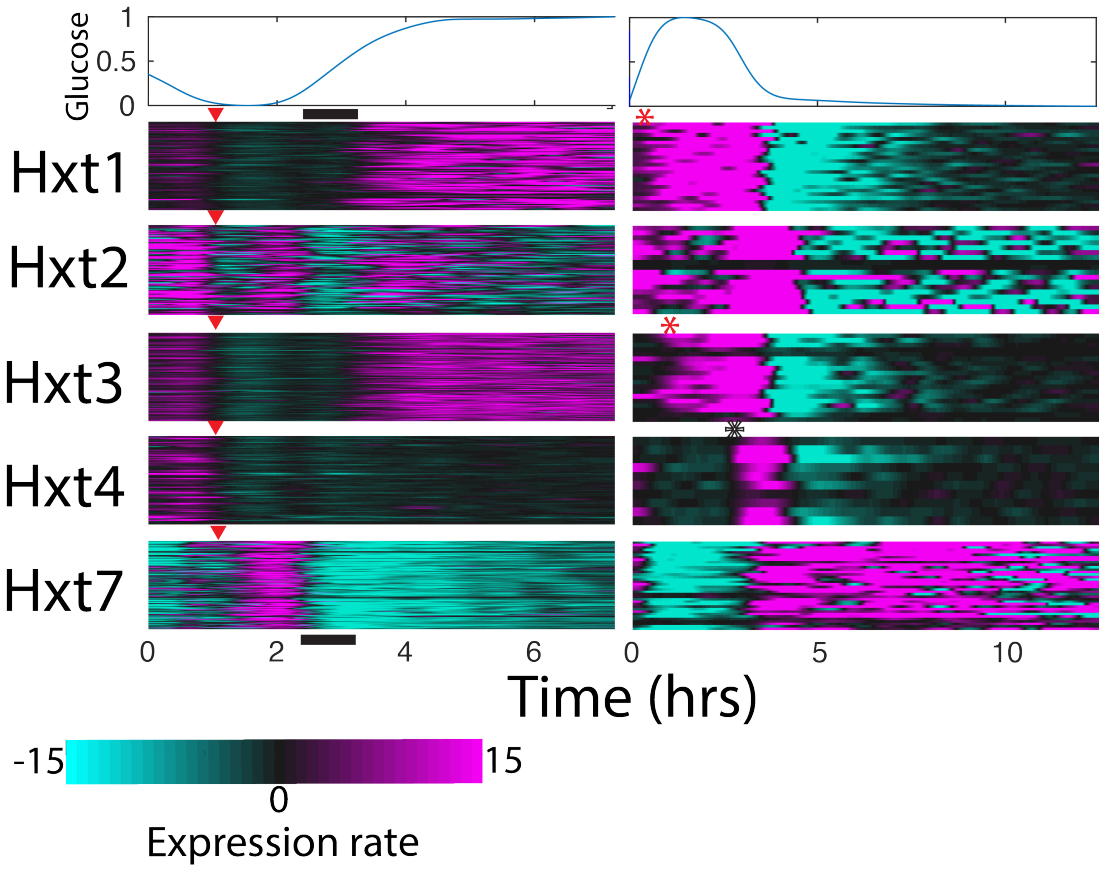

Figure 4.8: Glucose ramps reveal dynamic switching for different hexose transporters during transient glucose environments. Top row: normalised cy5 signal (% glucose) over time for 2 ramping experiments. Chymographs show expression rates over time for cells present in the whole experiment. Magenta and cyan indicate production and decay respectively. The rates (t^{-1}) saturate at 15 to allow comparison among strongly and weakly expressed Hxts. Each column corresponds to a different experiment. Red triangles indicate a depletion switch, which inactivates all Hxts shown except Hxt7. Black rectangles highlight a low upshift section where the transporters effectively decrease in concentration. Red asterisks indicate switching events (transition from an inactive to an active regime) for Hxt1 and 3, which are more divergent from each other compared to a slower ramp. The black asterisk indicates the switching time for Hxt4, which is mostly non–overlapping with the other Hxts shown.

in switching.

4.7.2 Hxt2, 4, and 7

As previously shown, Hxt2 is induced immediately upon entrance to a glucose environment (Figure 4.8, before the black rectangle region), and its production is stabilised upon transition to higher concentrations. This is consistent with the model that metabolism triggers repression of Hxt2 (perhaps caused by its own transport activity). In contrast, Hxt4 did not activate at any point during the upshifts, and activated fully in the downshifts (albeit within a concentration regime). Hxt7 showed activity mostly in non glucose environments, and when exposed to glucose hats, its activation occured at similar times as Hxt4. Yet, in batch cultures, Hxt4 would activate earlier than hxt7 (3.2).

Together, these results show that the glucose sensing network can dynamically allocate expression of transporters with similar reported affinities on the basis of environmental kinetics. The asymmetric activation patterns in rising and falling ramps suggest that the network's dynamics can activate different transporters depending on glucose history.

4.8 Dynamic Regime and slope analysis

In total, I performed 19 experiments, comprising a total of 37 rising and falling glucose ramps (see ramps in Appendix Figure B.2). The falling ramps were preceded by a 80 minute glucose step while changing the falling ramp's slope. To integrate results from all these experiments, each experiment was divided in 'regimes' separated by transition through 10% and 90% of the normalised glucose signal. The average expression rate in each of these regimes was obtained for every transporter (Figure 4.9, left panel). The heatmap averaging all the experiments (Figure 4.9, right panel) is in agreement with the two experiments shown in Figure 4.8. Hxt4 shows expression only in glucose downshifts and Hxt1 at higher glucose levels. Hxt1 showed a weaker signal during upshifts probably because the gene is inactive during the lower half of it.

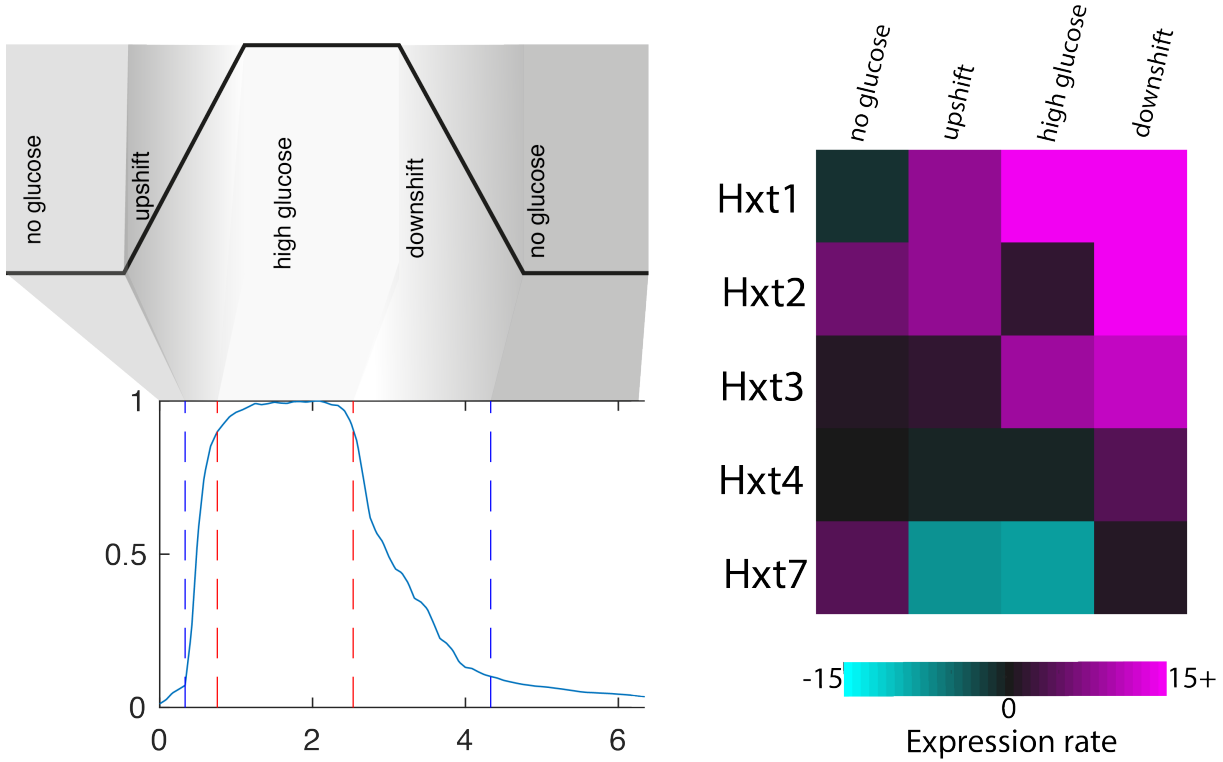

Figure 4.9: Hxts have different activation profiles across dynamic 'regimes'. Left: Experiments with a glucose upshift and downshift were heuristically divided in dynamic 'regimes' delimited by the crossing of 0.1 and 0.9 in the normalised cy5 signal (approximately the corresponding percentages of glucose), and each regime was classified as explained in the figure. 'No glucose' before and after the ramping were collapsed into the same category. Right: Heatmap of average expression rate (t^{-1}) per strain per regime. Rates saturate at -15 and 15 to compare across genes of varied expression strength.

The Hxt4 response may be caused by linking the environmental rate of change directly to th eexpression of Hxt4, such that the response of Hxt4 is proportional to the derivative of the environment, a strategy that could be exploited to the cell's advantage. To address whether the slope of the glucose ramp had an impact on the mean expression rate, I obtained linear fits for all the ramps in the experiments (see fits Figure B.3). A metric was proposed for transient response strength, which considered the total change in expression from the time of activation to the time of peak. (for details see section 2.7.2). Even though this metric recovered the sign sensitivity of Hxt4, no obvious trend was recovered regarding the slope and the Hxt response strength. This lack of trend could be because of confounding technical variation in some experiments [7].

4.9 Disruption of dynamic decoding in glucose sensing mutants

4.9.1 The falling glucose response of Hxt4 constitutes a model to decompose dynamic information processing in the glucose sensing pathway

The results shown above indicate transport regimes that are undoubtedly influenced by the glucose concentration. Hence we observe a coordinated switching of HXT gene activity at specific moments. Consider the switching events at t=1 hour or t=2.5 hours on the left panel of Figure 4.8. It is expected that those coordinated switching events are mediated by components of the network. One can hypothesise what components may play a role in particular transitions [8]. However, the previously highlighted dynamic asymmetries may be less straightforward to understand intuitively. Such is the particular case of the activation dynamics of Hxt4. While the activity of Hxt7 could be simply explained by glucose inhibition, similar concentrations of glucose lead to either activation or

[7] execution of ramps with identical slopes proved challenging

[8] For example, Mth1/Std1 are known to be in charge of repression in sugarless environments.

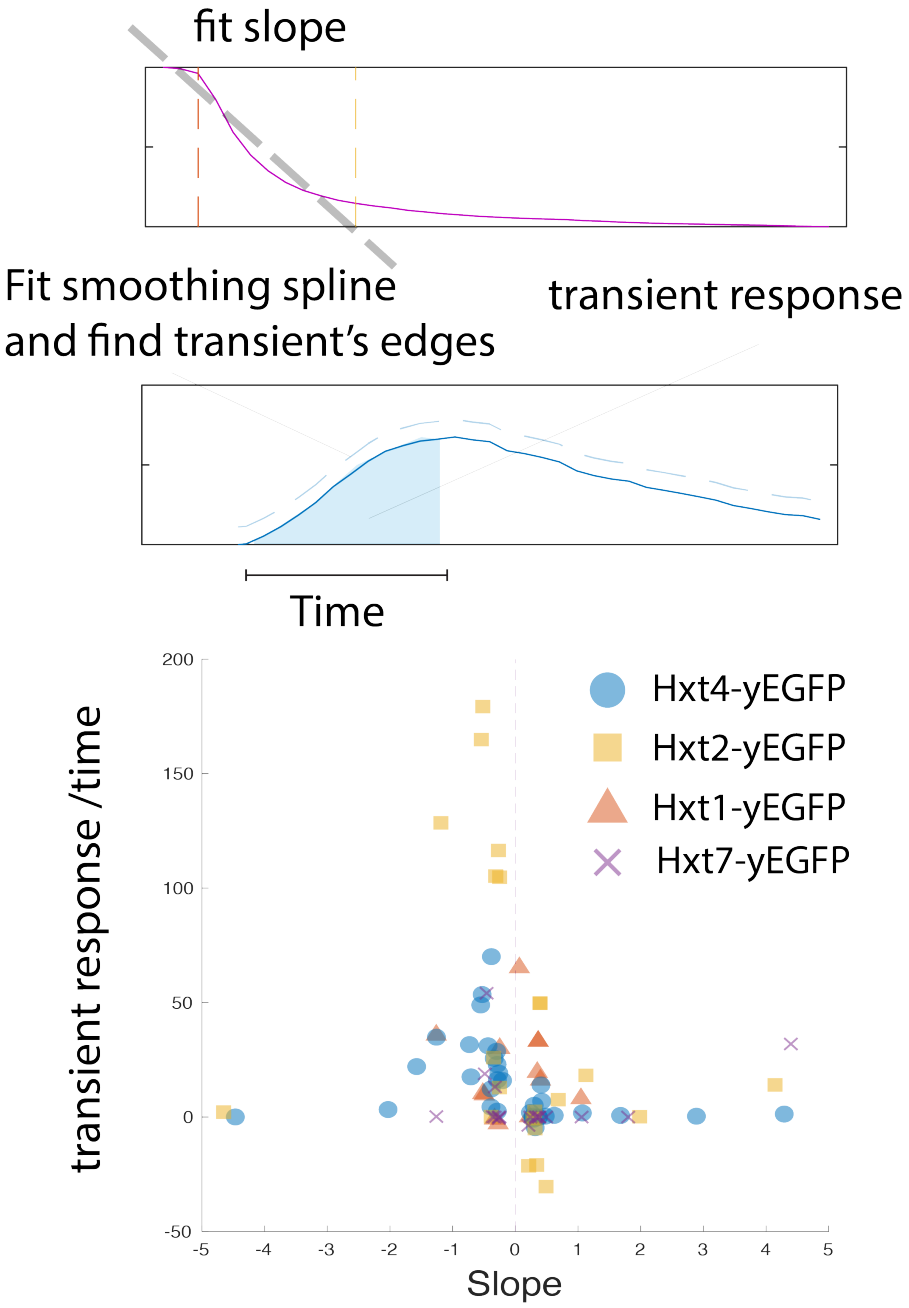

Figure 4.10: Quantification of transient responses to environmental rate of change. Top panel: The slope of a glucose ramp (magenta) was obtained by linear regression, and the transient response was obtained by fitting a spline to the mean expression, finding the transient's edges and averaging the positive production rates (see methods section 2.7.2. Bottom panel: graphs showing slope vs transient response over time in the ramp onset (left plot) or in the period after the ramp (right panel)

repression of Hxt4, conditioned by the environmental trajectory. The lower the repression threshold needed to explain repression during the upshift, the more difficult it will become to generate any response in the downshift, let alone a response half way through it, especially if the response must end upon depletion.

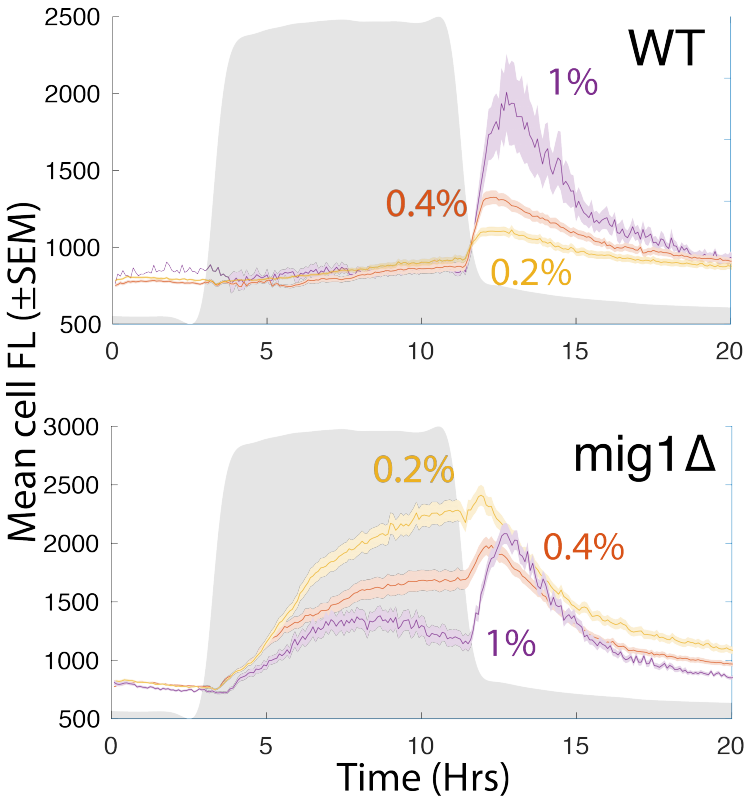

Figure 4.11: Hxt4 in the mig1Δ background is subject to additional repression by glucose. Shown are curves for hat transitions from sugarless medium to 0.2% (yellow), 0.4% (orange) and 1% (purple) glucose medium and back. Before the glucose downshift, the mean Hxt4 response (top panel) remains flat. Deletion of Mig1 was expected to render a constitutive Hxt4 activation regardless of glucose concentration. In the mig1Δ strain, Hxt4 activates during the upshift in all cases. However, total Hxt4 levels become lower with higher glucose, suggesting another layer of repression. Shaded grey area indicates the glucose regime. Lines are mean cell fluorescence ±SEM.

4.9.2 Dynamic alterations of the Hxt4 response in mutants

To gain deeper understanding about the activation dynamics of Hxt4 at a single cell level, I sought to investigate whether any genes in the pathway would disrupt

the observed glucose signal processing of HXT4. I hypothesised that the unequal responses of the paralogs in the network[9] could be driving the dynamic asymmetry observed (See section 1.7.2). Therefore I studied the dynamics of hxt4-yEGFP in strains where genes of the pathway were deleted.

The wild type and mutant strains were thus exposed to hats of 1%, 0.4% and 0.2% glucose starting from a reference, sugarless medium as previously shown. Similarly to the other sections, these hats were from sugarless, to glucose, back to sugarless medium. The data to be presented is from strains created in collaboration with Iseabail Farquhar, and are also used in chapter 3. Independent strains made through the knockout collection showed equivalent behaviour.

Appendix Figure B.6 describes the effect of the regimes in a 1% glucose hat to the expression rates in wild type and mutant backgrounds. From this overview it is clear that Mig1, Snf3, Rgt2 and Mth1 have different impacts in the response.

4.9.3 Dynamic layering of repression underlies the falling glucose response of Hxt4

Figure 4.12 shows chymographs for a mig1Δ strain in a 0.4% glucose step. Deletion of MIG1 caused the expression rate of Hxt4 to spike during (and only in) glucose upshifts, rendering the gene's response more symmetrical to environmental directionality. The fact that this response can become symmetrical by mutation constitutes further evidence that HXT4 has indeed been allocated to a strictly falling glucose regime by evolution, rather than it being an experimental artifact.

Given previous evidence that Hxt4 is majorly regulated by Mig1 (Westholm et al. (2008)), it was expected that its deletion would make the gene constitutively active. However, to my surprise, this was not the case. Exposure to higher glucose levels caused the maximum levels of Hxt4 to be lower (Figure 4.11), indicating another Mig1-independent, glucose level based repression of Hxt4. In contrast, the levels of the wild-type Hxt4 spike increased with higher levels of glucose. Finally, I note that the activation dynamics of Hxt4 in the mig1Δ strain beared strong resemblance to the response of Hxt2, though it was not identical.

[9]Specifically, MTH1-STD1, YCK1-YCK2, SNF3-RGT2, MIG1-MIG2-MIG3.

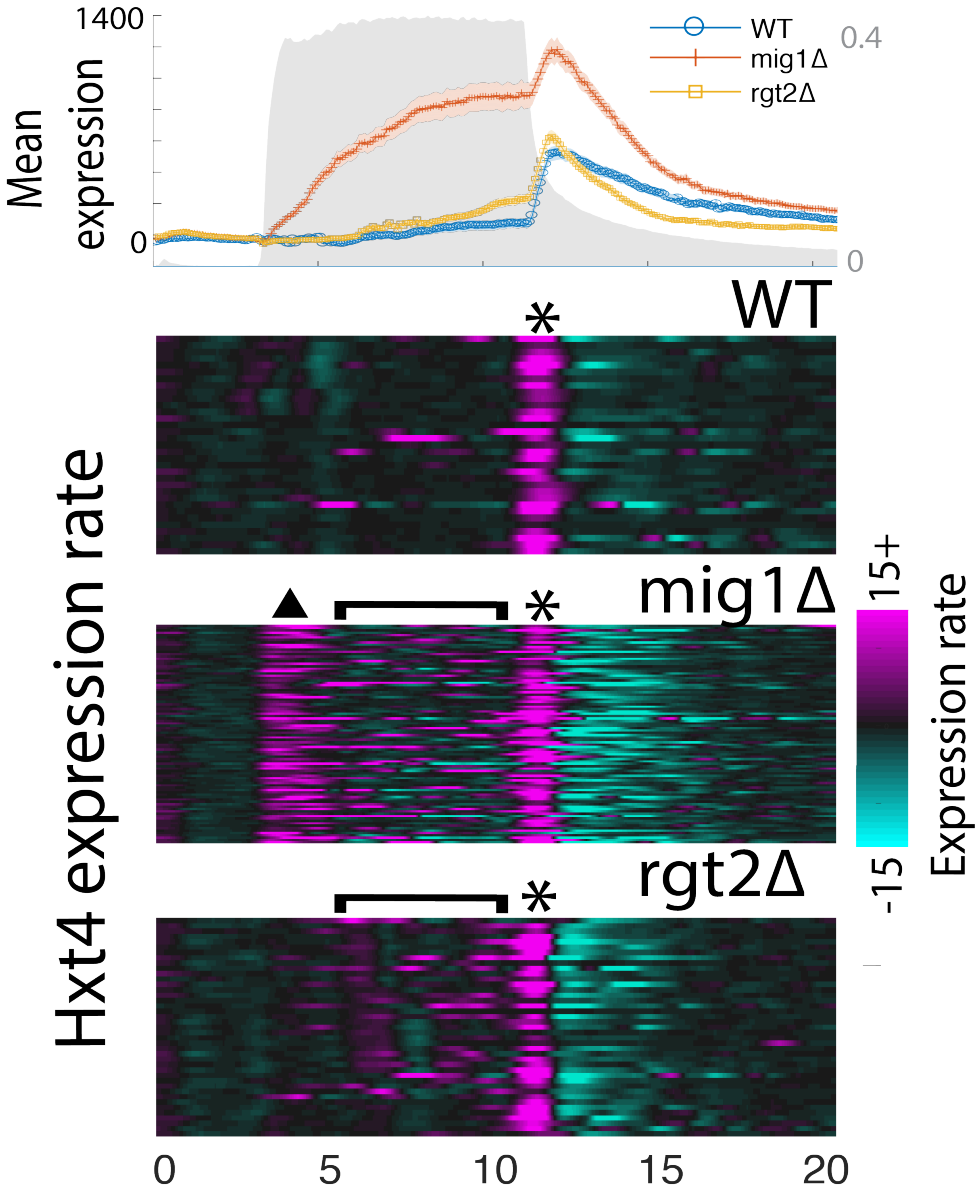

Figure 4.12: Mig1 and Rgt2 exert dynamic layers of repression over Hxt4. Cells were exposed to a 0.4% glucose hat (top panel) where strains showed the corresponding mean expression dynamics ($\pm SEM$). Chymographs show expression rates over time for individual cells (t^{-1}). Magenta and cyan correspond to production and decay respectively, with black as inactivity. Data is shown for wild type cells (2nd panel from top), which only activate in the downshift (black asterisks). In contrast, virtually all mig1Δ cells (3rd panel from top) activate in both the upshift (black triangle) and the downshift, with some cells remaining active during steady glucose (bracket region). The rgt2Δ strain (4th from top), remains fully repressed in the upshift (presumably because of Mig1) and follows a specific activation pattern during steady glucose. Rates saturate at —15— to emphasise more subtle activation dynamics.

Further screening revealed that deletion of glucose sensor Rgt2 did not affect the insensitivity of HXT4 to a glucose upshift, but derepressed the transporter's expression during longer, steady glucose environments (4.12, yellow line, bottom panel). This behaviour was consistent in 2 independently created strains. As derepression from a lack of RGT2 came later than that of a mig1Δ strain, for which a glucose upshift activated expression (Appendix Figures B.6, 4.19), it suggests that repression of Mig1 is not entirely dependent on Rgt2. It could be that Mig2 is responsible for this effect; however, Mig2 has been reported to repress HXT4 in concentrations around 10% glucose (Westholm et al. (2008)). Finally, de-repression of HXT4 due to a lack of sensor Rgt2 appears to be of through spiked, periodic bursts rather than of a simple cumulative dynamics. In glucose concentrations below 1%, some wild type cells behave similarly to the rgt2Δ background (Appendix Figure 4.19), suggesting that Rgt2 is a source of level-mediated control.

4.9.4 Deletion of paralogs Mth1 and Std1 results in divergent repression dynamics on Hxt4

While the behaviour of several strains had abundant overlap in 1% glucose, a 0.4% hat showed greater diversity across mutant phenotypes (Figure 4.13). To more directly compare the effects of each mutant versus the wild type, the mean fold difference relative to wild type was plotted (Figure 4.15). The plots show the wide range of dynamic effects that each deletion has over the dynamics of Hxt4.

If deletion of RGT2 caused a striking phenotype, even more striking was the dynamics of the std1Δ strain. Std1 is reported to be a corepressor of the HXT genes, so its deletion was expected to derepress Hxt4 to some extent. However, the std1Δ Hxt4 showed even stronger repression than the wild type wild type Hxt4 gene (Figure 4.13). I asked how a deletion of STD1 compared to that of MTH1, its functionally overlapping paralog. The role of Mth1 was more consistent with with a repressor degraded by glucose since the mth1Δ Hxt4 levels rose in the absence of glucose (Figure, 4.15, Figure 4.14). Paying close attention, the longer pulse of std1Δ Hxt4 upon glucose disappearance (Figure 4.13, purple line after downsift)

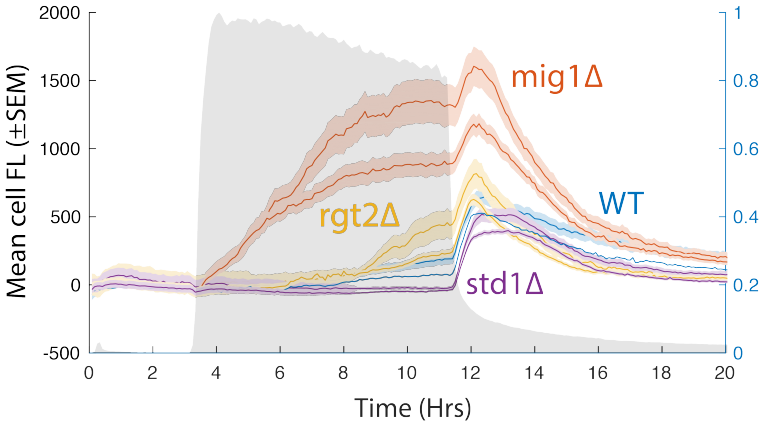

Figure 4.13: Hats of 0.4% glucose (shaded area) reveal dynamic differences among mutants. Data is the average GFP channel fluorescence after background subtraction ± SEM over time. Same coloured lines correspond to biological replicates. Note how the std1Δ achieves a flatter response than the wild type, yet presents a rounder pulse upon glucose disappearance. Ranks among strains are preserved at t=10 in both replicates ($P < 0.0003$)

suggests that Std1 can behave both as an activator or repressor depending on environmental trajectories.

Finally, the expression levels of Hxt4-yEGFP mth1Δ resembled those of Hxt7, so I wondered whether Hxt7 would be identical to Hxt4 without Mth1 regulation. Appendix Figure B.7 (top panel) shows that the mean levels of both proteins are similar. However, their vacuole internalisation dynamics with the Moment of Inertia B.7 (bottom panel) revealed divergent destinations for each during glucose exhaustion. This suggests that deletion of Mth1 is not enough to make both transporters equivalent.

These widely divergent behaviours of paralogs suggest that Mth1 and Std1 act through different repression mechanisms. This possibility is not entirely new (Horák (2013)), but a dynamically conditioned role of Std1 as a repressor or activator was not previously considered.

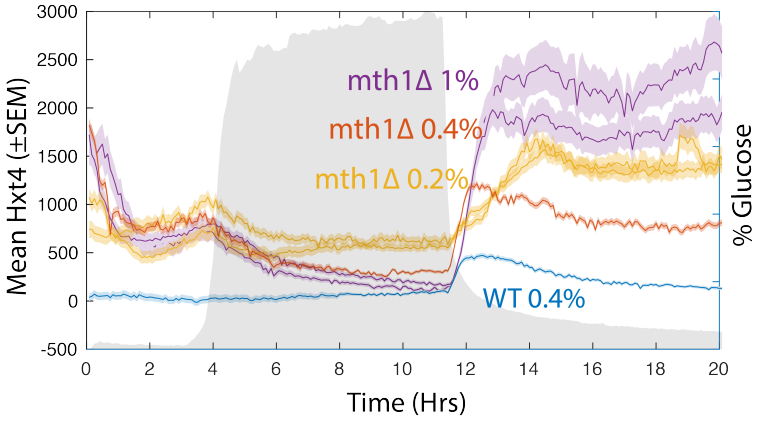

Figure 4.14: Deletion of Mth1 releases Hxt4 repression during non-glucose environments. Lines show mean cell fluorescence ±SEM from sugarless medium to 0.2% (yellow), 0.4% (orange) and 1% (purple) glucose medium and back. One wild type Hxt4 curve at 0.4% glucose is shown for reference. Shaded grey area indicates the glucose regime. The complexity of the curves shows how Hxt4 is subject to multiple control mechanisms. In the deletion, the basal non glucose level of Hxt4 has increased, and glucose level dependent repression is noticeable as levels of Hxt4 drop with higher glucose. Absence of Mth1 causes an overall higher level in the downshift than that achieved by the wild type.

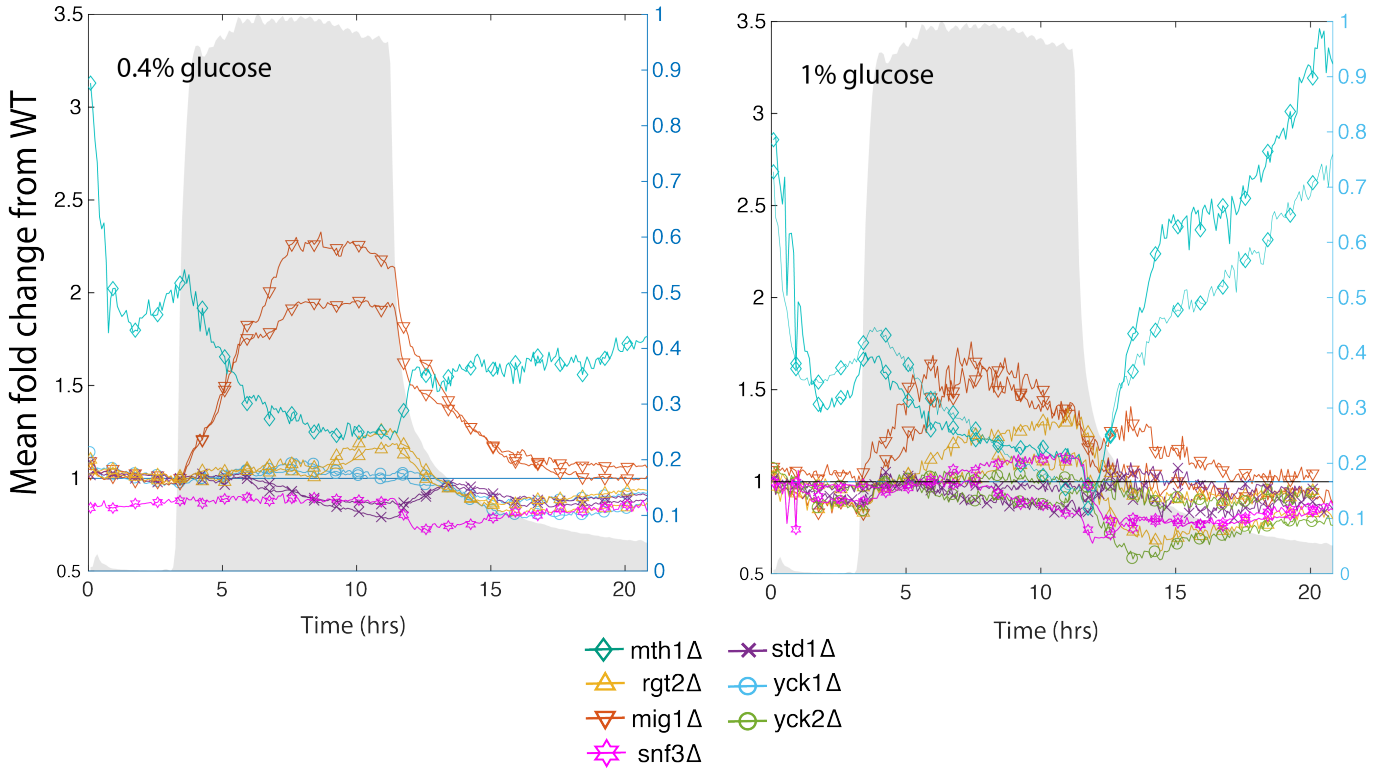

Figure 4.15: Mutants alter wild type signal processing in different ways. The mean GFP fluorescence of each of the mutant was divided by the mean GFP fluorescence of the wild type. The fold change from the wild type to each knockout is plotted over time. Duplicate lines correspond to independent biological replicates. Shaded grey area corresponds a reference for the occurrence of the glucose step; the cy5 signal from each experiment may vary from case to case, and the same reference is used for simplicity in both plots. Most mutants have dynamic effects that are different from each other mostly in uncorrelated ways. However, the rgt2Δ and std1Δ strain show negative correlation, suggesting both components are mechanistically interconnected.

4.9.5 Std1 and Rgt2 are opposing regulators of the same Hxt4 repression mechanism

Figure 4.15 also shows the rgt2Δ Hxt4 (yellow) and std1Δ Hxt4 (purple) dynamics. While the mth1Δ and mig1Δ strains diverge strongly from the wild type before or immediately after glucose addition, the rgt2Δ and std1Δ strains both take longer time to achieve a noticeable effect in the dynamics. At 0.4% glucose (t $\approx$ 10) (Figure 4.15 left panel), both mutants affect the wild type by similar factor in opposite ways. These results suggest that Rgt2 and Std1 may be antagonists regulating the same repression mechanism.

Finally, the yck1Δ and yck2Δ deletions remained close to wild type behaviour for most of the dynamics tested. However, along with the rgt2Δ and std1Δ strains, they showed a smaller falling glucose peak than the wild type (Figure B.6, fourth box plot panel). It is possible that the kinase levels at the membrane affect the maximal degradation rate of co-repressors Mth1 and Std1 or affect the transporter's degradation rate, thereby decreasing the final expression peak. But more data is needed to quantify a precise trend for the effects of these kinases. I conclude that yeast casein kinases do not contribute differentially to Hxt4 dynamics.

4.9.6 Mig1 localisation dynamics correlates with the time derivative of the glucose environment

Previously in the chapter I hypothesised that the ability of Hxt4 to bypass the response to a glucose upshift suggested that some moiety in the network was sensing the time derivative of the glucose signal, and linking it to Hxt4 such that a positive derivative would trigger repression, whereas a negative derivative was mapped to activation. The fact that a mig1 deletion rendered the Hxt4 response more symmetrical by enabling a fast upshift response (Figure 4.13) [10] hinted at Mig1 being at least part of this derivative processing. I thus set to address whether the nuclear localisation dynamics of Mig1 contained any clues toward

[10]This effect was almost exclusively during the upshift, as opposed to Rgt2

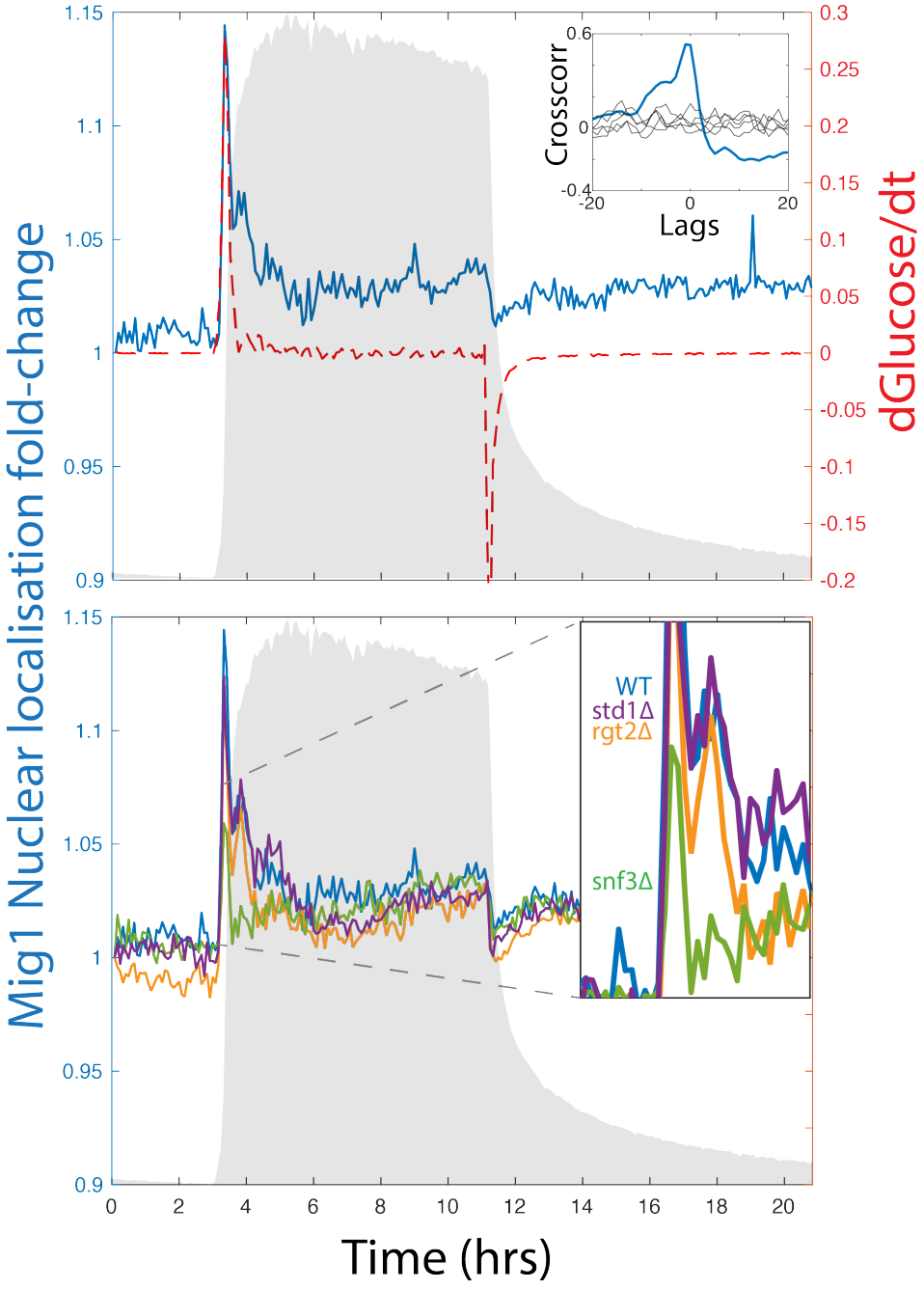

Figure 4.16: Nuclear localisation of glucose repressor Mig1 is temporally correlated with the time derivative of the glucose environment. Top panel: Fold change in nuclear localisation of Mig1 from a population of wild type cells (blue, left axis) in response to a 1% glucose step (shaded grey area). Shown is the mean localisation for all cells normalised by the value at $t = 0$. The derivative of the glucose step (dotted red line, right axis) is overlaid for comparison. Inset shows the cross–correlation with the derivative of the glucose signal of the nuclear localisation signal (blue), and 5 artificial time series sampled from a uniform distribution (black)). Bottom panel: Mean fold change in nuclear localisation of Mig1 for the wild type (blue) and glucose sensing deletion backgrounds snf3Δ (green), rgt2(orange), std1Δ(purple).

this derivative processing.

Figure 4.16 (top panel) shows the fold change in Mig1 nuclear shuttling from the beginning of the experiment, as measured through a commonly used metric (See methods 2.7.3). It can be seen that Mig1 undergoes a sharp nuclear spike, and the peak then drops, but reaches a level higher than pre-glucose conditions. Localisation sharply drops during the glucose downshift. Data exploration revealed that the spiking dynamics of Mig1 had a strong overlap with the temporal gradient of the glucose signal (the signal's time derivative), even though the repressor's dynamics is not exactly equivalent to the time derivative (Figure 4.16, top panel). Altogether, I conclude that the dynamic asymmetry observed in Hxt4 expression dynamics is a consequence of the reporting of the time derivative by its repressor, Mig1. The fast spike of Mig1 could therefore prevent hxt4 levels from immediately rising, and fast translocation of Mig1 back into the cytoplasm during a glucose drop would enable expression of Hxt4, provided that no other repressors are present.

4.9.7 A snf3Δ knockout affects nuclear shuttling dynamics of repressor Mig1

Having noticed that the rgt2Δ Hxt4 must escape Mig1 repression somehow to achieve expression late after addition of glucose (Figure 4.12, bottom panel;, yellow lines in Figures 4.15 and B.4) I reasoned there were at least two potential mechanisms for this escape. First, the Mig1 localisation valley after the initial spike (Figure 4.16) may be so low as to allow derepression of some targets such as Hxt4. Second, lack of Rgt2 may inhibit high glucose transport, which could decrease glucose metabolism and hamper the stability Hxk2/Mig1 complex at the HXT4 promoter (see Figure 1.4). Third, perhaps the general Mig1 dynamics has been altered in the glucose sensing mutant backgrounds such as Δrgt2. To distinguish among these alternatives, I asked whether Mig1 localisation dynamics would be altered in backgrounds defective in glucose sensing. To this end, a Mig1-yEGFP strain was crossed with strains carrying deletions for the glucose sensing pathway.

Figure 4.16 (bottom panel) shows how the localisation dynamics of Mig1 remains generally undistinguishable for most deletions assayed. However, to my surprise, the only noticeable effect on Mig localisation was seen in the snf3Δ were the size of the localisation spike is diminished, but still present. This suggests that alterations in the sensing pathway can ultimately feed back onto Mig1 mediated glucose repression. This could counterintuitively derepress HXT gene expression.

4.9.8 The HXT4 promoter recovers the activation dynamics of the Hxt4 protein, but not its depletion induced decay

In the previous chapter I showed that the promoter of HXT4 alone can recover the activation dynamics of Hxt4 in batch culture. It was therefore expected that the downshift response was similarly recovered with the promoter. Figure 4.17 shows that the microfluidics results are consistent with the batch culture experiments (Figure 3.7). That said, the levels of the transcriptional fusion remained steady after glucose was depleted, in contrast with the translational fusion. This suggests that the Hxt4 protein is actively degraded in response to glucose depletion.

4.9.9 Removal of potential Mig1 sites eliminates the upshift repression of pHXT4

In the previous chapter I introduced a synthetic version of the HXT4 promoter whose potential core Mig1 binding sites had been removed (Figure 3.10). This promoter lost the delayed timing present in the native version. Figure 4.18 shows that the pHXT4noSTRE promoter is strongly induced during the glucose upshift and achieves high steady state levels after about 4 hours. Importantly, steady state levels vary widely among cells, reaching up to 18 times higher than the wild type. The sharp entry to steady state suggests a layer of Mig independent regulation preventing further increase in Hxt4 levels after this point. It is possible that Rgt2 is (presumably in an indirect way) responsible for this repression.

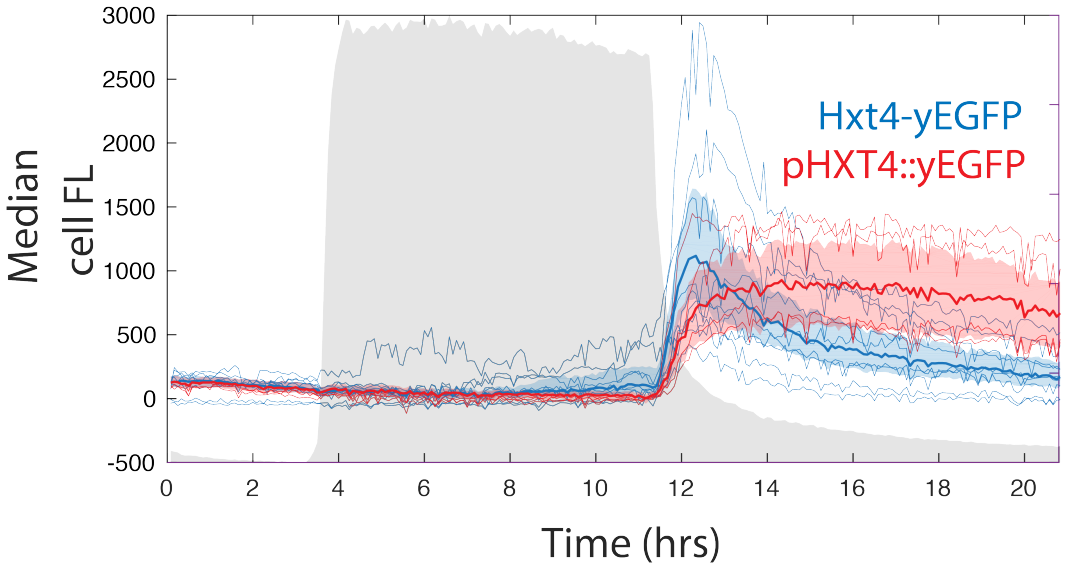

Figure 4.17: Different decay kinetics for Hxt4-yEGFP and pHXT4::yEGFP upon glucose depletion suggests active degradation of Hxt4. Plot shows the median cell fluorescence over time for translational fusion Hxt4-yEGFP of the native gene (blue) and an independent transcriptional fusion pHXT4::yEGFP (red) inserted into the URA locus. Thick line corresponds to the median. Coloured shaded areas correspond to the inter quartile range of the cell population. Shaded grey area corresponds to a 1% glucose step.

Alternatively, some growth mechanism may activate after 4 hours, for example, fast growth, which may allow to level Hxt4 expression [11]. Altogether, these results provide evidence that HXT4 is subject to tight, dynamic control caused mainly by Mig1 and other potential sources, even though the promoter's transcriptional capacity is at least as high as that of other major hexose transporters.

4.10 Chapter 4 Discussion

In this chapter, I have provided evidence that hexose transporters undergo extensive dynamic control orchestrated by glucose signals and that most transporters' expression have fundamentally different dynamics. However, the glucose sensing network must be able to provide the regulation necessary to satisfy all these dynamic states. The contribution to fitness of each transporter may be related to this dynamic allocation.

[11] Dilution by division, for example, would assume inheritance of Hxt4 to daughters. No evidence is presented in this direction

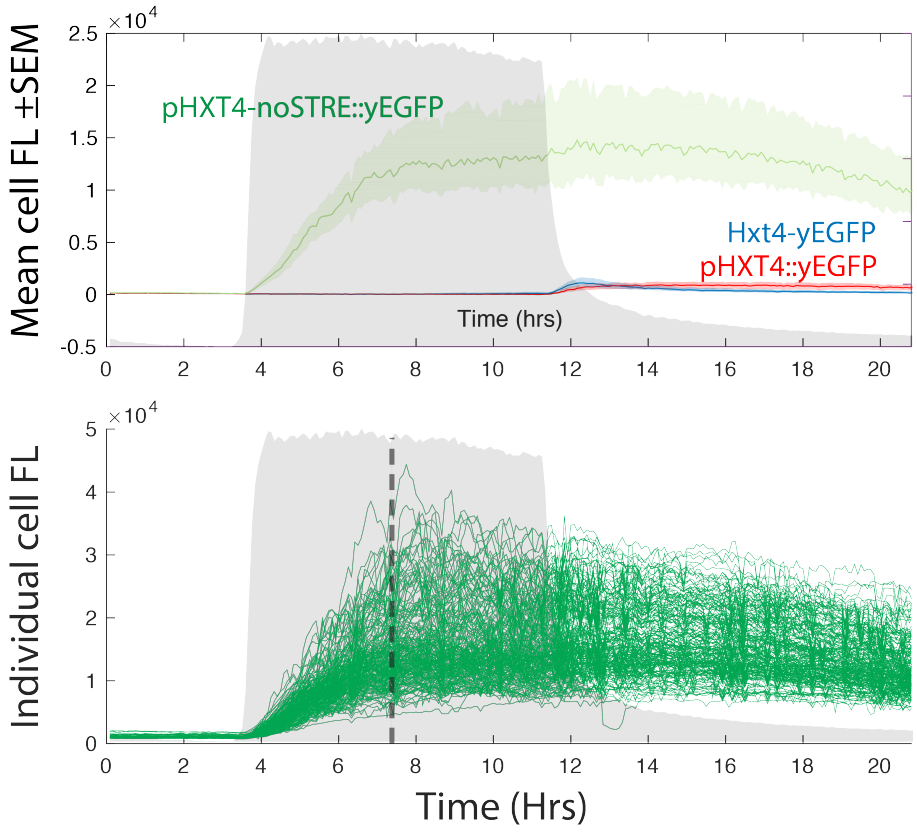

Figure 4.18: Removal of potential STRE sites fully derepresses the pHXT4 promoter during glucose upshifts. Top panel: Median fluorescence over time ± inter quartile range (coloured shaded areas) for promoter pHXT4noSTRE::yEGFP, whose potential Mig1 sites hae been removed. The Hxt4-yEGFP (blue) and pHXT4::yEGFP (red) plotted fully in Figure 4.17 are also shown for comparison. Shaded grey area indicates a 1% glucose step. Bottom panel: Single cell fluorescence traces (minus background) to show the extent of variation of the pHXT4noSTRE. Dotted line highlights an interval at which most traces stop increasing in fluorescence (steady state), suggesting that another mechanism is responsible for inhibiting expression after this point.

I have shown that hexose transporter Hxt4, despite being a transporter that is expressed to lower levels than other Hxts, is the only one of the major hexose transporters 1-7 that is dynamically conditioned to be expressed strictly in a glucose downshift regime (section 4.5.1). This downshift response explains the increasing delay in Hxt4 expression seen in batch cultures when glucose is higher (section 3.6).

The evidence I have provided for this phenomenon consists of two sources. First, I have designed dynamic environments to distinguish between a response based purely on glucose levels and one based on the kinetics. Glucose hats of 3 different concentrations were not enough to activate Hxt4, whereas a glucose downshift triggered a stronger response than 8 hours of glucose regardless of the concentration and duration of the glucose step (Figure 4.4). The strength of the downshift response correlates with glucose concentration (Figure 4.11, top panel). Second, I have shown that this downshift response can be ablated by engineering strains (through knockout or synthetic biology), where the exclusivity towards a downshift response is lost, thereby rendering the response more symmetrical to the directionality of the glucose input. These results constitute strong evidence that the glucose sensing network is invested in decoding the dynamic identity of environmental glucose, and exerting gene and transport regulation with this information.

4.10.1 A hypothetical mechanism driving the downshift response of Hxt4

The wild type and knockout data collected provides a temporal dimension to activation and repression of transporters. One working model obtained from this data can be observed in Figure 4.20. In general, as the deletion of Mth1 increased the basal levels of Hxt4, Mth1 must be repressing the gene in the absence of glucose. The spike of Mig1 localisation during the upshift (Figure 4.16) would then take over given that the absence of Mig1 activates a strong upshift response (Figure 4.13). Activation of Rgt2 during steady (high) glucose would then preserve the repressed state of the gene, even if cells may escape repression

of Mig1. Therefore, absence of Rgt2 would allow more cells to derepress later during glucose. The conclusions obtained here are consistent with those obtained in the batch culture chapter (Section 3.13).

4.10.2 A gene expression 'blind spot' in Hxt regulation

A surprising finding was that slow glucose upshifts manifested a 'blind spot' where no hexose transporter underwent production (Figure 4.8, region between black rectangles). This region presents cyan protein decay signals in the chymographs of all Hxts. I cannot claim that no other transporter is being produced there as there are 20 possible hexose transporters that could take this role. Nevertheless Hxt1-7 are the major transporters (Hxt6 behaves shows a highly similar dynamics to Hxt7 in hats (4.2) so Hxt7 was chosen because of limited space in the same experiments and higher uptake rate of Hxt7 (Reifenberger et al. (1997))). Even though there are transporter molecules present, it could be that excess transport is undesirable for this particular condition, or that the condition is not informative enough to decide for a specific type of transport. Hxt2 and 7 do activate at a lower concentration and remain at a high level, implying that at least Hxt2 is being preemptively produced for this regime (Hxt7 is targeted to the vacuole in glucose). Finally, neutralising production of transporters entirely may prevent the potential toxicity generated from a glucose overload in the initial steps of glycolysis, where too much energy investment in the initial reactions may cause a large accumulation of glucose-6-phosphate, energy depletion and subsequent growth arrest (Teusink, Walsh, Van Dam & Westerhoff (1998), van Heerden et al. (2014)).

4.10.3 Temporal effects of noise in gene expression depend on specific regulators

Studies on the noise in gene expression focus on the variance of expression levels for one gene or product like Hxt4. The current results suggest not only that the variance itself is important, but at what moment in time the variance of

Hxt4 is affected by the absence of a certain regulator. Figures 4.15, B.6 and 4.19 demonstrate how the lack of Mig1 causes expression variance soon after upon the appearance of glucose. In contrast, a Rgt2 knockout also induces variation among cells, but takes longer to do so (Figure 4.19). These two sources of repression are mostly non-overlapping as one begins were the other ends (C.3). Therefore, noisy activation of cells in either of these dynamic regimes is essentially informative about what moiety of the pathway is the source of noise. More concretely, cells that may show sporadic activation either in the first 4 hours or afterwards are likely experiencing noise either through the Mig1 than through Rgt2 moiety, and viceversa for the last 4 hours.

4.10.4 Judging network dependencies through dynamic effects

Levels of Hxt4 in the mig1 deletion stop increasing after 4 hours (figure 4.15 orange lines). Consistently, the levels of pHXT4noSTRE promoter, which has been stripped of all potential Mig1 sites, also stop increasing at 4 hours (Figure 4.18). If Rgt2 exerts repression through the exact same mechanism as Mig1, How then can it be that the rgt2 knockout *starts* derepressing at a later time? (Appendix Figures C.3 4.19) This leads to hypothesise that Rgt2 is acting *independently* of Mig1 regulation. It would be predicted that the levels of the pHXT4noSTRE fusion will be higher when screened in a rgt2Δ background. In contrast, the fact that rgt2Δ and std1Δ show opposing variance across the same temporal components (Appendix Figure B.5) invites to speculate that both genes are part of the same functional branch, perhaps cross–inhibiting each other.

4.10.5 Limitations

Technical limitations in the microfluidic switching

The approach herein presented limits any conclusions that may be desirable about the glucose concentration in transient regimes. The microfluidics devices often showed higher brightness in the cy5 channel after cy5 pumping ended. This is

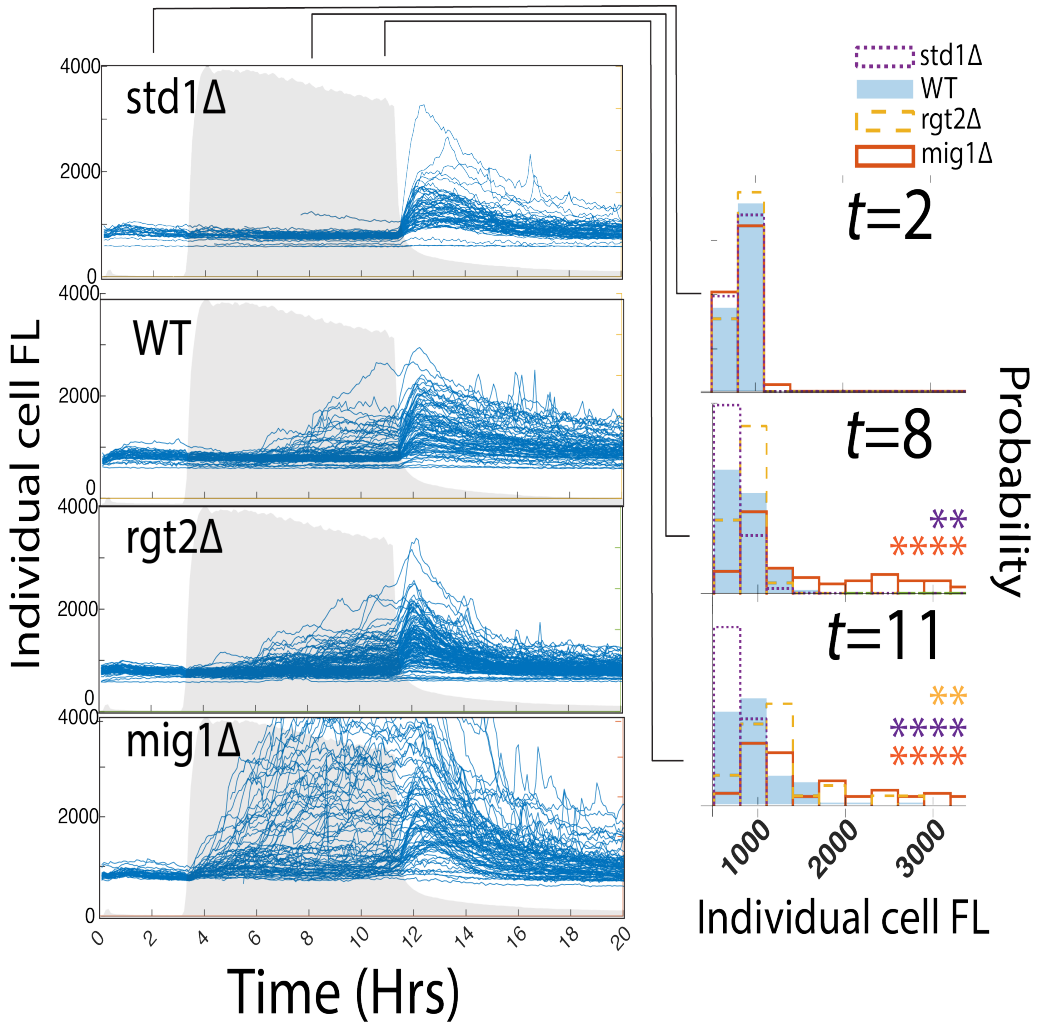

Figure 4.19: Temporal effects on Hxt4 variance in mutant backgrounds, for a hat of 0.4% glucose. Left panel: Hxt4 fluorescence in cells of different backgrounds, from most repressed (std1Δ, top) to earliest derepressed (mig1Δ, bottom). Right panel: Fluorescence distributions for WT (filled blue), mig1Δ (orange), rgt2Δ (yellow), std1Δ (purple) at 2 (top), 8 (middle) and 11 (bottom) hours. Each distribution was tested for equal median to the wild type with a Wilcoxon rank sum test. Asterisk number indicates P value significance for a strain: two for $P < 0.001$, four $P < 10^{-5}$ down to ($P < 10^{-10}$ for mig1Δ). A few mig1*Delta* outliers > 800 were cropped out for visualisation purposes.

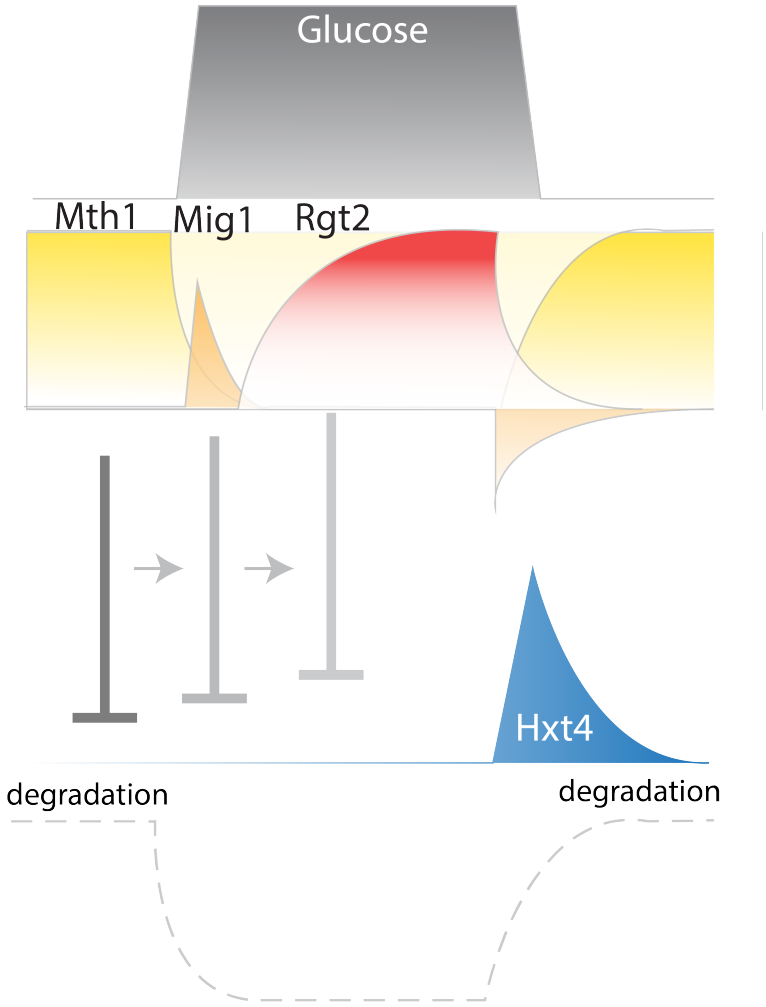

Figure 4.20: Cartoon model depicting the phenomenology that accounts for the downshift response of Hxt4 according to the chapter's results. Mth1 (yellow) represses in the absence of glucose. Mig1 (orange) represses during a glucose upshift. Derivative processing by Mig1 means that its levels can go down, at which point cells may escape repression. However, Rgt2 repression (red) takes over by glucose levels. The protein is degraded when glucose disappears (bottom, dotted line). In a downshift, all four repression mechanisms are temporarily absent, enabling a spike of Hxt4. The role of Std1 is less clear, but its knockout has the opposite effect that of an rgt2 knockout (Figure 4.15). Therefore Std1 may be an antagonist of Rgt2.

probably due to a high affinity of cy5 to PDMS, and an exponential decay of the fluorescence signal. These two events limited our capacity to monitor exactly when glucose would be depleted. Glucose assays (Figure 3.6) showed that the peak of Hxt4 expression was reached upon depletion. Taking an Hxt4 peak as a proxy for the moment of glucose depletion, the sugar appears to be depleted almost concomitantly with the end of most ramps, even in the downshifts that showed a smoother decay or a higher terminal cy5 level. The delay between the imaging and the passing of the liquid through the device complicated the sampling of the sugar in real time, especially through the fast slopes. To ameliorate these problems, I made sure that the glucose pump was set to 0 after the transition to guarantee a sugarless environment. Even though the environment is programmed to switch at similar times for any hat programme, Hxt4 takes longer to reach its peak in coming from a higher glucose, suggesting that the higher levels of Hxt4 may be just because of longer exposure to glucose (Figure 4.11).

Microfluidics may break feedbacks that are relevant for HXT function

The environment of the traps and the microfluidics is not exactly natural or comparable with a batch culture as in the former the media is constantly replenished for new media, thus preventing metabolites, toxins or even enzymes to accumulate in the surrounding environment of the cells. This could potentially break some feedbacks that are important to trigger the activity of some Hxts. An example of a feedback could be from communication or physical contact between neighbouring cells, which may affect gene expression. Some enzymes such as invertase (Suc2) are secreted to the periplasm to facilitate the breakdown of sucrose into glucose and fructose (Carlson et al. (1983)).

Other important metabolites being washed away are acetaldehyde and ethanol. In microfluidics, the entire medium is changed to fresh medium every few seconds, which is considerably faster than a chemostat, in which such dilution rate would likely cause an unsustainable culture. The absence of such metabolites may impact enzyme levels, metabolic fluxes and thereby influence transporter activity (Section 1.6.7, De JongGubbels et al. (1995), Richard et al. (1996)) For

example, ethanol may facilitate entry into respiration by inhibiting HXT1 or Rgt2, perhaps via Std1 activity (Tillman et al. (1995), Kuchin et al. (2003)). This can be tested by observing the derepression dynamics of Hxt4 in mixtures of glucose and ethanol.

Immediate turnover of medium may prevent any build up of functional extracellular secretion. Feedbacks like this, although more confounding, may prove important to activate or differentiate the hexose transporters. Despite this possibility, the behaviour of Hxt4 was robust, albeit with different magnitude. Nevertheless, the artificial features of the microfluidics environment may actually expose the environmental feedback mechanisms that otherwise would remain intractable.

Noisy and heterogeneous cellular activity is filtered out by central tendency statistics

Although an effort was made to represent the complexity of single cell data, it will be noted that individual cells may sometimes diverge largely from the mean of the population. For example, observe the single cell traces in Figures B.1 and 4.19. Studying the cells through central tendency statistics, as I have done here, may hamper the study of heterogeneous decision making. This is a valid concern: in many wild type experiments there were cells that passed as mutant genotypes. However, a large proportion of the population followed a similar trend, and some conditions showed a majorly (if not completely) uniform behaviour across cells. The biological replicate pairs (Figures 4.13,4.2) and chymographs (Figure 4.8) show that the the probability distributions of Hxt activation are biologically consistent. That said, heterogeneous activation of Hxt4 was particularly more frequent in the rgt2Δ background. Future work will pay closer examination to the heterogeneity in the responses, which could be influenced by cell size or cell cycle stage.

4.10.6 Mechanistic insights about the regulation of hexose transporters

The derivative reporting of Mig1 (Figure 4.16) is likely the main driver for glucose upshift repression. This finding, albeit informative about the biology of Mig1, is not surprising. Other groups have speculated that Mig1 performs rate measurements (Bendrioua et al. (2014)) and that there must be flux sensing system somewhere in the glucose sensing pathway (Huberts et al. (2012)). What has been striking is that this derivative processing is directly harnessed to determine the right environment to express a gene.

In terms of other findings about gene regulation, the intervention of Rgt2 as an inhibitor of a hexose transporter, and the potential role of Std1, are perhaps the most surprising finding. Most studies have analysed the effects of Rgt2 and Std1 on Hxt1, a transporter considered a flagship for glucose transport. The results presented reveal that knock out of Rgt2, which probably would lead to faulty activation of Hxt1, could cause a kickback effect and activate Hxt4. This could comprise a distributed emergency system to keep fermenting upon a sudden fault in environmental sensing or low affinity transport. Consistent with this, Hxt4 was found to be unaffected by blockage of respiration (See section 3.8).

The opposite regulatory effect of Rgt2 and Std1 may take place directly via interaction (Schmidt et al. (1999)) or indirectly. For example, the system could regulate repression at the promoter or via interaction of Std1 with Snf3 or Snf1 (Figure 1.4, Tillman et al. (1995), Kuchin et al. (2003)). Importantly, one study found that the lag time between a glucose/maltose transition was made shorter or longer only by mutations in STD1 or HXK2 (New et al. (2014)). Both proteins are able to bind promoters: Hxk2 establishes repression together with Mig1, whereas Std1 has been found to activate (Tillman et al. (1995)) or repress genes (Moriya & Johnston (2004), Sabina & Johnston (2009)). Therefore it is possible that escape of repression by Mig1 is the primary role of Std1 at the promoter. At this point, more information and modelling are needed to elucidate how the opposing role of these two proteins comes to be.

Chapter 5

Mathematical modelling to understand the mechanisms of Hexose transporter regulation

The observed effects of mutation and environmental kinetics on hexose transporters allow us to create an abstraction of the mechanisms that may be taking place (4.20). Even though it might be tempting to declare such models as facts, it must be kept in mind that they come from human intuition and, as such, as subject to bias, error, and omission. Additionally, several other plausible, non–exclusive mechanisms might equally explain the observations presented. In order to provide a more objective evaluation of our models, we must resort to mathematical modeling Albert (2007), Raue et al. (2013).

Mathematical modeling of biological phenomena has a long history (section 1.2.1) and, with a strong physics heritage, has provided insight about how biological phenomena can be explained and characterised through abstract principles and agents that often escape empirical observation Albert (2007). With the advent of the post genomic era in which merely descriptive approaches do not capture the complexity of the data, mathematical modelling has become a necessity to provide mechanistic and predictive insight about the biological processes that generate such data Kitano (2002).

5.1 The diverse approaches to modelling

Ultimately, the toolkits and mathematical formalisms used in modelling will depend on the specific aims of a given model. In general, models can be qualitative or quantitative.

In one category are qualitative (toy) models, which try to abstract the general principles of function of a system. Toy models are meant to study the generative mechanisms of a phenomenon, and how different conditions may bring a system in and out of steady state. In order to achieve this, they often remain detached from the physical reality of a system.

In contrast, quantitative approaches often explicitly model known processes in a system, and their goal is often both to approximate the real behaviour of a system (using real data) and ultimately create a simulation of a real system. Such models are useful to predict the behaviour of multiple interconnected processes with exactitude, and can often be useful to obtain mechanistic insights about certain phenomena, especially through perturbation. Each of the processes in the system may be described in precise detail through explicit equations. Quantitative models often have large numbers of parameters which are difficult to adjust to real values.

Large systems can also be described in terms of interconnected blocks that receive an input and produce a processed output. Although more abstract, these models are useful to mathematically identify and drive (i.e. control) a system to a particular state. However, the exact configuration of a system, or the details of how that processing is done, may remain unknown. This approach is often called input-output modelling, and its formalisms are inherited from signals and systems theory and control theory (Chaparro (2010)).

An additional category is that of data driven approaches, whose goal is often to 'learn' and predict the behaviour of a system based purely on the system's data, particularly its internal relationships in multiple dimensions. This approach is significantly less interested in the mechanisms that drive such relationships, and therefore it is often called black-box modelling. However, novel and relevant uses of machine learning involve the inference of hidden equations that govern a system

based on time series data (Dzeroski & Todorovski (2008)).

With regard to regulation of the glucose sensing network, qualitative modeling has been previously used to explain how glucose perception contributes to fitness in addition to glucose import (Youk & van Oudenaarden (2009)). Quantitative modeling (Christensen et al. (2009), Kuttykrishnan et al. (2010)) has been done to simulate the behaviour of the glucose sensing network, with steady states that are qualitatively consistent with the literature. However, some omissions are substantial, like the assumption of one single glucose sensor instead of two. While the model of Kuttykrishnan et al. (2010) predicted a pulse of HXT4 transcription, and was the first to suggest dynamic functions of the hexose transporters, the study generally described a steady state behaviour of the system.

In this small chapter I show efforts using data driven and quantitative modeling to understand the mechanistic basis of the glucose sensing network's behaviour. My aim is oriented toward system identification: that is, find the system that best explains the transient activation of Hxt4 activation given the rich dynamic data available (Villaverde & Banga (2014)).

5.2 Mig1 localisation can be linearly predicted from glucose history

Previously I showed that Mig1 localisation dynamics is concomitant with the derivative of the glucose signal (Figure 4.16). To test if there was a causal relationship between these two, I wondered whether the glucose history trace could be processed to predict the future nuclear localisation signal of Mig1. In other words, I took a trace of w timepoints of the glucose signal, and looked for a filter that, when applied to that glucose trace, would best predict the next datapoint in the nuclear localisation signal of Mig1.

More formally, given a glucose history trace x of w timepoints $x(t-w...t-1)$, and the future localisation value $g(t)$, I looked for a filter of coefficients $\hat{k} = [K_0, K_1, ...K_w]$ such that $K_0 + K_1x_1 + K_2x_2... + K_wX_w = g(t)$ for every t.

To find this filter, I constructed matrix X out of all possible glucose history

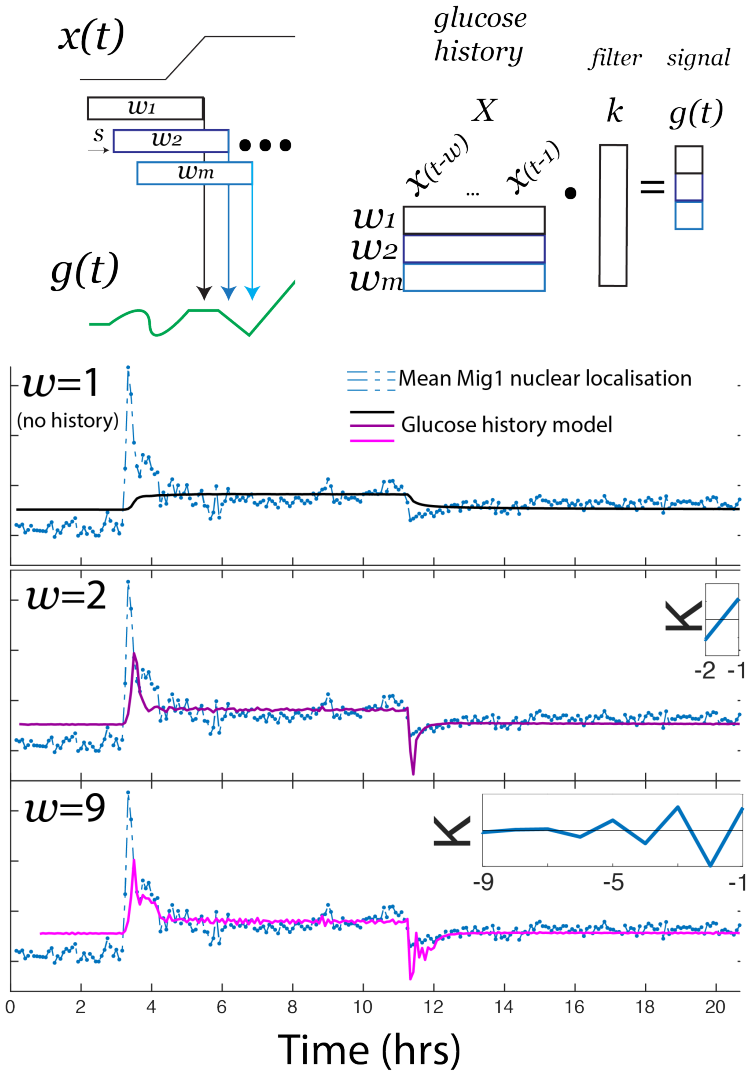

Figure 5.1: Glucose history contains sufficient information to accurately predict the upcoming nuclear localisation of Mig1. Top: windows of the glucose signal of size w are used to build build matrix X, row by row. Response vector $\hat{g}$ is made of all upcoming nuclear localisation values after each glucose trace. Windows are displaced by $s = 1$ timepoints. Regression is performed to find a filter $\hat{k}$ such that $X\hat{k} = \hat{g}$. Bottom: predictions of the glucose history based model on the relative Mig1 nuclear localisation. Filters of size $w \geq 2$ are able to obtain the time difference of glucose on consecutive timepoints (see filters in inset), and thus recover the the transtient 'jerk' of Mig1 localisation. The fit improves when only few more timepoints are added. Fits are shown for glucose trace windows of size $w = 1$ (no integration of history), $w = 2$ (middle) and $w = 9$, which corresponds to 45 minutes of history (bottom panel). Compared to the model where $w = 1$, models where $w \geq 2$, the least square error was $1.3\times - 1.5\times$ smaller.

traces, as well as vector $\hat{g}$ out of all possible upcoming nuclear localisation values for those traces. I then found the filter $\hat{k}$ such that $X\hat{k} = \hat{g}$ (Figure 5.1; see methods section 2.7.5). This filter can then be applied to any set of glucose traces to formulate predictions about the nuclear localisation of Mig1.

A glucose history window of 1 timepoint was not enough to recover the transients in the shuttling of Mig1, as it only shifted and rescaled the original glucose signal. However, inclusion of 2 or more timepoints in the window (Figure 5.1, bottom panel, middle and bottom) proved sufficient to capture the 'jerk' in the transient. Inclusion of more distant timepoints improved this prediction, up to $\approx$ 45 minutes. As these filters add and subtract consecutive time blocks (Figure 5.1, bottom panel insets, Appendix Figure B.12 bottom panel) this strongly suggests that the system governing Mig1 is calculating the time derivative of the glucose signal for a specific timescale. Altogether, I conclude that, effectively, the system governing Mig1 is able to dynamically process temporal sequences of glucose within a time frame of 45 minutes. A consistent processing was also obtained from single cell traces (Figure B.12).

5.3 Plate reader OD predicts the peak time of Hxt4 of wild type and mutants

Under the same logic I asked whether the OD history in the plate reader contained sufficient information to predict the expression dynamics of Hxt4, and to capture the dynamic effect of the mutants. Figure 5.2 shows the result of such models and the filters produced, which were relatively consistent (albeit scaled) across multiple glucose concentrations. While the mig1Δ and the rgt2Δ had the best fits, the wild type and std1Δ dynamics struggled to capture the strong delays in high glucose, particularly for the std1Δ strain (this was achieved when adding considerably more timepoints). It can be seen that the filters for the wild type and std1Δ strains subtract the first preceding timepoint, whereas the other two add it. Altogether, I conclude that Hxt4 peak (glucose depletion) times and the decay dynamics can be accurately predicted from the OD despite a less precise decoding

of the induction dynamics. With such filters one can potentially estimate the induction dynamics of Hxt4 in any given growth curve.

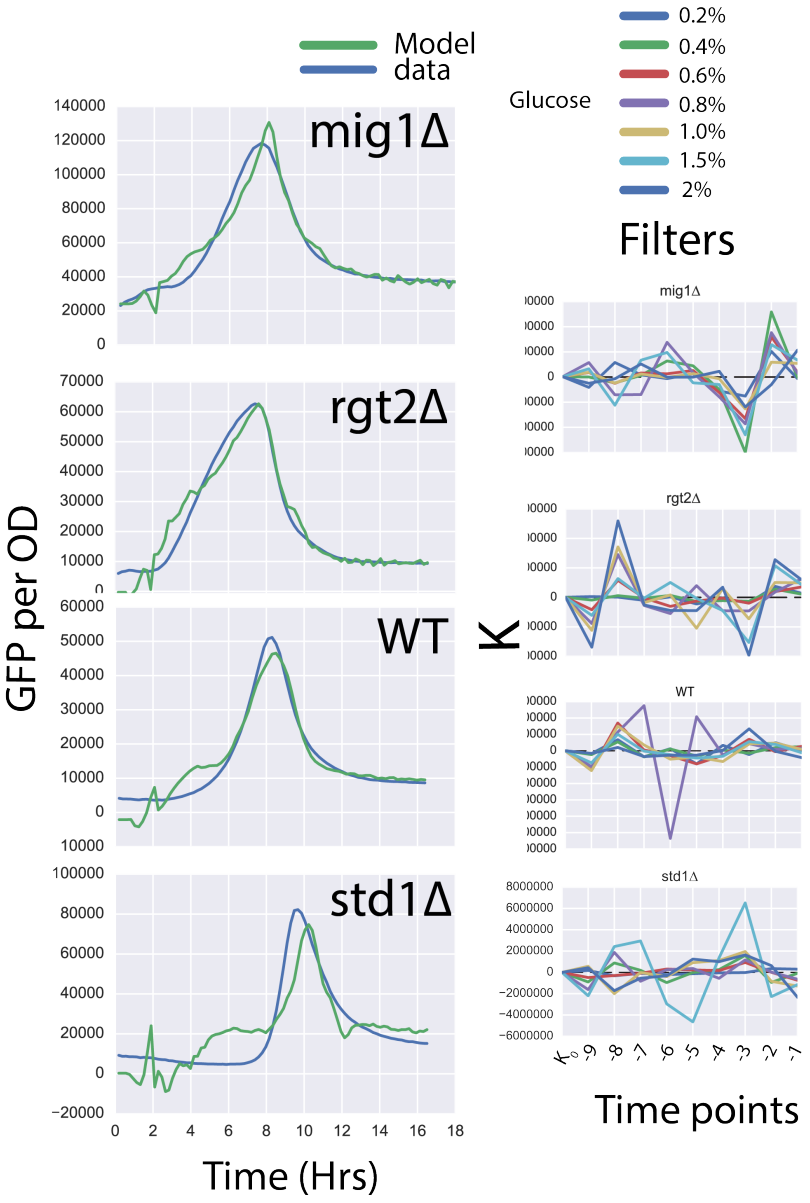

Figure 5.2: OD history accurately predicts Hxt4 peak times in the wild type and mutant genotypes. Left column: data (blue) and model predictions (green) for the expression level of Hxt4 in different strain backgrounds. Input data was the average of 2 biological replicates of OD, and GFP data is shown for the average of 2 fluorescence replicates in 2% glucose. Right column: 10 previous OD timepoints and constant K_0 were weighted (y axis) to predict the upcoming value of GFP fluorescence, for all glucose concentrations tested (curves of different colours). Filters are consistent, but the weights appear scaled for each concentration.

5.4 Bayesian model discrimination of downshift response mechanisms

The glucose sensing network is of high complexity, and therefore it is challenging to understand how the downshift response arises mechanistically from the large assembly of network components. It is therefore reasonable to systematically look for a minimal set of components that could be capable of producing a dynamic behaviour. Such strategy has been used before, where every single three node system (within a set of boundary conditions) was evaluated by its ability to perform biochemical adaptation (Ma et al. (2009)), with 2 non-redundant configurations found to be the most suitable for this performance. Similarly, my collaborator Melissa Bothe (Bothe (2016)) attempted to search for 3 node networks that were best able to fit the Hxt4 downshift response data, provided by me. 120 non redundant three node qualitative models were generated, and evaluated using an Approximate Bayesian Computation–Sequential Monte Carlo (ABC-SMC) algorithm, which allows to find posterior probability distribution for a particular network without having to calculate exact likelihoods (Toni et al. (2009)). Parameter sets are sampled from a prior (usually uniform) distribution, and parameter sets whose prediction error relative to the data is below a threshold are collected. These selected parameter sets are then used to build a posterior distribution, which becomes a prior for the parameter search in the next round. The algorithm (Lenormand et al. (2013)) was adapted by Anthony Bowman to dynamically calculate the best threshold error in each round. Then each model pair is compared directly by the Bayes factor B_{12}:

$$B_{12} = \frac{P(m_1|x)}{P(m_2|x)} \tag{5.1}$$

where $P(m_i|x)$ represents the posterior probability distribution of a model given the data.

Comparison of 120 possible topologies through this framework yielded 2 topologies that comprised 75% and 24% of the posterior probability distribu-

tion: an incoherent [1] Feed Forward Loop (IFFL) type 3 and type 2 (see Alon (2007)). The IFFL type 3 produced tighter fits for the data, particularly the steeper changes in he Hxt4 response. In this topology, the presence of glucose achieves direct repression of A to C, whereas the other branch must wait for the accumulation of B to exert activation. The drop of glucose below a threshold inhibits A, thereby triggering both derepression and activation of C at the same time, and hence a strong downshift response. Despite this elegant logic, the upshift response was not entirely absent from either FFL.

Altogether, from this work we conclude that a minimal set of components can generally (but not exactly) explain the downshift response, though additional processing is required to entirely eliminate the upshift response. Future work will involve extending these basic models to explain the derivative reporting of Mig1.

5.5 Efforts in dynamic modelling of Hxt4 function

The data in chapter 4 suggests that the Hxt4 downshift response is the combined action of three repressing agents, one of them being Rgt2. However, the mechanism through which Rgt2 may be exerting repression is not clear (Figure 5.4) . Rgt2 could derepress a transcriptional repressor, enhance Mig1 repression or promote the transporter's degradation. If the sensor is promoting Mig1 activity, it is likely through the interplay of Std1 and Hxk2, which have been found to have opposite effects in glucose derepression. In particular, eliminating Std1 would break its derepressive/activating effects on Mig1 (Tillman et al. (1995), Kuchin et al. (2003)), driving the equilibrium to the ultra repressed state observed (Figure 4.19 left, top panel). I sought to investigate which of these mechanisms of Rgt2 regulation is better supported by the data. To this end, I elaborated models that explicitly included these possibilities. The aim of the models was to fit the Hxt4 wild type data from 1% glucose hats (4.2), and to reproduce the behaviour of the mutants.

[1] They are called Incoherent because their 2 branches exert contradictory effects.

I therefore attempted to build a model that would capture the regulatory effects of Mth1, Mig1 and Rgt2 over Hxt4 (Figure 4.20). The quasi–steady state model (Equations 2.12) included additive Hill repression of Hxt4 by these three agents. Mth1 was repressed by Mig1, and Rgt2 was activated by glucose. Active degradation by glucose was added to Mth1 and Hxt4. Additionally, the decay of Rgt2 was made proportional to the concentration of Mth1. This was reasoned in order to capture the sensor's inactivity in low glucose.

To simplify the problem at this stage, the activity of Mig1 was not modelled explicitly (none of the mutants disrupted Mig1 localisation completely so no access to the responsible circuitry is available). I predicted the nuclear localisation directly from the glucose signal by applying the dynamic filter previously described to the glucose sequence (See Section 2.7.5; exact filter in Appendix Figure B.12). These predictions were consistent with the experimental result for Mig1 localisation.

Figure 5.5 shows initial results with this circuit, which is able to recover the activation trend of Hxt4, if not the exact shape or scale of induction. Using this model, I simulated cases in which Mth1, Rgt2 or Mig1 were deleted. Figure 5.5 panels on the right) shows how the model is also able to capture the the regulatory effects of the mutants, with the mth1Δ achieving steady state in the absence of glucose, the mig1Δ responding strongly in the upshift, and the rgt2Δ showing gradual accumulation. The experimental results for mutants reveal similar qualitative activation trends (Figure 5.5 bottom right). Altogether, these results suggest that the model presented, in which Rgt2 exerts independent action from Mig1, is indeed a plausible candidate to regulate the expression of Hxt4.

5.6 Chapter 5: Future work

Future work will closely examine the mechanism by which Mig1 exerts the derivative reporting, which is likely to be controlled by the Snf1 kinase complex, Reg1/Glc7 phosphatase and hexokinase 2 (Ozcan & Johnston (1995), Ludin et al. (1998), Treitel et al. (1998), Kuchin et al. (2003), Fernańdez-García et al. (2012),

Vega et al. (2016)), none of which were included in this model or experimented with. An obvious element missing in the current model is internal glucose and its key metabolic connections. A future model will initially include the HXT1 transporter, which will transform external glucose into internal at a high rate, which will affect the state of hexokinase 2 and thus the strength of glucose repression. Std1 could communicate with metabolism in several ways: its deletion could trigger superactivation of HXT1, creating an internal glucose overload and maximizing Hxt4 repression. An increase of Std1 levels due to less degradation could enhance activation of Snf1, and derepress Hxt4 by countering Mig1/Hxk2 activity. Another plausible hypothesis could be that ethanol or other metabolites could interfere with Rgt2 and HXT1 activity, perhaps via Std1. This would explain why a deletion of Std1 would impede such inhibition and enhance repression of Hxt4. A panorama of metabolic feedback could therefore include:

- A vicious repressive cycle with internal glucose- cAMP accumulation - Rgt1 inactivation - internal glucose/Hxk2 repression
- A derepressive feedback with lower internal glucose - higher Std1 and Snf1 activity (perhaps due to ethanol or other metabolites) -rise in trehalose 6 phosphate- lower Hxk2 activity (or Hxt1) - weaker glucose metabolism and lower mig1 repression

Also, I will evaluate the goodness of fit of this model and compare it with other models of Mig1-Rgt2 action. Finally, next steps will involve postulating hypotheses for the role of STD1 in this network, which remains unclear at the time of writing. The gene's circuitry is peculiar because, in contrast with its paralogue MTH1, it is subjected to negative self regulation which could yield interesting dynamic properties to the system (Kim et al. (2006)). The std1 deletion may be not be able to directly activate Hxt4 (Tillman et al. (1995)) or countering the action of Rgt2. These models will be compared quantitatively, but they will also be tested in their ability to predict the behaviour of double mutants in the pathway.

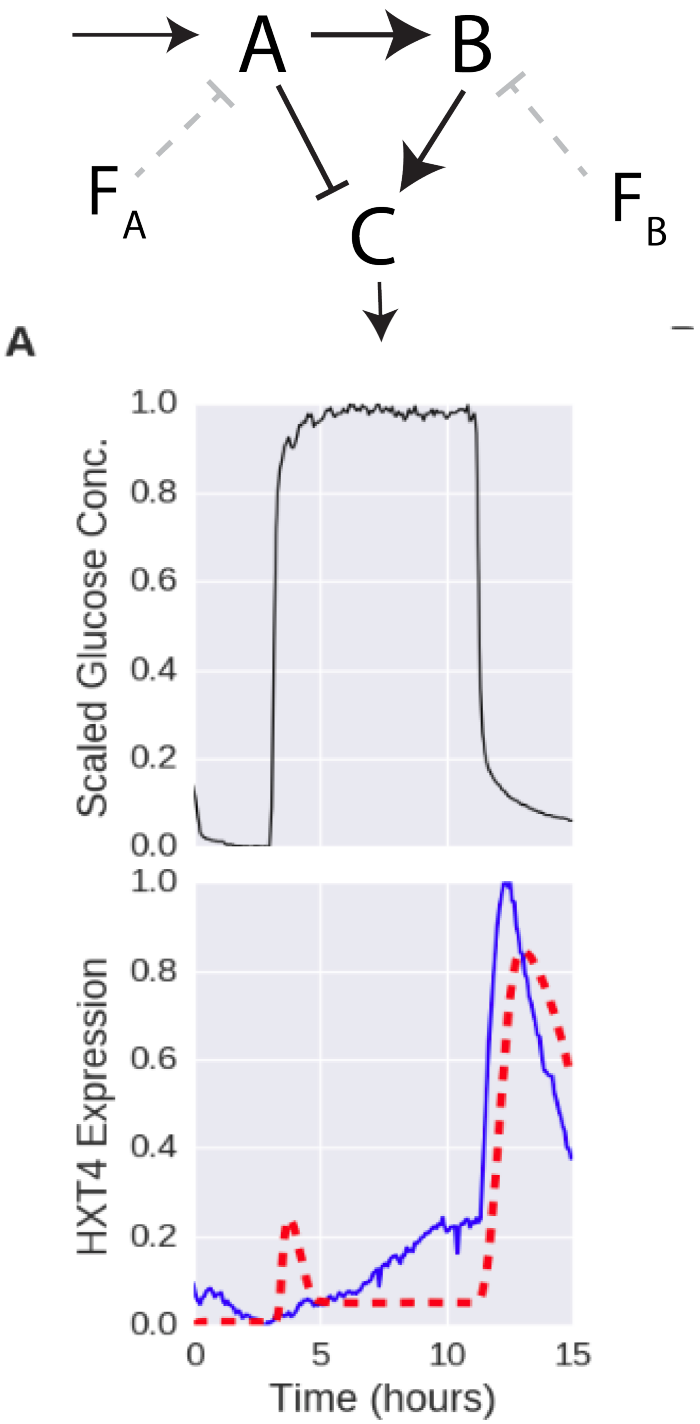

Figure 5.3: An incoherent type 3 Feed forward loop generally explains a strong downshift response. Figure taken from Bothe (2016), who found the best fit for the Hxt4 response across 120 three-node network topologies using ABC-SMC. In the resulting posterior distribution of best fits to the data, an incoherent type 3 Feed Forward Loop (top panel) comprised 75%. A receives the input, whereas C is the network's output. The model reproduced the downshift response, but did not achieve full repression during the upshift. Plots (bottom panel) show the internally normalised input (above, black) and output (below, blue) of Hxt4 plus simulation output (red) in different experiments.

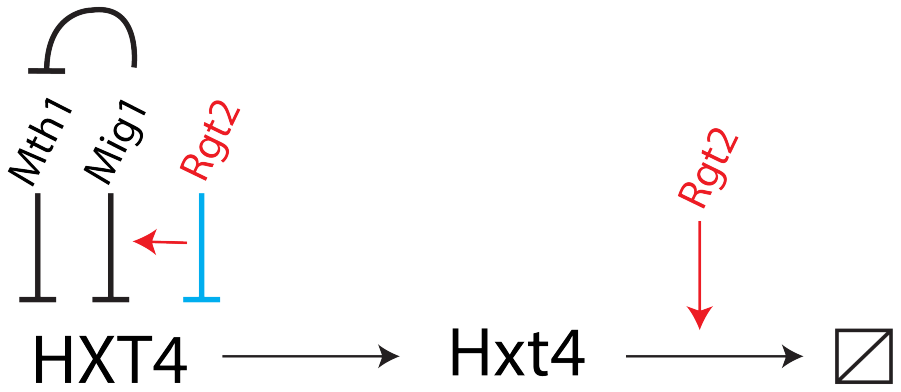

Figure 5.4: Potential roles for Rgt2 in repressing HXT4. Hypotheses of intervention of Rgt2 in distinct processes are shown in red, whereas blue shows the hypothesis modelled in this section. In it, Rgt2 exerts a (presumably indirect) transcriptional effect over HXT4. The other options involve Rgt2 modulating either the repressive activity of Mig1, or Hxt4 degradation.

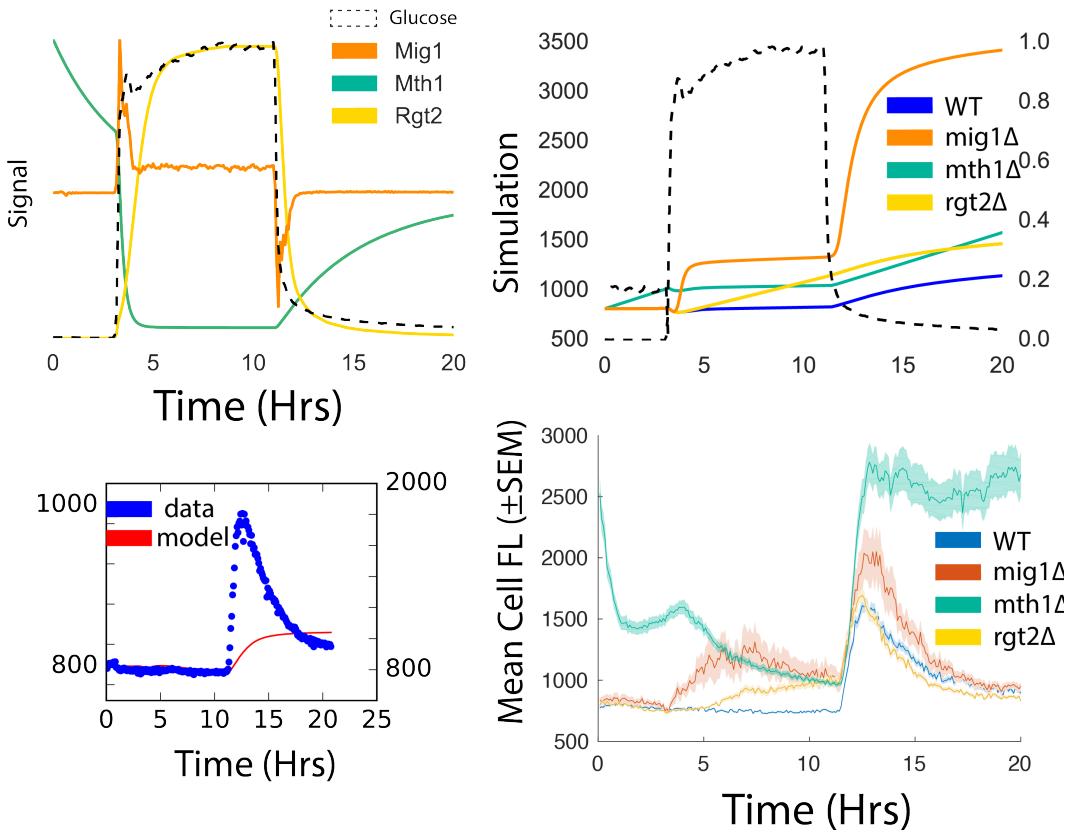

Figure 5.5: A dynamic model of Hxt4 recovers qualitative features in the wild type and mutants. Top Left: An ODE model was created to simulate the dynamics of unobserved repressors Mth1 (green) and Rgt2 (yellow). Mig1 localisation dynamics was predicted from a data driven model (Section 2.7.5) and incorporated. Values for these components were used to control the HXT4 gene. Bottom left: Results for a preliminary simulation of Hxt4 (red), which activates at similar times as the real Hxt4 (blue dots) Left Y axis corresponds to the simulation. Top/bottom right: Mutants for each of the repressors were simulated. The induction dynamics of each strain is qualitatively comparable. Std1, which has not been included in the model, may be involved in generating the sharp downshift peak in the data.

Chapter 6

Discussion

In this section I review the key overarching ideas laid out in the previous three chapters, which constitute the basis of the claim for novelty and relevance of this work.

I have postulated that the dynamic identity of an environment (not only its qualitative identity) constitutes a valuable asset that a single cell can exploit to optimise decision making in ambiguous, fluctuating conditions. In support of this hypothesis, I have provided substantial evidence that the gene for hexose transporter 4 (HXT4) of *Saccharomyces cerevisiae* is specifically activated in transient glucose downshifts rather than at a specific glucose concentration. This dynamic sensitivity comes from repressor Mig1, which tracks and channels information about time derivative specifically to the HXT4 gene and not the similar–affinity transporter HXT2. In addition, I have shown the plethora of dynamic effects of other genes over HXT4. This makes transporter an ideal model to study the role of glucose signalling in gene repression. The insights from this dynamic control could be potentially present in medically relevant systems, and could be harnessed for biotechnology.

Besides the context-specific results, these findings have several implications that expand our general expectations about gene regulation. First, a nutrient transporter (or any gene for that purpose) may be allocated to transient regimes (not only steady state ones), as opposed to presence/absence or concentration of a stimulus. Second, different environmental kinetics of the same stimulus may turn

a lowly expressed, nearly silent gene into a fast response one. Third, snapshot based phenotyping of a gene may not reveal any timing mechanisms in place, such as haste or delay in gene expression. I now elaborate on some of these implications.

6.1 The dynamics of hexose transporters bring the level based transport paradigm into question

Even though historically nutrient transporters have been found to be subject to several layers of regulation, the view on the function of transporters has remained based on a static paradigm. In other words, cells must sense the level of a desired molecule and adjust transport accordingly such that, at steady state, transport will be optimal. Under the current paradigm, a transporter is not readily suited for dynamic conditions. However, in many realistic scenarios, nutrient concentrations may drop fast enough so as to render a transporter unable to import any nutrient. The evidence I have presented about transporter Hxt4 being exclusively expressed and localised to the membrane in a non-steady state regime (section 4.5.1, Figure 4.7) directly challenges the established preconception of optimal use for a transporter. The experimental design used was the minimal setup needed to entertain this possibility, which was obscured by the snapshot approaches that dominate in transport biochemistry. This finding invites exploring novel ways in which the transporter may be able to contribute to the fitness of a cell.

6.2 Strong promoter, strong repression

From a level–centered viewpoint, it might be argued that HXT4 is a gene expressed at low levels, and therefore its function and impact on fitness may be minimal. However, removal of Mig1 sites from the promoter revealed that the maximum transcription rate achieved by the promoter is considerably high (higher

than the levels observed for Hxt1), judging by the levels of the transporter alone. Yet, Mig1 represses HXT4 to the point that the gene fully shuts down during a glucose uphsift. Upon Mig1 release, the promoter activates strongly yielding considerable levels of the protein for the short time window. Why are cells so invested in repressing a strong promoter with such vigour, if it is for a gene of little importance to fitness? Why retain such gene, when there are so many potential paralogs that could take over its function? Preliminary experiments investigated the impact on growth rate of a hxt4Δ deletion, but there were no obvious differences in plate reader experiments.

6.3 Dynamic link between glycogen production and Hxt4

Glycogen production, which takes place at the vacuole, is also triggered in an anticipatory fashion to glucose depletion (Lillie & Pringle (1980), Wilson et al. (2010)). Such regulation is also exerted by Mig1 (Wilson et al. (2010)) and, if there is one process that must be activated specifically during a glucose downshift, it would be glycogen synthesis (see section 1.5.3). This opens the possibility that the transcriptional regulation of Hxt4 is correlated with glycogen, and whether Hxt4 activity is somehow specifically linked to production of the reserve carbohydrate. Mutations in the glucose sensing pathway can delay or hasten the activation of Hxt4 during the glucose fall, and may as well regulate the timing of glycogen synthesis. Assuming, for a moment, that Hxt4 and glycogen are thus co-regulated exclusively in a glucose downshift, sharing activity in such specific circumstances may reveal equally specific regulatory signals. For example, there might be 20 potential Mig1 binding sites in the HXT promoters, but only 2 of those may have properties that enable a downshift response.

6.4 How the Hxt4 response may provide an advantage

A previous study showed that expression of a chimeric transporter enabled respiration even at high external glucose concentrations (Otterstedt et al. (2004)). If expression Hxt4 or other high affinity transporters is proven to have similar capabilities, it would be reasonable to provide tight regulation to it so that it does not enforce slower (respiratory) growth rates (Hoek et al. (1998)). Hxt4 is the first transporter to activate during the glucose downshift in a plate reader (Figure 3.2) and was found to be a overexpressed in a glucose limited, respiratory culture initiated at high glucose (Daran-Lapujade et al. (2004)). Assuming Hxt4 or other transporters have this capability, activation of such transporters during a glucose downshift may facilitate a concerted reduction in growth rate during the glucose downshift across all cells, thereby extending the preparation time before sugar depletion in the culture. Because the magnitude of the Hxt4 response showed some correlation with the magnitude of the glucose step (Figure 4.11), and there was a general correspondence between the duration of the slope and the duration of Hxt4 burst (Appendix 4.8), this hints at the possibility that Hxt4 may be performing fold change detection or a rate based response. At a concentration close to its Km, the transporter will be able to import sugar at half the max rate. However, this rate reduction might be compensated by doubling the amount of transporter available such that the same amount of sugar is imported. Support for this hypothesis will be explored in future work, but the influence of Hxt4 in preparation could be reflected by the glycogen concentration at the time of glucose exaustion.

6.5 The Hxt4 response as a scope into the physiology of glucose derepression

Even though the function of transporter Hxt4 may have relevant properties, the response itself is providing a dynamic signal of glucose derepression dynamics

and an uncountable set pf physiological decisions that come together with it. First, I have shown that the promoter acts as a direct transcriptional readout for the repressive activity of Mig1, enabling to explore how the magnitude of Mig1 pulsing actually influences transcription. The current model gene for glucose derepression is the Suc2 promoter, which is monitored statically by invertase activity or chromatin immuno precipitation. The response and decay of Hxt4 are fast and the signal does not depend on a particular product to be accumulated. This allows the collection of rich, noisy dynamics and activation time statistics before saturation (Appendix figures 4.19, B.4). The HXT4 promoter serves as an ideal model to elucidate the key events leading to transcriptional repression by Hxk2, and to distinguish the signals that lead to the differential silencing of some Mig1 regulated promoters and not others. A complete library of HXT4 promoters, where some repression earlier or later, can serve as a tool to elucidate the chromatin remodelling events during the transition towards glucose derepression. Similarly, these promoters will shed light on how the STRE elements coordinate the timing of the stress response and its robust achievement of gene timing during batch culture growth (Saldanha et al. (2004), Figure 3.11). Finally, One of the rate limiting steps of entry into respiration is the production of mitochondria, which are a costly resource (Shiota et al. (2015)), and thus the decision of commiting towards mitochondrial biogenesis could be subject to complex, dynamic environmental cues. Production of mitochondria during the anticipation towards glucose depletion could partially solve this cost allocation problem (there is no better moment than to invest in mitochondria where glucose will imminently run out) and could be related to or correlated with Hxt4 production. Altogether, Hxt4 opens a gate towards studying physiological processes for which little or no signal currently exists.

6.6 Revisiting the regulation of gene expression from a dynamic perspective

The fundamentals of microbial growth were established under conditions of balanced growth, a steady state in which the culture's growth rate is equal to the dilution rate in a nutrient-limited chemostat (Novick & Szilard (1950), Saldanha et al. (2004)). Such conditions allow the study of gene expression by controlling for any growth rate related effects. In contrast, a batch culture is highly dynamic environment for which the general stress response causes large unspecific temporal effects (Saldanha et al. (2004)) which are not present in a chemostat culture. Nutrient limited chemostats have thus been described to induce as 'poor, not starving' conditions (Saldanha et al. (2004)). Studies often approximate balanced growth with a point during logarithmic phase to investigate gene expression and enzyme activity (Reifenberger et al. (1997)). Valuable knowledge about gene function has been obtained through logarithmic and balanced growth studies, which allow to establish a steady state view of gene expression. However, such paradigm purposefully brings cells out of context (van Heerden et al. (2015)), in which the temporal correlations may be relevant for the functionality of genes.

In the above section I explicitly looked for the non steady state patterns of activation of the hexose transporters, which are distinguishable, reproducible and quantifiable despite deviating from balanced growth. The data presented shows that, outside balanced growth, the terms 'activation' or 'repression' can become ambiguous due to temporal effects in the mutants. Hxt4–yEGFP in the std1Δ strain may show a longer, stronger repression (delay), but given enough time, culminates in an overall higher expression peak than the wild type strain. If a lack of Std1 is causing a delay in the expression of Hxt4, it is worth considering whether this delay might be also affecting several other genes like SUC2 (Tillman et al. (1995)). From this perspective, Std1 would be neither a repressor nor an activator, but a 'timer' of certain biological processes. The existence of such timer systems may invite to reconsider whether any claims of expression change in mid-log transcriptomics or proteomics analyses are, in fact, temporal modulations of

gene expression.

6.7 Growth staging of hexose transporters could link perception to growth

Two previous studies have asked what is the contribution of glucose perception to growth and fitness, given that perception is not strictly necessary for survival. For instance, one single constitutive transporter would allow the sugar to enter the cell. However, in yeast, perception and import are highly intertwined. Glucose perception through sensors snf3 and rgt2 appeared to limit individual transporters' contribution to fitness (Youk & van Oudenaarden (2009)), but when the sensors were deleted, nearly every transporter increased growth rates in similar amounts. Another study (Schmidt-Glenewinkel & Barkai (2014)) found that the absence of both sensors caused an imbalance in biomass accumulation and cell division. Deletion of sensors has been also linked to derepression of respiration (Reddi & Culotta (2013)). I have shown that hexose transporters are organised during growth by the sensors: Rgt2 modulates how early must Hxt4 activate, whereas Snf3 impacts both the level of Hxt4 activation (Figure B.10, left column) and the overall nuclear localisation of Mig1 (Figure 4.16). The combined effects of the sensors are likely to cause large staging aberrations in a double sensor mutant. Unstaged expression of high affinity transport could itself decrease metabolic flux and trigger a 'default' respiratory growth. Alternatively, the timing of expression of respiratory enzymes could be simultaneously controlled by both Rgt2 and Mig1 in the same way that Hxt4 is controlled.

6.8 Practical relevance

6.8.1 Medicine

The study of fermentation is central to modern medicine. The ability of cells to ferment, even in aerobic conditions, is considered an emerging hallmark of

cancer (Hanahan & Weinberg (2011)). Human cancer cells initially achieve this state by upregulation of glucose transporters, particularly GLUT1 (DeBerardinis et al. (2008)). The ability of cells to harness complex environmental decoding could extend potentially to several systems like the one regulating GLUT1. For example, it has not been considered whether a drop in glucose may temporarily raise GLUT1 levels, thereby perpetuating the fermentative state.

Glucose sensing itself has important medical implications, specifically in beta pancreatic cell islets which are in charge of insulin secretion(Schuit et al. (2001)) among other tissues (Rolland et al. (2001)). Insulin secretion is likely to be subject to complex signal processing, as insulin can be released in anticipation to consumption and the appearance of glucose in the cell, which may produce hypoglycemia (MacDonald et al. (2005)). Ultimately, faults in such glucose sensing by these cells may directly drive type II diabetes (MacDonald et al. (2005)). It not yet understood how glucose sensing in these cells processes dynamic environmental changes, which ultimately trigger the insulin and glucagon spikes important to preserve glucose homeostasis.

6.8.2 A model for glucose derepression in industrial fermentation

In the biotechnology industry, catabolite repression enables preferential fermentation of glucose over maltose; however, transition from glucose to other sugars often causes a strong lag in microbial growth, which affects the times and costs of industrial fermentation. One group (New et al. (2014)) performed a directed evolution study that revealed variations in STD1 and HXK2 as the ones with the largest, opposing effects in the glucose-maltose lag. The Std1 variants exacerbated the lag, a result that is consistent with the stronger derepression delay in the std1 Δ background (Figures 3.13, B.10). The data presented across all chapters suggests specific roles for the Rgt2/Std1 interaction in modulating long term glucose repression. Future work using Hxt4 as a catabolite repression model will elaborate on how exactly these two genes, as well as RGT2, modulate metabolic reprogramming in yeast. Using synthetic biology, in a similar fashion as done

here (section 3.9), and could potentially guide precision engineering of lag and expression times. Finally, the induction of Hxt4 upon a drop of glucose (section 3.6) could also serve as a real time monitor of glucose consumption in a growing culture.

Bibliography

Ahuatzi, D., Riera, A., Peláez, R., Herrero, P. & Moreno, F. (2007), 'Hxk2 regulates the phosphorylation state of Mig1 and therefore its nucleocytoplasmic distribution', *Journal of Biological Chemistry* **282**(7), 4485–4493.

Alam, M. T., Zelezniak, A., Mülleder, M., Shliaha, P., Schwarz, R., Capuano, F., Vowinckel, J., Radmaneshfar, E., Krüger, A., Calvani, E., Michel, S., Börno, S., Christen, S., Patil, K. R., Timmermann, B., Lilley, K. S. & Ralser, M. (2016), 'The metabolic background is a global player in Saccharomyces gene expression epistasis', *Nature Microbiology* **1**(3), 15030.
URL: *http://www.nature.com/articles/nmicrobiol201530*

Albert, R. (2007), 'Network inference, analysis, and modeling in systems biology.', *The Plant cell* **19**(11), 3327–3338.

Alon, U. (2007), *Introduction to Systems Biology & the Design Principles of Biological circuits (Mathematical & Computational Biology Series, Vol. 10)*, Librairie Lavoisier.

Alon, U., Surette, M. G., Barkai, N. & Leibler, S. (1999), 'Robustness in bacterial chemotaxis.', *Nature* **397**(6715), 168–171.

Babu, P., Deschenes, R. J. & Robinson, L. C. (2004), 'Akr1p-dependent palmitoylation of Yck2p yeast casein kinase 1 is necessary and sufficient for plasma membrane targeting', *Journal of Biological Chemistry* **279**(26), 27138–27147.

Bakker, E., Swain, P. S. & Crane, M. (2017), 'Morphologically constrained and data informed cell segmentation of budding yeast', *bioRxiv* .
URL: *http://www.biorxiv.org/content/early/2017/02/06/105106*

Balaban, N. Q. (2004), 'Bacterial Persistence as a Phenotypic Switch', *Science* **305**(5690), 1622–1625.
URL: *http://www.sciencemag.org/cgi/doi/10.1126/science.1099390*

Balázsi, G., van Oudenaarden, A. & Collins, J. J. (2011), 'Cellular decision making and biological noise: from microbes to mammals.', *Cell* **144**(6), 910–25.

Barford, J. P. & Hall, R. J. (1979), 'An Examination of the Crabtree Effect in Saccharomyces cerevisiae: the Role of Respiratory Adaptation', *Journal of General Microbiology* **114**(2), 267–275.
URL: *http://mic.sgmjournals.org/content/114/2/267.abstract*

Baudin, A., Ozier-kalogeropoulos, O., Denouel, A., Lacroute, F. & Cullin, C. (1993), 'A simple and efficient method for direct gene deletion in Saccharomyces cerevisiae', *Nucleic Acids Research* **21**(14), 3329–3330.

Bendrioua, L., Smedh, M., Almquist, J., Cvijovic, M., Jirstrand, M., Goksör, M., Adiels, C. B. & Hohmann, S. (2014), 'Yeast AMP-activated protein kinase monitors glucose concentration changes and absolute glucose levels', *Journal of Biological Chemistry* **289**(18), 12863–12875.

Bernard, C. (1885), 'Lecons sur les phenomenes de la vie communs aux nimaux et aux vegetaux', *Cours de Physiologie Generale du Museum d'Histoire Naturelle* .

Blázquez, M. A., Lagunas, R., Gancedo, C. & Gancedo, J. M. (1993), 'Trehalose-6-phosphate, a new regulator of yeast glycolysis that inhibits hexokinases', *FEBS Letters* **329**(1-2), 51–54.

Bothe, M. (2016), Dynamic signal processing in the yeast glucose sensing network, Master's thesis, Imperial College London.

Bowsher, C. G., Voliotis, M. & Swain, P. S. (2013), 'The Fidelity of Dynamic Signaling by Noisy Biomolecular Networks', *PLoS Computational Biology* **9**(3).

Broach, J. R. (2012), 'Nutritional control of growth and development in yeast', *Genetics* **192**(1), 73–105.

Brown, M. & Wittwer, C. (2000), 'Flow cytometry: Principles and clinical applications in hematology', *Clinical Chemistry* **46**(8 II), 1221–1229.

Burke, D., Dawson, D. & Stearns, T. (2000), *Methods in yeast genetics: A Cold Spring Harbor Laboratory course manual*, Cold Spring Harbor Laboratory Press.

Cai, L., Dalal, C. K. & Elowitz, M. B. (2008), 'Frequency-modulated nuclear localization bursts coordinate gene regulation', *Nature* **455**(7212), 485–490.
URL: *http://www.nature.com/doifinder/10.1038/nature07292*

Carlson, M., Taussig, R., Kustu, S. & Botstein, D. (1983), 'The secreted form of invertase in Saccharomyces cerevisiae is synthesized from mRNA encoding a signal sequence.', *Molecular and cellular biology* **3**(3), 439–447.

Caudron, F. & Barral, Y. (2009), 'Septins and the Lateral Compartmentalization of Eukaryotic Membranes', *Developmental Cell* **16**(4), 493–506.

Chadwick, A., Van Rossum, M. C. W. & Nolan, M. F. (2015), 'Independent theta phase coding accounts for ca population sequences and enables flexible remapping', *eLife* **2015**(4), 1–51.

Chambers, P. J. & Pretorius, I. S. (2010), 'Fermenting knowledge: the history of winemaking, science and yeast research.', *EMBO reports* **11**(12), 914–20.

Chaparro, L. (2010), *Signals and systems using MATLAB*, Academic Press.

Christensen, T. S., Oliveira, A. & Nielsen, J. (2009), 'Reconstruction and logical modeling of glucose repression signaling pathways in Saccharomyces cerevisiae', *BMC Systems Biology* **3**(1), 7.
URL: *http://bmcsystbiol.biomedcentral.com/articles/10.1186/1752-0509-3-7*

Cooper, S. J. (2008), 'From Claude Bernard to Walter Cannon. Emergence of the concept of homeostasis', *Appetite* **51**(3), 419–427.

Crane, M. M., Clark, I. B. N., Bakker, E., Smith, S. & Swain, P. S. (2014), 'A microfluidic system for studying ageing and dynamic single-cell responses in budding yeast', *PLoS ONE* **9**(6).

Daran-Lapujade, P., Jansen, M. L. A., Daran, J.-M., van Gulik, W., de Winde, J. H. & Pronk, J. T. (2004), 'Role of transcriptional regulation in controlling fluxes in central carbon metabolism of Saccharomyces cerevisiae. A chemostat culture study.', *The Journal of biological chemistry* **279**(10), 9125–38.

De JongGubbels, P., Vanrolleghem, P., Heijnen, S., Van Dijken, J. P. & Pronk, J. T. (1995), 'Regulation of carbon metabolism in chemostat cultures of Saccharomyces cerevisiae grown on mixtures of glucose and ethanol', *Yeast* **11**(5), 407–418.

De Kok, S., Kozak, B. U., Pronk, J. T. & Van Maris, A. J. A. (2012), 'Energy coupling in Saccharomyces cerevisiae: Selected opportunities for metabolic engineering'.

de Virgilio, C. (2012), 'The essence of yeast quiescence', *FEMS Microbiology Reviews* **36**(2), 306–339.

DeBerardinis, R. J., Lum, J. J., Hatzivassiliou, G. & Thompson, C. B. (2008), 'The Biology of Cancer: Metabolic Reprogramming Fuels Cell Growth and Proliferation', *Cell Metabolism* **7**(1), 11–20.

DeRisi, J. L. (1997), 'Exploring the Metabolic and Genetic Control of Gene Expression on a Genomic Scale', *Science* **278**(5338), 680–686.
URL: *http://www.sciencemag.org/cgi/doi/10.1126/science.278.5338.680*

Diallinas, G. (2014), 'Understanding transporter specificity and the discrete appearance of channel-like gating domains in transporters', *Frontiers in Pharmacology* **5 AUG**.

Diderich, J. A., Schuurmans, J. M., Van Gaalen, M. C., Kruckeberg, A. L. & Van Dam, K. (2001), 'Functional analysis of the hexose transporter homologue HXT5 in Saccharomyces cerevisiae', *Yeast* **18**(16), 1515–1524.

Dodd, A. N., Salathia, N., Hall, A., Kévei, E., Tóth, R., Nagy, F., Hibberd, J. M., Millar, A. J. & Webb, A. A. R. (2005), 'Plant Circadian Clocks Increase Photosynthesis, Growth, Survival, and Competitive Advantage', *Science* **309**(5734), 630–633.
URL: *http://www.sciencemag.org/content/309/5734/630.abstract*

Dubuis, J. O., Tkacik, G., Wieschaus, E. F., Gregor, T. & Bialek, W. (2013), 'Positional information, in bits', *Proceedings of the National Academy of Sciences* **110**(41), 16301–16308.
URL: *http://www.pnas.org/content/110/41/16301.abstract*

Dzeroski, S. & Todorovski, L. (2008), 'Equation Discovery for Systems Biology: Finding the Structure and Dynamics of Biological Networks from Time Course Data', *Current Opinion in Biotechnology* **19**(4), 360–8.
URL: *http://www.ncbi.nlm.nih.gov/pubmed/18672061*

Elowitz, M. B., Levine, A. J., Siggia, E. D., Swain, P. S., Guptasarma, P., Spudich, J. L., McAdams, H. H., Heitzler, P., Ko, M. S., Fiering, S., Lutz, R., Deuschle, U., Maloney, P. C., Rotman, B., Paulsson, J., Ehrenberg, M., Boyd, D., Becskei, A., Serrano, L., Elowitz, M. B., Leibler, S., Thattai, M., van Oudenaarden, A., Alon, U., Capaldo, F. N., Barbour, S. D., Casadaban, M. J., Parkinson, J. S., Houts, S. E., Meyer, B. J., Maurer, R. & Ptashne, M. (2002), 'Stochastic gene expression in a single cell.', *Science (New York, N.Y.)* **297**(5584), 1183–6.
URL: *http://www.ncbi.nlm.nih.gov/pubmed/12183631*

Engel, S. R., Dietrich, F. S., Fisk, D. G., Binkley, G., Balakrishnan, R., Costanzo, M. C., Dwight, S. S., Hitz, B. C., Karra, K., Nash, R. S., Weng, S., Wong, E. D., Lloyd, P., Skrzypek, M. S., Miyasato, S. R., Simison, M. & Cherry, J. M. (2014), 'The Reference Genome Sequence of Saccharomyces cerevisiae : Then and Now', *G3 Genes—Genomes—Genetics* **4**(3), 389–398.
URL: *http://g3journal.org/lookup/doi/10.1534/g3.113.008995*

Engelhart, A. E., Adamala, K. P. & Szostak, J. W. (2016), 'A simple physical mechanism enables homeostasis in primitive cells', *Nature Chemistry* **8**(5), 448–453.
URL: *http://www.nature.com/doifinder/10.1038/nchem.2475*

ERASO, P., MAZÓN, M. J. & GANCEDO, J. M. (1987), 'Internal acidification and cAMP increase are not correlated in Saccharomyces cerevisiae', *European Journal of Biochemistry* **165**(3), 671–674.

Escalante-Chong, R., Savir, Y., Carroll, S. M., Ingraham, J. B., Wang, J., Marx, C. J. & Springer, M. (2015), 'Galactose metabolic genes in yeast respond to a ratio of galactose and glucose', *Proceedings of the National Academy of Sciences* **112**(5), 1636–1641.
URL: *http://www.pnas.org/lookup/doi/10.1073/pnas.1418058112*

Ettinger, A. & Wittmann, T. (2014), 'Fluorescence live cell imaging', *Methods in Cell Biology* **123**, 77–94.

Fernańdez-García, P., Peláez, R., Herrero, P. & Moreno, F. (2012), 'Phosphorylation of yeast hexokinase 2 regulates its nucleocytoplasmic shuttling', *Journal of Biological Chemistry* **287**(50), 42151–42164.

Fersht, A. (1999), *Structure and mechanism in protein science: A guide to enzyme catalysis and protein folding.*, Vol. 13409.

Flick, K. M., Spielewoy, N., Kalashnikova, T. I., Guaderrama, M., Zhu, Q., Chang, H.-C. & Wittenberg, C. (2003), 'Grr1-dependent inactivation of Mth1 mediates glucose-induced dissociation of Rgt1 from HXT gene promoters.', *Molecular biology of the cell* **14**(8), 3230–41.

Fraenkel, D. G. et al. (2011), *Yeast intermediary metabolism*, Cold Spring Harbor Laboratory Press.

Gabbiani, F., Krapp, H. G., Koch, C. & Laurent, G. (2002), 'Multiplicative computation in a visual neuron sensitive to looming', *Nature* **420**(6913), 320–324.
URL: *http://www.nature.com/doifinder/10.1038/nature01190*

Gadura, N., Robinson, L. C. & Michels, C. A. (2006), 'Glc7-Reg1 phosphatase signals to Yck1,2 casein kinase 1 to regulate transport activity and glucose-induced inactivation of saccharomyces maltose permease', *Genetics* **172**(3), 1427–1439.

Gayon, J. (2015), 'Enzymatic cybernetics: An unpublished work by Jacques Monod', *Comptes Rendus - Biologies* **338**(6), 398–405.

Goentoro, L., Shoval, O., Kirschner, M. W. & Alon, U. (2009), 'The Incoherent Feedforward Loop Can Provide Fold-Change Detection in Gene Regulation', *Molecular Cell* **36**(5), 894–899.
URL: *http://www.sciencedirect.com/science/article/pii/S1097276509008594*

Gordon, A., Colman-Lerner, A., Chin, T. E., Benjamin, K. R., Yu, R. C. & Brent, R. (2007), 'Single-cell quantification of molecules and rates using open-source microscope-based cytometry', *Nature Methods* **4**(2), 175–181.
URL: *http://www.nature.com/doifinder/10.1038/nmeth1008*

Granados, A. A., Crane, M. M., Montano-Gutierrez, L. F., Tanaka, R. J., Voliotis, M. & Swain, P. S. (2017), 'Distributing tasks via multiple input pathways increases cellular survival in stress', *eLife* **6**.

Hanahan, D. & Weinberg, R. A. (2011), 'Hallmarks of cancer: The next generation', *Cell* **144**(5), 646–674.

Hansen, C. H., Endres, R. G. & Wingreen, N. S. (2008), 'Chemotaxis in Escherichia coli: A molecular model for robust precise adaptation', *PLoS Computational Biology* **4**(1), 0014–0027.

Hernndez, J. A. & Lisboa, J. C. V. (2004), 'Reduced kinetic models of facilitative transport', *Biochimica et Biophysica Acta (BBA) - Biomembranes* **1665**(1), 65 – 74.
URL: *http://www.sciencedirect.com/science/article/pii/S0005273604001683*

Hersen, P., McClean, M. N., Mahadevan, L. & Ramanathan, S. (2008), 'Signal processing by the HOG MAP kinase pathway', *Proceedings of the National Academy of Sciences* **105**(20), 7165–7170.
URL: *http://www.pnas.org/content/105/20/7165.abstract*

Hoek, P. I. M. V. a. N., Dijken, J. P. V. a. N. & Pronk, J. T. (1998), 'Effect of Specific Growth Rate on Fermentative Capacity of Baker ' s Yeast', *Society* **64**(11), 4226–4233.
URL: *http://aem.asm.org/cgi/content/abstract/64/11/4226*

Horák, J. (2013), 'Regulations of sugar transporters: insights from yeast', *Current Genetics* pp. 1–31.

Huberts, D. H. E. W., Niebel, B. & Heinemann, M. (2012), 'A flux-sensing mechanism could regulate the switch between respiration and fermentation', *FEMS Yeast Research* **12**(2), 118–128.

Ingolia, N. T., Brar, G. A., Rouskin, S., McGeachy, A. M. & Weissman, J. S. (2013), 'Genome-wide annotation and quantitation of translation by ribosome profiling', *Current Protocols in Molecular Biology* **10**(SUPPL.103).

Jacob, F. & Monod, J. (1961), 'Genetic regulatory mechanisms in the synthesis of proteins', *Journal of Molecular Biology* **3**(3), 318–356.

Janke, C., Magiera, M. M., Rathfelder, N., Taxis, C., Reber, S., Maekawa, H., Moreno-Borchart, A., Doenges, G., Schwob, E., Schiebel, E. & Knop, M. (2004), 'A versatile toolbox for PCR-based tagging of yeast genes: New fluorescent proteins, more markers and promoter substitution cassettes', *Yeast* **21**(11), 947–962.

Josephides, C. & Swain, P. S. (2017), 'Predicting metabolic adaptation from networks of mutational paths', *Nature Communications* **8**(1), 685.
URL: *http://www.nature.com/articles/s41467-017-00828-6*

Kaniak, A., Xue, Z., Macool, D., Kim, J. H. & Johnston, M. (2004), 'Regulatory Network Connecting Two Glucose Signal Transduction Pathways in Saccharomyces cerevisiae', *Eukaryotic Cell* **3**(1), 221–231.

Kayikci, Ö. & Nielsen, J. (2015), 'Glucose repression in Saccharomyces cerevisiae', *FEMS Yeast Research* **15**(6).

Kim, J.-H., Brachet, V., Moriya, H. & Johnston, M. (2006), 'Integration of transcriptional and posttranslational regulation in a glucose signal transduction pathway in Saccharomyces cerevisiae.', *Eukaryotic cell* **5**(1), 167–73.

Kim, J.-H. & Johnston, M. (2006), 'Two glucose-sensing pathways converge on Rgt1 to regulate expression of glucose transporter genes in Saccharomyces cerevisiae.', *The Journal of biological chemistry* **281**(36), 26144–26149.

King, A. D. (1998), 'Inertial navigation - Forty years of evolution', *Gec Review* **13**(3), 140–149.

Kitano, H. (2002), 'Systems biology: a brief overview.', *Science (New York, N.Y.)* **295**(5560), 1662–4.

Kopp, R. E., Kirschvink, J. L., Hilburn, I. A. & Nash, C. Z. (2005), 'The Paleoproterozoic snowball Earth: A climate disaster triggered by the evolution of oxygenic photosynthesis', *Proceedings of the National Academy of Sciences* **102**(32), 11131–11136.
URL: *http://www.pnas.org/cgi/doi/10.1073/pnas.0504878102*

Krampe, S., Stamm, O., Hollenberg, C. P. & Boles, E. (1998), 'Catabolite inactivation of the high-affinity hexose transporters Hxt6 and Hxt7 of Saccharomyces cerevisiae occurs in the vacuole after internalization by endocytosis', *FEBS Letters* **441**(3), 343–347.

Kregiel, D. (2012), *Succinate Dehydrogenase of Saccharomyces cerevisiae – The Unique Enzyme of TCA Cycle – Current Knowledge and New Perspectives*, INTECH Open Science, chapter 9.

Kuchin, S., Vyas, V. K., Kanter, E., Hong, S.-P. & Carlson, M. (2003), 'Std1p (Msn3p) Positively Regulates the Snf1 Kinase in Saccharomyces cerevisiae', *Genetics* **163**(2), 507–514.

Kuttykrishnan, S., Sabina, J., Langton, L. L., Johnston, M. & Brent, M. R. (2010), 'A quantitative model of glucose signaling in yeast reveals an incoherent feed forward loop leading to a specific, transient pulse of transcription', *Proceedings of the National Academy of Sciences* **107**(38), 16743–16748.
URL: *http://www.pnas.org/content/107/38/16743.abstract*

Lee, M. E., DeLoache, W. C., Cervantes, B. & Dueber, J. E. (2015), 'A highly characterized yeast toolkit for modular, multipart assembly', *ACS Synthetic Biology* **4**(9), 975–986. PMID: 25871405.

Lehninger, A., Nelson, D. & Cox, M. (2008), *Lehninger Principles of Biochemistry*, MacMillan Learning.

Lenormand, M., Jabot, F. & Deffuant, G. (2013), 'Adaptive approximate Bayesian computation for complex models', *Computational Statistics* **28**(6), 2777–2796.

Levy, S., Kafri, M., Carmi, M. & Barkai, N. (2011), 'The Competitive Advantage of a Dual-Transporter System', *Science* **334**(6061), 1408–1412.
URL: *http://www.sciencemag.org/cgi/doi/10.1126/science.1207154*

Lichten, C. a., White, R., Clark, I. B. & Swain, P. S. (2014), 'Unmixing of fluorescence spectra to resolve quantitative time-series measurements of gene expression in plate readers.', *BMC biotechnology* **14**(1), 11.
URL: *http://www.ncbi.nlm.nih.gov/pubmed/24495318*

Lillie, S. H. & Pringle, J. R. (1980), 'Reserve carbohydrate metabolism in saccharomyces cerevisiae: responses to nutrient limitation.', *Journal of Bacteriology*

143(3), 1384–1394.
URL: *http://jb.asm.org/content/143/3/1384.abstract*

Longtine, M. S., McKenzie, A., Demarini, D. J., Shah, N. G., Wach, A., Brachat, A., Philippsen, P. & Pringle, J. R. (1998), 'Additional modules for versatile and economical PCR-based gene deletion and modification in Saccharomyces cerevisiae', *Yeast* **14**(10), 953–961.

Ludin, K., Jiang, R. & Carlson, M. (1998), 'Glucose-regulated interaction of a regulatory subunit of protein phosphatase 1 with the Snf1 protein kinase in Saccharomyces cerevisiae.', *Proceedings of the National Academy of Sciences of the United States of America* **95**(11), 6245–50.

Ma, W., Trusina, A., El-Samad, H., Lim, W. A. & Tang, C. (2009), 'Defining Network Topologies that Can Achieve Biochemical Adaptation', *Cell* **138**(4), 760–773.

MacDonald, P. E., Joseph, J. W. & Rorsman, P. (2005), 'Glucose-sensing mechanisms in pancreatic beta-cells.', *Philosophical transactions of the Royal Society of London. Series B, Biological sciences* **360**(1464), 2211–25.

Medina-Rivera, A., Defrance, M., Sand, O., Herrmann, C., Castro-Mondragon, J. A., Delerce, J., Jaeger, S., Blanchet, C., Vincens, P., Caron, C., Staines, D. M., Contreras-Moreira, B., Artufel, M., Charbonnier-Khamvongsa, L., Hernandez, C., Thieffry, D., Thomas-Chollier, M. & Van Helden, J. (2015), 'RSAT 2015: Regulatory sequence analysis tools', *Nucleic Acids Research* **43**(W1), W50–W56.

Meijer, M. M. C., Boonstra, J., Verkleij, A. J. & Verrips, C. T. (1998), 'Glucose repression in Saccharomyces cerevisiae is related to the glucose concentration rather than the glucose flux', *Journal of Biological Chemistry* **273**(37), 24102–24107.

Miesenböck, G., De Angelis, D. A. & Rothman, J. E. (1998), 'Visualizing secretion and synaptic transmission with pH-sensitive green fluorescent proteins', *Nature* **394**(6689), 192–195.
URL: *http://www.nature.com/doifinder/10.1038/28190*

Mihalcescu, I., Van-Melle Gateau, M., Chelli, B., Pinel, C. & Ravanat, J.-L. (2015), 'Green autofluorescence, a double edged monitoring tool for bacterial growth and activity in micro-plates', *Physical Biology* **12**(6), 066016.

Millar, A. J. (2016), 'The Intracellular Dynamics of Circadian Clocks Reach for the Light of Ecology and Evolution', *Annual Review of Plant Biology* **67**(1), 595–618.

Milo, R. (2002), 'Network Motifs: Simple Building Blocks of Complex Networks', *Science* **298**(5594), 824–827.
URL: *http://www.sciencemag.org/cgi/doi/10.1126/science.298.5594.824*

Mitchell, A., Romano, G. H., Groisman, B., Yona, A., Dekel, E., Kupiec, M., Dahan, O. & Pilpel, Y. (2009), 'Adaptive prediction of environmental changes by microorganisms', *Nature* **460**(7252), 220–224.
URL: *http://dx.doi.org/10.1038/nature08112*

Montano-Gutierrez, L. F. (2017), 'ACCESSPR: a Python-based software for plate reader data integration and analysis.', *GitHub* .
URL: *http://github.com/nandomgu/accesspr*

Mony, V. K., Benjamin, S. & O'Rourke, E. J. (2016), 'A lysosome-centered view of nutrient homeostasis', *Autophagy* **12**(4), 619–631.

Moriya, H. & Johnston, M. (2004), 'Glucose sensing and signaling in Saccharomyces cerevisiae through the Rgt2 glucose sensor and casein kinase I.', *Proceedings of the National Academy of Sciences of the United States of America* **101**(6), 1572–7.

Muzzey, D., Gómez-Uribe, C. A., Mettetal, J. T. & van Oudenaarden, A. (2009), 'A Systems-Level Analysis of Perfect Adaptation in Yeast Osmoregulation', *Cell* **138**(1), 160–171.

Naylor, E., Bergmann, B. M., Krauski, K., Zee, P. C., Takahashi, J. S., Vitaterna, M. H. & Turek, F. W. (2000), 'The circadian clock mutation alters sleep homeostasis in the mouse.', *The Journal of neuroscience : the official journal of the Society for Neuroscience* **20**(21), 8138–43.
URL: *http://www.ncbi.nlm.nih.gov/pubmed/11050136*

New, A. M., Cerulus, B., Govers, S. K., Perez-Samper, G., Zhu, B., Boogmans, S., Xavier, J. B. & Verstrepen, K. J. (2014), 'Different Levels of Catabolite Repression Optimize Growth in Stable and Variable Environments', *PLoS Biology* **12**(1).

Nilsson, A. & Nielsen, J. (2016), 'Metabolic Trade-offs in Yeast are Caused by F1F0-ATP synthase', *Scientific Reports* **6**(1), 22264.
URL: *http://www.nature.com/articles/srep22264*

Novick, A. & Szilard, L. (1950), 'Description of the Chemostat', *Science* **112**(1), 715–716.

Okada, S., Leda, M., Hanna, J., Savage, N. S., Bi, E. & Goryachev, A. (2013), 'Daughter Cell Identity Emerges from the Interplay of Cdc42, Septins, and Exocytosis', *Developmental Cell* **26**(2), 148–161.
URL: *http://www.cell.com/developmental-cell/fulltext/S1534-5807(13)00354-7*

Otterstedt, K., Larsson, C., Bill, R. M., Ståhlberg, A., Boles, E., Hohmann, S. & Gustafsson, L. (2004), 'Switching the mode of metabolism in the yeast Saccharomyces cerevisiae', *EMBO Reports* **5**(5), 532–537.

Özcan, S., Dover, J. & Johnston, M. (1998), 'Glucose sensing and signaling by two glucose receptors in the yeast Saccharomyces cerevisiae', *EMBO Journal* **17**(9), 2566–2573.

Ozcan, S., Dover, J., Rosenwald, A. G., Wölfl, S. & Johnston, M. (1996), 'Two glucose transporters in Saccharomyces cerevisiae are glucose sensors that generate a signal for induction of gene expression', *Proceedings of the National Academy of Sciences* **93**(22), 12428–12432.
URL: *http://www.pnas.org/content/93/22/12428.abstract*

Ozcan, S. & Johnston, M. (1995), 'Three different regulatory mechanisms enable yeast hexose transporter (HXT) genes to be induced by different levels of glucose.', *Molecular and cellular biology* **15**(3), 1564–72.

Pasteur, L. (1876), *Études sur la bière: ses maladies, causes qui les Provoquent, procédé pour la rendre inaltérable; avec une theorie nouvelle de la fermentation.*, Gauthier-Villars, Paris.

Peláez, R., Herrero, P. & Moreno, F. (2010), 'Functional domains of yeast hexokinase 2', *Biochemical Journal* **432**(1), 181–190.
URL: *http://biochemj.org/lookup/doi/10.1042/BJ20100663*

Perkins, T. J. & Swain, P. S. (2009), 'Strategies for cellular decision-making', *Molecular Systems Biology* **5**.
URL: *http://msb.embopress.org/cgi/doi/10.1038/msb.2009.83*

Qin, D., Xia, Y. & Whitesides, G. M. (2010), 'Soft lithography for micro- and nanoscale patterning', *Nature Protocols* **5**(3), 491–502.
URL: *http://www.nature.com/doifinder/10.1038/nprot.2009.234*

Raue, A., Schilling, M., Bachmann, J., Matteson, A., Schelke, M., Kaschek, D., Hug, S., Kreutz, C., Harms, B. D., Theis, F. J., Klingmüller, U. & Timmer, J. (2013), 'Lessons Learned from Quantitative Dynamical Modeling in Systems Biology', *PLoS ONE* **8**(9).

Reddi, A. R. & Culotta, V. C. (2013), 'SOD1 integrates signals from oxygen and glucose to repress respiration', *Cell* **152**(1-2), 224–235.

Reifenberger, E., Boles, E. & Ciriacy, M. (1997), 'Kinetic Characterization of Individual Hexose Transporters of Saccharomyces Cerevisiae and their Relation to the Triggering Mechanisms of Glucose Repression', *European Journal of Biochemistry* **245**(2), 324–333.
URL: *http://doi.wiley.com/10.1111/j.1432-1033.1997.00324.x*

Richard, P., Bakker, B. M., Teusink, B., Van Dam, K. & Westerhoff, H. V. (1996), 'Acetaldehyde mediates the synchronization of sustained glycolytic oscillations in populations of yeast cells.', *European journal of biochemistry / FEBS* **235**(1-2), 238–241.
URL: *http://www.ncbi.nlm.nih.gov/pubmed/8631335*

Rolland, F., Winderickx, J. & Thevelein, J. M. (2001), 'Glucose-sensing mechanisms in eukaryotic cells', *Trends in Biochemical Sciences* **26**(5), 310–317.

Rubenstein, E. M., McCartney, R. R., Zhang, C., Shokat, K. M., Shirra, M. K., Arndt, K. M. & Schmidt, M. C. (2008), 'Access denied: Snf1 activation loop phosphorylation is controlled by availability of the phosphorylated threonine 210 to the PP1 phosphatase', *Journal of Biological Chemistry* **283**(1), 222–230.

Sabina, J. & Brown, V. (2009), 'Glucose Sensing Network in Candida albicans: a Sweet Spot for Fungal Morphogenesis ', *Eukaryotic Cell* **8**(9), 1314–1320.
URL: *http://ec.asm.org/content/8/9/1314.short*

Sabina, J. & Johnston, M. (2009), 'Asymmetric Signal Transduction through Paralogs That Comprise a Genetic Switch for Sugar Sensing in Saccharomyces cerevisiae', *Journal of Biological Chemistry* **284**(43), 29635–29643.
URL: *http://www.jbc.org/content/284/43/29635.abstract*

Saldanha, A. J., Brauer, M. J. & Botstein, D. (2004), 'Nutritional homeostasis in batch and steady-state culture of yeast.', *Molecular biology of the cell* **15**(9), 4089–104.

Schmidt-Glenewinkel, H. & Barkai, N. (2014), 'Loss of growth homeostasis by genetic decoupling of cell division from biomass growth: implication for size control mechanisms', *Molecular Systems Biology* **10**(12), 769–769.
URL: *http://msb.embopress.org/cgi/doi/10.15252/msb.20145513*

Schmidt, M. C., McCartney, R. R., Zhang, X., Tillman, T. S., Solimeo, H., Wölfl, S., Almonte, C. & Watkins, S. C. (1999), 'Std1 and Mth1 proteins interact with the glucose sensors to control glucose-regulated gene expression in Saccharomyces cerevisiae.', *Molecular and cellular biology* **19**(7), 4561–4571.

Schuit, F. C., Huypens, P., Heimberg, H. & Pipeleers, D. G. (2001), 'Glucose sensing in pancreatic ??-cells: A model for the study of other glucose-regulated cells in gut, pancreas, and hypothalamus', *Diabetes* **50**(1), 1–11.

Scialdone, A., Mugford, S. T., Feike, D., Skeffngton, A., Borrill, P., Graf, A., Smith, A. M. & Howard, M. (2013), 'Arabidopsis plants perform arithmetic division to prevent starvation at night', *eLife* **2013**(2).

Sen, A., Acosta-Sampson, L., Alvaro, C. G., Ahn, J. S., Cate, J. H. D. & Thorner, J. (2016), 'Internalization of heterologous sugar transporters by endogenous ??-arrestins in the yeast Saccharomyces cerevisiae', *Applied and Environmental Microbiology* **82**(24), 7074–7085.

Shashkova, S., Wollman, A., Leake, M. C. & Hohmann, S. (2017), 'The yeast mig1 transcriptional repressor is dephosphorylated by glucose-dependent and independent mechanisms', *bioRxiv* .
URL: *http://www.biorxiv.org/content/early/2017/04/25/130690*

Sheff, M. A. & Thorn, K. S. (2004), 'Optimized cassettes for fluorescent protein tagging in Saccharomyces cerevisiae', *Yeast* **21**(8), 661–670.

Shiota, T., Traven, A. & Lithgow, T. (2015), 'Mitochondrial biogenesis: Cell-cycle-dependent investment in making mitochondria', *Current Biology* **25**(2), R78–E79.

Shoemaker, D. D., Lashkari, D. A., Morris, D., Mittmann, M. & Davis, R. W. (1996), 'Quantitative phenotypic analysis of yeast deletion mutants using a highly parallel molecular bar-coding strategy', *Nat Genet* **14**(4), 450–6.

Siso-Nadal, F., Ollivier, J. F. & Swain, P. S. (2007), 'Facile: a command-line network compiler for systems biology.', *BMC systems biology* **1**, 36.

Swain, P. S., Elowitz, M. B. & Siggia, E. D. (2002), 'Intrinsic and extrinsic contributions to stochasticity in gene expression', *Proceedings of the National Academy of Sciences* **99**(20), 12795–12800.
URL: *http://www.pnas.org/cgi/doi/10.1073/pnas.162041399*

Swain, P. S., Stevenson, K., Leary, A., Montano-Gutierrez, L. F., Clark, I. B., Vogel, J. & Pilizota, T. (2016), 'Inferring time derivatives including cell growth rates using Gaussian processes', *Nature Communications* **7**, 13766.

Tagkopoulos, I., Liu, Y.-C. & Tavazoie, S. (2008), 'Predictive Behavior Within Microbial Genetic Networks', *Science* **320**(5881), 1313–1317.
URL: *http://www.sciencemag.org/content/320/5881/1313.abstract*

Tanida, I., Ueno, T. & Uchiyama, Y. (2014), 'A super-ecliptic, phluorin-mkate2, tandem fluorescent protein-tagged human LC3 for the monitoring of mammalian autophagy', *PLoS ONE* **9**(10).

Teusink, B., Diderich, J. A., Westerhoff, H. V., Van Dam, K. & Walsh, M. C. (1998), 'Intracellular glucose concentration in derepressed yeast cells consuming glucose is high enough to reduce the glucose transport rate by 50%', *Journal of Bacteriology* **180**(3), 556–562.

Teusink, B., Walsh, M. C., Van Dam, K. & Westerhoff, H. V. (1998), 'The danger of metabolic pathways with turbo design'.

Tillman, T. S., Ganster, R. W., Jiang, R., Carlson, M. & Schmidt, M. C. (1995), 'STD1 (MSN3) interacts directly with the TATA-binding protein and modulates transcription of the SUC2 gene of Saccharomyces cerevisiae', *Nucleic Acids Research* **23**(16), 3174–3180.

Toni, T., Welch, D., Strelkowa, N., Ipsen, A. & Stumpf, M. (2009), 'Approximate Bayesian computation scheme for parameter inference and model selection in dynamical systems', *Journal of the Royal Society Interface* **6**(1), 187–202.
URL: *http://www.scopus.com/inward/record.url?eid=2-s2.0-58149142997&partnerID=40&md5=d26ab2a93f87c39123680c07b13b1285*

Treitel, M. A., Kuchin, S. & Carlson, M. (1998), 'Snf1 protein kinase regulates phosphorylation of the Mig1 repressor in Saccharomyces cerevisiae.', *Molecular and cellular biology* **18**(11), 6273–80.

Tu, B. P. (2005), 'Logic of the Yeast Metabolic Cycle: Temporal Compartmentalization of Cellular Processes', *Science* **310**(5751), 1152–1158.
URL: *http://www.sciencemag.org/cgi/doi/10.1126/science.1120499*

van Heerden, J. H., Bruggeman, F. J. & Teusink, B. (2015), 'Multi-tasking of biosynthetic and energetic functions of glycolysis explained by supply and demand logic', *BioEssays* **37**(1), 34–45.

van Heerden, J. H., Wortel, M. T., Bruggeman, F. J., Heijnen, J. J., Bollen, Y. J. M., Planque, R., Hulshof, J., O'Toole, T. G., Wahl, S. A. & Teusink, B. (2014), 'Lost in Transition: Start-Up of Glycolysis Yields Subpopulations of Nongrowing Cells', *Science* **343**(6174), 1245114–1245114.
URL: *http://www.sciencemag.org/cgi/doi/10.1126/science.1245114*

Vega, M., Riera, A., Fern??ndez-Cid, A., Herrero, P. & Moreno, F. (2016), 'Hexokinase 2 Is an intracellular glucose sensor of yeast cells that maintains the structure and activity of mig1 protein repressor complex', *Journal of Biological Chemistry* **291**(14), 7267–7285.

Vemuri, G. N., Eiteman, M. A., McEwen, J. E., Olsson, L. & Nielsen, J. (2007), 'Increasing NADH oxidation reduces overflow metabolism in Saccharomyces cerevisiae', *Proceedings of the National Academy of Sciences* **104**(7), 2402–2407.
URL: *http://www.pnas.org/cgi/doi/10.1073/pnas.0607469104*

Venturelli, O. S., Zuleta, I., Murray, R. M. & El-Samad, H. (2015), 'Population Diversification in a Yeast Metabolic Program Promotes Anticipation of Environmental Shifts', *PLoS Biology* **13**(1).

Verduyn, C., Postma, E., Scheffers, W. A. & Vandijken, J. P. (1992), 'Effect of benzoic acid on metabolic fluxes in yeasts - a continuous culture study on the regulation of respiration and alcoholic fermentation', *Yeast* **8**(7), 501–517.

Verwaal, R., Paalman, J. W. G., Hogenkamp, A., Verkleij, A. J., Verrips, C. T. & Boonstra, J. (2002), 'HXT5 expression is determined by growth rates in Saccharomyces cerevisiae.', *Yeast (Chichester, England)* **19**(12), 1029–38.
URL: *http://www.ncbi.nlm.nih.gov/pubmed/12210898*

Villaverde, A. F. & Banga, J. R. (2014), 'Reverse engineering and identification in systems biology: strategies, perspectives and challenges.', *Journal of the Royal Society, Interface / the Royal Society* **11**(91), 20130505.

Vincent, O., Townley, R., Kuchin, S. & Carlson, M. (2001), 'Subcellular localization of the Snf1 kinase is regulated by specific β subunits and a novel glucose signaling mechanism', *Genes and Development* **15**(9), 1104–1114.

WADDINGTON, C. H. (1957), *The strategy of the genes. A discussion of some aspects of theoretical biology. With an appendix by H. Kacser.*, London: George Allen; Unwin, Ltd.

Wang, P., Robert, L., Pelletier, J., Dang, W. L., Taddei, F., Wright, A. & Jun, S. (2010), 'Robust growth of escherichia coli', *Current Biology* **20**(12), 1099–1103.

Warburg, O. (1956), 'Injuring of Respiration the Origin of Cancer Cells', *Science* **123**(3191), 309–14.
URL: *http://www.ncbi.nlm.nih.gov/pubmed/13298683*

Waters, J. C. (2009), 'Accuracy and precision in quantitative fluorescence microscopy.', *The Journal of cell biology* **185**(7), 1135–48.
URL: *http://www.ncbi.nlm.nih.gov/pubmed/19564400*

Wells, J. (2013), 'Center of Mass.', *MATLAB File Exchange* .
URL: *https://uk.mathworks.com/matlabcentral/fileexchange/41675-center-of-mass*

Westholm, J., Nordberg, N., Murén, E., Ameur, A., Komorowski, J. & Ronne, H. (2008), 'Combinatorial control of gene expression by the three yeast repressors Mig1, Mig2 and Mig3', *BMC Genomics* **9**(1), 601.
URL: *http://bmcgenomics.biomedcentral.com/articles/10.1186/1471-2164-9-601*

Wheeler, A. R., Throndset, W. R., Whelan, R. J., Leach, A. M., Zare, R. N., Liao, Y. H., Farrell, K., Manger, I. D. & Daridon, A. (2003), 'Microfluidic device for single-cell analysis', *Analytical Chemistry* **75**(14), 3581–3586.

Wieczorke, R., Krampe, S., Weierstall, T., Freidel, K., Hollenberg, C. P. & Boles, E. (1999), 'Concurrent knock-out of at least 20 transporter genes is required to block uptake of hexoses in Saccharomyces cerevisiae', *FEBS Letters* **464**(3), 123–128.

Wilson, W. A., Roach, P. J., Montero, M., Baroja-Fernández, E., Muñoz, F. J., Eydallin, G., Viale, A. M. & Pozueta-Romero, J. (2010), 'Regulation of glycogen metabolism in yeast and bacteria', *FEMS Microbiology Reviews* **34**(6), 952–985.

Wolpert, L. (1969), 'Positional information and the spatial pattern of cellular differentiation', *Journal of Theoretical Biology* **25**(1), 1–47.
URL: *http://linkinghub.elsevier.com/retrieve/pii/S0022519369800160*

Wulff, P., Ponomarenko, A. A., Bartos, M., Korotkova, T. M., Fuchs, E. C., Bahner, F., Both, M., Tort, A. B. L., Kopell, N. J., Wisden, W. & Monyer, H. (2009), 'Hippocampal theta rhythm and its coupling with gamma oscillations require fast inhibition onto parvalbumin-positive interneurons', *Proceedings of the National Academy of Sciences* **106**(9), 3561–3566.
URL: *http://www.pnas.org/cgi/doi/10.1073/pnas.0813176106*

Yaakov, G., Lerner, D., Bentele, K., Steinberger, J. & Barkai, N. (2017), 'Coupling phenotypic persistence to DNA damage increases genetic diversity in severe stress', *Nature Ecology & Evolution* **1**(1), 0016.
URL: *http://www.nature.com/articles/s41559-016-0016*

Yates, G. T. & Smotzer, T. (2007), 'On the lag phase and initial decline of microbial growth curves', *Journal of Theoretical Biology* **244**(3), 511–517.

Yi, T.-M., Huang, Y., Simon, M. I. & Doyle, J. (2000), 'Robust perfect adaptation in bacterial chemotaxis through integral feedback control', *Proceedings of the National Academy of Sciences* **97**(9), 4649–4653.
URL: *http://www.pnas.org/cgi/doi/10.1073/pnas.97.9.4649*

Youk, H. & van Oudenaarden, A. (2009), 'Growth landscape formed by perception and import of glucose in yeast', *Nature* **462**(7275), 875–879.

Young, R. (1992), 'Bacteriophage lysis: mechanism and regulation', *Microbiological reviews* **56**(3), 430–481.

Zampar, G. G., Kummel, A., Ewald, J., Jol, S., Niebel, B., Picotti, P., Aebersold, R., Sauer, U., Zamboni, N. & Heinemann, M. (2013), 'Temporal system-level organization of the switch from glycolytic to gluconeogenic operation in yeast', *Mol Syst Biol* **9**.

Zare, R. N. & Kim, S. (2010), 'Microfluidic Platforms for Single-Cell Analysis', *Annual Review of Biomedical Engineering* **12**(1), 187–201.
URL: *http://www.annualreviews.org/doi/10.1146/annurev-bioeng-070909-105238*

Appendix A

Effects of pre-culture conditions in the hexose transporter expression dynamics

A.1 Plate age affects growth, but does not alter Hxt4 growth staging

As expression of Hxt4 is associated with growth features, variability in growth could propagate into the variance of Hxt4 dynamics. Different experiment sets showed growth rate differences, To minimise these differences, I asked how the age of the initial plate, or different colony origin affected growth. To this aim, I harvested agar plates for 4 months, 2 months and 2 days, and picked 4 colonies of each plate to innoculate cultures of LFSC with 2% glucose. A plate reader experiment was prepared following our standard procedure. As can be seen in A.1, the variability in growth and even fluorescence across all the colonies and technical replicates screened was minor, with only one colony out of 12 displaying distinct growth rate differences; however the initial OD for that colony was lower. Therefore I conclude that, at least for high glucose, plate and colony origin have minor influence in batch culture growth for these purposes. This suggests that specific experiments' external variables, like media batch composition, shaking

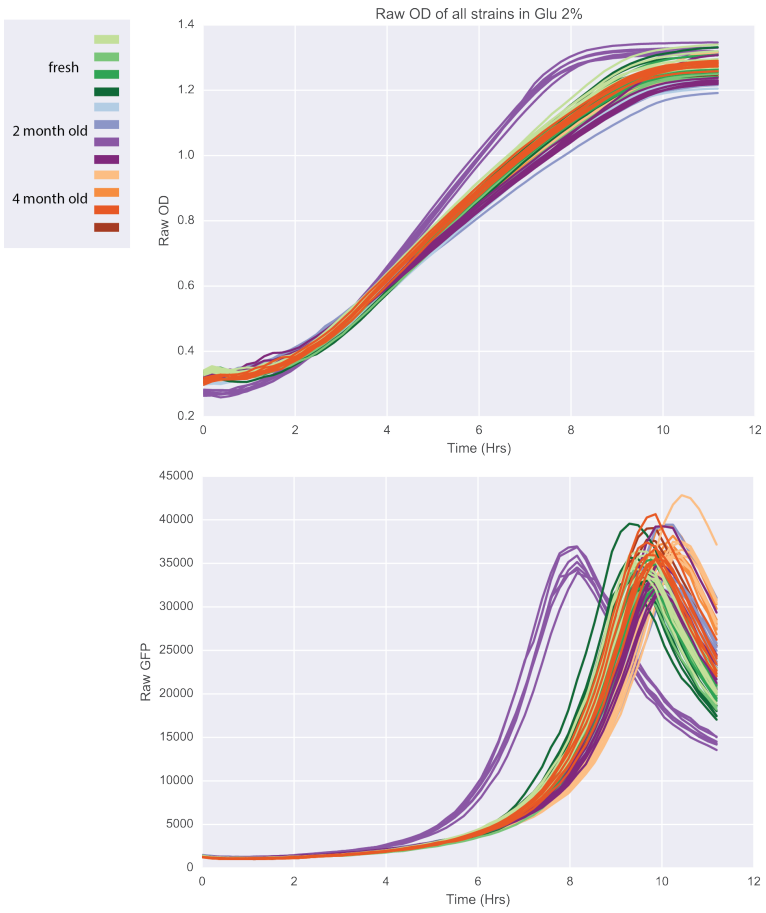

Figure A.1: Plate age does not significantly influence Hxt4 expression variability. Shared plate origin is shown with similar colours, whereas same coloured lines indicate up to 7 technical replicates for the same colony.

properties, temperature and innoculate size could have a greater combined effect than plate and colony origin.

A.2 Pre-culture on different carbon sources does not alter Hxt4 staging in glucose growth

Control of hexose transporter expression could come from the specific carbon source history. Cells grown in glucose, for example, may show glucose memory effects, whereas cells grown in galactose may show specific transition-dependent effects. In order to test how carbon source pre-culture history influenced Hxt4

expression dynamics, I incubated Hxt4-yEGFP and untagged cells for 24 hours in sugarless SC, 2% glucose, 2% galactose, 2% pyruvate or 2% raffinose. Cells were then placed in a plate reader experiment in 1% glucose. At least for the conditions tested, no significant change in the expression dynamics was noted amongst cultures of different treatment (Figure A.2), suggesting that the plate reader preparation procedure, along with high glucose, erase most of the existing memory that could impact the shape of expression dynamics. Interestingly, however, there were some changes in the total expression level, particularly for pyruvate, plus diauxic growth showed differences in the cultures of different treatment (Figure A.2, t¿6) and some of the cultures. Later tests revealed that incubation time in pyruvate affected the expression rate of other Hxts, like Hxt1 (Figure A.3). These changes in cell fluorescence could be due to different proportions of cell subpopulations caused by the preculture conditions. This possibility will be explored using FACS to screen for subpopulations of cells as done by van Heerden et al. (2014).

A.3 Innoculate size does not alter growth staging of Hxt4

I then asked how the innoculate size, and therefore cell density, impacted growth features and the Hxt4 response. With this purpose, I grew both the Hxt4-yEGFP strain and the BY4741 reference in 2% glucose, but diluted them to start at different ODs. The results of this experiment A.4) provided three major insights. First, the final OD of the medium was largely determined by the initial OD of the medium. Second, lower cell densities corresponded to increasingly higher growth rates achieved and longer net growth times; the area under the growth rate curve, which integrates both increments, is therefore inversely correlated with cell density. Third, the activation time of Hxt4 and the lag time are inversely correlated with initial cell density. That is, at lower cell densities it takes longer for cells to activate Hxt4. Fourth, the total fluorescence of Hxt4 per cell is similar across all conditions. As can be seen in Figure A.4, Hxt4 activates expression

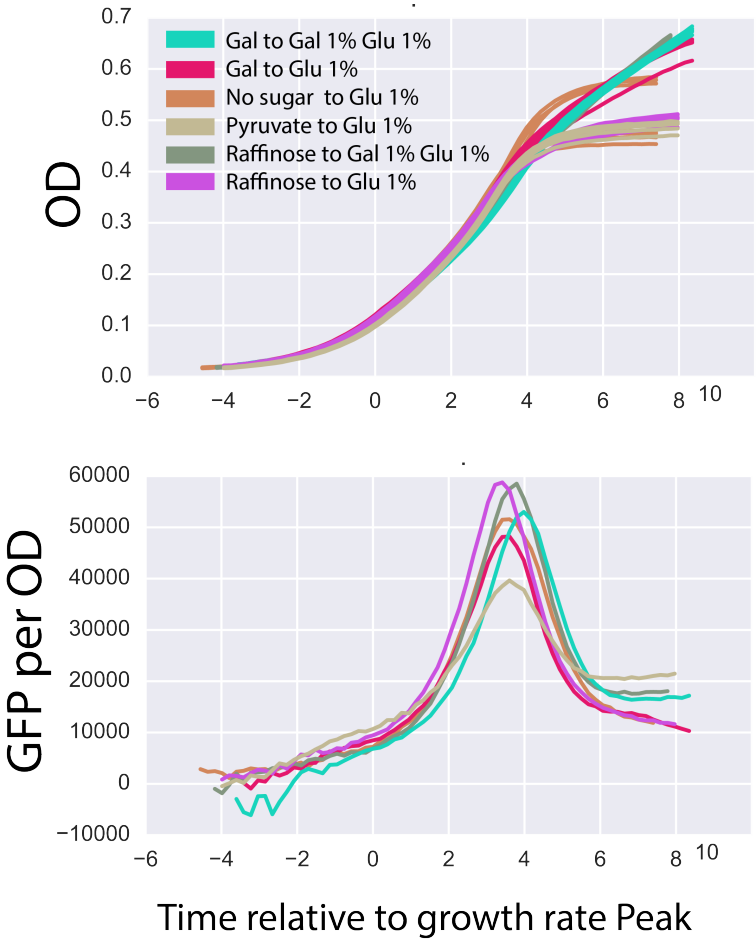

Figure A.2: Pre–culture conditions do not significantly affect the growth staging of Hxt4, even though they may impact exact expression level. Results are shown for a Hxt4-yEGFP tagged strain grown overnight in several carbon sources, washed and then placed in a microplate with either 1% glucose or a mixture of 1% glucose 1% galactose. Top: Growth curves for all pre–culture conditions, after alignment relative to the maximum growth rate. Bottom: corrected GFP fluorescence per OD of all the cultures. Note that the timing for all overlaps significantly, yet the exact values of the fluorescence may vary from condition to condition. This plot shows fluorescence values captured at gain GFP100.

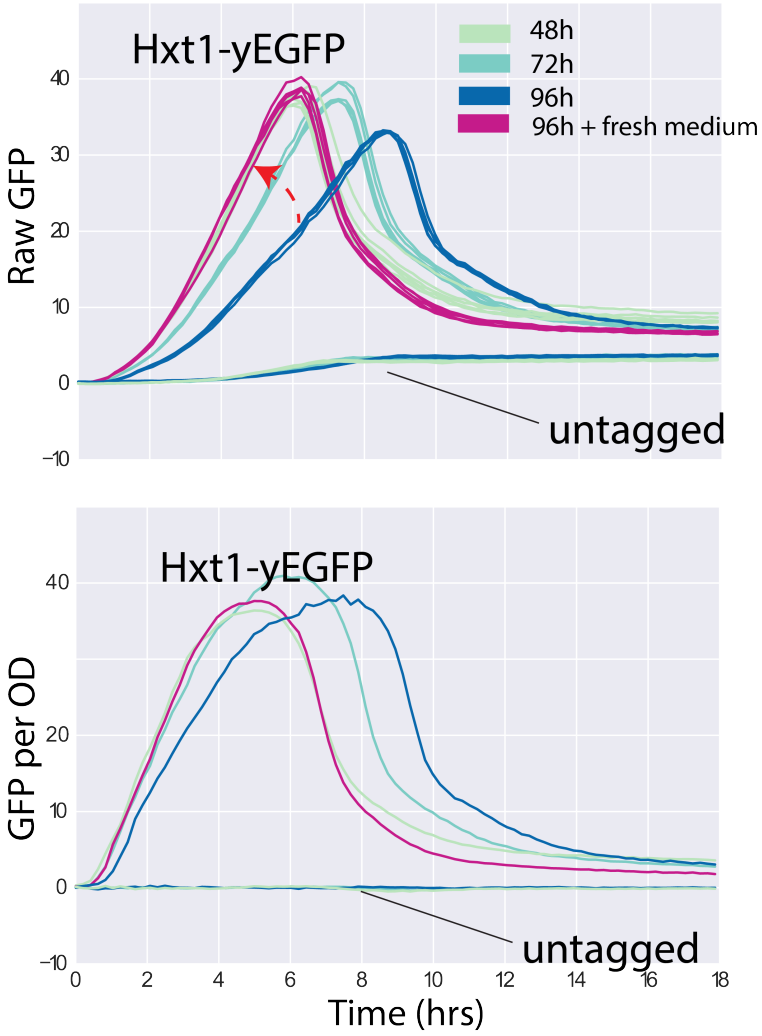

Figure A.3: Pyruvate consumption and incubation impact the expression rate of Hxt1. Cells were incubated in 2% pyruvate for 48 (lightest tone), 72 (cyan tone) or 96 hours (dark blue), and then either placed in the plate reader following the standard procedure (see methods) or incubated in fresh pyruvate medium 3 hours before plate reader set up (magenta). The red arrow highlights the difference in expression rate from the longest to the shortest incubation time. Such difference is lost when replenishing the culture with pyruvate, as the replenished magenta lines overlap almost completely with the 48 hr lines. Panels show the Raw GFP fluorescence and the corrected GFP per OD over time.

and peaks at different cell density and time. However, when projecting Hxt4 dynamics over growth rate features (magnitude and derivative of growth rate), expression of all cultures collapses into the same trajectory. (Figure A.4, inset).

Altogether,setting aside the non-trivial mapping between initial and final OD for a moment, this experiment shows that a delay in the onset of Hxt4 in high glucose can be countered by a higher cell density, and is correlated with dynamic growth rate features rather than a specific cell density. This is a consistent result with the previously shown glucose assay. These results therefore suggest that the cell is able to precisely couple growth rate magnitude and dynamics and with gene expression independently of cell density.

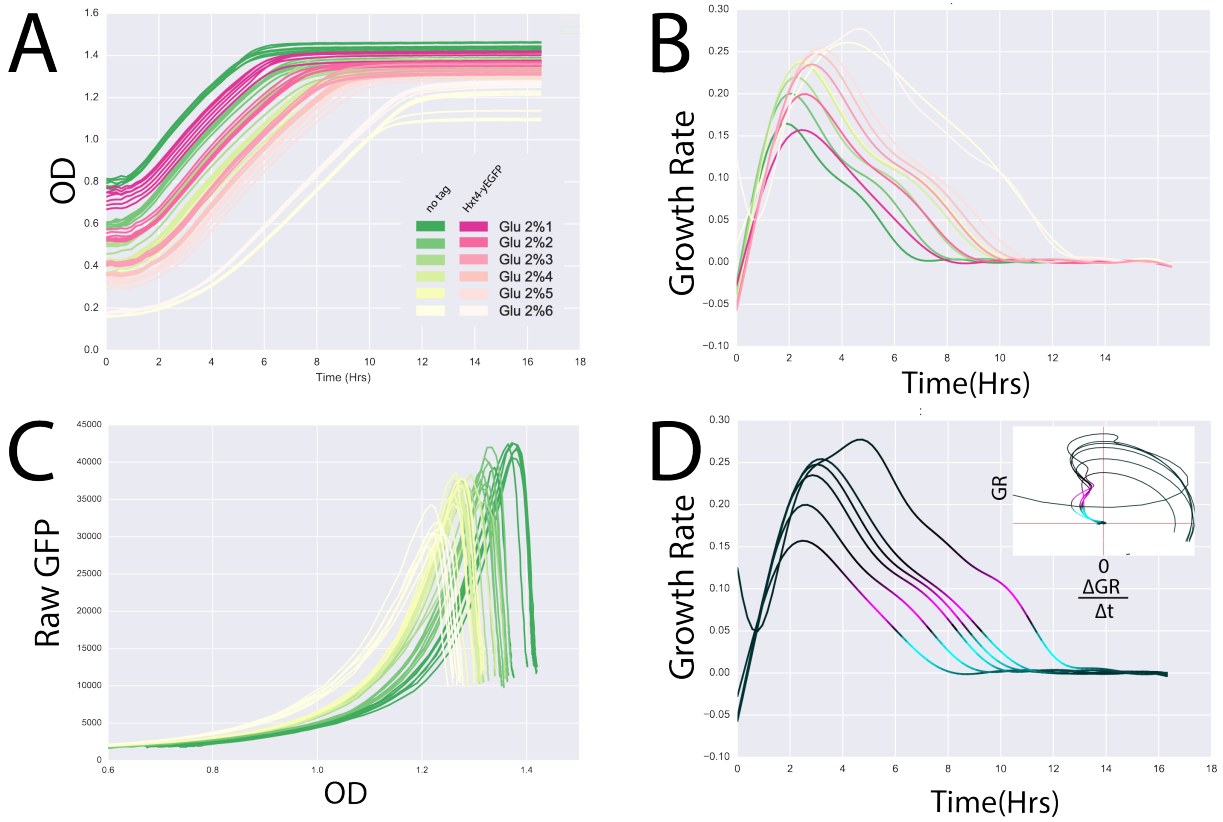

Figure A.4: Hxt4-yEGFP expression is staged during growth regardless of cell density. A) OD curves of a tagged and untagged strain starting from different innoculate sizes. B) corresponding growth rates over time for the OD curves in A. C) Hxt4 activates and peaks at multiple cell densities. D. Growth rate curves in B, coloured by the Hxt4 normalised expression rate. Magenta indicates production whereas cyan indicates decay. Inset shows the same trajectories over the growth rate derivative (x) and growth rate magnitude(y). red indicates the zero crossings.

A.4 Pre-culture time affects the lag phase time, but does not alter Hexose transporter kinetics in glucose

Plate reader experiment design involves standard overnight culture incubation, which could have a historical influence in growth and gene expression dynamics. For example, a 'young' overnight culture may still be undergoing the effects of recently depleted sugar, whereas longer times may induce starvation or, in the case of cerevisiae, respiration. Diauxic growth after glucose depletion is known to carry on for several days before growth reaches complete saturation. Therefore I set to address the impact of incubation times on growth and on the dynamics of multiple Hxts. The following experiments were performed by Jill Zhang and the data has been reported (with different analysis) in her Master's dissertation. Jill conducted these experiments with direct guidance and help from me; Peter Swain and I designed the experiments and the I performed the analysis herein described.

We kept continuous cultures for up to 9 days, and took 1 ml aliquots at the same time every day to start a plate reader experiment, for a total of 9 experiments. At the time, these experiments were done using strains whose transporters were tagged with super ecliptic phluorin (SEP). The brightness of SEP has been reported to be affected by pH (Tanida et al. (2014)). We noticed the fluorophore to be less bright than GFP, but, as will be seen, the qualitative differences across transporters were conserved across fluorophores.

A.4.1 Combining replicates with ACCESSPR

Even though technical performance was of high quality judging by the variability across experimental replicates, analysis imposed several challenges: the experiments were run in two different plate readers: one with a defect which caused artificial oscillations in the fluorescence measurements, and the other one brighter than the first one. Additionally, the most notorious effect from day to

day was that later day cultures showed an increasingly longer lag before logarithmic growth, which caused a temporal shift in the curves. To address these issues, I implemented the software ACCESSPR (Montano-Gutierrez (2017)) which enabled to properly process the data. Among the procedures applied linear mapping was used to account for plate reader differences (2.7.1). Then the growth curves were centered at the peak time of growth rate in order to account for diverging lag times (Figure 3.1). Figure A.5 shows how the initial variance is reduced by this processing, thereby revealing precise expression dynamics for all the different genes. This is true despite the fact that SEP fluorescence was about 8 times lower than that of yEGFP. Moreover, the relative timing and expression of each transporter was remarkably distinct and conserved across incubation times and concentrations, given that the growth curves have been aligned.

Despite the fact that growth rate peak alignment was not perfect, analysis revealed that longer incubation time mainly increased the lag time of the culture (Figure C.1, yet this effect was largely accounted for by growth curve alignment. Additionally, incubation time had a gradual, moderate impact in the max growth rate reached, which was not captured by the net growth. However, by and large, the initial OD of the culture was still the largest determinant of net growth regardless of the incubation time. Altogether, we conclude that the delay induced by longer incubation times does not significantly affect Hexose transporter expression dynamics, other than by their effect on the growth shape.

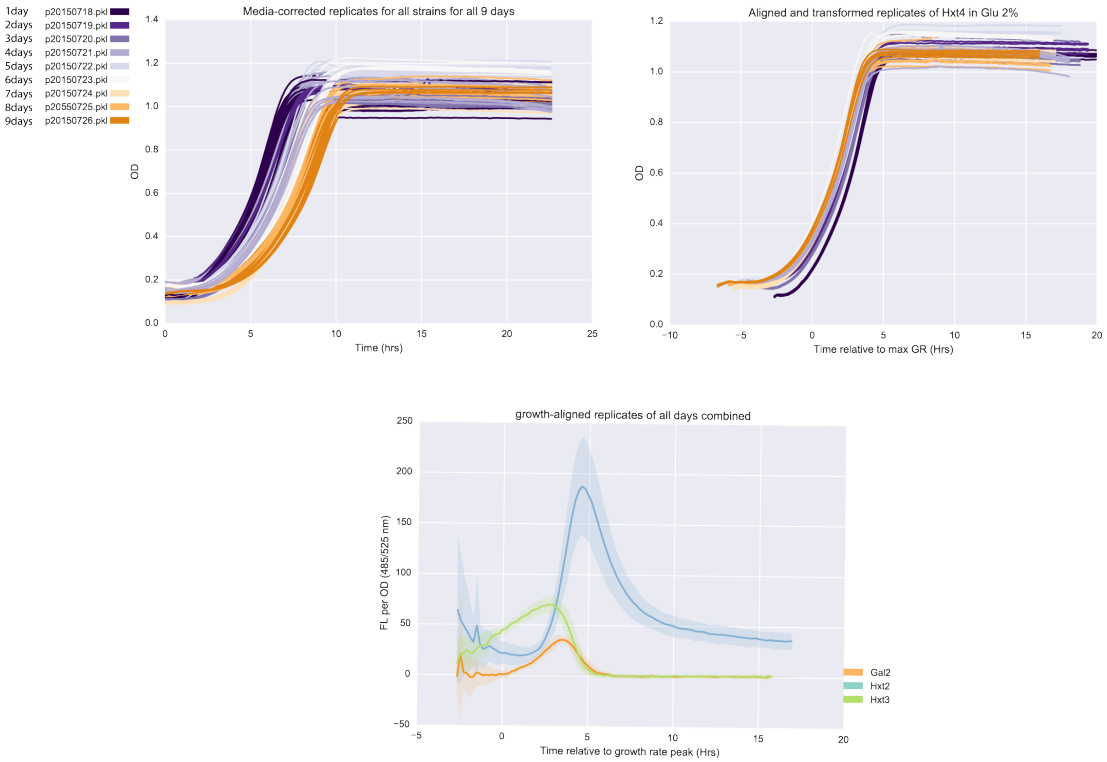

Figure A.5: Incubation time and lag do not influence Hxt expression dynamics. Data corresponds to Plate reader experiments whose starting pre culture was incubated from 1 day up to 9 days. Each day the experiment was prepared using the same standard conditions for all other experiments (See methods). Top Left: Raw OD curves for all experiments. Colour (purple-white-orange) indicates the increasing age of the starting culture. Top right: Same curves on the right, now aligned with reference to the point of maximum growth rate. Bottom: The dynamics of different Hxt-SEP remains highly reprocible even when mixing all the experiments from different ages. It is possible to conclude this because of the alignment, mapping and interpolation of all experiments (as shown in the in the top right) with software ACCESSPR (Montano-Gutierrez (2017)) before averaging replicate values. Coloured lines correspond to Hxt4-SEP (orange), Hxt3-SEP, Hxt7-SEP (Blue)

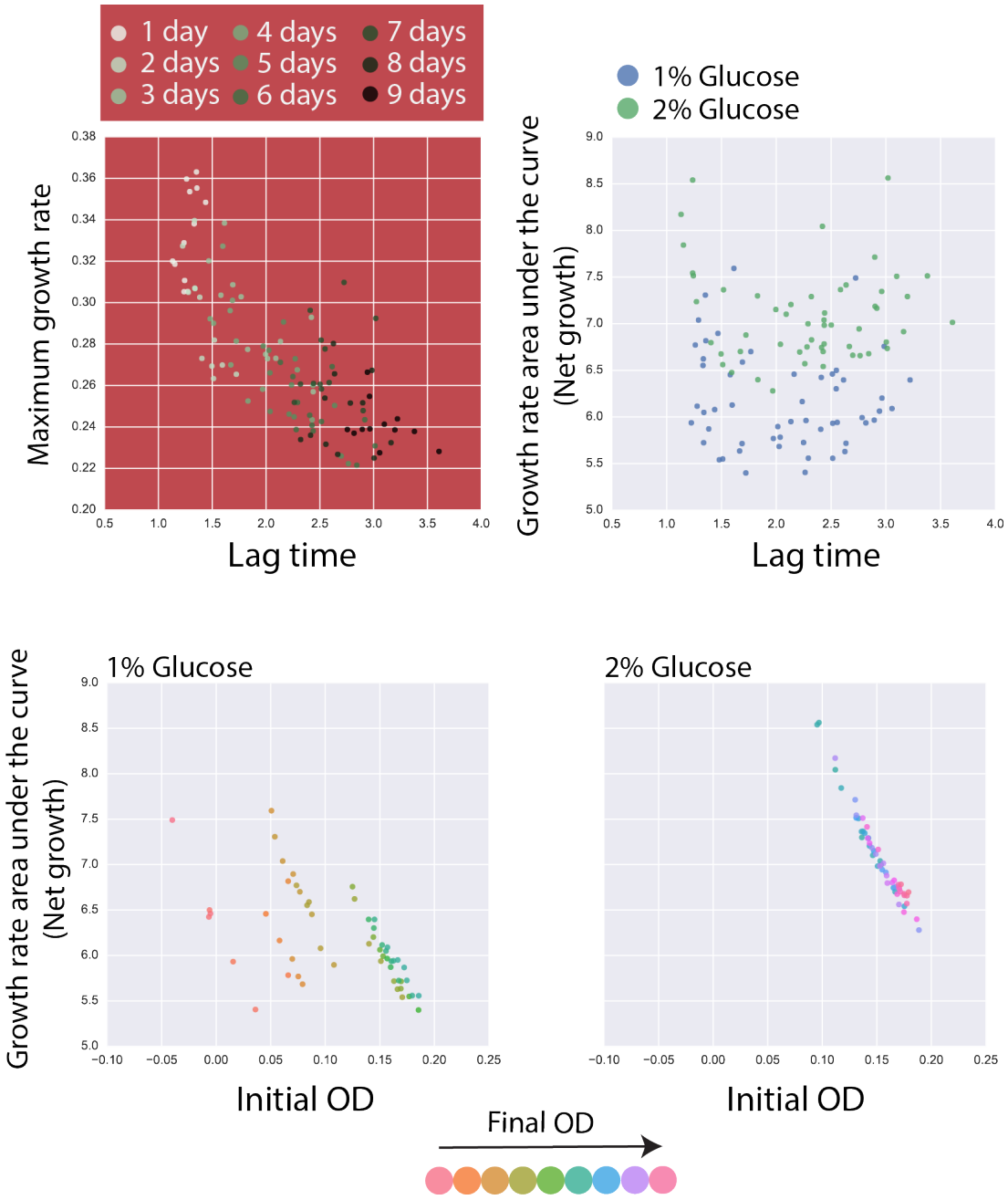

Figure A.6: Initial OD and lag time constrain growth rate. **Top left**: increasing days of culture increase lag time and reduce the maximum growth rate. Each point is the quantification for one independent culture. Colors (from brighter to darker) depict increases of 24 hours in culture age. **Top right**: the net growth, as measured by the area under the growth rate curve, is not affected by lag time, but by initial sugar concentration. **Bottom left and right**: Higher initial OD negatively impacts total growth for a given final OD, but other factors constrain growth variance globally. Colours correspond to different final ODs in the culture (which are implicitly correlated with the initial OD).

Appendix B

Supplementary figures

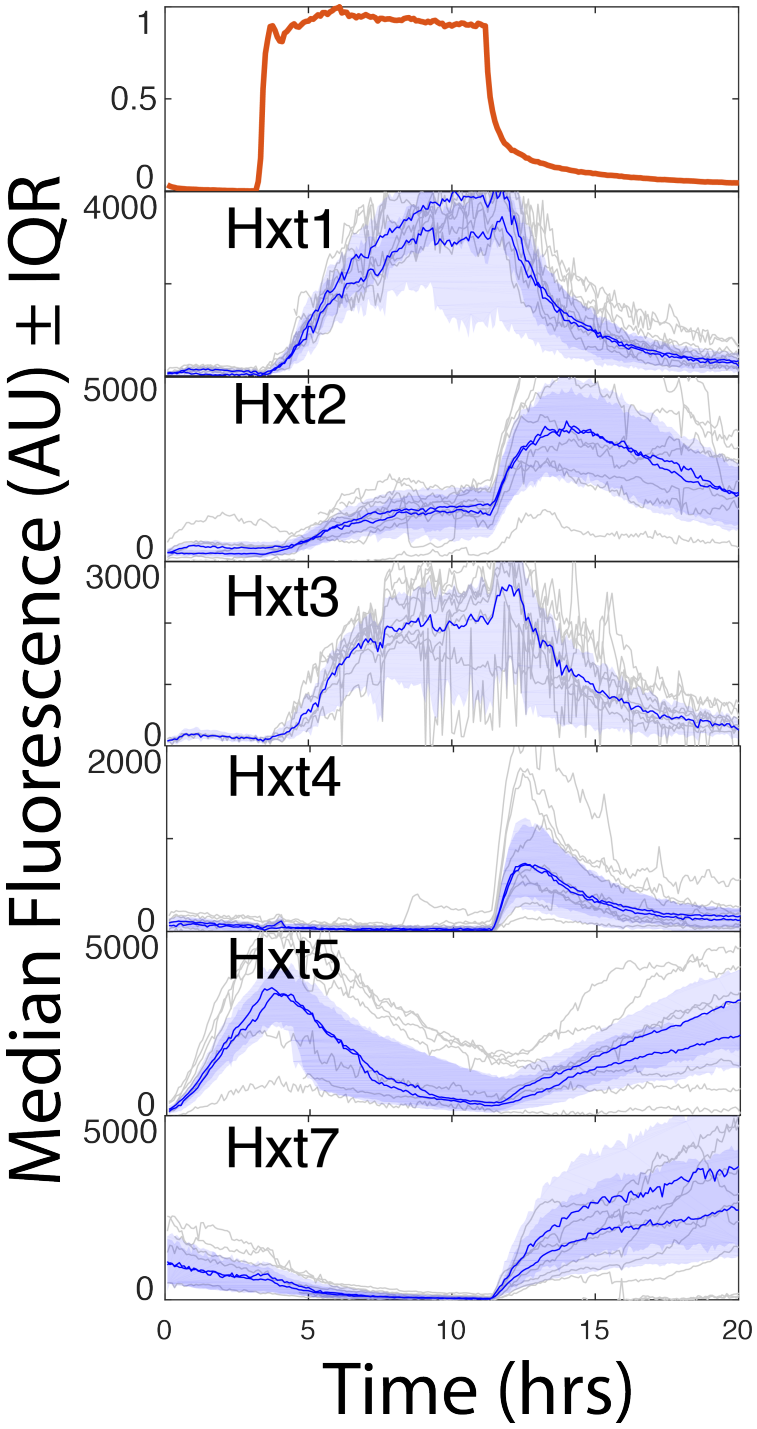

Figure B.1: Hat experiment results are consistent for the Hxts screened. Each Hxt was exposed to sugarless SC, followed by an upshift to 1% glucose and then a downshift to sugarless SC. Top panel: normalised cy5 (% glucose) over time. Strain panels show median cell fluorescence (GFP channel) over time (blue lines), inter-quartile ranges (shaded blue regions), and a sample of 5 cells each (grey lines) for 2 independent, biological replicates. Experiments were subtracted a background of 800 units.

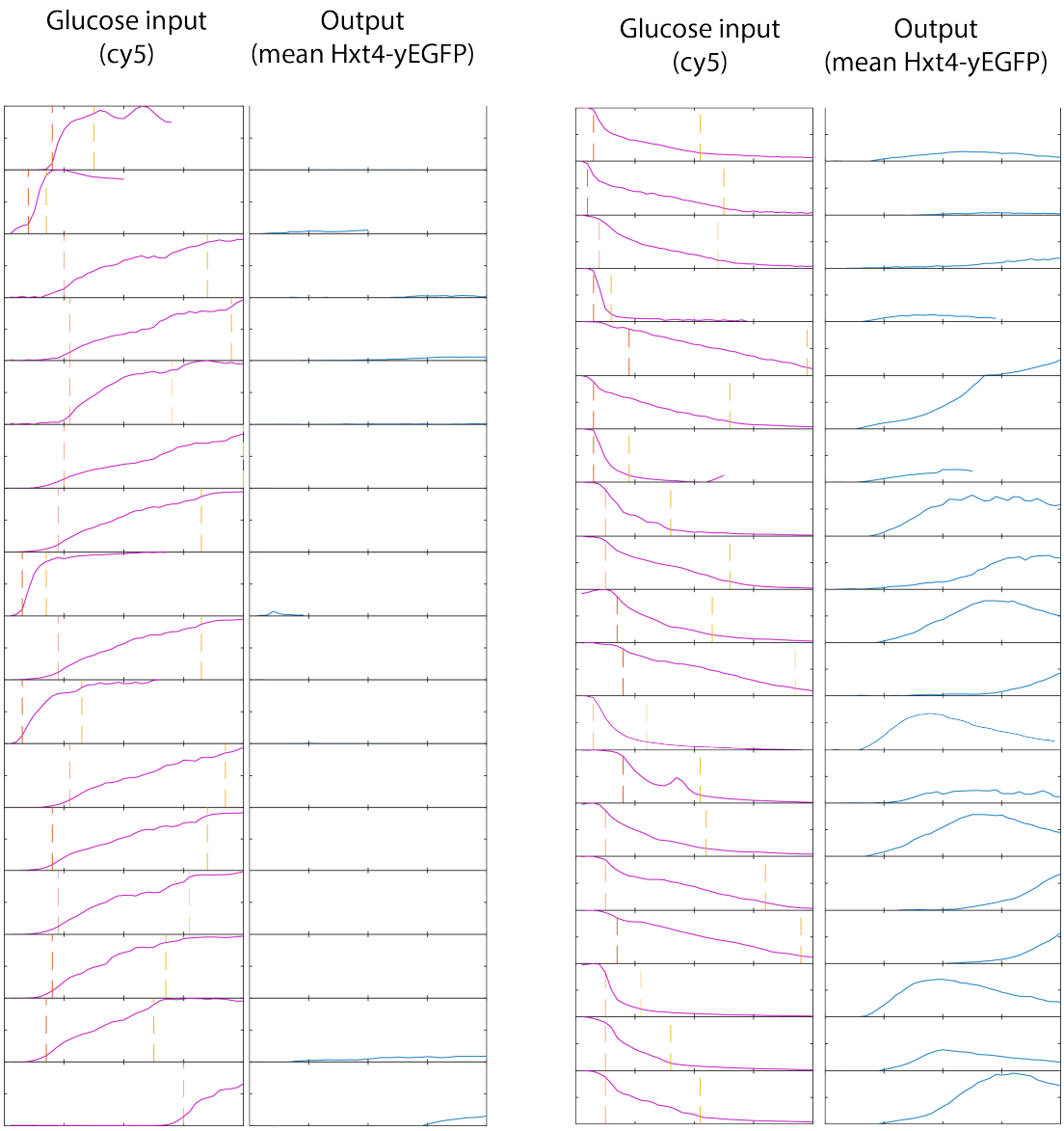

Figure B.2: Overview of all the gradual glucose transitions (ramps) to which Hxt4 was subjected. Magenta lines indicate a tansition from 0 to 1% glucose. Blue lines indicate the mean response of Hxt4 to the ramp on the immediate left column. Orange and yellow lines indicate the the regime between 0.1 and 0.9 % glucose and vice versa. Left panel: rising ramps. Right panel: falling ramps.

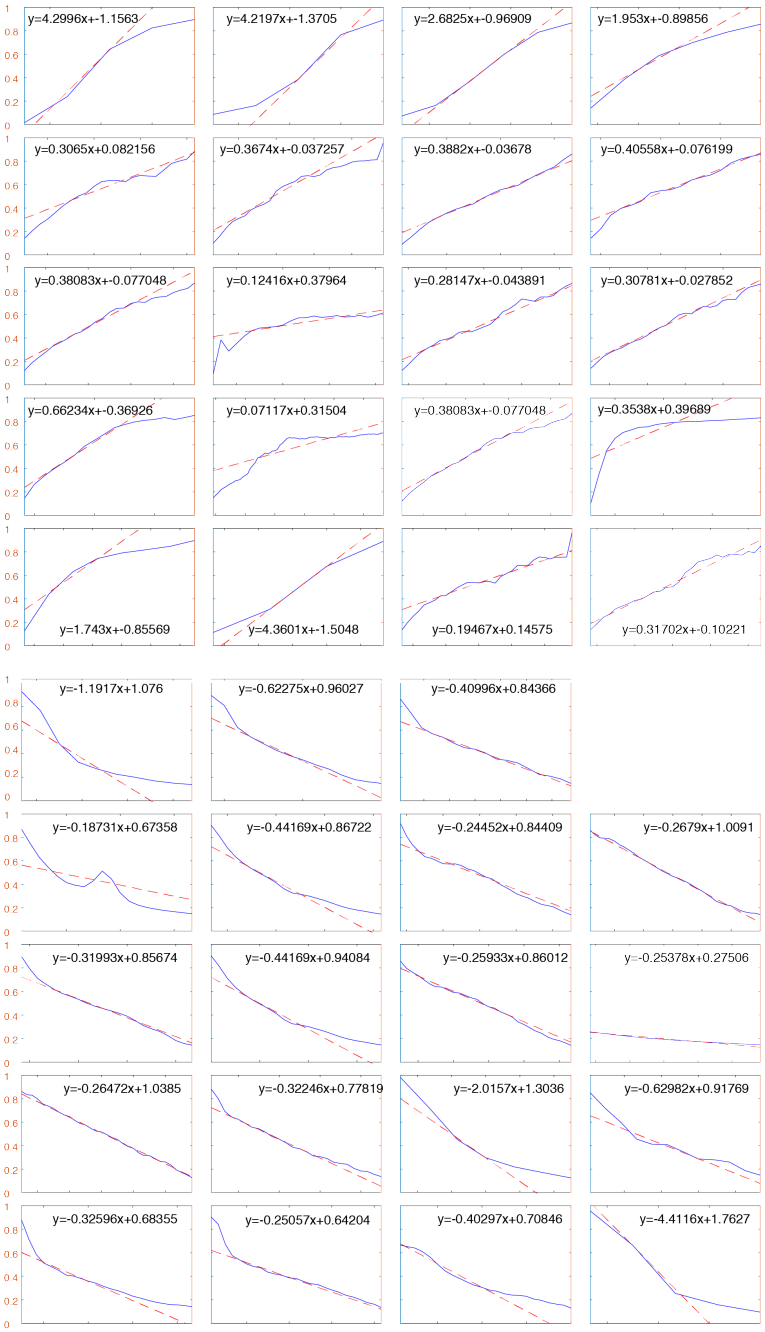

Figure B.3: Results of linear regression for the calculation of glucose slopes. Shown are all the glucose ramps considered for the calculations of Figure 4.10. x axis is time (Different time scale in each panel). Blue lines are the normalised cy5 signal for each experiment, while dashed red lines are the linear regression on the slope with more weight on the midpoints of the ramp (see section 2.7.2. Equation in panel corresponds to the equation for the slope of that experiment.

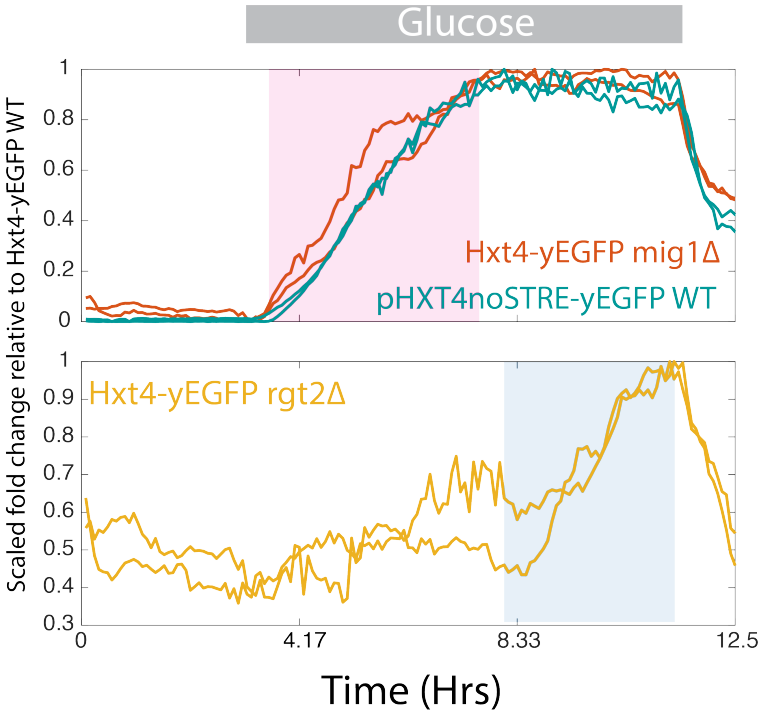

Figure B.4: Dynamic differences of repression by Mig1 and Rgt2. Lines shown the scaled fold change (relative to wild type) over time for different strains. Scaling was done relative to the maximum value as the real fluorescence differed in magnitude. Replicate colours correspond to experimental replicates. Top panel: the activation pattern of Hxt4-yGEFP mig1Δ and the pHXT4noSTRE promoter (in which all potential Mig1 sites have been removed) is highly similar for the first 4 hours (highlighted in pink) to then enter a repressive/steady period. Bottom panel: The activation pattern of a Hxt4-yEGFP rgt2Δ strain. It remains relatively steady/repressed for the first 4 hours in glucose, to then activate (light blue highlight). I conclude that the repression dynamics of Mig1 and Rgt2 is complementary, and therefore likely to be independent.

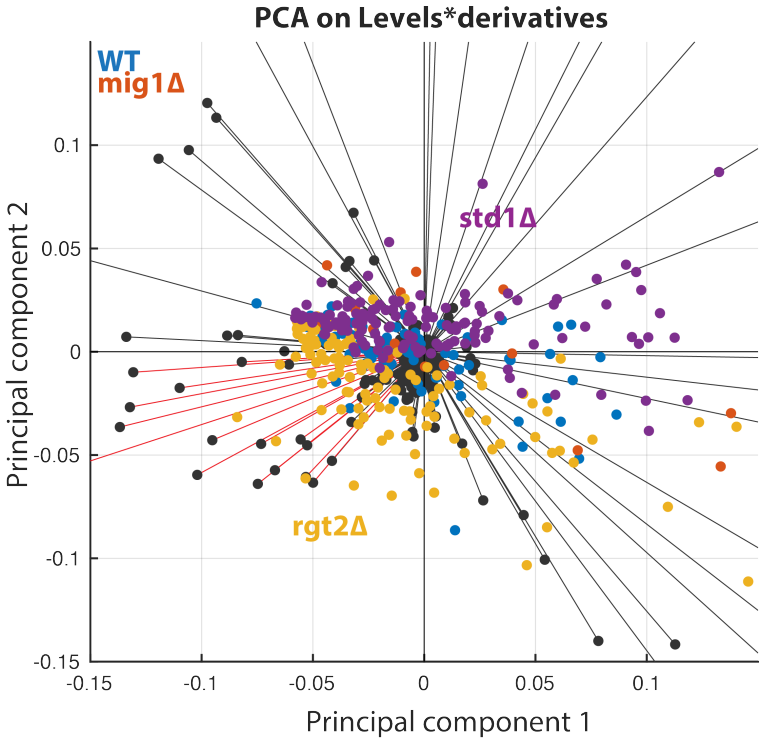

Figure B.5: Rgt2 and Std1 act on the same temporal components to regulate Hxt4. At a given time, both the expression levels and the cell rates describe the state of a cell. Mutants affecting signal processing therefore may impact either the levels or the rates, or both. To integrate information from both level and rate, the matrix $A_{m,t-1}$ of expression levels (where m is the number of cells and t is the number of timepoints) was multiplied entrywise by the matrix $B_{m,(t-1)}$ of expression rates to generate matrix $C_{m,t-1}$. Then, to see if the variance in the dataset could be explained in by fewer temporal dimensions, a Principal Components Analysis (PCA) was run on C. The projection of each cell along the 2 largest components is shown. Each temporal dimension, a variable in the data (black stems), is also projected on the two principal components. It can be seen that the rgt2Δ (yellow) and the std1Δ are accurately separated by the 2 components shown. The component along which rgt2Δ and std1Δ are separated appears to arise from a few covarying timepoints (red stems), Leading to conclude that that both mutants show a phenotype at the similar times. The mig1Δ and WT strains (orange and blue) do not show clear cut separation, perhaps because of sample size differences.

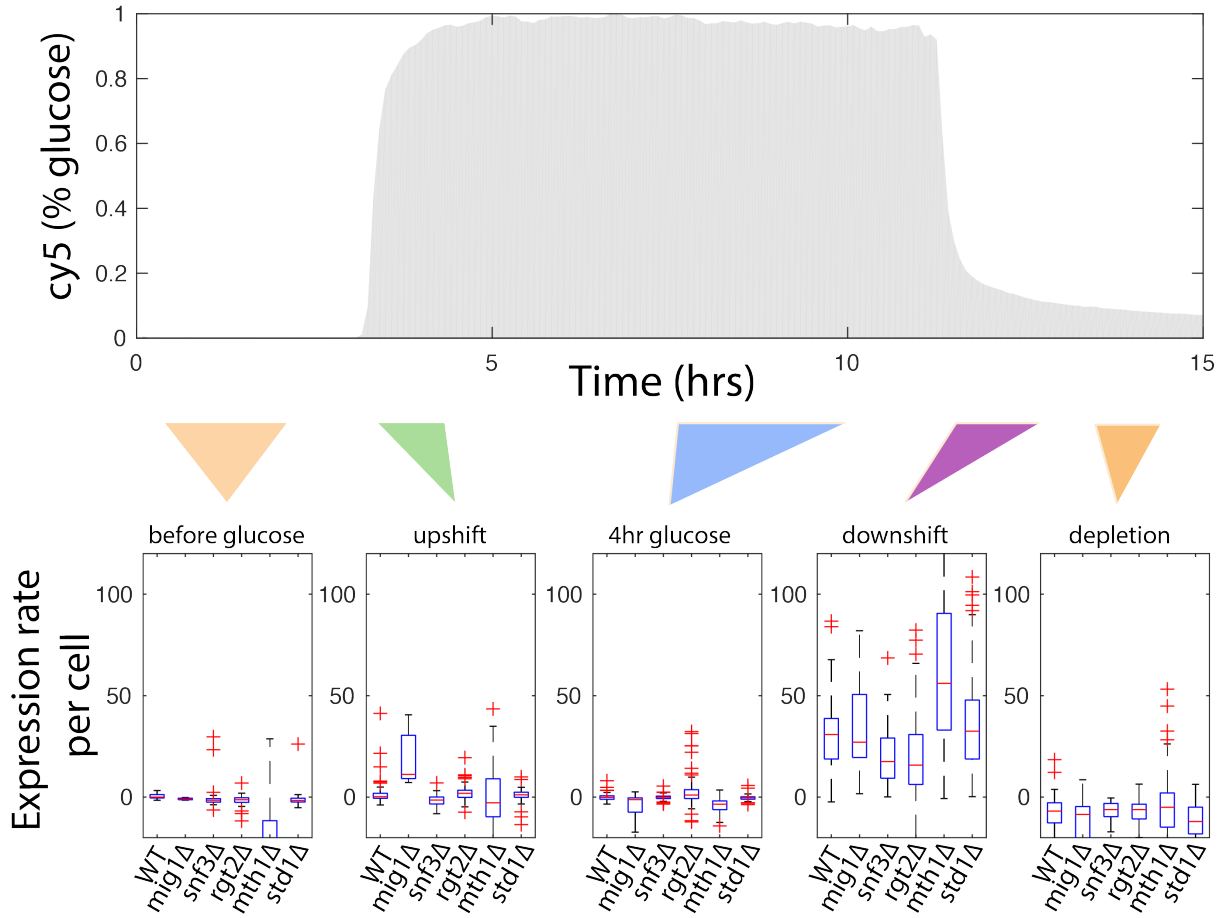

Figure B.6: Single cell effects on the expression rate of Hxt4 depending on the genetic background and the dynamic glucose regime. Top panel: 1% glucose hats over time was sampled over different time windows with different glucose dynamics. Bottom panel: Boxplots showing the distribution of expression rates for Hxt4 per mutant in each of the dynamic regimes. Negative rates, such as those in the last panel, correspond to protein decay. Note how Mig1 activity increases in the upshift but shuts down later. In the window of 4 to 7 hours, the rgt2Δ background is the only one showing derepression, albeit for some cells. Lack of sensors Snf3 and Rgt2 causes a lower overall expression rate in the glucose downshift.

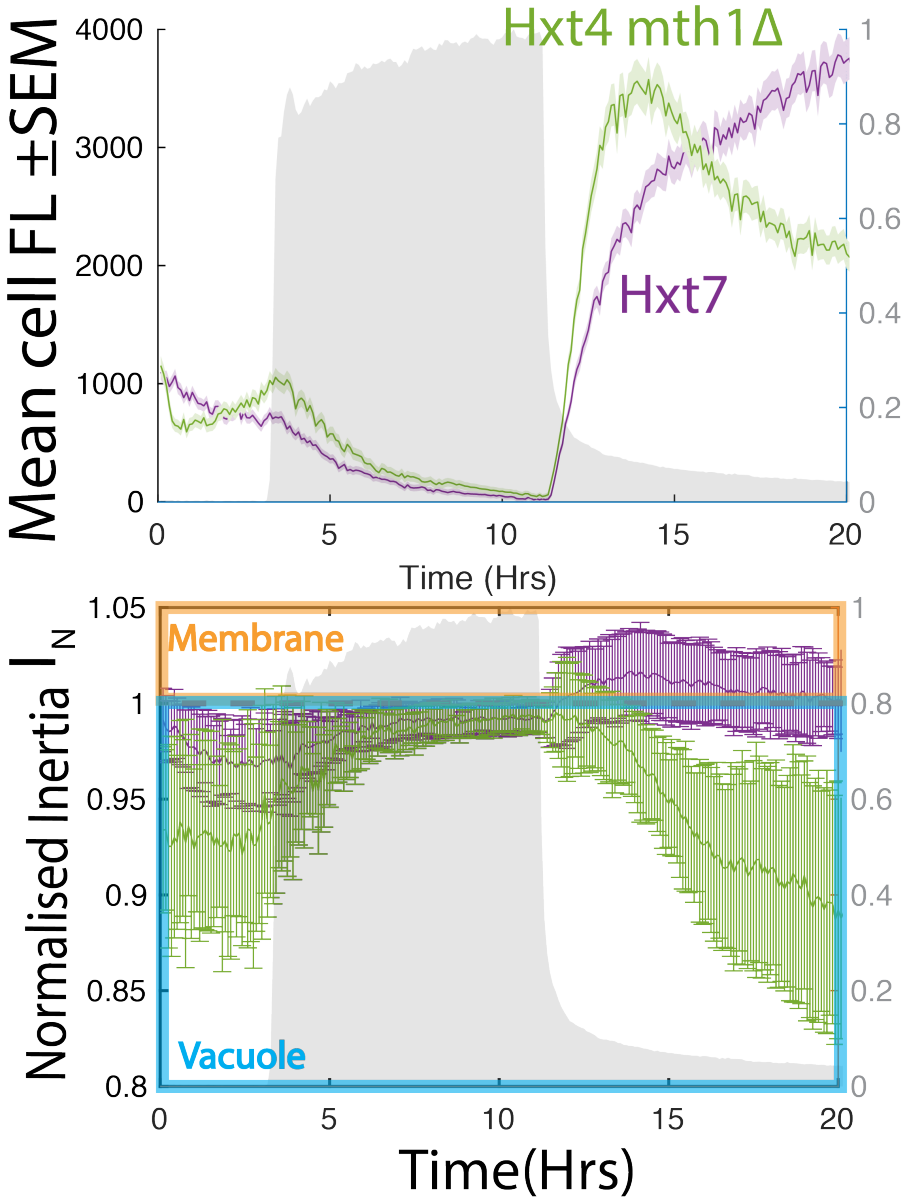

Figure B.7: Similar transporter fluorescence levels can show different vacuole internalisation dynamics. Data is shown for Hxt7-yEGFP (purple) and a Hxt4-yEFGP mth1Δ (green) strains. Grey shows the glucose step in transitions towards-from sugarless SCM. Top panel: Mean expression level ± standard error of the mean for both strains. Bottom panel: Normalised moment of inertia I_N, showing the median ± inter quartile range of localisation for each cell, with values > 1 and < 1 classifying as membrane or vacuole localisation respectively. Note the wide deviation in I_N during glucose exaustion.

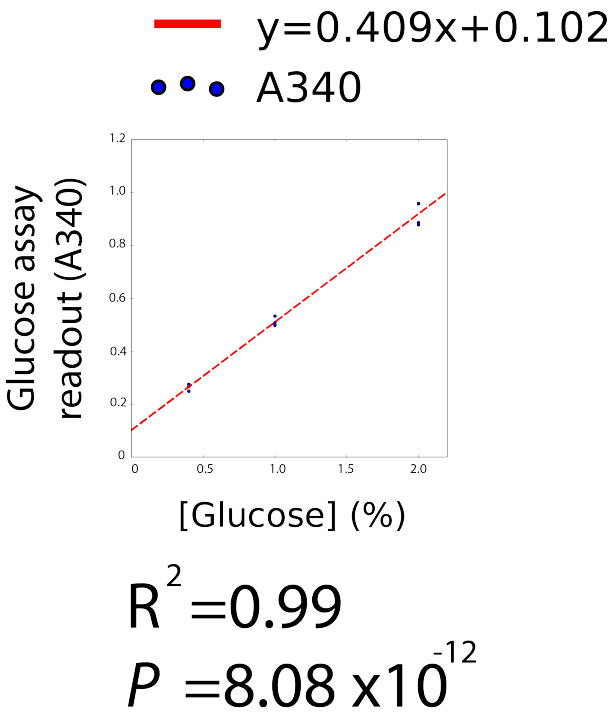

Figure B.8: Calibration standard for the glucose assay presented in Figure 3.6. Samples (0.4%, 1% and 2%) were obtained immediately after innoculation of sugar into the cell medium (in order to account for cell-medium effects in the measurement, which was seen to have an effect. Each point comes from a distinct culture.

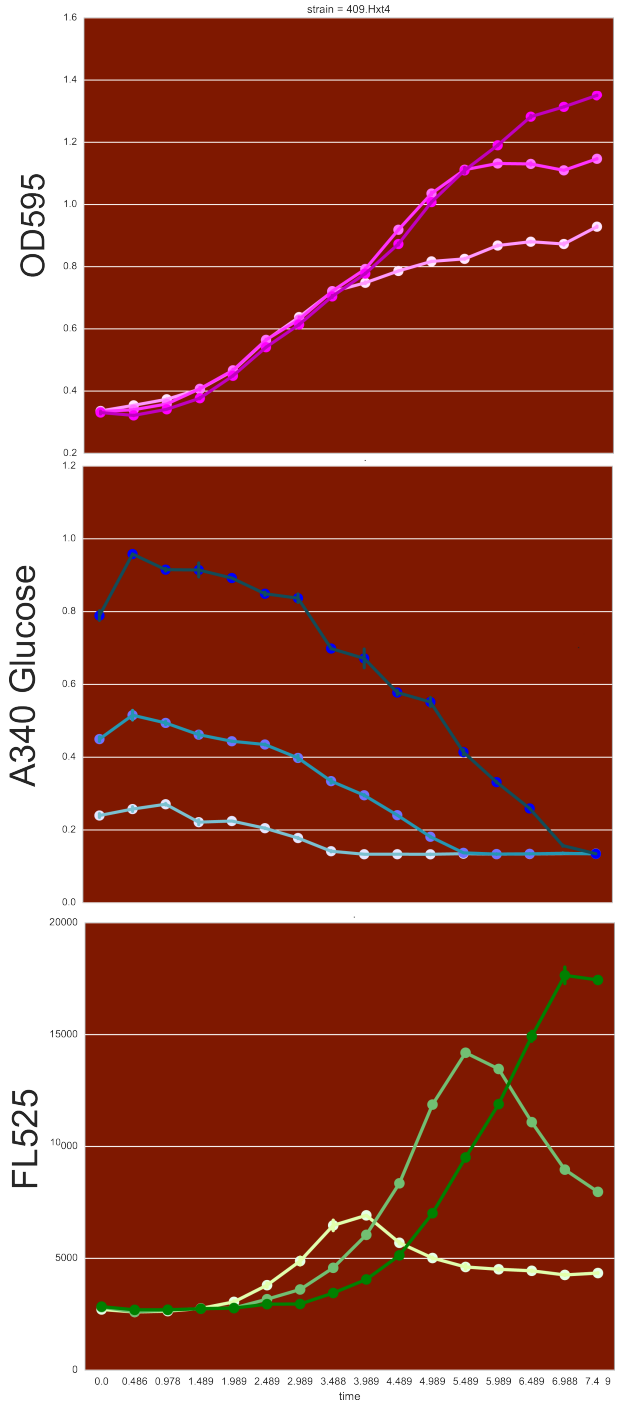

Figure B.9: Curves of glucose assay measurements of section 3.6 grouped by type. Stronger tones depict higher initial glucose concentration. Top (magenta): OD_{595}. Middle: A340 (glucose). Bottom: raw GFP. Each line corresponds to the average of 2 technical replicates. Bars indicate ± standard deviation.

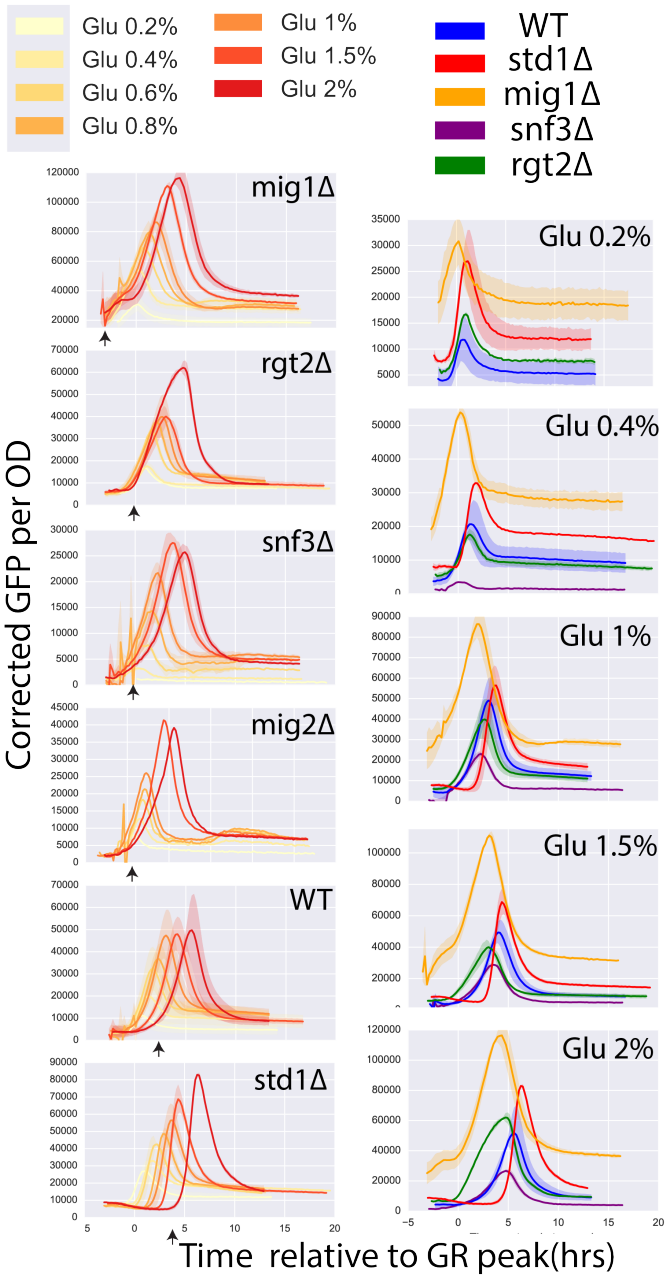

Figure B.10: Dynamic alterations of expression of Hxt4 in different mutant backgrounds. Left column: corrected Hxt4-yEGFP curves over time are shown for many glucose concentrations (red tones) in different mutant backgrounds. Strains were ordered according to the strength of the delay in Hxt4 expression, from no delay (mig1Δ, top panel) to the strongest delay (std1Δ, bottom panel). Arrows indicate the activation time for Hxt4. Right column: The timing effects are preserved at different concentrations of glucose. Time (x axis) is displayed relative to the time of maximum growth rate (0). Error bars show the standard deviation of more than one biological replicate per condition, which have been interpolated to the same sampling times.

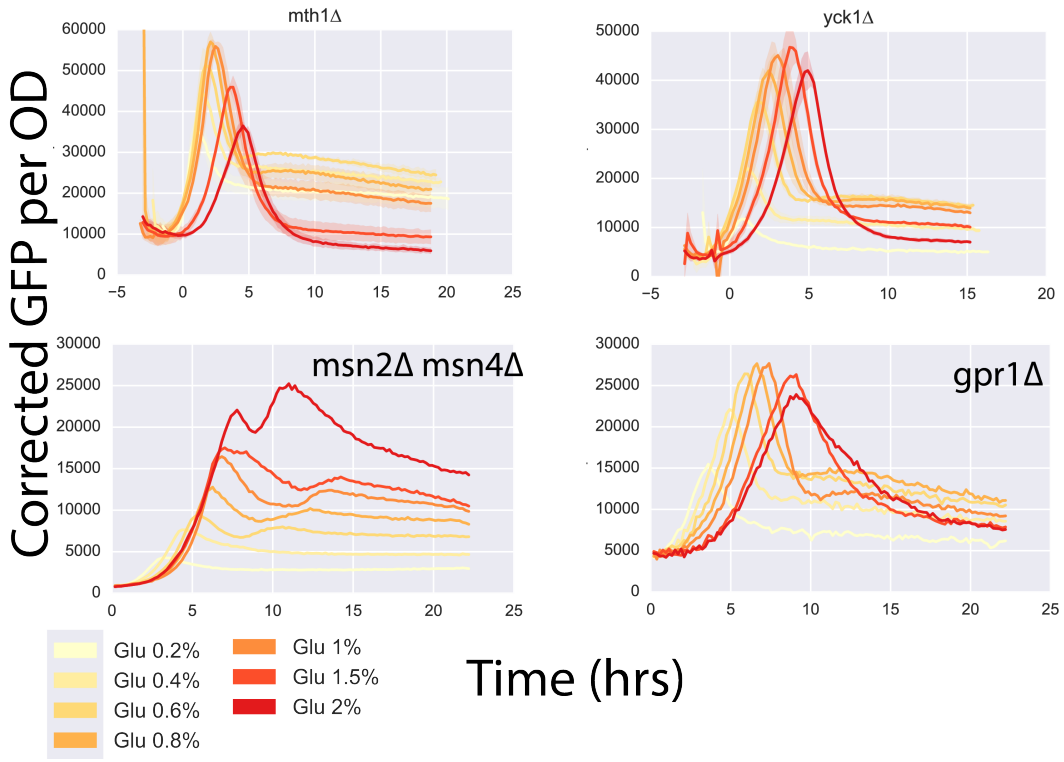

Figure B.11: Additional effects of pathway mutants on Hxt4 dynamics. Expression dynamics data is shown of Hxt4-yEGFP in multiple concentrations of glucose. Top left: Deletion of mth1Δ causes scale effects in expression, but the delays are still present. Top right: A yck1Δ strain has no obvious defect in timing. Bottom row: Hxt4 expression does not depend on activation by the general stress response or alternative glucose sensing. Bottom left: Hxt4 dynamics in a (msn2Δmsn4Δ) strain, showing that Hxt4 is still activated (and subject to timing) in their absence. Additional Hxt4 peaks are an artifact from technical problems in the OD curve in the given experiment. Bottom right: Expression of Hxt4 in the gpr1Δ strain.

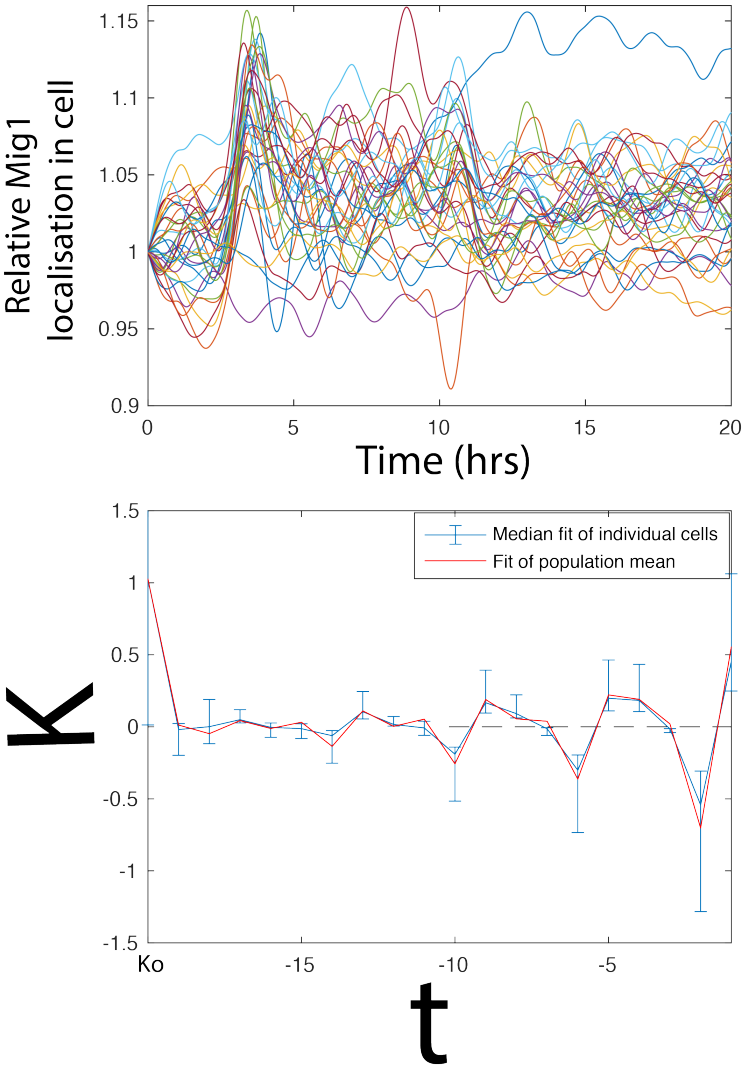

Figure B.12: Prediction of nuclear localisation of Mig1 based on glucose history in single yeast cells. Top panel: single cell traces of mig1 localisation relative to the first timepoint. The traces have been smoothed with a spline to eliminate high frequency noise. Bottom: a regression of each localisation trace above based on glucose history was performed and compared with fitting the mean localisation in the population. Plot shows the filter K applied to the preceding glucose trace x(t-w..t-1) to approximate the upcoming glucose value g(t). Blue line shows the median filter ($\pm IQR$) for the individual cell fits, whereas magenta shows the result when fitting the population mean. The filter has length 19 as opposed to 9 in figure 5.1 because the time values were interpolated, causing a double size of the filter for the same time duration.

Appendix C

Supplemental Notes

C.1 On the linear relationship between initial OD and final OD

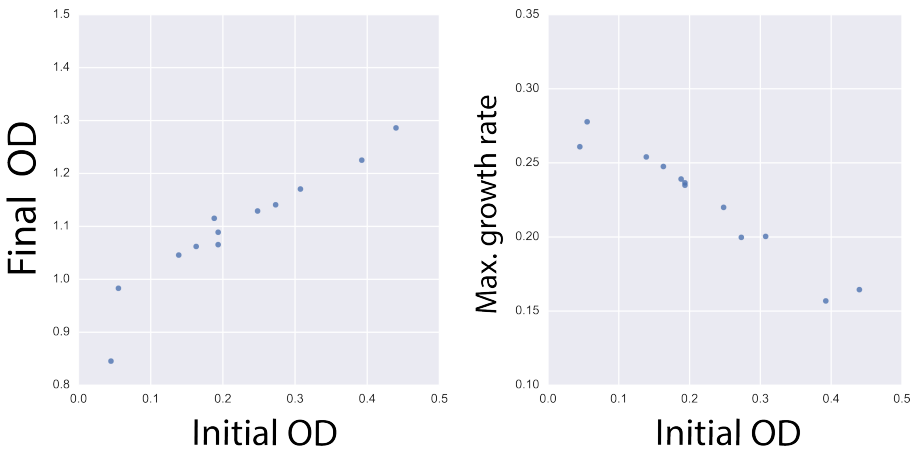

Figure C.1: Linear effects of the initial OD in growth. Data corresponds to the curves shown in Figure A.4. Initial OD negatively has a positive correlation with the Final OD (Left) and a negative impact on the max growth rate achieved.

Throughout the plate reader experiments performed, it was observed that the initial OD had a positive impact on the final OD reached by a culture and a negative effect in growth (Figures C.1, A.6).These results are striking given that microbial growth theory posits a fixed loading capacity. In other words, the growth saturation point is fixed and is provided by the availability of rate-limiting nutrients. Higher innoculates imply that this rate-limiting nutrient will be de-

pleted quicker, but the same biomass accumulation should eventually be achieved. hence it is not completely understood why the final OD would increase. Another interpretation of these results is that, nutrient-wise, the loading capacity of the medium has not been reached, but the growth limitation is dictated by toxin accumulation. This would explain why the densest cultures are the first ones to reach saturation: they produce toxic byproduct at the highest rate, even though they reach higher cell densities and divide the fastest. However, an implicit assumption is that all cells in an innoculate ultimately become dividing cells. An alternative is that a specific fraction of cells dominates the culture after innoculation. Therefore, the dividing cells are active contributors to consumption of nutrients in the culture, while the others have just increased the basal culture density. Through this mechanism, the initial OD of the culture would rise, and so would the final OD. Altogether, despite the inability to explain the tight relationship between initial and Final OD, this experiment shows that a delay in the onset of Hxt4 in high glucose can be countered by a higher cell density.

C.2 On the apparent initial rise of glucose during the glucose assay in section 3.6

As can be seen in figure 3.6, the time course showed an unexpected apparent initial rise in the measured glucose concentration, leading to an ambiguity about the absolute value of glucose concentration throughout the experiment. This unexpected result does not interfere with the conclusions obtained from the assay because a) the final value in the assay coincides with the value of the blank b) the same blank value is reached at different times for all cultures, and c) the linear relationship between initial glucose and A340 holds for both the first and the second timepoint. Since the relative differences among the cultures are key to my claims, and not the precise measurement of glucose concentration, and because the phenomenon affected all cultures in the same way, I conclude that this technicality does not affect the claims I make. I hypothesise the causes of this phenomenon to be 2. First, the assay was prepared with a multichannel pipette,

in which a pipeting error in this timepoint could propagate through all conditions. Second, the assay used is based on hexokinase, G6PDH and NADH, all of them existent metabolites in the yeast's environment. Rupture of some cells would therefore release of these agents into the cell environment, particularly NADH, especially after washing the cells with distilled water (see section 2.6.2). This issue will be addressed in future work using an alternative glucose assay based on glucose oxidase as well as washing with PBS.

C.3 Rationale behind rate based analysis of gene expression

Gene expression is usually measured through expression levels. After all, the amount of a gene product should be proportional tothe gene's rate of activity. However, at least in the case of the HXT genes, levels are not fully informative of a gene's activity. One reason is that its function is not only dependent on expression level, but also on localisation and licensing[1] (section 4.1.3). Another reason is that membrane-bound components cannot be directly inherited to the daughter [2], eliminating the possibility to passively dilute the concentration of a protein. Transporters that were needed for a previous environment linger in the cell for longer than usual unless they are actively degraded, and even so, active degradation may be a slow process. In sum, protein levels may not relate to a functional protein.

In contrast to levels, expression rates offer several advantages. First, they offer a proxy [3] for the moment in which the cell makes the decision to express a transporter. Second, significant non-linear or short expression pulses or spikes will still be recovered, even though the total expression levels of the gene may remain low. A potential disadvantage is that the rate is more sensitive to noise in the

[1]reports have found highly expressed, membrane bound transporters that are unable to import maltose because a kinase was deleted (Gadura et al. (2006)).

[2]The formation of a septin ring between mother and daughter creates a diffusion barrier for membrane-bound proteins forces daughters to synthesise their own membrane (Caudron & Barral (2009), Okada et al. (2013)

[3]disregarding the delay in detection of the reporter's signal.

measurement. However, high frequency noise can be disregarded by smoothing. Third, the saturation of a transporter's levels may decrease the signal coming from the rate. However, as can be seen from the fast changes in rate across the dynamic glucose regimes, the experiments are likely well below the saturation level of the transporters.